STREAMBANK EROSION HAZARD MAPPING: CONCEPTS, METHODOLOGY AND APPLICATION ON THE VENOGE RIVER (SWITZERLAND)

THÈSE N^{O} 3523 (2006)

PRÉSENTÉE LE 21 JUIN 2006

À LA FACULTÉ ENVIRONNEMENT NATUREL, ARCHITECTURAL ET CONSTRUIT

Laboratoire d'hydrologie et aménagements

SECTION DES SCIENCES ET INGÉNIERIE DE L'ENVIRONNEMENT

ÉCOLE POLYTECHNIQUE FÉDÉRALE DE LAUSANNE

POUR L'OBTENTION DU GRADE DE DOCTEUR ÈS SCIENCES

PAR

John Raymond BECK

B.Sc. in Engineering, University of Iowa, Etats-Unis
et de nationalité américaine

acceptée sur proposition du jury:

Prof. A. Buttler, président du jury
Prof. A. Mermoud, Prof. A. Musy, directeurs de thèse
Prof. M. Altinakar, rapporteur
Dr A. Petrascheck, rapporteur
Prof. A. Schleiss, rapporteur

ÉCOLE POLYTECHNIQUE
FÉDÉRALE DE LAUSANNE

Lausanne, EPFL
2006

Abstract

Streambank erosion hazard mapping has received much less attention than flood inundation mapping in the past due to the complexity of the task as well as bank protection works that have reduced bank erosion and unfortunately, the ecological functions of our watercourses at the same time. Damages due to streambank erosion in some flooding contexts are greater than the flood water damages (Loat and Petrasheck, 1997). For these reasons, streambank erosion hazard mapping should be an integral part of flood hazard mapping and methods must be developed to accomplish it. This research proposes a methodology for mapping streambank erosion hazards based on the directives of the Swiss Federal Office for Water and Geology (now within the Swiss Federal Office for the Environment). It permits the calculation of bank failure widths and their probability as opposed to future channel migration paths. This research also investigates the input data necessary for streambank erosion hazard modeling.

Geomorphological mapping must be the first step to streambank erosion hazard mapping as it permits the identification of the sediment movements in the catchment. After this step, modeling of streambank erosion can be undertaken. Geofluvial models that combine hydraulic sediment transport and geotechnical modeling are well suited for streambank erosion modeling. The model CCHE1D is such a model and was adapted for the calculation of the streambank erosion hazard on an 8 kilometer reach of the Lower Venoge River, Switzerland.

CCHE1D performs one dimensional hydraulic calculations. A shear stress correction function based on channel curvature distributes mean boundary shear stress appropriately to outer and inner bank toes and the phase lag of maximum toe shear stress compared to the apex of the bend curvature is ensured by a convolution of upstream shear stresses. Tension cracking was added to the slab failure algorithm due to its significant effect on bank failure widths. After a bank failure, the cross section shape does not change which allows the flow conditions to remain the same and in turn allows the probability of failure for the modeled bank profile to be evaluated.

To gain a better understanding of streambank erosion on the Lower Venoge River, detailed erosion and flow depth monitoring were done on two 1 kilometer river reaches from November 2003 through September 2005. These measurements showed the mass failures to be mainly soil falls and cantilever failures. Measured bank erosion was linearly related to the product of maximum discharge and flood volume. Bank and bed sediment data were also collected for the study reach.

Eighty-two cross sections were surveyed in 2004 in the 8 kilometer study reach. A new cross section tool was developed to properly reproduce scour holes in bends. It calculates transverse position and distance, graphs the cross section to allow identification of bank definition points, linearly interpolates, calibrates bed topography parameters based on surveyed cross sections, and interpolates with respect to channel curvature.

Hydrological modeling allowed for the generation of input hydrographs for the period January 1979-February 2005. This information was combined with historically based low probability floods to construct three 300 year discharge series.

Flow and erosion measurements allowed for the calibration of roughness and critical shear stress parameters, respectively, in the CCHE1D model. Where detailed erosion measurements were not available, past channel migration served as a guide for estimating the critical shear stress. Calibrated critical shear stress was poorly correlated with measured bank properties indicating the necessity of

measuring critical shear stress. A regression equation involving the percentage of fine sand - large silt and the fraction of non-vegetated bank explained 75% of the variation.

The three 300 year discharge series were simulated with CCHE1D. Bank failures series were output for each of the banks of the 1149 computational nodes in the study reach. Empirical frequency was used to determine the bank failure width of a given probability. These bank failure widths and their probabilities were used to calculate a streambank erosion danger. To further qualify this danger, it was mapped with a bar proportional to the mean annual simulated erosion rate. The extreme failure width for the entire reach was determined by multiplying the maximum simulated failure width by a safety factor. The erosion hazard in straight reaches is too high showing that the shear stress reduction due to the highly vegetated banks needs to be taken into account better in the shear stress correction function.

This research has demonstrated the feasibility of streambank erosion hazard mapping, although the quantity of input data necessary is prohibitive. Data acquisition methods must be researched and improved to reduce costs, and research must be continued to improve understanding of bank failure processes to be included in geofluvial models.

Keywords: bank erosion, bank failure, bank stability, shear stress, critical shear stress, erosion pin, bank profiling, cross section interpolation, geofluvial modeling, hydrologic modeling

Résumé

La cartographie des dangers liés à l'érosion des berges d'un cours d'eau a reçu moins d'attention dans le passé que celle des dangers liés aux inondations. Cette différence est due à la difficulté de la tâche, et à la présence d'ouvrages de protection, réduisant l'érosion, mais malheureusement aussi les fonctions écologiques de nos cours d'eau. Dans certains contextes, les dommages dus à l'érosion des berges sont cependant plus importants que ceux causés par l'eau (Loat et Petrasheck, 1997). De ce fait, la cartographie des dangers liés à l'érosion des berges devrait faire partie intégrante de la cartographie des dangers liés aux crues, et des méthodes devraient être développées pour ce faire. Le présent travail de recherche propose une méthodologie pour la cartographie des dangers liés à l'érosion des berges basée sur les directives de l'Office Fédérale Suisse de l'Eau et de la Géologie (maintenant intégré à l'Office Fédérale de l'Environnement). Cette méthodologie permet le calcul des largeurs et probabilités d'effondrement des berges, et non la position future du cours d'eau. Le présent travail de recherche fait par ailleurs une revue des données nécessaires pour la modélisation de l'érosion des berges.

La cartographie géomorphologique doit être la première étape dans la cartographie des dangers liés à l'érosion des berges car elle permet l'identification des mouvements de sédiment dans le bassin versant. La modélisation de l'érosion des berges peut être entreprise ensuite. Les modèles géo-fluviaux qui combinent des modèles hydrauliques de transport de sédiments et des modèles géotechniques sont particulièrement adaptés pour ce faire. Le modèle CCHE1D est un modèle de ce type. Il a été adapté dans le cadre de cette étude pour le calcul des dangers liés à l'érosion des berges, sur un tronçon de rivière de 8 kilomètres de la Venoge, Suisse.

CCHE1D est un modèle hydraulique unidimensionnel. Basée sur la courbure du cours d'eau, une fonction de correction des contraintes de cisaillement distribue celles-ci entre les pieds des berges intérieures et extérieures. Le décalage de la contrainte maximale de cisaillement au pied par rapport à la courbure maximale est assuré par une convolution des contraintes de cisaillement à l'amont. La fissure de tension est intégrée à l'algorithme d'effondrement en plan du fait de son effet significatif sur la largeur d'effondrement. Dans l'approche proposée, la géométrie du profil en travers n'est pas modifiée après un effondrement de berge. Ceci permet que les conditions d'écoulement restent inchangées et ceci permet aussi l'évaluation de la probabilité d'effondrement du profil modélisé.

Pour une meilleure compréhension du phénomène d'érosion des berges de la Venoge, des mesures de hauteurs d'eau et d'érosion ont été effectuées sur deux tronçons de 1 kilomètre, de novembre 2003 à septembre 2005. Ces mesures ont démontré que les effondrements des berges correspondent principalement à des chutes de sol et des effondrements en levier. L'érosion mesurée est corrélée linéairement au produit du débit maximum et du volume de crue. Des données sur les sédiments du lit et des berges ont également été collectées pour le tronçon d'étude.

Quatre-vingt-deux profils en travers ont été levés en 2004 dans le tronçon d'étude de 8 kilomètres. Un nouvel outil de traitement des profils en travers a été développé pour reproduire les affouillements du fond dans les méandres. Cet outil calcule position et distance transversale, dessine le profil en travers pour l'identification des points de définition des berges, interpole linéairement, cale les paramètres de la topographie du lit, et interpole en respectant la courbure du cours d'eau.

Une modélisation hydrologique a permis la génération des hydrogrammes d'entrées pour la période de janvier 1979 à février 2005. Cette information a été combinée avec des crues rares, construites à partir des crues observées, pour préparer trois séries temporelles de débit d'une durée de 300 ans chacune.

Des mesures de hauteur d'eau et d'érosion ont permis le calage de la rugosité et des contraintes de cisaillement critiques pour le modèle CCHE1D. Dans les zones n'ayant pas bénéficié de mesures d'érosion, les divagations historiques du cours d'eau ont guidé l'estimation de la contrainte de cisaillement critique. Les valeurs calées des contraintes de cisaillement critiques ne sont pas bien corrélées avec les propriétés des berges mesurées, ce qui indique la nécessité de mesurer la contrainte de cisaillement. Une régression utilisant le pourcentage de sable fin et de limon grossier et la fraction de berge non couverte de végétation a pu expliquer 75% de la variation, et peut être utilisée pour le tronçon étudié.

Les trois séries temporelles de débit ont été simulées avec CCHE1D. Les séries d'effondrements pour chaque berge des 1149 nœuds de calcul ont été produites par le modèle. Pour une probabilité donnée, la fréquence empirique a été utilisée pour déterminer la largeur d'effondrement. Ces probabilités et leur largeur d'effondrement ont été utilisées pour calculer le danger lié à l'érosion des berges. Pour qualifier le niveau de danger, ce dernier a été cartographié avec des lignes proportionnelles à l'érosion annuelle moyenne simulée. La largeur d'effondrement relative à un événement extrême pour le tronçon a été déterminée en multipliant l'effondrement maximal simulé par un facteur de sécurité. Le danger d'érosion est trop élevé dans les tronçons droits, ce qui montre que la réduction des contraintes de cisaillement due à la végétation des berges doit être mieux prise en compte dans la fonction corrigeant les contraintes de cisaillement.

Le présent travail de recherche a montré la possibilité de réalisation de cartes des dangers liés à l'érosion des berges, bien que la quantité des données nécessaires y soit restrictive. Les méthodes d'acquisition des données doivent être améliorées pour réduire les coûts, et des recherches supplémentaires doivent être mise en œuvre pour mieux comprendre les processus d'effondrement des berges afin de les inclure ensuite dans les modèles géo-fluviaux.

Mots-clés: érosion de berge, effondrement de berge, stabilité de berge, contrainte de cisaillement, contrainte de cisaillement critique, fiche d'érosion, profil de berge, interpolation de profils en travers, modélisation géo-fluviale, modélisation hydrologique

Acknowledgements

For such a multidisciplinary fieldwork thesis, a considerable number of people were necessarily involved. Fortunately, I have this section to thank them. I will inevitably forget someone or some aspect. Please forgive me and know that I appreciated your help.

First of all I thank God, who has given me the opportunity to study his magnificent creation that we will never finish to contemplate.

I want to thank my thesis directors, Professor André Musy and Professor André Mermoud, who provided me the opportunity to start, develop, and finish my thesis! The HYDRAM laboratory was an excellent place to work under the direction of Prof. Musy and still is under the new direction of Prof. Mermoud. The great environment is also due to my incredible HYDRAM colleagues, who are too numerous to invoke here, and to whom I wish to thank not only for their provocative discussions, but also for the kindness and good spirits they brought to work.

Among my HYDRAM colleagues, I wish to thank Richard Metzger, who helped me countless times with HydroRoute, Delphi, and Mapinfo, and who verified a portion of the draft. Jean-Marc Lance laid the foundation for this thesis by his erosion work on the Venoge River and also helped out with the draft verification. Benoît Hingray was always kind to discuss the hydrologic modeling with me. Anne-Catherine Favre provided excellent advice for statistical analyses. My appreciation also goes out to Bettina Schaefli, Cécile Picouet, and Colin Schenk for their verification of portions of the draft. I couldn't have done it without you all!

The amount of fieldwork accomplished during this thesis wouldn't have been possible without the help of the HYDRAM technical staff. Discussions with Alexis Amiguet, Bernard Sperandio, and Karine Vernez-Thomas allowed for the fieldwork techniques to be transferred from paper to reality. Cold weather and getting dirty did not discourage them from getting the measurements event after event! Gabrielle Schwab will probably never count as many rocks as she did in the summer of 2004. Bernard Sperandio also helped out with several figures in this document. Thanks to you all and bravo!

This thesis was given a boost by Professor Mustafa Altinakar and Professor Sam Wang when they provided me the opportunity to work with the CCHE1D code. Dalmo Vieira and Weiming Wu exchanged countless emails with me during my code modifications and debugging, and Dalmo also verified a portion of my draft. I met Andrew Simon and Eddy Langendoen during my visit to Oxford, Mississippi. Their advice and input were greatly appreciated.

Closer to home, Pierre-Yves Gillieron, Ivan Spassov, and Hervé Gontran provided valuable advice and help on the survey work. Christophe Bonnard and Gilbert Steinmann gave me advice on geotechnical aspects and fieldwork. Pascal Turberg contributed with geological information. Discussions with Koen Blanckaert concerning hydraulic theory were insightful. Thank you all for taking the time!

I am grateful to the jury members for the pain they took to judge my work and for their remarks to improve this document. I appreciated the fruitful discussions with Professor Anton Schleiss and Dr. Armin Petrascheck throughout the thesis.

The Interreg IIIb NWE project "Strategies and Actions/Implementations for Flood Emergency Risk Management" partially financed this thesis. I am grateful to the project designers who had the foresight to see the necessity of including this work in the SAFER project and to the project partners for their

fruitful discussions on streambank erosion. Thanks goes out to the SESA and SIT of the Vaud Canton, the national hydrological service (SHN) of the Swiss Federal Office for the Environment, the Swiss Federal Statistical Office, and MeteoSwiss for the data they provided.

Lastly, but definitely not least, I thank my family. Damaris, thank you from the bottom of my heart for the immense support you gave me during these last few years. Lucas, Daniel, and Samuel, you guys were patient with your Daddy when he was working weekends, and you were fantastic when you made him forget about work at times! To the rest of my family, thank you for your prayers and encouragement.

Table of Contents

List of Figures

List of Tables

Chapter 1

Introduction

1.1 Streambank erosion in the flood damage context

1.1.1 Streambank erosion damages

The streambank failure on the unique access road to the Engelberg mountain resort in the Swiss Central Alps on August 22, 2005 illustrates quite well the extreme damages that can be caused by streambank erosion (figure 1.1). This streambank failure caused the collapse of the roadway foundations which led to the collapse of approximately 80 meters of roadway. This perturbation of traffic had enormous consequences as the village of Engelberg was accessible only by helicopter during a two week period.

Although the Engelberg case is an extreme one, streambank failures which perturb traffic are not uncommon. Roadways and railways are often located along rivers. They are usually protected by bank protection works, but in extreme floods those works sometimes fail leading to the collapse of the roadway or railway. Sometimes, it is the foundations of bridges or their pillars which are attacked causing structural damage to the bridge and significant traffic perturbation or at minimum important reparation costs (figure 1.2).

The actual cost of streambank erosion damages is poorly known. They usually are not differentiated from flooding damages, and when no floods occur but streambank protection must be put in place, the costs are often not tallied as flood damage. The other difference compared to flood water damages is that streambank erosion causes protection work degradation. The protection works must then be restored or

replaced. This is also a hidden streambank erosion damage cost. Even if the streambank protection doesn't degrade rapidly, it must be surveyed regularly to ensure its stability.

Figure 1.1. Destruction of the roadway leading to the mountain resort in Engelberg, Switzerland. The village was accessible only by helicopter during a two week period. (from Blick, 2005)

Considering only land value, Graf (1984) estimated the value of land lost due to streambank erosion over a 50 year period for the Rillito Creek to be 5 times the floodwater losses estimated by the US Army Corps of Engineers. "In 1978, the US Army Corps of Engineers estimated that there were over 1,130,000 km of eroding river banks in the USA, with the resulting annual land loss valued at about $270 million and with annual bank-protection costs nearly three times that amount" (Wood et al., 2001 citing Blackmar, 1995). In many countries today, the rivers are not allowed to meander anymore, removing the question of loss of land, but in these countries the pertinence of the cost of bank protection implementation, maintenance, and replacement as well as the sometimes dramatic damages to structures or transportation networks comes into play.

Figure 1.2. Undermining of a bridge pillar (from Loat and Petrascheck, 1997)

1.1.2 Streambank erosion mapping and prevention

The Federal Office for Water and Geology (FOWG) in their booklet (Loat and Petrascheck, 1997) on recommendations to take into account flood hazards in the framework of spatial planning states that streambank erosion, is, in many cases, the type of hazard causing the most damages. This has led the Swiss government to require that streambank erosion be included in flood hazard maps. The directives for mapping the streambank erosion hazard are shown in figure 1.3 (Loat and Petrasheck, 1997). The map of the streambank erosion hazard is called the streambank erosion danger map. A danger level on a map aggregates the streambank erosion hazard information. The streambank erosion danger mapping directives, contrary to the flood inundation directives, are very difficult to evaluate. Knowledge of historical bank failure widths is often very poor and rarely measured precisely, and their probability is usually not known at all. Even if a rough estimation of a bank failure width is possible with a relatively simple calculation, the estimation of the bank failure probability is much more difficult. Once a bank has failed, the hydraulic flow conditions affecting the bank will be changed so that preceding bank failures can not be used in the probability calculation of the present bank. This presents a major problem for Swiss engineers to produce the streambank erosion danger maps according to the Federal Office for Water and Geology directives.

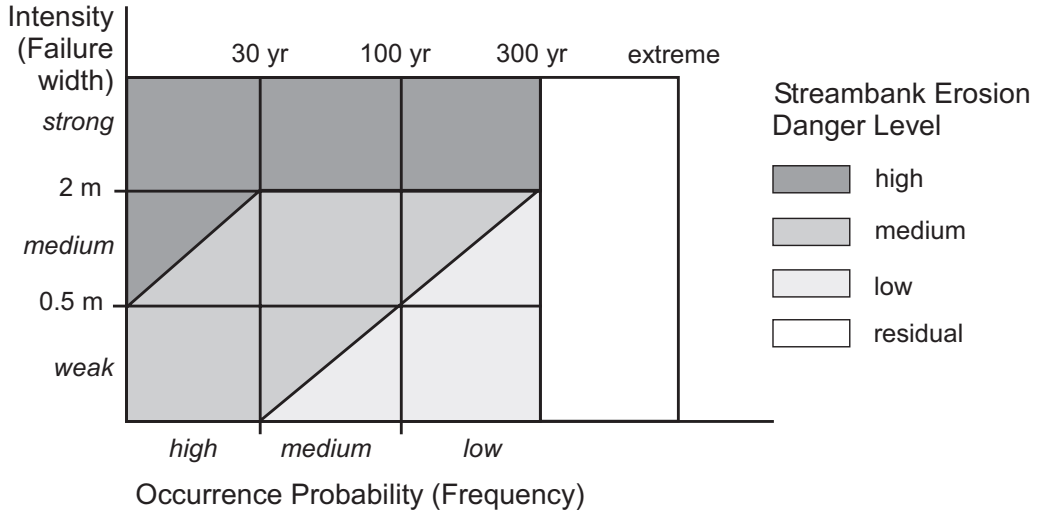

Figure 1.3. Swiss Federal Office for Water and Geology (Loat and Petrascheck, 1997) directives for mapping streambank erosion

Many other governments have also recognized the importance of mapping streambank erosion. The Federal Emergency Management Agency (FEMA) of the United States published the "Riverine Erosion Hazard Areas - Mapping Feasibility Study" (FEMA, 1999). It concluded that mapping of riverine erosion hazard areas is technologically feasible. Contrary to the Swiss approach, it is recommended to delineate the "riverine erosion hazard area" (REHA) for a 30-60 year period. The report expresses the fact that the 30 year estimation will be more reliable, but a 60 year estimation can be drawn up to comply with Section 577 of the National Flood Insurance Reform Act (NFIRA). The erosion hazard area is defined in the act as follows:

"Erosion hazard area means, based on erosion rate information and other historical data available, an area where erosion or avulsion is likely to result in damage to or loss of buildings and infrastructure within a 60-year period." (section 577 of NFIRA quoted in FEMA, 1999)

This definition of course can be criticized in that it confuses the definitions of hazard and risk.

The above two approaches illustrate two types of streambank erosion hazard maps. One which is related to the bank failure width due to a single event or the other which maps the river channel planform change over a number of years. Both maps have their purposes. The Swiss streambank erosion hazard map, called a streambank erosion danger map, is important for describing how much erosion could happen during a single event. This information is sometimes roughly known for rapidly moving channels, but for relatively stable banks it is usually unknown. The REHA is also an important information for flood risk management and for spatial planners (assuming the erosion hazard is mapped regardless of vulnerability). The REHA will help the flood manager to decide where bank protection works will be necessary and the spatial planner where development zones should be avoided.

A third type of streambank erosion hazard map is the streambank erosion intervention map. A prototype of this map was developed in the Venoge study (Lance and Consuegra, 1998) done by the HYDRAM laboratory of the EPFL. Figure 1.4 shows an example of this type of map. What is important in this map is that a stream corridor is defined. This stream corridor in the example of the Venoge study was

determined according to the historical locations of the river visible in historical maps, aerial photos, and Digital Terrain Models (DTM) and according to the confining nature of the river valley. With knowledge from either a streambank erosion danger map or from observations, a maximum possible channel change is used as a security distance. Land use maps superimposed on the stream corridor will show the existing conflicts. An additional security distance, let's call it the infrastructure security distance, can be added to the erosion security distance as an extra protection for infrastructure. Thus, spatial planners can use this map to make appropriate decisions on land use and riverway managers can use the map to decide when they must react to stop an erosion. This map has the advantage that it does not try to use the perilous calculation of a 30 year or 60 year possible river channel change, but rather shows the maximum possible space allowed for channel movement. Usually the stream corridor can be more easily defined than the possible channel movement during the next 60 years.

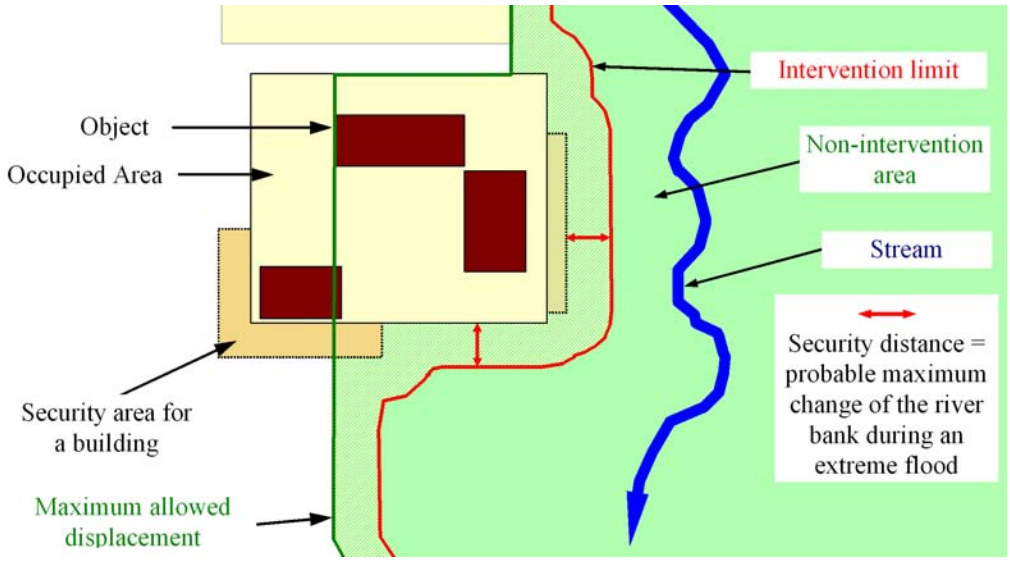

Figure 1.4. Streambank intervention map (adapted from Lance and Consuegra, 1998)

1.2 Thesis objectives

Due to the importance of damages caused by streambank erosion during flood events, and the lack of tools available to calculate bank failure widths and their probability, the primary objective of this thesis is to develop a methodology to map streambank erosion hazards. This will necessitate the improvement of existing models. To test such a model, a case study is necessary. The Venoge River is chosen for the case study and bank erosion data is acquired.

1.2.1 Modeling streambank erosion

Near-bank hydraulic processes require a 3-D representation of the flow field to attempt to estimate the boundary shear stress that is responsible for the fluvial entrainment of bank materials. This poses of course the problem of the significant computational time and data necessary for such a model. Two

dimensional flow models are most often used due to the lateral variation of the flow parameters they provide. One dimensional flow models have also been used, but a correction to the shear stress estimation on the outer bank must be applied for realistic erosion-producing shear stresses to be simulated.

Due to the computational consequences of 2-D and 3-D flow and sediment transport models, the first objective of this thesis is to adapt an existing 1-D model to simulate erosion and bank failures. This will require that the complexities of the longitudinal extent of bank erosion and the estimation of the near-bank shear stress be addressed.

1.2.2 Acquisition of streambank erosion data

The second objective of this research is to explore the practicality of obtaining sufficient data for simulating streambank erosion with spatially varying data. If streambank erosion models are to be used for streambank erosion hazard mapping, data collection methods must also be considered and their optimization must also be carried out.

Besides the importance of estimating the practicality of acquiring data for streambank erosion modeling, this research could provide a valuable data set for further streambank erosion modeling efforts. In their article on "River Width Adjustment", the ASCE Task Committee (1998b) cites only three data sets "that are suitable for use with numerical models of width adjustment". This significant lack of data is a major hurdle to overcome for developing streambank erosion models.

1.3 Report organization

Chapter 2 of this dissertation starts with a description of the important processes involved in streambank erosion. It goes on to explore the modeling possibilities available for streambank erosion. Finally, a methodology for calculating the streambank erosion hazard map based on the model CCHE1D is presented.

Chapter 3 gives the geomorphological context of the Venoge catchment (geology, land-use, soil, topography, hydrographic network, climate, and hydrologic regime) and river (channel morphology) as background information for the case study.

Chapter 4 goes into detail about the data that was obtained for the case study on the Lower Venoge River. Two experimental reaches were setup on the Venoge to gather bank erosion data. The studied reaches and equipment are described and the measured values are given. Orthophotos are available for the Venoge River and their importance is discussed concerning channel planform and erosion measurement. LIDAR (LIght Detection And Ranging) topographic data was obtained for the Lower Venoge River and its comparison with and integration with surveyed topographic points is expounded on. The interpolation of cross section data poses a significant problem for the topographic description of banks. Methods are developed to improve conventional interpolation. The methods used for gathering information on bed and bank sediment information are also described. The calculation of boundary conditions (flow depth

and sediment input) finish this chapter.

Although infrequent in hydraulic studies, a detailed hydrologic analysis was performed and is reported in Chapter 5. It is well known that the sequence of flood hydrographs is very important to streambed fluctuations and streambank erosion. A continuous hydrologic model, HydroRoute, is used to generate the important tributary hydrographs. This chapter presents in the case of the Venoge how data can be spatialized and how this spatialization permits the variability of tributary discharges and consequently the tributary sediment input. By generating low probability floods and combining them with the historical discharge series, three 300 year discharge series are constructed for the hydraulic simulations.

Chapter 6 describes the detailed streambank erosion modeling done with the model CCHE1D. The model setup and preparation are explained. The calibration of the model as well as the simulation of bank erosion and sediment transport with the historical discharges from 1979-2005 is accomplished. Bank mechanical strength tests were done and are compared to the calibrated bank parameters to determine the utility of those tests. Simulated and measured event erosion are examined to examine the capability of the model to reproduce event erosion. A program to permit the frequency analysis of the bank failures is developed and its use with the simulation results is illustrated. The results are mapped to produce a streambank erosion danger map. Finally, a hypothetical test is performed to investigate a possible improvement to the shear stress formulas and to analyze the sensitivity of the model to planform digitization.

These chapters lead to the final conclusions of this dissertation and also to a section dedicated to the numerous ideas generated by this thesis for future research.

Chapter 2

Streambank Erosion Hazard Assessment and Mapping Methodology

2.1 Introduction

The simulation of streambank erosion has until present eluded commercial software packages. This is not because of its insignificance, but rather because of the complexity of the processes involved. This chapter will serve to review the processes involved in streambank erosion. Secondly, it will briefly describe different type of models used in research today. Thirdly, the methodology chosen for the assessment of streambank erosion hazards of single-threaded, subcritical flow streams is elaborated.

2.2 Streambank erosion processes

Streambank erosion is best referred to as streambank retreat. Bank retreat refers to the combined processes of bank erosion and bank mass failure. Bank erosion, simply put, occurs when the shear strength of sediment is overcome by the boundary shear stress exerted by the streamflow. Bank mass failure occurs when a large mass of bank collapses because the bank soil strength can no longer resist the bank weight and is often provoked by bank steepening or heightening by bank erosion or bed scour, respectively. Bed scour can play a significant role and this necessitates the understanding of sediment transport. Catchment and climate configuration produces the water and sediment discharges and the channel morphology that in turn produce the boundary shear stresses. The reviewed processes below then will be structured according to these main themes: catchment, fluvial, and bank processes.

2.2.1 Catchment processes

Schumm's (2005) diagram (figure 2.1) describes quite well the catchment processes that dictate river type and reach variability which in turn will dictate the streambank erosion potential of a reach. Thorne (1997) describes channel form as depending on the driving variables of water and sediment inflow and boundary characteristics of valley slope and topography, bed and bank materials, and riparian vegetation. These two conceptualizations of catchment processes are represented in figure 2.1.

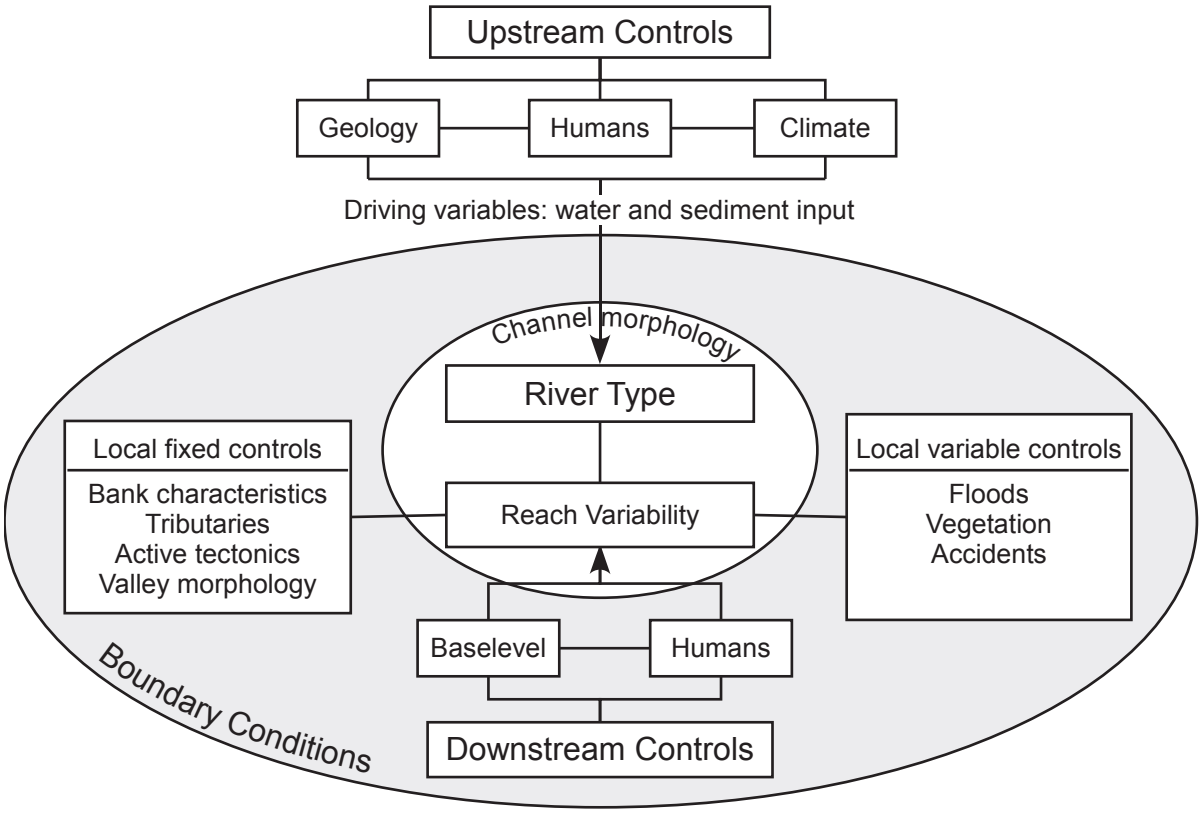

Figure 2.1. Controls of river morphology and behavior (after Schumm, 2005)

Upstream controls include geology, climate, and humans. These controls interact and produce numerous river types. Schumm (2005) also includes history and subdivides geology into tectonics and lithology. History is not included in figure 2.1 because time evolution is, in the author's opinion, a significant part of each of the upstream controls. Tectonics and the geological formation is responsible for the catchment relief and lithology. Uplift or subsidence due to plate activity or isostatic adjustment continues to change the relief of the earth although at very long time scales. The geological formation of a catchment is often dependant on many systems: weathering, slope mass movement, river, groundwater, glacier, and eolian systems. These systems are products of the upstream controls of geology and climate. Weathering is produced by the interaction of geology and climate. Physical and chemical breakdown of the catchment rock will be dependant on the climate. Slope mass movement also is a result of climate and geological controls. A more pronounced catchment relief in friable soil and rock will promote a high downslope mass movement. Climate plays a very important part in downslope movement due to soil saturation or by freezing and thawing. Earthquake activity can also be significant in downslope mass movement. River systems are extremely important in relief development by their sediment erosion and deposition.

River systems can be divided into three systems: collection (sediment source), transport (transfer), and dispersal (sediment sink) (Hamblin and Christiansen, 1998). Over geological periods, these three systems can significantly form a relief. Groundwater systems are intricately related to river systems. They can also be determinant in forming relief by dissolution of bedrock. This is especially the case of sinkholes in karst topography. Glacier systems are extremely effective in their eroding and depositing action. During the last Ice Age, much of the world's drainage systems were largely modified by the Pleistocene glaciers. Wind is also responsible for sediment erosion, transport, and deposition, although Eolian systems are the least effective in landscape transformation.

Besides the significant historical effect of climate on the geological formation of a catchment, it is of course responsible in connection with the catchment relief for the present hydrological regime of the catchment. Climate of course produces the precipitation events which dictate the subsurface moisture conditions and produce the stream discharge events. Connected with the subsurface moisture conditions, slope mass movement provides sediment input into the drainage network.

Schumm (2005) includes humans also as an upstream control and rightfully so. Graf (2001, in Schumm, 2005) estimated that 79 percent of American rivers have been influenced by humans. Dams and reservoirs, interbasin diversions, irrigation, channelization, levees, and mining are the most common human disturbances to natural catchment processes.

Local controls, fixed and variable, create reach variability. Local fixed controls are those that are geographically fixed. Schumm (2005) lists bedrock, tributaries, active tectonics, and valley morphology as fixed local controls. Bedrock and resistant alluvium will resist channel erosion. This can maintain longitudinal profile convexities or cause irregular meander development. Clay plugs resulting from meander chutes or cutoffs are known for their ability to resist meander migration. Tributaries offer their water and sediment to the main river which in the case of small tributaries may only have slight repercussions, but in the case of large tributaries could cause a complete regime change or significant changes in longitudinal slope, sinuosity, and channel width downstream from the tributary. Active tectonics can also cause changes to the valley floor. Subsidence due to petroleum or groundwater also effects the valley floor and is called pseudotectonics by Schumm (2005). Valley morphology provides the convexities and concavities in the longitudinal profile that are critical to channel form and sediment transport.

Variable local controls are those that are variable in space and time according to Schumm (2005). He lists floods, vegetation, and accidents in that category. Including floods could be questionable in that the upstream controls produces the sediment and water input into the drainage network, but floods can have significant sediment transport that can vary from flood to flood. In this respect, it is reasonable to include it as a reach variability control. It is strongly connected to the accident control. Accidents are unanticipated events such as log jams, ice jams, and natural dams produced by earthquakes and landslides. The significant, usually temporal, change in channel discharge and sediment discharge can cause significant channel changes that can take a long time to reestablish. It is well known that vegetation influences significantly channel width. Hey and Thorne (1986) determined hydraulic geometry relations that showed that the width of the channel increases with increasing bank vegetation density. Recently, though, Hession et al. (2003) showed that channel width was greater for forested riparian zones than

grassy ones. Abernethy and Rutherfurd (1998) indicated that the effectiveness of vegetation on width control depends on the location of the reach, whether it be upstream, middle, or downstream.

Downstream controls are that of base level and humans (Piégay and Schumm, 2003). Base level is the lowest point to which a river flows. It is sea level for large rivers, but for smaller rivers could a large lake or a resistant bedrock. Humans can influence the baselevel by river damming. River damming creates an artificial baselevel for the river upstream and creates an upstream control for the river downstream.

Besides looking only at the driving and boundary conditions that will dictate the channel form, long profile, and planform, it is convenient to look at catchment processes in terms of the three river systems mentioned above: sediment source, transfer, and sediment sink zones. It is fundamental in sediment transport studies to identify the type of the river system. Sediment source zones are usually supply limited. Mountainous and hilly headward zones are usually sediment source zones. Bed movement can be significant in these zones due to the limited sediment supply and sediment bursts caused by slope failures. Transfer zones are zones in which the sediment transport is in balance. Erosion can occur in these zones, but deposition will keep up with the erosion. Sediment sink zones are transport limited. The streamflow does not have a sufficient transport capacity to carry all of the sediment. Alluvial fans and deltas are the most flagrant sediment sink zones.

2.2.2 Fluvial processes

Natural river flows are extremely complex. Hydraulic research has not yet unraveled the physical laws that can completely describe river flow. It is beyond the context of this thesis to fully describe what is known about the physical laws that govern them, but a brief description will be given here to describe the important fluvial processes acting in streambank retreat.

All river flows, whether it be in straight or bending flow, have secondary flows. These secondary flows are more pronounced in river bends. Secondary flows can be stress induced (anistropic turbulence) or skew induced (streamwise curvature) (ASCE, 1998a). Stress induced secondary flows are the reason for their existence in straight sections, while secondary flows in bends are mostly skew induced. These strong bend secondary flows are represented in figure 2.2 by the well known helical flow motion in bends. This flow motion results from the centrifugal force on the water elements in the bend. Those forces are higher at the surface. They cause the superelevation that is observed in bends. Superelevation causes a greater pressure on the flow in the outer bottom. This difference of pressure results in a bottom flow from the outer bank towards the inner bank. These two lateral flows are superimposed on the streamwise flow to create the helical flow pattern. Blanckaert and Graf (2001) call this helical motion the center-region cell. As can be seen in figure 2.2, an outer region cell exists. Blanckaert and Graf (2001) suggest that the outer-bank cell protects the outer bank from the high velocities of the center-region cell and reduces the turbulent activity. Boundary shear stress is often expressed by mean values, but that shear stress varies around the mean. These variations are caused by turbulent bursts: sweeps and ejections. Those bursts have been found to be extremely energetic by Franca (2005). Including equations to represent those bursts to better characterize the instantaneous boundary shear stress is not yet feasible for practical engineering application (ASCE, 1998a).

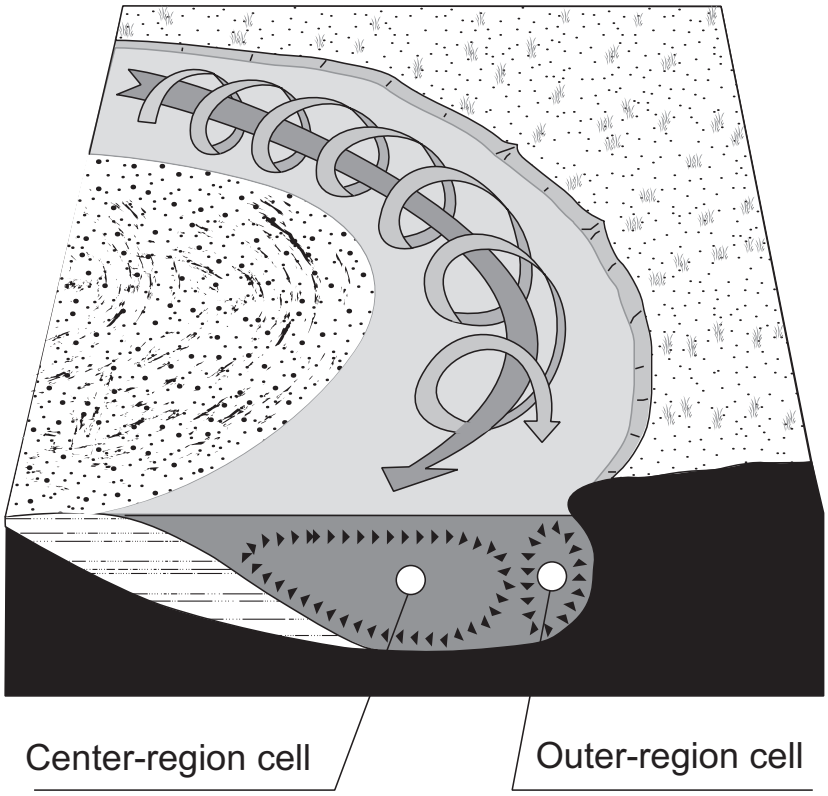

Figure 2.2. Helical flow motion in channel bends (adapted from Hamblin and Christiansen, 1998)

The Navier-Stokes equations are classically used to represent open channel flow. The most well known form of these equations is the Saint-Venant equations for 1-D open channel flow (e.g. Cunge et al., 1980). The Saint-Venant Exner equations include sediment transport with the hydrodynamic flow. These equations use the momentum and continuity equations of the Saint-Venant equations and a continuity equation for solid transport, leaving the energy slope and sediment discharge to be computed by empirical formulas (Graf and Altinakar, 2002). As in the Saint-Venant equations, a resistance law, such as that of Manning, must be used to determine the energy slope.

Sediment transport is initiated by the boundary shear stress that overcomes the critical shear stress of the sediment. Boundary shear stress, τ_o, can be estimated by:

$$\tau_o = \rho g R_h S \qquad \textit{Eq. 2.1}$$

where ρ is the density of water, g is gravity, R_h is the hydraulic radius and S is the energy slope. Other variations of equation 2.1 exist (ASCE, 1998a) such as the one that replaces R_h with water depth. Critical shear stress, τ_c, is often based on Shield's work (1936) and the well known Shield's diagram. It can be estimated by:

$$\tau_c = \theta_c g(\rho_s - \rho)D \qquad \textit{Eq. 2.2}$$

where θ_c is the critical dimensionless shear stress known as Shield's value, ρ_s is the density of the grain, and D is the grain diameter. On hydraulically rough beds, θ_c ranges from 0.03 to 0.06 and is usually taken to be around 0.45 which is less than the original Shield's value of 0.06 (Knighton, 1998). The varying range of Shield's value is partially due to grain shape and packing. For cohesive sediments, there is no

unique critical shear stress. This results from the electrochemical binding of the soil particles and the fact that erosion occurs by aggregate movement and not by particle movement.

Sediment transport modeling often relies on sediment transport capacity equations. The Smart and Jaeggi formula is often used in Switzerland due to its reported validity domain of (0.04 to 20% slopes) (Smart, 1984) and is given by the following formula:

$$\phi = 4\left(\frac{d_{90}}{d_{30}}\right)^{0.2} S^{0.6} C\theta^{0.5}(\theta - \theta_c) \qquad \textit{Eq. 2.3}$$

where ϕ is the dimensionless sediment transport ($q_b/[g(s\text{-}1)d^3]^{0.5}$, in which q_b is the volumetric sediment discharge per unit channel width, d is the mean grain diameter, and s is the specific weight of sediment, and d_{90} and d_{30} are the grain diameters for which 90% and 30% weight, respectively, of a nonuniform sample is finer, S is the bed slope, C is a flow resistance factor, and θ is the dimensionless shear stress. More detailed developments on sediment transport equations can be found in Graf and Altinakar (2002) and the implementation of other currently used formulas can be found in (Wu and Vieira, 2002).

Johannesson and Parker (1989) proposed a model that combined the flow field, bedload transport, and bed topography calculations. Their model is important because of the physical explanation given to bend pools and phase lag via the incorporation of a secondary flow parameter. A simplified equation for bend topography is given by

$$\sin\alpha = K\frac{h}{r} \qquad \textit{Eq. 2.4}$$

where K is a coefficient, h is local depth and r is the radius of curvature. After integration this formula becomes:

$$\frac{h}{h_0} = \left(\frac{r}{r_0}\right)^K \qquad \textit{Eq. 2.5}$$

where h_0 is the centerline water depth, *and* r_0 is the centerline radius of curvature. The value of K has been approximated as $7 \cdot \tan\phi$ by Engelund (1974, in Hersberger 2003) where ϕ is the dynamic shear angle. Bridge (1976, in Hersberger 2003) estimated that K is $11 \cdot \tan\phi$ with values of ϕ in the range of 0.32 to 0.75 and has proposed other estimates as well (Bridge, 2003).

In recent years, two and three dimensional models of flow and sediment transport have been developed. One recent example of the use of a 2D model based on the equations developed by Rodi (1993) for solving flow in curved bends is that of Wu and Wang (2004). They proposed a semi-empirical formula for the determination of the helical flow intensity. This allowed them to evaluate the dispersion terms of the depth-averaged 2D momentum equations and suspended-load transport equation. It also allowed them to evaluate the bedload transport angle. The quantification of the dispersion terms is very important for the representation of the secondary flow.

In spite of the advances in modeling 2D and 3D flows in curved channels, the variability of natural rivers poses many problems for modeling (ASCE, 1998a). Adequately representing the topography, roughness, and sediment variability is impossible for long reaches. Topographic variability occurs from the changing cross section and planform shapes. Roughness variability occurs due to the distribution of grain

sizes in the section, but also due to bed forms. Sediment variability occurs due to selective entrainment and fining processes.

2.2.3 Bank processes

Definitions of bank retreat terms, as defined by Lawler et al. (1997), are:

> "*Bank erosion*: detachment, entrainment and removal of bank material as individual grains or aggregates by fluvial and subaerial processes.
> *Bank failure*: collapse of all or part of the bank en masse, in response to geotechnical instability processes.
> *Bank retreat*: net linear recession of bank as a result of erosion and/or failure
> *Bank erodibility*: the ease with which bank material particles and aggregates can be detached, entrained and removed (normally by flow processes)."

As can be seen in these definitions, bank erosion should not be confused with bank failure and the two are combined in the term bank retreat. Channel cutoffs are also extremely important in terms of channel planform change, but since the modeling in this dissertation does not concern middle or long-term planform changes, it will not be dealt with.

2.2.3.1 Bank erosion

Fluvial

As is the case for the river bed, the force exerted by the boundary shear stress must overcome the resisting forces of the sediment as given by the critical shear stress. For non-cohesive soils, the critical shear can be determined by equation 2.2. This equation must be multiplied though by a coefficient, λ, that takes into account the additional instability caused by the bank slope. It was defined by Lane (1953) as:

$$\lambda = \cos\theta \sqrt{1 - \frac{\tan^2\theta}{\tan^2\phi}} \qquad \textit{Eq. 2.6}$$

where θ is the bank angle with the horizontal, and ϕ is the internal friction angle of repose of the bank material.

Fluvial erosion of cohesive materials is much more complicated. The ASCE Task Committee (1998a) indicates that in addition to the interparticle, electrochemical bonding that resist the driving forces, the soil structure due to its formation and soil moisture history influence a soil's critical shear stress. Although, critical shear strength testing (see section 4.6.1 for testing methods) must be undertaken to determine a soil's value, generally, it is higher for cohesive soils than non-cohesive soils, especially for higher clay content soils.

For cohesive banks, Arulanandan et al. (1980, in Osman and Thorne, 1988) developed a method for estimating lateral erosion. Their method consists of:

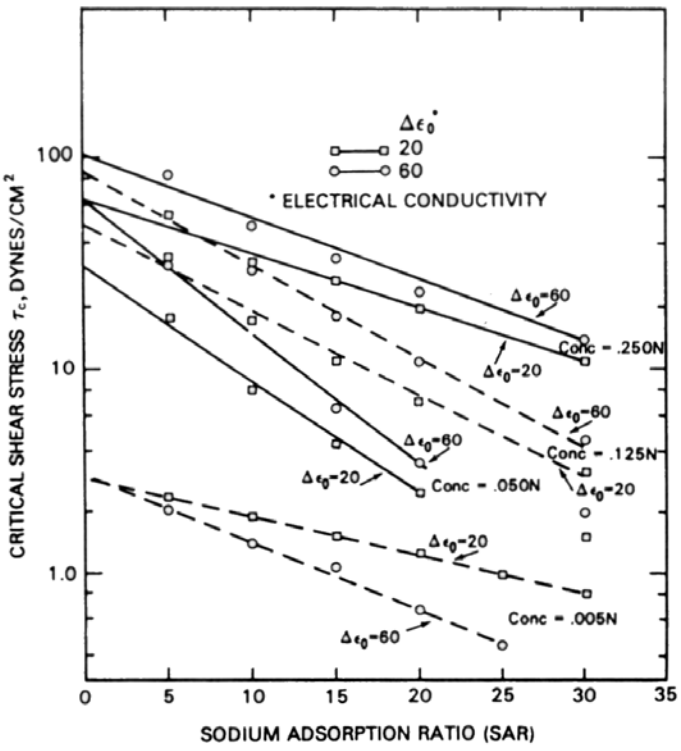

Figure 2.3. Critical shear stress as a function of SAR, soil salt concentration, and dielectric dispersion (from Osman and Thorne, 1988, after Arulanandan et al., 1980 and reprinted with permission from the American Society of Civil Engineers)

1.Estimating the shear stress.

2.Estimating the critical shear stress. This can be done by determining the sodium adsorption ratio (SAR), pore fluid salt concentration, and dielectric dispersion. With these values, the critical shear stress can be determined with figure 2.3.

3.An erosion rate, ε_r, can be determined by the formula,

$$\varepsilon_r = 223 \cdot 10^{-4} \tau_c e^{-0.13\tau_c} \quad \textit{Eq. 2.7}$$

where τ_c is the critical shear stress in dynes/cm², and ε_r is in g/(cm²•min).

4.A lateral erosion rate can then be determined by:

$$\frac{dW}{dt} = \frac{\varepsilon_r}{\gamma_s}\left(\frac{\tau - \tau_c}{\tau_c}\right) \quad \textit{Eq. 2.8}$$

where γ_s is the specific weight of the soil, and *dW/dt* is the lateral erosion rate for all τ greater than τ_c.

Subaerial

The effectiveness of subaerial processes in erosion is poorly known. What is sure is that, whether by actual erosion or by weakening of the soil structure, subaerial processes can be a significant factor in erosion. The most commonly cited subaerial processes are freeze-thaw and wetting-drying cycles. Couper (2003) exposed riverbank samples to repeated freeze-thaw and wetting-drying cycles in the laboratory and measured erosion. Due to the laboratory conditions, her work can not be used directly to estimate erosion from subaerial conditions, but she did confirm that banks with higher silt-clay content have a higher susceptibility to subaerial erosion. Compared to fluvial erosion, the role of subaerial erosion though is subsidiary (Knighton, 1998). It can be, though, the dominant process, especially in small drainage basins that do not produce enough shear stress to erode cohesive banks (Lawler et al., 1997).

Among freeze-thaw activity, ice needles are probably the most effective eroding agent. They can lift and incorporate bank material during their growth, thus weakening or eroding the bank (Lawler et al., 1997). Wetting-drying cycles can produce swelling and shrinking that induce cracks which will increase bank erodibility (ASCE, 1998a).

Vegetation

Vegetation, generally, reduces bank erosion. This is largely due to (ASCE, 1998a): root systems that physically retain soil particles, the reduction of near-bank velocities, and the dampening of peak

turbulence to reduce shear stresses. Erosion of well vegetated banks is reduced by one to two orders of magnitude as reported by the ASCE Task Committee (1998a) according to many studies.

Seepage

Within fluvial processes, erosion by the main river current is the most frequent eroding agent, but water within the bank can also be responsible through seepage (ASCE, 1998a). Strong seepage often occurs in stratified banks in layers of higher permeability. If this seepage is strong enough, it can entrain soil particles. This process is called piping. After significant piping, mass wasting (failure) of the upper bank soil is likely to occur.

2.2.3.2 Bank failure

Bank mass failure occurs when the driving gravitational force overcomes the resisting force provided by soil friction and cohesion, and by root reinforcement. Bed scour and/or bank toe erosion often causes bank instability. Different bank failure modes exist depending on bank soil, stratification, height, and vegetation conditions (figure 2.4). These bank failure modes are difficult to clearly observe in nature because of the combination of bank weakening effects and fluvial scour (Thorne, 1982).

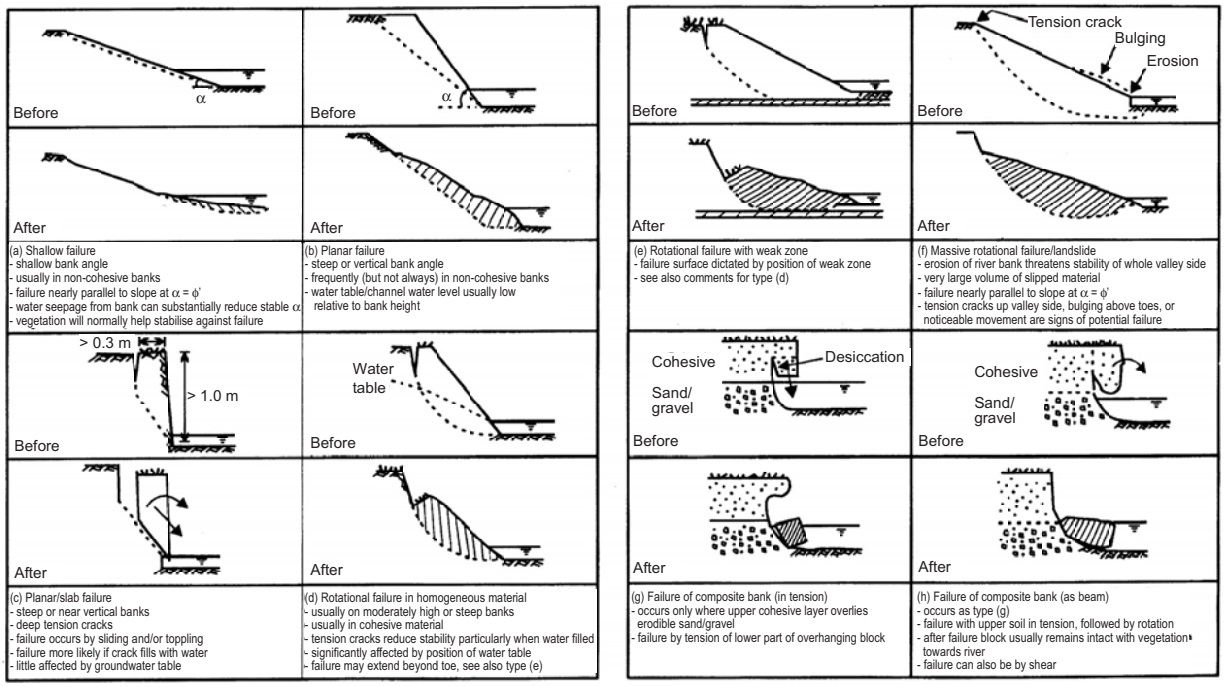

Figure 2.4. Modes of bank mass failure (from Hey et al., 1991, in Lawler et al., 1997)

Mass failure is significantly different for cohesive and non-cohesive soils. Failures will be shallow for non-cohesive banks (figure 2.4 a, b), while those in cohesive banks can be deep. This is mainly due to the fact that shear stress increases less quickly than shear strength, while in cohesive banks it is the opposite, promoting deeper failures (Terzaghi et al., 1996). The non-cohesive failure shown in figure 2.4 (a) occurs by the dislodgement and/or avalanching of the sand or gravel particles. It is often induced by toe erosion. Planar failure as shown in figure 2.3 (b) can occur in non-cohesive and cohesive soils. Planar

and planar/slab failures (figure 2.4 b and c) are very common for steep bank slopes. In medium to high bank slopes, rotational slips have been observed to occur (figure 2.4 d, e, f). These rotational slips have a curved base which depends on the bank stratigraphy (especially weak layers) and this failure surface can pass through the bank slope, toe, or below it. Tension failures in overhanging/cantilevered banks are also very common. This often occurs in stratified banks. This stratification can occur because of a composite bank soil configuration as in figure 2.4 (g) and (h), but can also occur simply by a root reinforcement of the upper soil layer.

Stability analysis for the various modes of bank failure exist, although planar failure is the stability analysis that has been most commonly implemented into streambank erosion models described in literature. Rotational slip failures are at the crossroad between landslide hazard assessment and streambank erosion hazard assessment. The multiple factors (see Hutchinson, 1995 for a listing of those factors) involved in deep seated rotational slip failures precludes their analysis within a long river reach streambank erosion hazard analysis. The detailed lithographic information needed as well as the hydrogeologic and geotechnical modeling necessary are net yet feasible within a streambank erosion hazard model. Optimally, regional streambank erosion hazard mapping or regional landslide hazard mapping should detect potentially unstable slopes along rivers. These slopes should then be analyzed by geotechnical means, more or less sophisticated, depending on the risk involved. Overhang tension failure analysis formulas exist (Thorne and Tovey, 1981, Langendoen, 2000), but have not been implemented in streambank erosion hazard models. The hydraulic analysis of such complex cross sections is usually not incorporated in hydraulic models.

Since planar failure analysis is common for low to medium cohesive steep streambanks, and will be used in the modeling within this thesis, planar failure analysis will be described in more detail here. For steep cliffs in brittle granular soils exhibiting tension cracking, slips are planar requiring an analysis such as the Culmann wedge analysis (Selby, 1993). This analysis determines the factor of safety, F_s, as the resisting force, F_r, divided by the driving force, F_d (figure 2.5). The bank is considered stable if F_s is greater than 1. The weight of the failure block, W_t, is the driving force, given by:

$$F_d = W_t \sin\beta = \frac{\gamma_s}{2}\left(\frac{H^2 - y_d}{\tan\beta} - \frac{H'^2}{\tan\alpha}\right)\sin\beta \qquad \textit{Eq. 2.9}$$

where β is the failure plane angle, γ_s is the unit weight of the soil, H is the bank height, y_d is the tension crack depth, H' is the non-eroded bank height, and α is the bank slope. The resisting force is derived from a shear strength equation. The importance of taking into consideration saturated or unsaturated conditions has been demonstrated by many authors (Simon et al., 2000 for example) and thus the appropriate resisting force equation is:

$$F_r = Lc' + N\tan\phi' + \psi L\tan\phi^b \qquad \textit{Eq. 2.10}$$

where L is the length of the resisting plane, c' is the effective cohesion, N is the normal stress due to the weight of the soil block, ϕ' is the effective friction angle, ψ is the matric suction, and ϕ^b is the increase in shear strength associated with an increase in matric suction. The length of the resisting plane can be found to be $(H-y_d)/\sin\beta$ and $N = W_t\cos\beta$. Matric suction can be estimated as the negative pore water pressure by $\gamma(z_s-z_g)$ where z_s is the elevation of the soil and z_g is the elevation of the groundwater table

assuming hydrostatic pore water pressure distribution. The matric suction can be negative in the case of a high water table representing the case of high pore water pressure. Groundwater modeling is possible but has not been incorporated into present-day streambank erosion hazard models. Usually, the groundwater table is assumed to be the same as the water level in the river. Simon et al. (2000) note that "the value of ϕ^b is generally between 10° and 20° and increases with the degree of saturation". They evaluated its value with linear regression after having determined the apparent cohesion, c_a, which is $c'+\psi tan\phi^b$, by in situ shear strength testing. The failure plane angle and the tension crack depth must still be determined for the application of equation 2.10. Failure plane angle, β, can be determined by the formulation of Osman and Thorne (1988):

$$\beta = 0.5\left\{ \text{atan}\left[\left(\frac{H}{H'}\right)^2\left(1-\left(\frac{y_d}{H}\right)^2\right)\tan\alpha\right] + \phi \right\} \qquad \textit{Eq. 2.11}$$

This equation uses the hypothesis that the most dangerous failure angle occurs when the developed cohesion is maximum, which is criticized by Langendoen (2000). He implemented a search algorithm to search for the failure plane which minimizes the factor of safety, F_s. Maximum tension cracking depth, y_d, is not well known. It has been estimated by Taylor (1948) as:

$$y_d = \frac{2c'}{\gamma}\tan\left(45+\frac{\phi}{2}\right) \qquad \textit{Eq. 2.12}$$

Darby and Thorne (1994) reported improvements in the determination of the crack depth with their new formula, but it uses the tensile shear strength of the soil which is difficult to determine and to which they partly attribute the mediocre results of their calculated tension crack locations compared to observed ones.

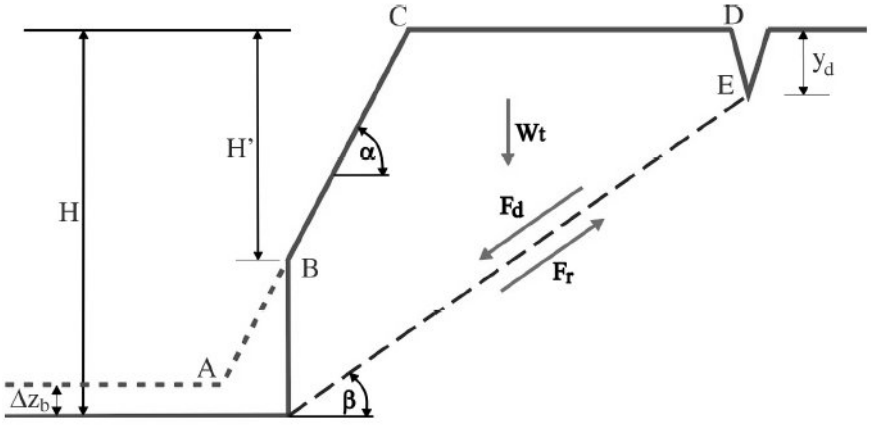

Figure 2.5. Planar failure analysis (from Wu and Vieira, 2002 after Osman and Thorne, 1988)

Vegetation effects

The effect of vegetation on bank failures is poorly known. It has both positive and negative effects according to the ASCE task committee (1998a) on river width adjustment. They listed the positive effects as:

1. an increase in shear strength due to the tensile shear strength of root systems for low banks in which the vegetation root systems cross the shear failure plane
2. a decrease in soil moisture levels due to canopy interception and increased evapotranspiration
3. buttressing or abutment of slopes

and the negative effects as:

1. a weight surcharge
2. wind loading of the vegetation that can cause a significant destabilizing moment
3. wedging and prying in soil cracks and fissures to decrease soil strength.

Basal endpoint control

Mass failures come to rest at the base of the bank and are known as basal sediments. The rate of entrainment by streamflow of these sediments will determine the medium and long term retreat rate of a bank and will determine the frequency of bank failures. Thorne (1982) described the three states of basal endpoint control as follows:

1. Impeded removal: Basal accumulation is important and the rate of entrainment is slow. Bed elevation will increase to promote lower banks resulting in lower bank supply rates to promote progression towards the second state.
2. Unimpeded removal: Bank supply rates are in balance with the entrainment rates. The bed level remains stable.
3. Excess basal capacity: Fluvial entrainment is rapid, promoting frequent bank failures. Bed lowering will result until the bank height is significant enough to supply greater volumes of bank material. The rate of supply will increase promoting a progression to the second state.

These three states could be associated with stream reaches that are aggrading, in dynamic equilibrium, and degrading, respectively.

Wood et al. (2001) showed that failed soil blocks that come to rest at the base of the bank develop cohesion with the substrate to aid in their resistance to fluvial entrainment. This means that large failed blocks will have to be eroded particle by particle until they become small enough for the streamflow to able to entrain the entire cohesive aggregate.

Sections 2.2.2 and 2.2.3 summarize the fluvial processes and bank processes responsible for bank retreat. More details, especially on bank processes, can be found in Thorne (1982), Lawler et al. (1997), and ASCE (1998a). The book section by Thorne (1982) is particularly interesting because of the field observations enumerated.

2.3 Streambank erosion assessment models

This section will serve to briefly review the state of the art in streambank erosion modeling. This has largely been done already by the ASCE Task Committee (1998b) on river width adjustment, especially

on numerical modeling, but additions to the models they present will be shown here to emphasize models that can be practically put into use for streambank erosion hazard mapping. The Federal Emergency Management Agency (FEMA, 1999) has also produced a guide on "Riverine Erosion Hazard Areas". Their document describes geomorphological, engineering, and mathematical models. Although, this document claims riverine erosion hazard mapping to be feasible, it shows that mathematical modeling has rarely been used to calculate riverine erosion hazards and the document is vague about the analyses involved in geomorphological and engineering analysis. In general, geomorphological analysis is described as the qualitative and sometimes quantitative understanding of the discharge and sediment movements in the river reach of interest based on field observations and the use of historical information. Most studies have used orthophotos to calculate mean erosion rates (see chapter 4.3 for details on use of remotely sensed data). Engineering analysis usually draws on geomorphological analysis and goes beyond it by quantifying discharge, sediment discharge and bank retreat with empirical formulas. This section will present conceptual models and engineering analysis as well as geofluvial models. "Geofluvial" refers to models that couple flow and sediment-routing models and treat bankline adjustments mechanistically (ASCE, 1998b).

It must be remembered that the goal of the modeling will be to calculate the streambank erosion hazard. This hazard as defined by the Swiss Federal Office for Water and Geology (Loat and Petrscheck, 1997) is the combination of the probability of occurrence and intensity. In terms of streambank erosion, this is interpreted to be the intensity of a bank failure (figure 2.6), given in meters, and its probability. If the guidelines of the FOWG are strictly followed, the erosion intensity is determined by the distance of the erosion perpendicular to the bank face, or in the case of a channel change, the depth of the newly eroded channel. This distance is not very meaningful, though, and it makes more sense to consider it to be the bank failure width, the distance between the original bank top and the bank top after failure, at least in the case of non-braided rivers.

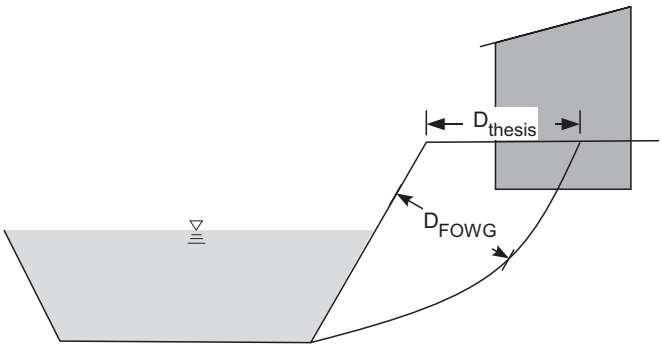

Figure 2.6. Erosion intensity, given as D (m), according to the Swiss FOWG guidelines

2.3.1 Engineering analysis and conceptual modeling

Richardson meander bend migration rate model (Richardson, 2002)

This model uses results issued from a 1D hydraulic model such as HEC-RAS. Average bottom shear stress from the 1D results is corrected according to planform geometry to produce an estimation of the outer bank shear stress. The average shear stress and outer bank shear stress are then used in sediment transport relations. The difference in the average sediment transport and the outer bank sediment transport is assumed to come from bank erosion. Then based on bank height, a bank erosion rate is calculated. Richardson calibrated the sediment transport relations according to measured bedload and was able to verify the bank erosion rates against historical data. This model is intended as a preliminary

assessment for determining bend migration rates. The model is limited at present because channel curvature and slope are not incorporated into the 1D hydraulic model and thus channel curvature and slope have to be updated periodically after non-negligible changes have occurred due to migration.

This model obviously makes the assumption that the river bed is stable and that deposition at bend inner banks keeps up with outer bank erosion. This model does not take into account the effect of the resistance of the bank material via an excess shear stress erosion equation, as in equation 2.8, and does not use bank instability relations to determine failure widths. A relationship between bend migration rate and the probability and widths of bend failures would have to be determined to use this model.

Rosgen streambank erosion potential method (Rosgen and Silvey, 1996)

Rosgen is well known for his stream classification system that has been widely applied. In his book that describes stream classification (Rosgen and Silvey, 1996), he also has presented a streambank erosion potential method. He proposes the calculation of bank erosion potential by ranking five different criteria from 1 to 10 and summing the ranks to determine a bank erosion hazard index (BEHI). Those criteria are: the ratio of bank height to bankfull water depth, the ratio of rooting depth to bank height, the root density, the bank angle, and the surface protection. The sum of the ranks of the five categories are also increased or decreased depending on the bank composition and stratigraphy. The BEHI must be compared to the near bank shear stress index (NBS) to find an erosion rate. The NBS is the ratio of the near bank shear stress to the average bed shear stress. A linear relationship can be sought for the relation of the erosion rate to the NBS for each BEHI category, preferably by calibration. From field observations, the BEHI for all banks within a reach can be determined and an erosion rate then calculated for each bank.

This model again calculates an erosion rate and not bank failure widths and probabilities, as in the Richardson model. It is also dependant on calibration.

Evaluation of potential instability in alluvial channels (Simon and Downs, 1995)

This method proposes site evaluations to characterize alluvial channel stability. For a state agency, it gives recommendations on the hydraulic, including bridges, geomorphological, and vegetative variables to be collected at a site evaluation for introduction into a state database. Enough site evaluations to characterize the rivers throughout the region must be planned. The site evaluation should include the status of channel evolution. Simon and Downs (1995) encourage the use of the Simon and Hupp (1986) channel evolution model (figure 2.7). Their model is important because of the characteristic forms and geobotanical evidence they suggest that characterize each stage of evolution, which can help the observer to correctly identify channels in evolution and stabilized channel systems. They suggest that the variables collected at site evaluations should be put into a Geographical Information System (GIS) and ranking of the variables in terms of channel instability be done. A sum of the ranks of the different variables can then be done to calculate a channel instability index. Such an index, in combination with the vulnerability of land-use, can be used to prioritize reaches for further investigation. Further investigation can then be based on numerical alluvial modeling, channel evolution models (figure 2.7), regime equations (discussed further in chapter 3.7.4), or empirical relations to predict future channel changes.

This method is essentially the geomorphological analysis that precedes engineering analysis and/or numerical modeling. Here again, the information in the geomorphological analysis alone is insufficient to calculate bank failure widths and their probability.

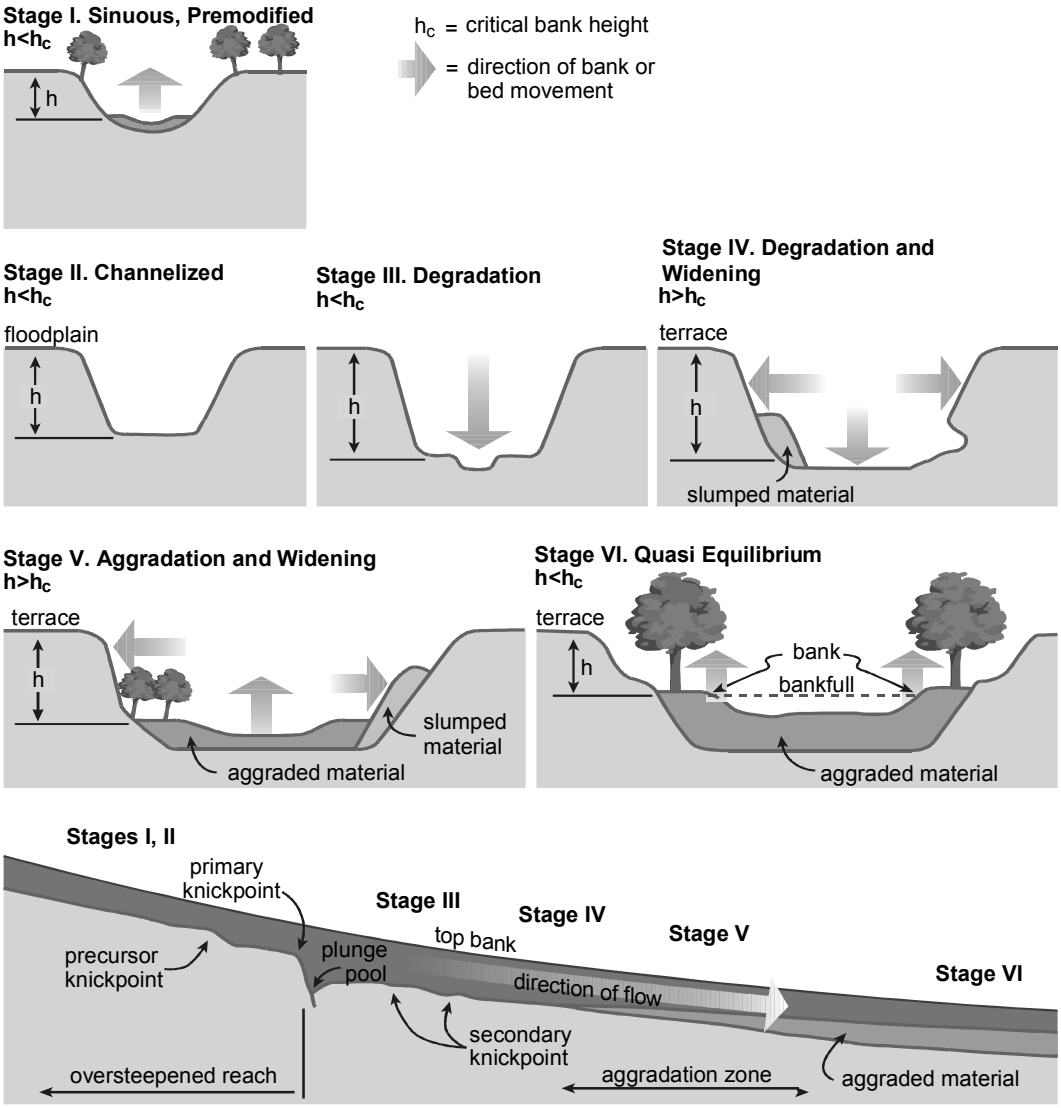

Figure 2.7. Channel evolution model (provided courtesy of Andrew Simon)

A GIS-based approach to mapping probabilities of river bank erosion (Winterbottom and Gilvear, 2000)

This method is quite attractive because it calculates the probability that a land cell adjacent to the river will retreat. The method was originally developed by Graf (1984). Winterbottom and Gilvear (2000) reused and adapted the method to study bank retreat on the regulated River Tummel, Scotland. The original method (Graf, 1984) specifies that the probability that the i-j cell, p_{ij}, will be eroded is:

$$p_{i,j} = f\left(d_l, d_u, \sum_{t=1}^{n} r\right) \qquad \text{Eq. 2.13}$$

where d_l is the lateral distance to the river, d_u is the upstream distance to the river, and r is the recurrence interval of the high flows (1 through n) during the period for which the probability is to be evaluated. In the case of a meandering stream, it would seem obvious that another variable should be present in equation 2.13, that of the presence of the cell on the exterior or interior of a river bend. Winterbottom and Gilvear (2000) recognized the other weakness of the Graf model: it must be applied to homogeneous banks. They added a variable in equation 2.13: er_c, which they called the erosion risk class. Based on observations, they classified the banks of their reach into five erosion risk classes. They also discarded the upstream distance to the river variable as it did not improve the probability calculation. Winterbottom and Gilvear (2000) then calibrated the following equating using historic discharge records and river channel changes:

$$\log_{10} p_{i,j} = \log_{10} a_0 + b_1 \log_{10} d_l + b_2 \log_{10} er_c + b_3 \left(\log_{10} \sum_{t=1}^{n} r \right) \qquad \text{Eq. 2.14}$$

where a_0, b_1, b_2, and b_3 are calibration coefficients.

This model makes many assumptions. The river needs to be in dynamic equilibrium for such a model to be applied. It should also be applied only to homogenous flow reaches. The recurrence interval variable could be improved in the author's opinion by considering the volume of water flow above a critical discharge during a period. This model deserves further exploration in the author's opinion as it is capable of producing a probability of bank retreat for a given flood or floods.

Howard and Knutson (1984) and Venoge river meandering models

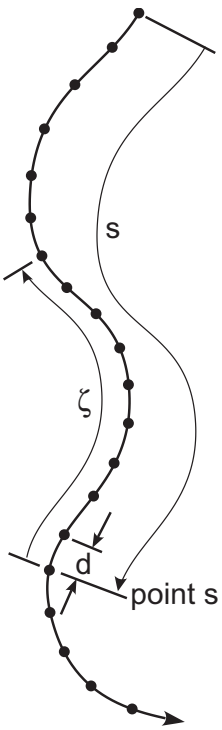

Figure 2.8. Channel centerline and distances used in upstream influence equations

Howard and Knutson's (1984) model was developed to explore conditions to explain river meandering. A first approximation of meander migration can be based on calibrated power law equations in which migration rate is a function of the ratio of the radius of curvature to the streamwidth, R_c/w, such as those of Hickin and Nanson (1975). They showed that lateral migration on the Beatton River tended to be greatest when R_c/w is approximately 2.9. Such a relationship, though, is insufficient to produce realistic meandering, as meanders translate not only laterally, but also downstream. Howard and Knutson (1984) suggest that the actual migration rate for a bend must be determined not only by the nominal migration rate, such as that of Hickin and Nanson (1975), but also by an upstream weighting of the nominal migration rates. They express this in the following equation:

$$R_1(s) = \Omega R_0(s) + \left[\Gamma \int_0^{\infty} R_0(s-\zeta) G(\zeta) d\zeta \right] \left[\int_0^{\infty} G(\zeta) d\zeta \right]^{-1} \qquad \text{Eq. 2.15}$$

where $R_1(s)$ and $R_0(s)$ are the adjusted and nominal migration rates, respectively, at the location s (measured downstream from the upstream starting point), $R_0(s\text{-}\zeta)$ is the nominal erosion rate at a

distance ζ upstream from *s*, Ω and Γ are weighting parameters, and $G(\zeta)$ is an upstream weighting function (c.f. figure 2.8 for distance definitions). The upstream weighting function can be expressed as an exponential decay equation:

$$G(\zeta) = e^{-\alpha\zeta} \qquad \textit{Eq. 2.16}$$

where α is the decay parameter. Using this form of weighting necessitates a value of Ω=-1 in equation 2.15. Howard and Knutson (1984) propose relationships to determine α and Γ, as functions of hydraulic parameters.

The Howard and Knutson model is limited by the fact that banks must be homogenous if the same migration rate function is to be used throughout the channel network and the flow must also be homogenous if the same values of α and Γ are to be used throughout the channel network, and that erosion rates are determined rather than bank failure widths and their probabilities.

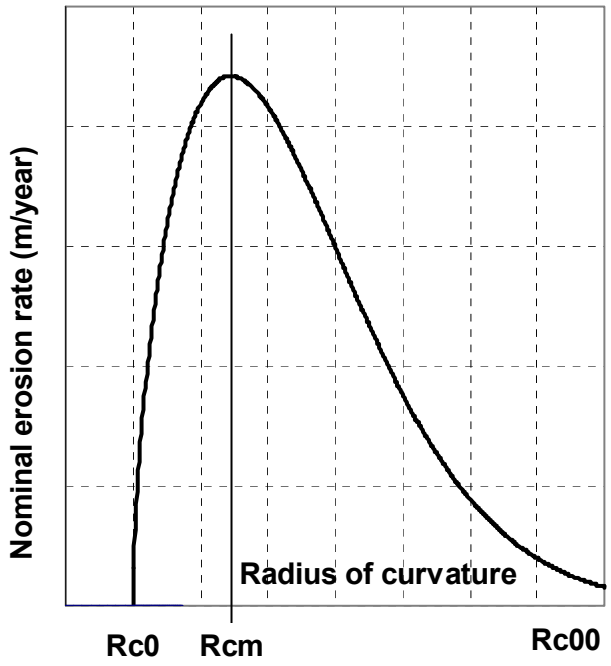

Figure 2.9. Nominal erosion rate as a function of radius of curvature (adapted from Consuegra et al., 1999)

The Venoge model (Consuegra et al., 1999) developed further Howard and Knutson's model. Rather than using two power functions as did Hickin and Nanson (1975), it is possible to approximate a bend migration rate function with a gamma type function as follows (Consuegra et al., 1999):

$$R_0(s) = k_1 X(s)^{(b-1)} e^{-k_2 X(s)^b} \qquad \textit{Eq. 2.17}$$

where X(s) is defined as $R_c(s)$-$R_{c0}(s)$, $R_c(s)$ is the radius of curvature in meters at point *s*, $R_{c0}(s)$ is the radius of curvature for which no erosion occurs at point s, and k_1, k_2, and *b* are parameters that define the shape of the function as shown in figure 2.9. If the variation of R_0 between point *s* and its upstream point is assumed to be linear, an analytical solution can be found for the integral in the numerator of equation 2.15:

$$\int_0^s R_0(s-\zeta)G(\zeta)d\zeta = \int_0^d (a\zeta + c)e^{-\alpha\zeta}d\zeta + e^{-\alpha d}\int_d^s R_0(s-\zeta)e^{-\alpha\zeta}(d\zeta) \qquad \textit{Eq. 2.18}$$

where *s* is the distance to the upstream starting point, *d* is the distance to the point just upstream from the point *s* (c.f. figure 2.8) , and *a* and *c* are the coefficients determined by a linear regression between the

values of $R_0(s)$ and $R_0(s\text{-}d)$. The spacing of channel points should be such that the linear regression estimation is acceptable. The first term of the right hand side can be determined analytically as:

$$\int_0^d (a\zeta + c)e^{-\alpha\zeta}d\zeta = \frac{-e^{-\alpha\zeta}}{\alpha}\left(a\zeta + \frac{a}{\alpha} + c\right)\Bigg|_0^d \qquad \textit{Eq. 2.19}$$

This equation allows the influence of the erosion at the point upstream from s to be calculated. Equation 2.18 recovers the influence of all other upstream points and diminishes their influence according to the distance between point s and its upstream point and then combines it with the result of equation 2.19. Equation 2.18 is important computationally as it eliminates the need to calculate the complete integral from 0 to s at each channel point. Equations 2.18 and 2.19 were determined in the framework of the Venoge modeling (Consuegra et al., 1999). Furbish (1991) treated the convolution of dimensionless curvature integral of Parker and Andrews (1986) in a similar way as expressed in equation 2.18.

The Venoge model (Consuegra et al., 1999) also considers meander cutoffs by calculating a cutoff distance, dc_s, expressed as:

$$dc_s = k_3 W \frac{d(s)}{max[d(s)]} \qquad \textit{Eq. 2.20}$$

where k_3 is another calibration parameter, W is the average river width, and $d(s)$ is the channel displacement at point s. The ratio of $d(s)$/max[$d(s)$] weights the current river displacement as compared to the maximum displacement. This allows the meander cutoff distance to be greatest when the meander is actively progressing. If dc_s intersects the downstream channel, a cutoff occurs and the channel computational nodes are changed accordingly.

Consuegra et al. (1999) also attempted to resolve the problem of associating meander bend migration rates to event migration rates. They hypothesized that a proportionality coefficient, k_{100}, could be multiplied against a mean meander migration rate to determine the migration distance due to a flood.

The Venoge model has 6 variables to calibrate: k_1, k_2, b, α, k_3, and k_{100}. These variables must be calibrated for each homogeneous bank area. Twelve homogeneous bank areas were determined in the Venoge study. The model needs to know the channel centerline (or thalweg) at different historical periods. Good topographic maps or orthophotos must be available and preferably at long time periods. Observations of bank failures must be at hand to give an appropriate value to k_{100} or orthophotos before and after a significant event must be available for its calibration.

This model has a significant number of variables to calculate and the calibration procedure becomes difficult if there are a wide variety of bank types. This model as in the other reviewed models assume that flow conditions do not change. This model has attempted to calculate a bank failure width for high flows. More work should be done to refine the formulation that translates meander migration rate into event migration rates.

Lancaster and Bras (2002) river meandering model

This research model conceptualizes the calculation of the near bank shear stress responsible for bank migration. A lateral force increment generated in meanders is calculated as a function of the mean depth,

mean downstream velocity and the changing bed topography. Mean depth and downstream velocity are based on continuity and Manning equations. Bed topography is estimated with a transverse bed slope that depends on bend curvature, friction, and the median bed particle size. The lag between the channel curvature and the secondary flow development, downstream lag (or phase lag) is estimated. The near bank shear stress is then calculated according to the lateral force increment, phase lag, bank height, and a dissipation length variable. They relate their dissipation length variable to the effect of bank roughness. They calculate bank migration then as a function of an erodibility coefficient and the near bank shear stress.

This model has not been applied to a real river case study with spatially varying data. It could be imagined though to use it in connection with a 1D model, such as proposed in the Richardson model above. The model also assumes a river in dynamic equilibrium such that mean flow conditions do not change with time. Here again bank migration is calculated and not bank failure distances.

Use of conceptual models for determining the probability of bank failure width

The above models conceptualize bank retreat and/or channel changes. The geomorphological analysis of the Simon and Downs method is a good starting point for determining channel instabilities. In combination with their model, a catchment geomorphological analysis should be done. In Switzerland, this catchment geomorphological analysis is called the phenomena map (Loat and Petrascheck, 1997). A phenomena map, or geomorphological map, will indicate sediment sources and localize erosion or aggradation problems (Kienholz and Krummenacher, 1995). This map in conjunction with a GIS database based on the Simon and Downs method will give the elements necessary to determine if a river reach is in dynamic equilibrium or if it is undergoing channel evolution. The other conceptual models can then be used to estimate bank migration in situations of dynamic equilibrium.

The Venoge model (Consuegra et al., 1999) is the only model that tried to estimate an event bank retreat. Their conceptualization of the event bank retreat should be further investigated. If the relationship between mean annual bank retreat can be better correlated with event bank retreat, this will allow a more widespread use of the above conceptual models to determine the probability of a bank failure width.

2.3.2 Geofluvial

With the incapacity of the above conceptual models to calculate bank failure widths and their probability, it is necessary to turn to fluvial and bank failure mechanistic models (geofluvial) models to try to make this calculation. The ASCE Task Committee (1998b) on river width adjustment reviewed twelve numerical river width adjustment models. Of those twelve models, four models incorporate fluvial entrainment and cohesive bank failures: Darby and Thorne ((1996) and Darby et al., 1996), RIPA (Mosselman, 1992 and Mosselman, 1998), STREAM2 (Borah and Bordoloi, 1989), and WIDTH (Osman, 1985 and Osman and Thorne, 1988). Since the writing of the ASCE review article, three other important models have been developed: CONCEPTS - Conservational Channel Evolution and Pollutant Transport System (Langendoen, 2000), CCHE1D (Wu and Vieira, 2002), and a modified version of RIPA (Darby et al., 2002), called RIPA2 here.

The difference between RIPA and RIPA2 is that the bank erosion and failure mechanisms of the Osman and Thorne (1988) model replace the previous bank erosion algorithms of RIPA.

The models CONCEPTS and CCHE1D are quite similar in their basic equations and algorithms. Both models are 1D unsteady models providing the possibility to simulate flows with the full dynamic equations or the diffusive wave approximation. Both models can handle the following hydraulic structures: bridge crossings, culverts, drop structures, and a generic structure based on a rating curve. None of the models in the ASCE (1998b) review implement hydraulic structures. Manning values as specified by the user provide flow resistance estimations in CONCEPTS and CCHE1D. These two models are 1D so secondary flow or lateral shear is not taken into account.

Sediment transport in CONCEPTS and CCHE1D is different due to some of the equations which are different. Both models treat the 1D non-equilibrium sediment transport of cohesionless beds, although CONCEPTS can also be applied to beds with cohesion. CONCEPTS uses 13 predefined classes for sediment transport and assigns an appropriate sediment transport capacity formula to each of the predefined classes. CCHE1D can have a variable number of sediment classes and the user can choose among the SEDTRA module, Wu, Wang, and Jia's formula, a modified Acker and White formula, or a modified Engelund and Hansen formula for the sediment transport capacity calculation. Both models treat suspended load and washload in combination with bedload. Both models employ mixing layer models so sorting in the 1D direction can occur.

Bank erosion and failure in CONCEPTS is more developed than it is in CCHE1D. Both models estimate fluvial entrainment based on excess critical shear and both models inject eroded sediment into the sediment continuity equation as a lateral input. Both models verify bank stability based on planar failure analysis. The CONCEPTS manner though is more sophisticated, though, in that pore-water pressure, and hydrostatic confining pressure are taken into account. CONCEPTS also searches for the failure plane that minimizes the factor of safety. CONCEPTS injects failed bank material into the sediment continuity equation immediately while CCHE1D uses a virtual reservoir to release these basal sediments at the rate of fluvial entrainment. As in all of the models in the ASCE review article, CONCEPTS and CCHE1D do not deposit on the inner bank and do not permit layered banks.

All of the geofluvial models mentioned above incorporate fluvial entrainment and planar failure analysis, although the planar failure analysis of CONCEPTS includes pore-water pressure and confining pressure, and can calculate a non-toe bank failure. The Darby-Thorne model and the WIDTH models are the only models to incorporate rotational failures. The chosen models only treat cohesive banks. No existing model treats both cohesive and non-cohesive banks. The only model that tries to explicitly treat the longitudinal extent of a bank failure is that of the Darby and Thorne (1996) model. Based on probability distribution functions of bank parameters, they calculate a probability of bank failure. When the probability of bank failure is greater than 0, they attribute a bank failure volume that corresponds to the calculated probability of failure and the reach length.

The comparison of the four ASCE reviewed models along with RIPA2, CONCEPTS and CCHE1D in terms of hydraulic flow and sediment transport capabilities is given in table 2.1.

Model	Planform	Dimension	Discharge variation	Secondary flow	Lateral shear	Friction factor	Flow resistance formula	Hydraulic structures
Darby and Thorne	straight	Quasi 2D	Stepped hydrograph	No	Yes	time and space variable	Strickler	No
RIPA	arbitrary single thread	2D	Stepped hydrograph	Yes	No	constant	Specified	No
RIPA2	arbitrary single thread	2D	Stepped hydrograph	Yes	No	constant	Specified	No
STREAM2	straight	1D	Stepped hydrograph	No	No	constant	Specified	No
WIDTH	straight	1D	Stepped hydrograph	No	No	time and space variable	Strickler	No
CCHE1D	straight	1D	Unsteady	No	No	constant	Strickler	Yes
CONCEPTS	straight	1D	Unsteady	No	No	constant	Strickler	Yes

Model	Dimension	Streamwise flux difference	Transverse flux difference	Bed load	Suspended load	Sorting	Bed material
Darby and Thorne	Quasi 2D	Yes	Yes	Yes	Yes	Yes	sand
RIPA	2D	Yes	Yes	Yes	No	No	sand and gravel
RIPA2	2D	Yes	Yes	Yes	No	No	sand and gravel
STREAM2	1D	Yes	No	Yes	Yes	Yes	sand and gravel
WIDTH	1D	Yes	No	Yes	Yes	No	sand and gravel
CCHE1D	1D	Yes	No	Yes	Yes	Yes	sand and gravel
CONCEPTS	1D	Yes	No	Yes	Yes	Yes	cohesive and non-cohesive

Model	Bank failure type	Pore-water	Non-toe failure	Lateral extent
Darby and Thorne	planar/curved	No	No	Yes
RIPA	planar	No	No	No
RIPA2	planar	No	No	No
STREAM2	planar	No	No	No
WIDTH	planar/curved	No	No	No
CCHE1D	planar	No	No	No
CONCEPTS	planar	Yes	Yes	No

Table 2.1. Comparison of geofluvial streambank erosion models capable of simulating cohesive bank erosion and failures (adapted from ASCE (1998b))

2.4 Proposed streambank erosion hazard methodology

Stream managers need to know what streambank failures might happen suddenly during a flood event and the channel migration that is likely to occur during the next 30-60 years. Flow conditions in natural streams are such that only in the simplest streams will channel migration models have a high success rate

of predicting the future channel planform. Channel migration models should output results in terms of the probability of a future channel placement. All uncertain parameters within a channel migration model should be varied according to their Probability Distribution Function (PDF), possibly in the framework of Monte-Carlo simulations, and the resulting channel planforms be used to calculate probabilistic future channel planforms. Knowledge of those PDF's is often poor, though, and sometimes important factors are not taken into account. For example, the influence of woody debris on channel migration is very significant, but this aspect has hardly been treated in channel migration studies. A tree that falls into a river causes small damming or important flow diversions. A fallen tree can also reduce near bank shear stresses and inhibit future channel migration. The effects of trees should also be incorporated into channel migration models in terms of the probability that a fallen tree will influence channel migration. Cutoffs are also extremely important for channel migration models.

Although knowledge of the future channel migration is beneficial, a truly probabilistic approach of producing future channel planform in natural streams for a period of 30-60 years should in most cases produce a wide variety of possible channel planforms. In this thesis, it is proposed to follow the logic of the Swiss Federal Office for Water and Geology and to estimate the probability of a given bank failure width to characterize the streambank erosion hazard (Loat and Petrasheck, 1997). Following this logic is also helpful to land-use management. This is because of the importance of knowing what bank failures could occur during a flood event so as to ensure significant setback of vulnerable objects. This logic of land-use management has been shown in the streambank erosion intervention map in figure 1.4. The problem, though, to follow this logic is that it is unknown how to calculate the probability of a given bank failure width. This is understandable because of the near bank flow conditions that change with time. Such non-stationarity makes it difficult to apply frequency analysis to bank failures to be able to produce a bank failure width probability. Darby and Thorne (1996) calculated the probability of failure of a bank considering only bank parameter uncertainty. Their probability is for a specific moment only and does not consider the entire possible flow conditions.

A methodology is proposed here for assessing and mapping the streambank erosion hazard for single-threaded streams with subcritical flow. This methodology will use the CCHE1D model, although adaptations to the model will be needed. A collaboration with the National Center for Computational Hydroscience and Engineering (NCCHE) was possible to adapt the CCHE1D model to the needs of this thesis. CONCEPTS was also considered for the modeling, but since the source code was not available for modifications, it was not chosen. The CCHE1D adaptations necessary for this thesis will be also be outlined.

2.4.1 Streambank erosion hazard assessment and mapping

1. Catchment geomorphological mapping (Kienholz and Krummenacher, 1995) is the starting point. A stream manager must understand the sediment and water flow through the stream reach. This will permit detection of reaches which are most likely aggrading, degrading, or in equilibrium. All locations where bank erosion or bed aggradation or degradation are observed are noted. Such observations help also to determine the type of bank erosion processes occurring. Historical maps and orthophotos are critical for understanding past channel migration. The geomorphological

mapping should be done in combination with the Simon and Downs (1995) channel instability method. Variables for evaluating a channel instability index should be decided upon for entry into a GIS. The results of geomorphological analysis and the channel instability index ranking can be used to draw up a preliminary streambank erosion hazard map that outlines the maximum expected channel movement during an extreme flood and potential unstable bank slopes.

2. Although geomorphological mapping is the recommended starting step, a possible regional model is outlined here. The idea behind such a method would be to run it to prioritize stream reaches for geomorphological mapping. The method would involve the characterization of the flow by stream power and bank resistance by available information as follows:
   - Stream power ($\Omega=\gamma QS$) or unit stream power ($\omega=\gamma QS/w$), where γ is the specific weight of water, Q is the discharge, S is the channel slope, and w is the channel width, can be used to characterize the flow condition of the river. It can be classified into three classes of high, medium, and low stream power. For important variations of stream power, which will probably reflect aggradational or degradational zones, the stream power rank could be increased to the next higher category to reflect the possible channel instability. Approximations for discharge exist for most rivers, or can be estimated by relationships that estimate discharge as a function of catchment area. The bankfull discharge, or the one or two year return period discharge, can be used. Slope and channel width can be estimated from an appropriately interpolated digital terrain model (DTM) (see chapter 4.4 for more details).
   - Bank resistance can be determined from available information. Minimally, bank height can be estimated from a high resolution DTM. If surface and terrain LIDAR elevation points are available, it is expected that the difference in point density along river banks can give an estimation of the vegetation density and consequently the root reinforcement of the banks that will resist fluvial erosion. Information on bank soils is rare. Geological information is more common though and if available, categories of stability could be assigned to the geological units that surround the stream. With the available bank information, a ranking system could combine the information into a bank resistance index (similar to the BEHI of Rosgen and Silvey (1996)). The bank resistance indices could then be classified into high, medium, or low bank resistance.
   - A streambank erosion hazard index is then determined according to a hazard level matrix as shown in figure 2.10.

   This methodology has not been tested so its pertinency can not yet be guaranteed. Once again, it is recommended to do geomorphological analysis and mapping throughout the region so that such a regional method is not needed. This method is shown though as a possibility for prioritizing the geomorphological mapping as its cost over a large region is considerable.
3. Based on geomorphological analysis and mapping, a decision must be made on where detailed streambank erosion hazard mapping must be conducted. If a large rotational streambank failure could occur or a planar failure on a high bank, it is suggested that a detailed geotechnical study be performed. Such a failure falls more into landslide hazard assessment than streambank erosion hazard assessment. For planar/slab failures on low to medium high banks (less than 15-20 meters high), a geofluvial model can be used.
4. Input data for the geofluvial model must be collected. This includes:
   - channel planform data
   - cross section data including roughness

- bank data
- bed data
- tributary and boundary condition sediment and discharge input

Details on the data to collect and methods are given in chapters 4 and 5.

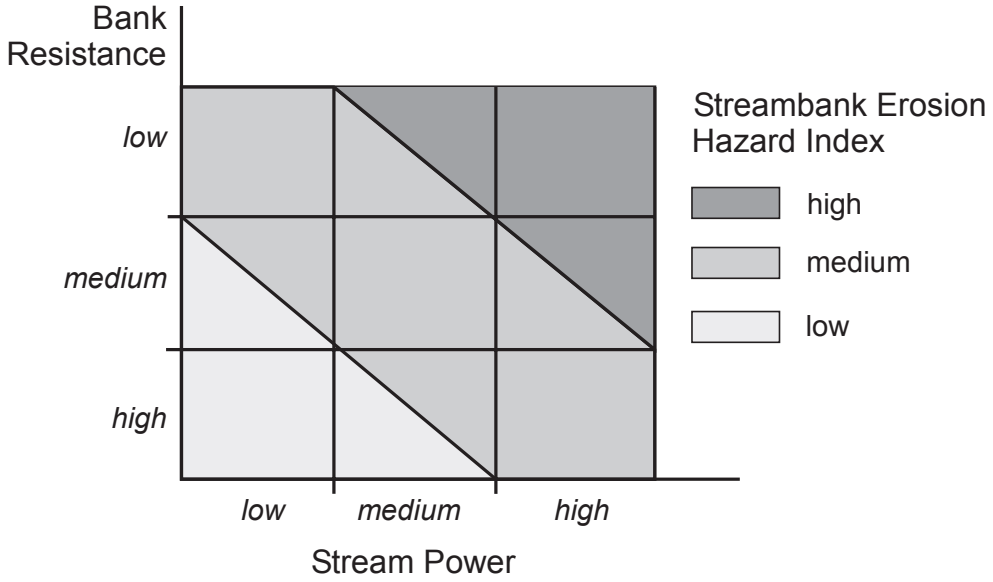

Figure 2.10. Streambank erosion hazard index based on stream power and bank resistance

5. Simulations are done with a geofluvial model. Calibration of water depth should be done with historically observed flood depths. Bedload transport parameters can be adjusted to reproduce historical changes in bed level changes. Calibration of bank parameters can be done to reproduce approximate historical channel migration. Simulations to produce bank failure widths is tricky. The problem is that a frequency analysis of the bank failures will not be pertinent if the cross section and planform change significantly altering the near bank shear stress. In the adaptations to the CCHE1D model, it will be seen in the next section that cross section width and planform will be kept constant to avoid non-stationarity associated with these changes. Bed level change can be allowed though to try to take into account bed fluctuations during a flood. Simulations can be done with a long historical period or with a generated discharge series.
6. An extreme flood is simulated so as to calculate the maximum bank failure widths expected.
7. The probability of a given failure width can then be evaluated with the simulated bank failure widths. Failure width probability where bank protection exists involves the multiplication of the probability of the bank protection failure and the failure width probability. Bank protection failure probability depends on the protection work type and its condition and should be evaluated by experts. Its foundation depth relative to the present or potential future bed depth is a very helpful information for the expert in evaluating the stability of the work.
8. Mapping a streambank erosion hazard in terms of bank failure width and probability is difficult due to the many small failures that occur. A very fine resolution map is necessary to show very small bank failures. To overcome this while respecting the danger level calculation of the Swiss Federal Office for Water and Geology directives (figure 1.3), it is proposed to map the danger level with a line or polygon in the danger color (the most critical danger level according to figure 1.3) and to

map it to a specified factor of the mean annual erosion rate. This mean annual erosion rate can be determined by integrating the frequency distribution of the bank failure width. The multiplication factor will be determined by the mapper according to the readability of the map. By using the mean annual erosion rate, the user can interpret the danger level in terms not only of instantaneous bank failure width, but also in terms of the mean annual migration rate. Besides the mapping of the danger level, the danger map should also show a maximum failure distance as calculated in step 6. The distance to be mapped for a particular bank will be based on the maximum failure value throughout the reach.

2.4.2 CCHE1D model modifications

CCHE1D (version 3.0) is a one-dimensional model. For the calculation of fluvial erosion in a meandering river this raises the problem of the calculation of the bank shear stresses. A correction method based on channel planform is used. Streambank erosion and bank failures originally implemented in CCHE1D are for the purpose of determining channel widening in straight channels due to bed instabilities. For this reason, channel planform is not kept track of. Input of the channel planform coordinates will need to be implemented. The bank failure algorithm of the current CCHE1D model does not take into account tension cracks. Tension cracks have a very significant effect on bank failure widths so they must be implemented in the bank failure algorithm. The current version of the model does not output bank failure widths. This also must be implemented. CCHE1D is described in detail by its user and technical manuals, quick-start guide, and capabilities report that can be found on the internet (http://www.ncche.olemiss.edu/index.php?page=cche1d_documents). Only the modifications to the model will be described here.

Correction of bank shear stresses

Correction of the bank shear stresses is based on the Venoge planform modeling (Consuegra et al., 1999) that was adapted for the correction of bank shear stresses in the Seymaz, Switzerland project (Consuegra et al., 2000). Assuming bank migration rate is proportional to the excess bank shear stresses (Hanson, 1990), nominal and adjusted migration rates are replaced by the shear stress exerted at the bank toe in equation 2.15 to give:

$$\tau_1(s) = \Omega\tau_0(s) + \left[\Gamma\int_0^{\infty}\tau_0(s-\zeta)G(\zeta)d\zeta\right]\left[\int_0^{\infty}G(\zeta)d\zeta\right]^{-1} \qquad \textit{Eq. 2.21}$$

where τ_0 is the nominal bank toe shear stress and τ_1 is the planform adjusted bank toe shear stress. In initial trials of this shear stress correction, using the Venoge planform modeling values for Ω=-1 and Γ=2 forced unrealistic shear stresses in straight sections. More realistic shear stress values in straight sections occur with values of Ω=0 and Γ=1.

Nominal bank toe shear stress is based on a correction value that resembles the function shown in figure 2.9. The function implemented in CCHE1D calculates a shear stress correction factor with the following equation:

$$c_b(s) = k_5(s) + k_1(s)X(s)^{(b(s)-1)}e^{-k_2(s)X(s)^{b(s)}} \qquad \textit{Eq. 2.22}$$

where $c_b(s)$ is the shear stress bend correction factor, $k_1(s)$, $k_2(s)$, and $b(s)$ are the shape parameters, $k_5(s)$ regulates the correction factor to be applied in straight river reaches, and X(s)=$R_c(s)/w(s)$. The parameters k_1, k_2, b, k_5 are initially set at 0.785, 0.0845, 1.7, and 1 for all cross sections, respectively, although they can be different for each cross section. This function is graphed in figure 2.11. Nominal outer bank shear toe stress, $\tau_{OB,0}$, at point s, is then calculated as:

$$\tau_{OB,0}(s) = k_4 c_b(s)\rho g R_h(s)S(s) \qquad \textit{Eq. 2.23}$$

where k_4 is a coefficient that takes into account the bank angle, set to 0.75 for this thesis, and the other variables are those defined in equations 2.1 and 2.22. Nominal inner bank shear toe stress, $\tau_{IB,0}$, at point s, is calculated as:

$$\begin{aligned} \tau_{IB,0}(s) &= k_4(2k_5(s) - c_b(s))\rho g R_h(s)S(s) \;:\; cb \le 2k_5(s) \\ \tau_{IB,0}(s) &= 0 \;:\; cb > 2k_5(s) \end{aligned} \qquad \textit{Eq. 2.24}$$

The inner and outer bank shear stresses are attributed to the left or right cross section side according to the planform and then left and right nominal toe bank shear stresses are weighted according to the upstream values with equation 2.21 to calculate the adjusted toe bank shear stress.

Figure 2.11. Correction factor applied to outer bank toe shear stresses based on the ratio of radius of curvature over width

Channel centerline input

To calculate the radius of curvature needed in the above equations, the model must have the coordinates of each cross section center. The center of the channel is defined here as the middle point between the bank tops. This definition is adopted because it is much easier to approximate the channel centerline when digitizing it from orthophotos than the channel thalweg. The procedure for producing the coordinates of the channel centerline, based on the procedure used during the Venoge model study, are as follows:

1. Digitization of the channel centerline based on remotely sensed data, usually orthophotos.
2. Smoothing of the channel centerline based on the following algorithm:
   - A downstream channel centerline point that is closer than a minimum distance is eliminated.
   - An intermediate channel centerline point is added between a channel point and the following downstream point when the distance is greater than a maximum allowed distance (figure 2.12). This is done by calculating the point 1 based on the curcumscribed circle through points i, j, and k, calculating point 2 based on the curcumscribed circle through points j, k, and l, and then averaging these two points to get the new intermediate point to be placed in between points j and k.
   - The channel centerline points are looped through over and over until all channel points are within the maximum allowed distance.
3. Channel longitudinal distance is calculated with an appropriate GIS tool and points representing the channel centerline are extracted. In this study 1 meter spacing was chosen.
4. Points representing real cross sections are selected by the GIS. Other intermediate nodes between real cross sections must also be selected so that the computational network for bank erosion sufficiently represents possible longitudinal failure distances. Through GIS scripting, in this study Mapbasic® was used in connection with Mapinfo® Professional®, other intermediate nodes are selected so that a maximum distance between nodes is respected.

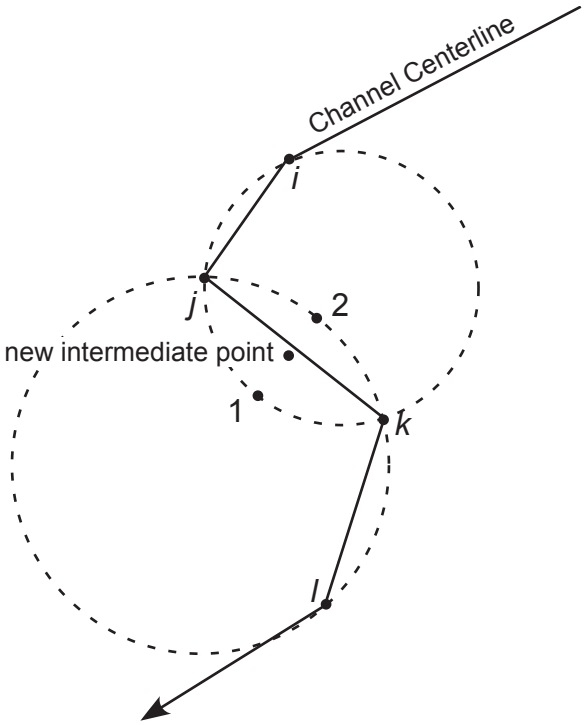

Figure 2.12. Channel centerline smoothing procedure

5. Each point is given a cross section identifier and those identifiers and their coordinates are exported from the GIS.

Bank erosion and failure algorithm changes

1. Toe erosion is always lateral. In the previous version toe erosion could also deepen the bed.

Depending on the bed geometry, this caused oversteepening of the bank in some cases.

2. In the unmodified version of CCHE1D, banks are considered stable if any lower portion of the bank has an angle between the toe and a bank point that is lower than the failure angle, β (figure 2.13). This condition has been eliminated so that bank stability calculations always progress up to or beyond the top of the bank.
3. Tension cracking has been implemented. Tension crack depth is determined by equation 2.12. If the predicted depth is greater than half the bank height, the tension crack depth is limited to half the bank height.
4. The failure angle is no longer calculated according to equation 2.11. Failure angles are computed at 10 cm intervals starting at 20 cm from the bank top until a minimum factor of safety is found. The failure angle giving the smallest factor of safety is retained.
5. Bank failures are output from the model. The location given by the cross section identifier and the bank side, the bank failure distance, and the time are output. Other hydraulic variables, beyond the standard model output variables, can also be output for analysis purposes, such as mean or maximum event toe shear stress.

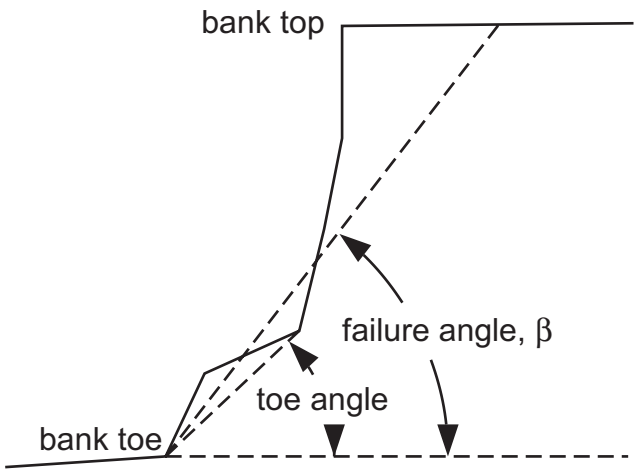

Figure 2.13. Bank stability is no longer guaranteed by the toe angle being lower than the failure angle

6. No cross sectional change occurs due to bank failure (figure 2.14). Initial bank or bed erosion is allowed to steepen or heighten the bank. If it is significant enough, the bank will eventually fail. In the unmodified CCHE1D, the bank geometry is then changed according to the failure. For this thesis, bank geometry is left unchanged. The bank is left unstable. The bank will not fail again, though, until the virtual tank that holds the failed sediment is empty. In this way, the virtual tank models the basal sediments. Until the basal sediments are eroded away, another bank failure can not occur. This conceptualization is appropriate for a discharge controlled bank retreat. If channel migration is to be studied, then cross section updating would be necessary. But in the case where we want to calculate the probability of failure for the modeled bank, it makes sense to adopt this modeling procedure to keep the cross sectional and planform conditions the same.

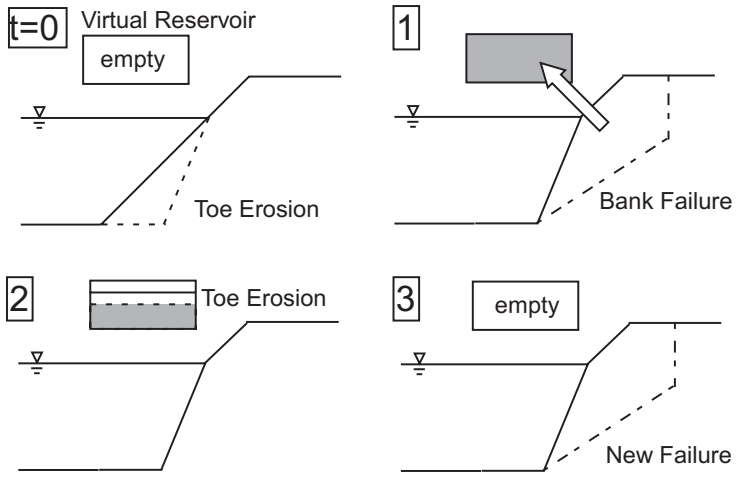

Figure 2.14. Cross sectional adjustments in the modified CCHE1D model. Toe erosion destabilizes the bank causing bank failure. Bank geometry does not change although the bank failure material is added to the virtual reservoir. Subsequent toe erosion empties the reservoir so a new bank failure can occur.

Chapter 3

The Venoge River

3.1 Introduction

The Venoge River in the Vaud Canton in Switzerland was chosen for streambank erosion monitoring. This choice was not arbitrary as the Venoge River is one of the closest rivers to the EPFL and has been the object of an important hydrologic and hydraulic study conducted by the HYDRAM laboratory from 1996-1998 (Lance et al., 1997, Lance and Consuegra, 1997, and Lance and Consuegra, 1998). More important than the proximity of the river to the EPFL, the Venoge River is allowed to meander through three major alluvial zones and partially in a few other reaches. Streambank erosion occurs in an observable manner each year giving the possibility to record significant erosion during the time of a PhD thesis.

This chapter will give a brief introduction to the Venoge catchment and the morphology of the Lower Venoge River.

3.2 Location of the Venoge catchment

The Venoge catchment is located in the west of Switzerland (figure 3.1). The topographic drainage basin has an area of 238 km². The upper catchment to the northwest is dominated by the karstic Jura mountains while the majority of the catchment lies on the Swiss Plateau. The catchment outlet is on Lake Geneva.

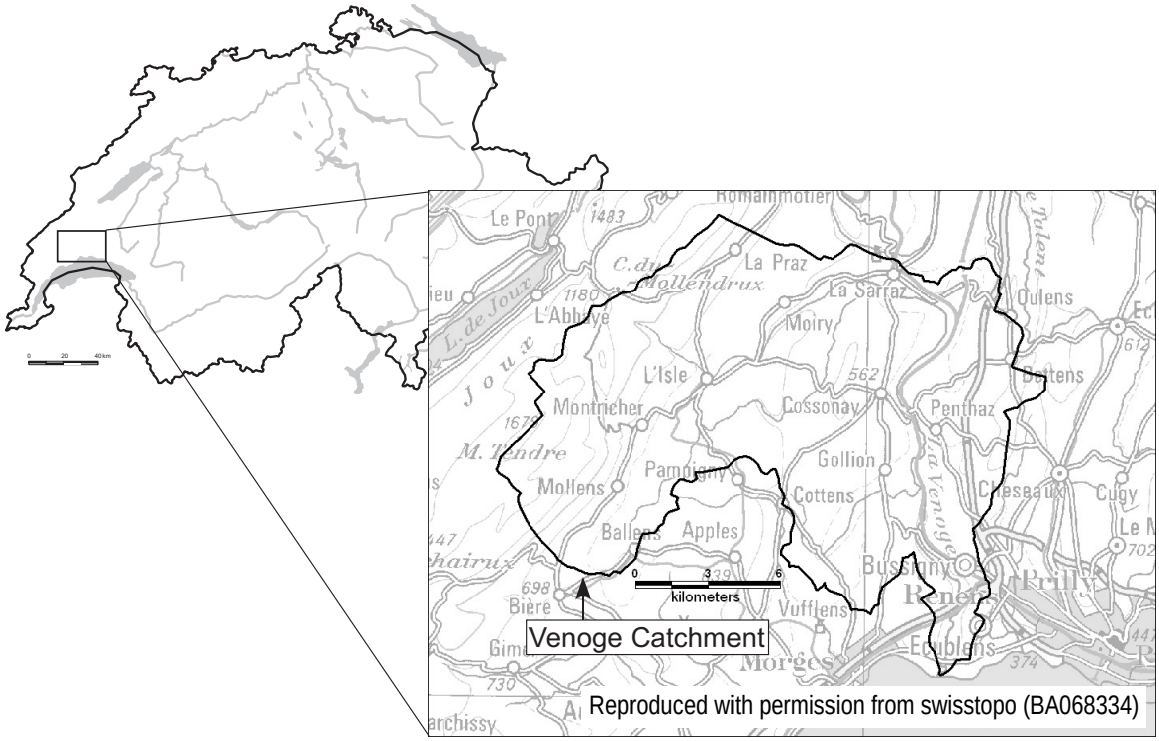

Figure 3.1. Venoge catchment topographical limit (background map: CP500 ©1997, Swisstopo)

3.3 Geology

Geologic history of the Venoge catchment

To understand the type of sediments that are found in the Venoge catchment, and especially in the bed and the banks of the Venoge River, it is important to understand the geologic history of the catchment and the type of rock and deposits encountered. The majority of the catchment lies on the Swiss Molasse. This sandstone plateau is the result of the erosion of the Alps during its formation during the Oligocene period. The sediment accumulation has a depth of 2.5 km (Grattier, 1980).

The Stampien formation of the Swiss Molasse (figure 3.2) is largely made up of lacustrine sediments, while sandstone proportions are greater in the Aquitanien and the Burdigalien formations due to the increased marine influence during these epochs (Grattier, 1980).

During the Pliocene, the folded Jura mountain belt detached from the Alps. As the folds separated from the Alps, the space in between was left for the formation of the Swiss Plateau (Collet, 1955). During the Quaternary, the Rhone glacier invaded the plateau, eroding the layers of Molasse. The moraines of the Venoge catchment are essentially those left from the Würm glacial period (Grattier, 1980).

After the glacial periods, during a period of tundra, the landscape was transformed by the eroding action of water and wind. The resulting layers of restructured silts forms what is the present day soil of the

Venoge catchment. Basins were filled up with colluvial material and formed marshes. Morainic material was picked up and deposited to form the alluvial zones of the lower plains (Grattier, 1980).

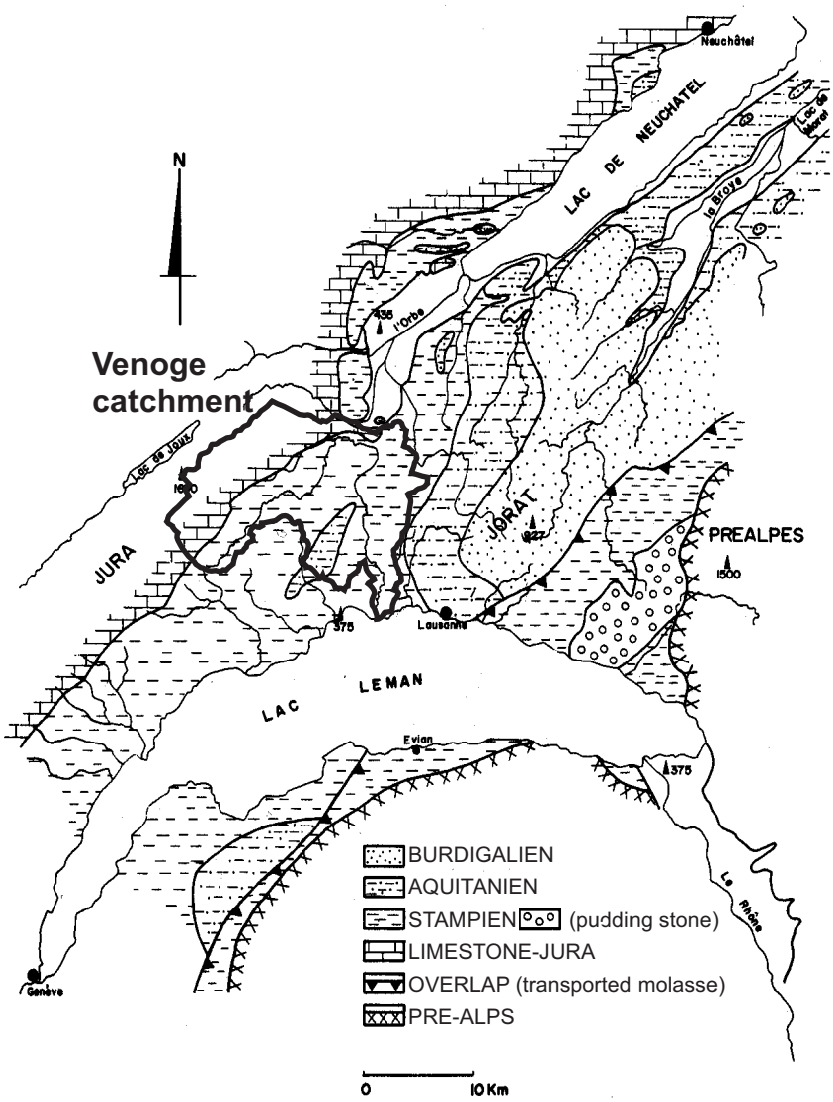

Figure 3.2. Geologic substrates of the Vaud Canton, Switzerland (adapted from Grattier, 1980)

Characteristics of the geologic deposits

Figure 3.3 shows a description of the geologic deposits based on the Swiss geologic maps (1:25'000).

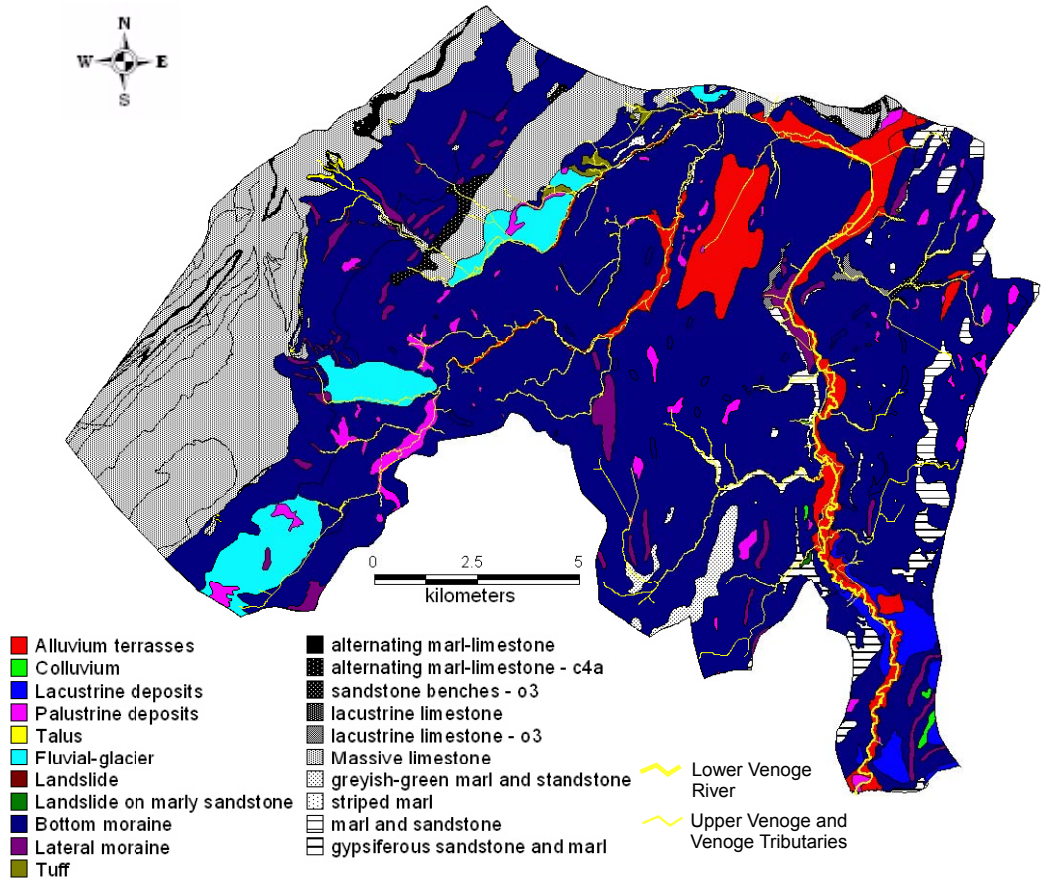

Figure 3.3. Bedrock and quaternary sediment of the Venoge catchment (data from Schneider, 2001)

Grattier (1980) described the deposits in five categories: cretaceous Jura limestone, oligocenic molasse, glacial deposits, silt and decarbonated colluvium, and alluvium and carbonated colluvium. The following is a summary of the characteristics of each of these deposits as described by Grattier (1980):

1. Cretaceous Jura limestone: These limestones are very hard, clastic, and cut into compartments by their faults. Fragmentation is slow, although the clasts have favored a karstic erosion.
2. Oligocene molasse: The molasse is a feldspatic-micaceous sandstone cemented by calcite or clayey-calcite. In terms of its petrography, it is rich in quartz and contains a lot of debris from crystalline and carbonated rocks, micas, chlorites, and other varied heavy minerals. In terms of its facies, the molasse is composed of alternating benches of marl-marly sandstone and sandstone. As mentioned above, the proportion of sandstone usually increases with decreasing age. The molasse is usually rich in silt. Marly molasse is especially rich in fine silt particles. The proportion of calcite varies from bench to bench; it is less frequent in the clayey molasse (red molasse). The marls are often rich in calcite.
3. Glacial deposits: Morainic deposits are quite variable in their spatial distribution and thickness. All of the degrees of mixes are found between the restructured molasse and the deposits of the Rhone and Jura. In terms of petrography, the gravels and pebbles are dominated by the limestones, and the sands and associated heavy minerals come mainly from the molasse. The three main facies are the

bottom, fluvio-glacier, and the superficial moraine. The bottom moraine is usually rich in silt and poor in gravel. The fluvio-glacier moraine has lenses of sand and gravel that were deposited in the front of the glacier. The superficial moraine is an intermediate moraine between the bottom moraine and the fluvio-glacier in which there is a lot of gravel and the different particle proportions are relatively equal. Figures A.1 and A.2 in the appendix shows textural triangle representations of the particle distribution of various samples taken from molassic and morainic deposits from the Vaud canton.

4. Silts from restructuring and decarbonated colluvium: These silts have very little gravel and were formed from the restructuring of older deposits. Their composition is more silty for the Stampien derived formations, and more sandy-silt when derived from the Aquitanien formations. This type of deposit occurs in a very limited way (either in its extension or its depth).
5. Alluvium and carbonated colluvium: These deposits are post-glacial. They are usually finer except near streams. In the alluvial plains, a finer silt layer, with varying degrees of organic matter, often covers a courser layer of sands and gravels. In the marsh basins, the succession from bottom to top is often a glacial clay, lacustrine lime, peat, and finally an organic clayey silt. Laterally, the finer alluvial deposits give way to bottom slope colluvium.

3.4 Soil and land use

The land-use of the Venoge catchment is dominated by cultivated fields (figure 3.4). Forests dominate the slopes of the Jura mountains. The catchment is essentially rural as the percentage of urbanized surface is only 8.6%, and of that only 3.5% was considered impermeable in the 1997 mapping.

Table 3.1 shows the percentages of the different land-use categories for 1985 and 1997 as extracted from the GESREAU[1] database. There is very little change from 1985 to 1997, and those being the conversion of some farmland to urban development.

Land-use category	1997	1985
Urban impermeable	3.5	3.2
Urban permeable	5.1	4.7
Forests	32.8	32.9
Cultivated Fields	51.1	51.5
Prairie, Pasture	6.8	7.1
Vineyards	0.3	0.3
Wetlands, lakes	0.2	0.2
Scree	0.1	0.1

Table 3.1. Venoge catchment land-use and changes from 1985 to 1997 (Data extraction from GESREAU)

1. GESREAU is the integrated water management database of the Vaud canton in Switzerland. See http://hydram.epfl.ch/gesreau/menu.htm for more information.

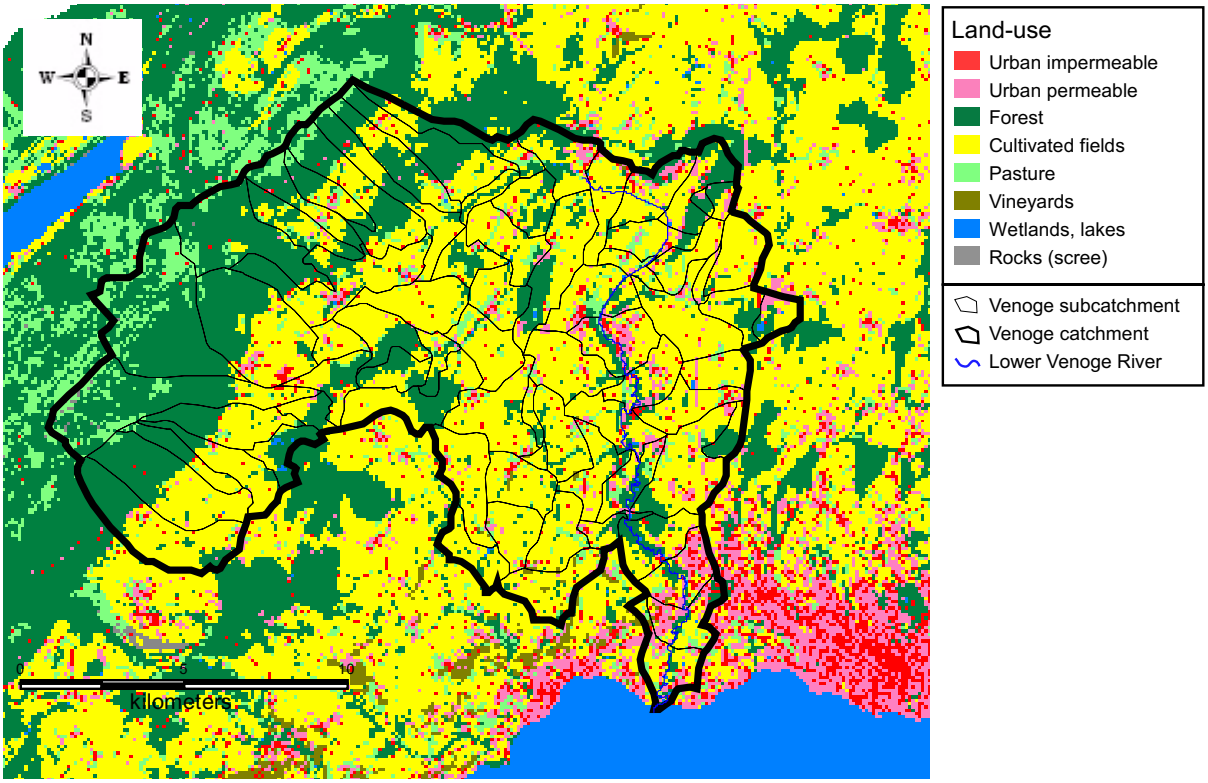

Figure 3.4. Venoge 1997 land-use (data from the Swiss Federal Office of Statistics (OFS))

Prétorian (1994) summarizes the soils of the Venoge catchment to be generally silt or fine silt. On average, the particle size distribution contains 15% clay, 28% fine silt, 23% large silt, and 35% sand. The pH varies from 5.3 to 7.8, the percentage of calcium from 0 to 20%, and the organic material from 2.5 to 3.8%. In general, the soils of the Venoge are strongly erodible with a factor K of Wischmeier between 0.2 and 0.4. The most erodible zones are the Upper Senoge, and on the Venoge the areas of Eclépens, Lussery and downstream from Cossonay (percentage of silt greater than 60% and little organic matter).

3.5 Topography and the hydrographic network

The limits of the Venoge catchment as determined within the GESREAU database are shown in figure 3.5. The total surface is 238 km^2. The maximum elevation within the catchment, 1680 m, is at the Mont-Tendre. The Lake Geneva typical water surface elevation at the outlet is 372 m. There are three relatively distinct topographic zones of the catchment (figure 3.5). The upper catchment formed by the Jura mountains has several sources connected to the karst system. In the middle catchment, water from the Jura sources and from the marshes at the foot of the Jura then runs through the impermeable molassic plateau where the waters of the Veyron join the waters of the Venoge at the Tine de Conflens. Finally, the Venoge flows through its alluvia in the lower catchment.

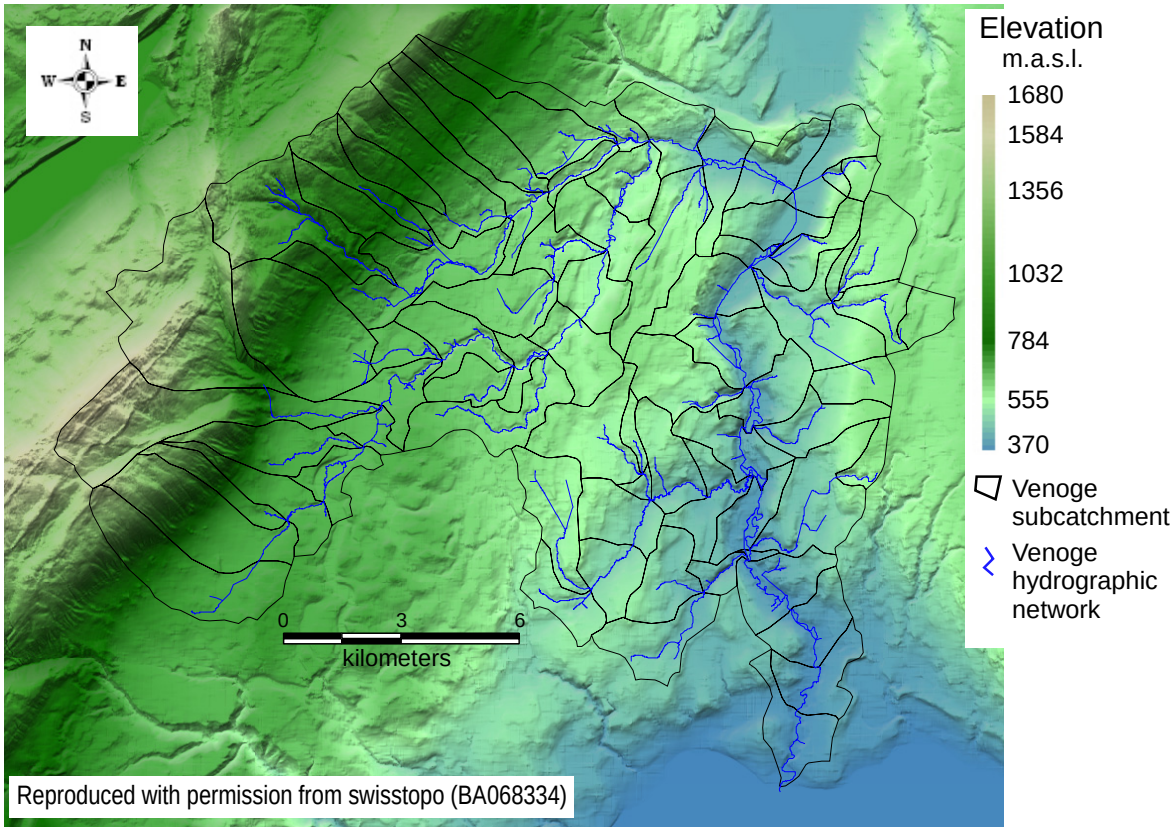

Figure 3.5. Venoge digital terrain model, subcatchments, and hydrographic network. Relief data is from the DTM25 ©1995, Swisstopo, and catchment and hydrographic network data come from GESREAU.

3.5.1 Catchment topography

The hypsometric curve of the Venoge catchment (figure 3.6) shows a basin in the monadnock phase according to the descriptions of Strahler (in Maxey, 1964). The monadnock phase is characterized by a resistant rock body, in this case the Jura mountains, and a relatively subdued relief, the Swiss molassic plateau. The mean elevation of the catchment is 700 m.a.s.l. and the median is 600 m.a.s.l. The mean slope is 10.9% while the median is 7.1% (figure 3.6).

The coefficient of compactness of Gravelius (Musy and Higy, 2004) indicates the effect of the form of the basin on the streamflow. It is defined as:

$$K_G = 0.28 \bullet \frac{P}{\sqrt{A}} \qquad \textit{Eq. 3.1}$$

where P is the catchment perimeter (smoothed) and A is the catchment area. For a round basin, K_G is approximately 1, while for a very long rectangular basin K_G is around 1.6 (Musy and Higy, 2004). The smoothed Venoge perimeter is approximately 76 km. Using this value and the catchment area, the value of K_G is 1.4. This demonstrates that the Venoge is a relatively long basin. Such basins typically produce attenuated hydrographs, longer concentration times, and lower peak discharges.

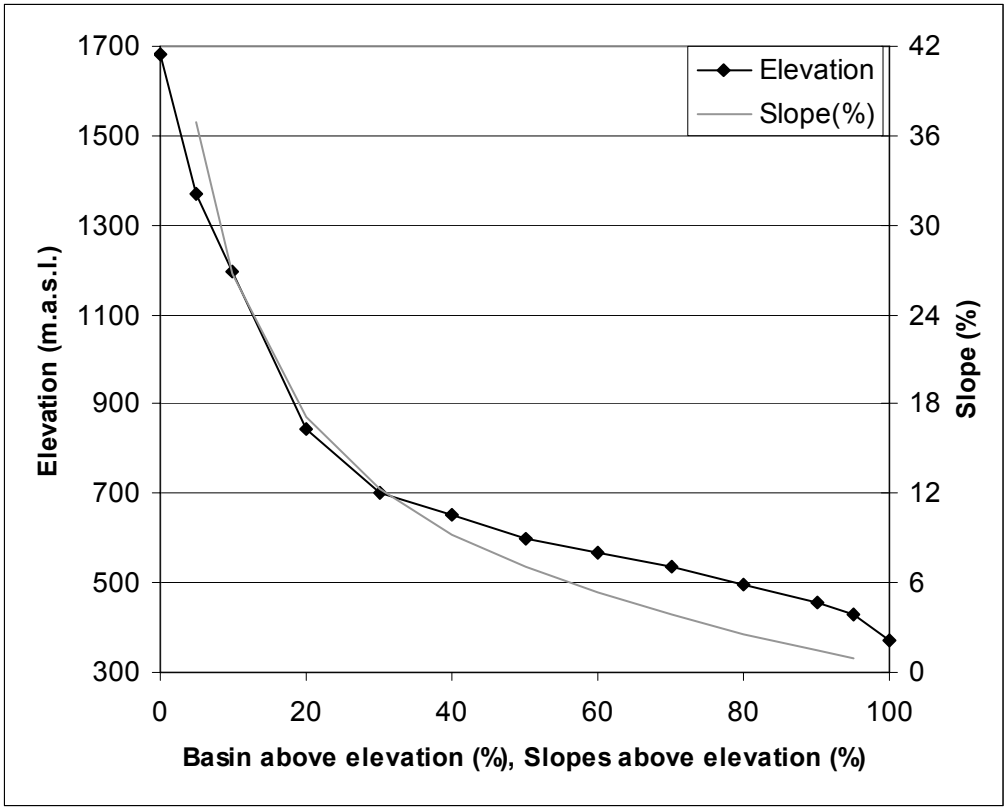

Figure 3.6. Venoge catchment hypsometric curve and slope frequency.

3.5.2 Subcatchment limits and stream network

The GESREAU subcatchments are shown in figure 3.5 and the main subcatchments are shown in figure 3.7. The Veyron is the principal subcatchment of the Venoge collecting waters from the marshy plain at the foot of the Mont-Tendre slopes. The Upper Venoge collects the remainder of the waters issued from the Jura karst. In his report on the hydrologic behavior of the Venoge catchment, Prétorian (1994), estimated the real Venoge catchment to be 15.5 km^2 greater than the topographic catchment according to hydrogeologic studies. The limit of the Venoge catchment from Mont-Tendre to the northern most point of the catchment should most likely be farther northwest stealing a part of the water from the Orbe catchment. There seems to be three levels of sources that feed the Venoge: 630-720 m.a.s.l., 850-950, and 1000-1150 as visible in the 1:25'000 geological maps of the Jura slopes, while the Veyron is only fed by the bottom level of sources at around 700-720 m.a.s.l. During low summer flow, the water table falls below 700 m.a.s.l. so that the Malagne et the Etremble become dry and only the Morand feeds the Veyron. The lower sources of the Upper Venoge continue to flow during low summer flows.

When the Veyron (86.6 km^2) joins with the Upper Venoge (43.6 km^2), combined they form 130 km^2 of the 238 km^2 of the Venoge catchment. During the inter-glacial period Riss-Würm, these two streams flowed through the Sarraz canyon (Custer, 1935). Post-Würm, due to moraines that filled the passages (Sarraz et Mormont) toward the Nozon of the Orbe catchment and the regressive erosion that eroded the

lower Venoge valley after the lowering of Lake Geneva, the Lower Venoge River was able to capture the Veyron and the Upper Venoge River (Custer, 1935).

The Lower Venoge valley is elongated and receives no major tributary. The Venoge essentially flows through its alluvium. Besides the areas surrounding the Venoge (intermediate catchments in figure 3.7), the other significant tributaries of the Lower Venoge River are the Molomba (13.5 km^2), the Senoge (22.5 km^2), the Vaube (6.7 km^2), and the Arena (7.3 km^2). The lengths, positions, and slopes of the above mentioned tributaries are indicated in the longitudinal profile of the Venoge and its tributaries in figure 3.8. As can be seen on the graph, the only torrential river slopes occur on the Jura tributaries of the Upper Venoge.

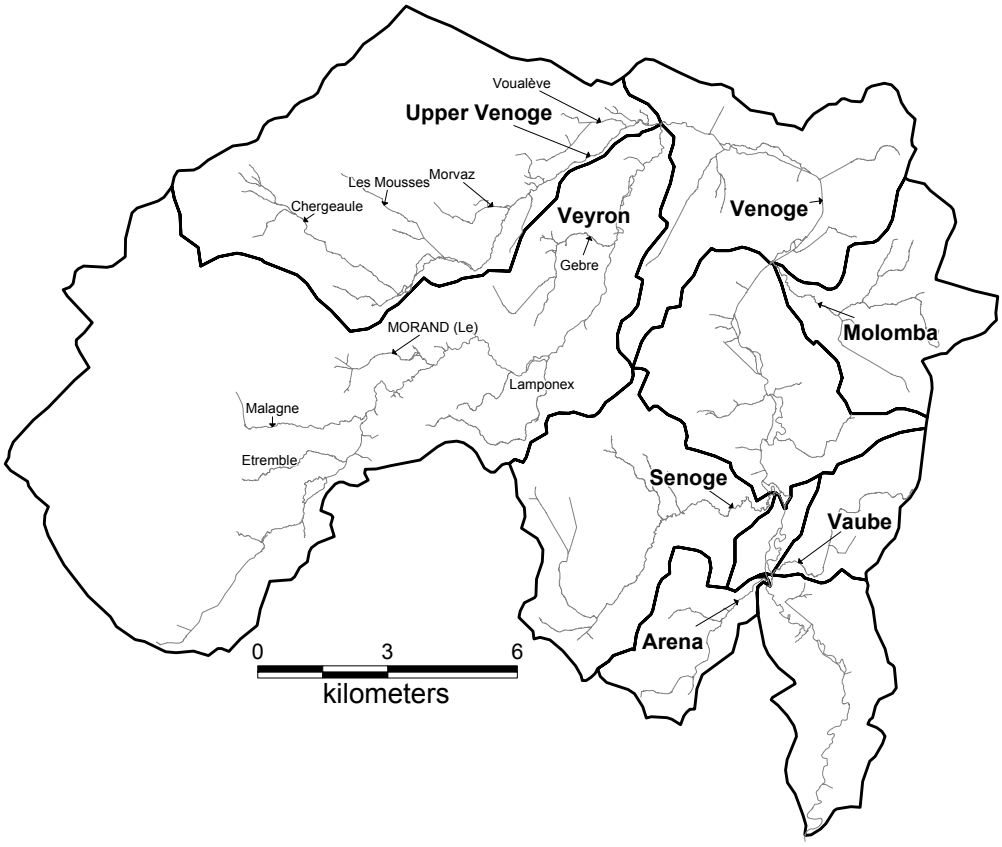

Figure 3.7. The Venoge River and its tributaries and subcatchments. Background map: CP500 ©1997, Swisstopo.

The drainage density is indicative of the type of runoff that occurs in the basin. Those with permeable structures will have a low value, while those that occur in cohesive materials will usually have a high value due to the important superficial runoff (Musy and Higy, 2004). The drainage density is defined as:

$$D_d = \frac{\sum L}{A} \qquad \text{Eq. 3.2}$$

where L is the length of an individual stream and A the area of the basin. Of course, depending on how the beginning of the stream is defined, the resulting value can easily change by 2 or 3 times. The length of the stream network for the Venoge basin according to the GESREAU system is 208 km, giving a value

of 0.9 for the drainage density. This value is very low indicating the important infiltration that occurs in the karstic and morainic formations. With such an important infiltration, a long response time is expected.

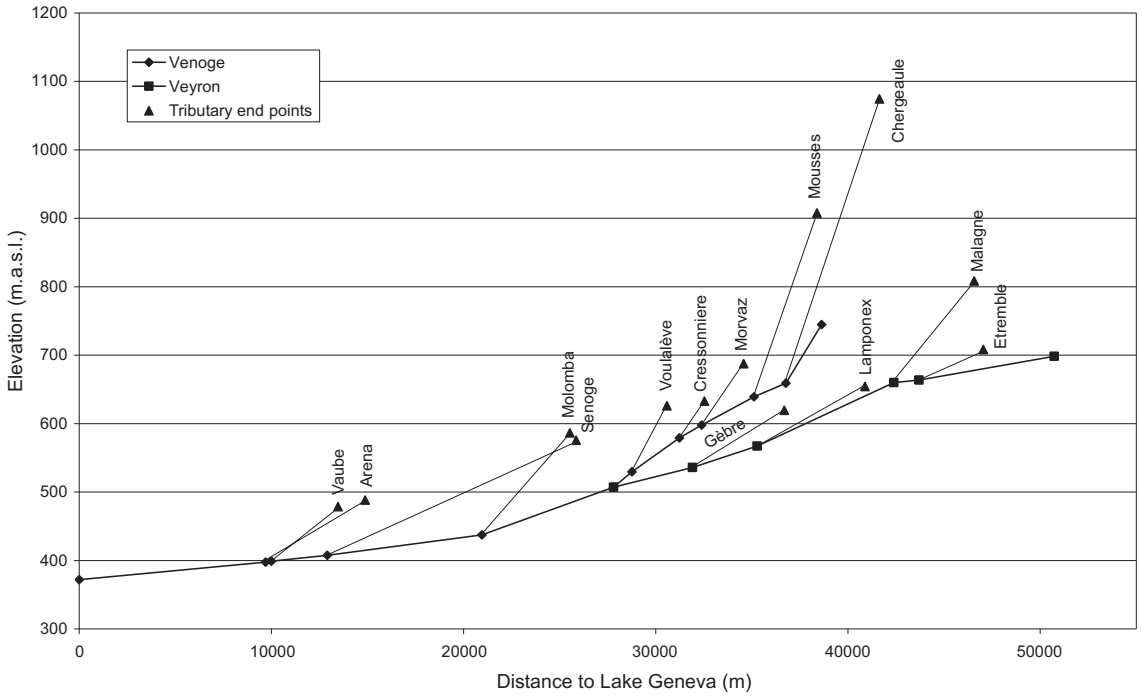

Figure 3.8. Longitudinal profile of the Venoge River and its important tributaries. Only starting and ending elevations are represented. Elevations based on the DTM25 ©1995, Swisstopo.

3.6 Climate and hydrologic regime

The climate of the Swiss plateau is considered to be humid temperate, with a continental tendency. The climate of the Venoge catchment deviates from a typical continental climate due to the effect of the Jura mountains. The ratio of summer precipitation to winter precipitation is approximately 1 for the Jura mountains and at the foot of the Jura there can be more winter rainfall than summer rainfall. This explains the small variation in monthly rainfall in figure 3.9. This figure equally shows the water deficit that can occur in the summer months due to an evapotranspiration potential that is greater than the rainfall. Mean annual Venoge precipitation is approximately 1250 mm, varying from 950 mm towards Chavornay (inland from the Jura and the lake) to 1800-2000 at Mont-Tendre (see chapter 5 for more details). Temperature variation over the catchment is represented in figure 3.9 by the Changins and Dole monthly mean temperatures. Although slightly outside of the Venoge catchment, they represent relatively well the elevation effect felt in the Venoge catchment. The Changins mean annual temperature is 10.1 °C for an elevation of 430 meters and the Dole mean annual temperature is 3.6 °C for an elevation of 1670 meters. The mean discharge in terms of depth is 600 mm. Assuming no other rainfall losses (deep percolation, hydrogeologic losses,...), this would give an ETR of approximately 650 mm. This is higher than what is indicated by the Swiss hydrological atlas (approximately 600 mm) (Spreafico, 1992),

but is realistic due to the important effect of the Joran winds that descend from the Jura mountains (Primault, 1972).

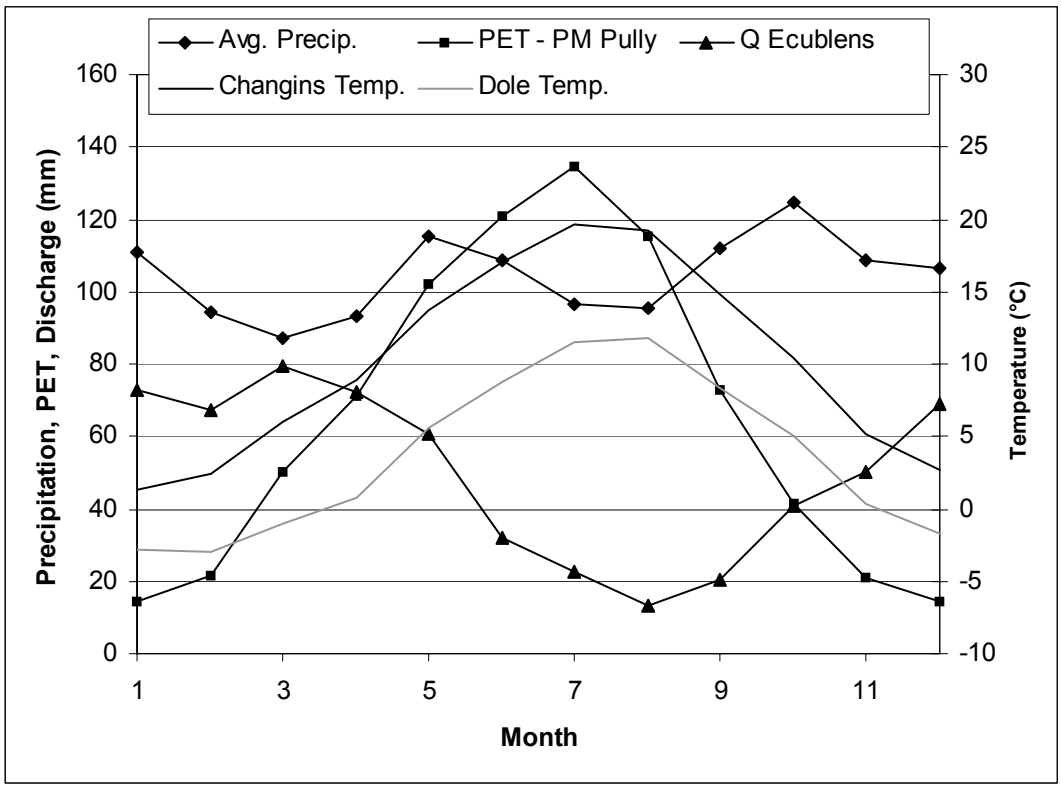

Figure 3.9. Seasonal variation of precipitation, potential evapotranspiration (PET calculated with the Penman-Monteith formula), discharge, and temperature. Data is from the period 1983-2003.

The hydrologic regime of a catchment can be defined by its variation of discharge. Usually this variation is examined by calculating each monthly discharge coefficient which is the mean monthly discharge divided by the mean annual discharge. In the Hydrologic Atlas of Switzerland (Spreafico et al., 1992), 16 regime classifications are proposed. The Venoge is classified as a "nivo-pluvial jurassien" regime. This classification is based on the Venoge Lussery discharge data collected from 1949-1978. Its name is indicative of the discharge generating mechanisms of the catchment, the Jura snow and rain. The typical nivo-pluvial jurassien regime has a peak monthly discharge in April and a minimum between July and October. Within this classification, the Venoge has the most marked difference between high spring flow and low summer flow. Figure 3.9 shows the discharge variation for the Venoge based on measured values (Ecublens 1983-2003) near the outlet. The difference between the high flows in March and low flows in August is even greater than that of the Venoge at Lussery, and thus no longer follows very well the classification of nivo-pluvial jurassien. The classification of pluvial jurassien is better, but does not yet capture the significant August low flow (monthly discharge coefficient of 0.26).

3.7 Channel morphology

In the above sections, the Venoge catchment has been described in its entirety. In this section, only the channel morphology of the last 25 kilometers of the Lower Venoge River, the river reach of interest, will

be considered. Channel morphology is dependant on the driving variables of water and sediment input and the boundary conditions (valley slope and topography, bed and bank material, and riparian vegetation). The resulting channel form is characterized by its longitudinal profile, cross sectional geometry, and its planform (Thorne, 1997).

3.7.1 Channel type

Leopold and Wolman (1957) defined channel forms as ranging from straight, single threaded channels through to multithread, braided systems. They classified a straight stream as having a sinuosity of less than 1.1, a slightly sinuous stream between 1.1 and 1.5, and a meandering stream greater than 1.5. Besides these three main categories of straight, meandering, and braided streams, a forth classification has been deemed necessary by Nanson and Croke (1992), that of anastomoses streams. These streams are low energy compared to braided streams which are usually high energy.

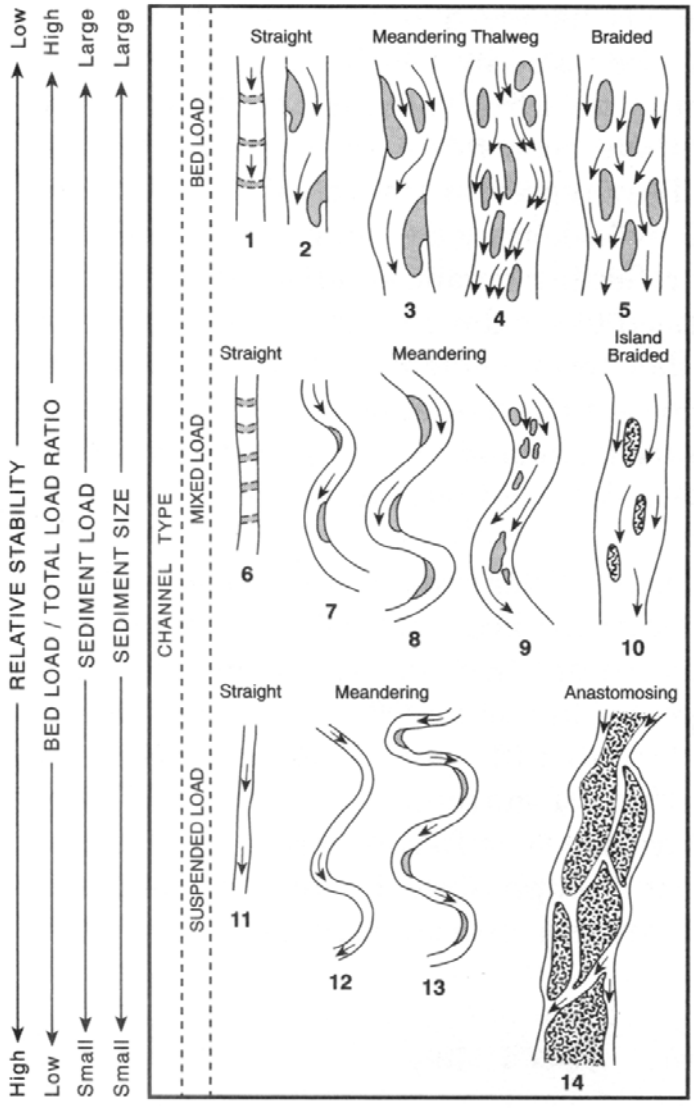

Figure 3.10. Classification of channel pattern (from Knighton,1998 based on the original work of Schumm, 1981). (Reproduced by permission of Stanley Schumm and Edward Arnold (Publishers)).

The Lower Venoge, as demonstrated by the orthophotos in figure 3.11, can be classified as a 3, 7, or 8 stream (figure 3.10). Some areas of the Lower Venoge do exhibit middle bars so that the 3rd classification is sometimes appropriate, although the Lower Venoge is mainly a meandering stream according to the 7th classification. Meandering must also be classified as active or passive (Thorne, 1997) or anchored, entrenched, or free (Bravard and Petite, 1997). The Lower Venoge was mostly free, although confined by the valley sides, but in the past century has been mostly fixed in place by bank protection. This leaves a minority of reaches to be truly freely meandering.

Figure 3.11. Two of the three alluvial zones of the Lower Venoge River. To the left - Lovataire and to the right - the islands of Bussigny. Orthophotos from 1996 EPFL student field study.

In figure 3.11, especially in the left picture, the Venoge exhibits compound and multibend loops. Another important feature of the Venoge morphology, is the meander cutoffs that occur. In the left picture, we see quite distinctly a meander cutoff that appears to be a chute cutoff. Cutoffs are either neck cutoffs, in which two bends of a loop meet so as to cutoff the meander, or chute cutoffs, in which significant overbank flow will erode a path (often following depressions) to cutoff the bend. Figure 3.12 shows four meander cutoffs that occurred in the Bussigny islands alluvial zone, three of which occurred

since 1964. The 1st cutoff is very small and occurred between 1996 and 2002. The second and third cutoffs occurred during the period 1964-1996, and the timing of the fourth one is unknown. The first three seem most likely to be chute cutoffs, while the fourth one is less clear. The orthophoto of figure 3.12 shows the important downstream planform modifications that occur after a meander cutoff, in addition to the significant slope change that occurs.

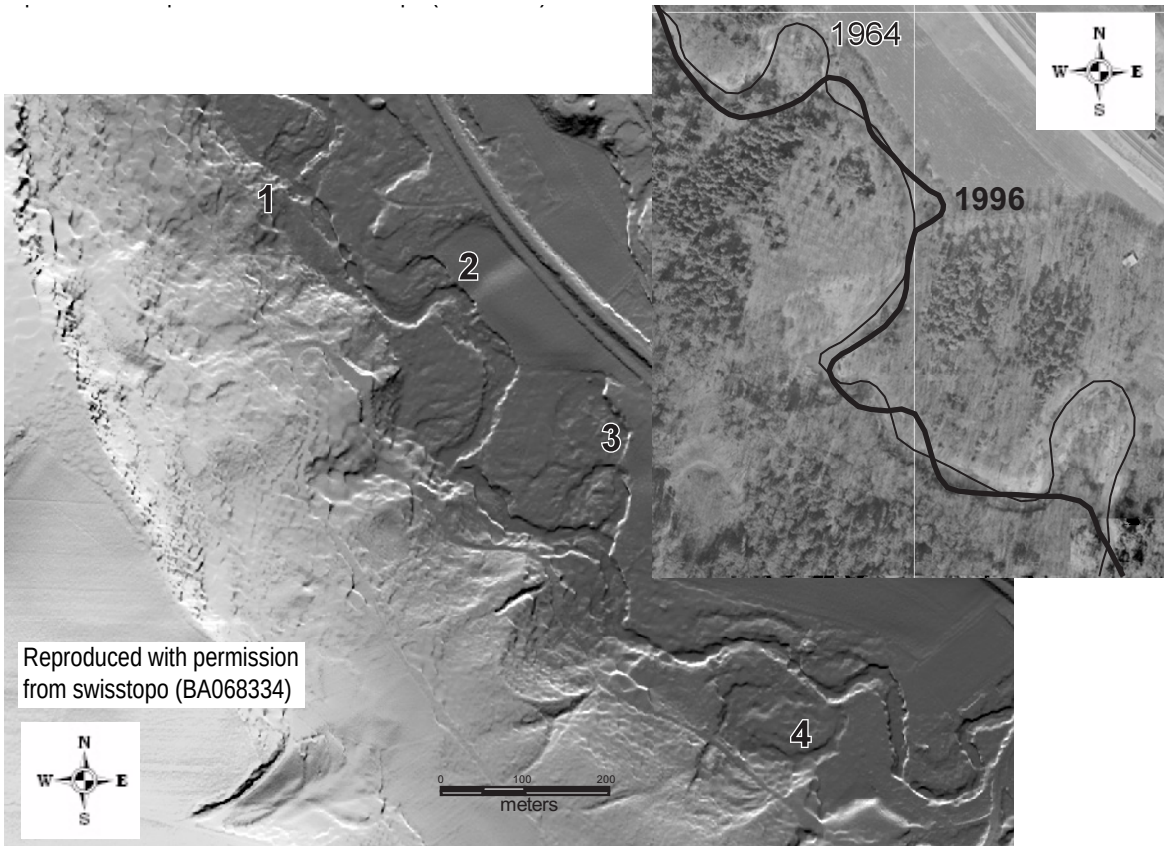

Figure 3.12. LIDAR DTM (DTM-AV ©2004, Swisstopo (DV043683)) showing four meander cutoffs in the Bussigny islands alluvial zone. The 1964 orthophoto shows the 2nd and 3rd meander cutoffs.

3.7.2 Planform

Being a meandering river, largely single thread, it is standard practice to describe the Venoge planform by its sinuosity. In theory (figure 3.13), defining meander planform geometry is simple, but in practice is much more difficult because of asymmetric planform patterns (figure 3.11). For simple bends in natural freely meandering zones of the Venoge, point bar spacing is in the range of 50-80 meters so that the wavelength is in the range of 100-160 meters. The sinuosity index is defined as the real channel length divided by the straight line. For the simple Venoge bends, it is in the 1.1 to 1.2 range. If the straight line distance that is used is the valley centerline, then for the Lower Venoge, the sinuosity is 1.5. This is a result of multiple loop bends and meandering that crosses the valley bottom. Figure 3.14 shows the distribution of the radius of curvature of the Lower Venoge River. The median radius of curvature is 170 meters.

To express the ranges in sinuosity possible over various reach lengths, Lancaster and Bras (2002) developed a new sinuosity-based method for analyzing planforms of meandering channels. Their method consists of calculating a mean channel sinuosity and its variance for every pair of digitized channel points at a given channel length. As the channel length increases, they suggest that the mean and variance will reveal two or three characteristic channel lengths. The first characteristic length they propose is that of the single bend length which is revealed by the mean sinuosity that increases less rapidly. The second and third characteristic lengths are found by peaks in the variance. They suggest that a first peak in the variance will determine the characteristic length of a long simple or compound bend loops. A second peak in the variance will determine the characteristic length of multibend loops.

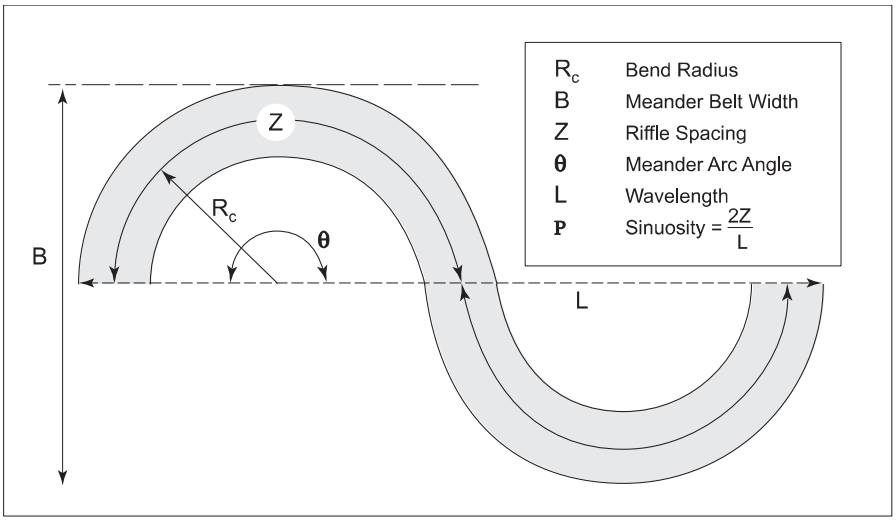

Figure 3.13. Meander planform geometry (adapted from Thorne, 1997)

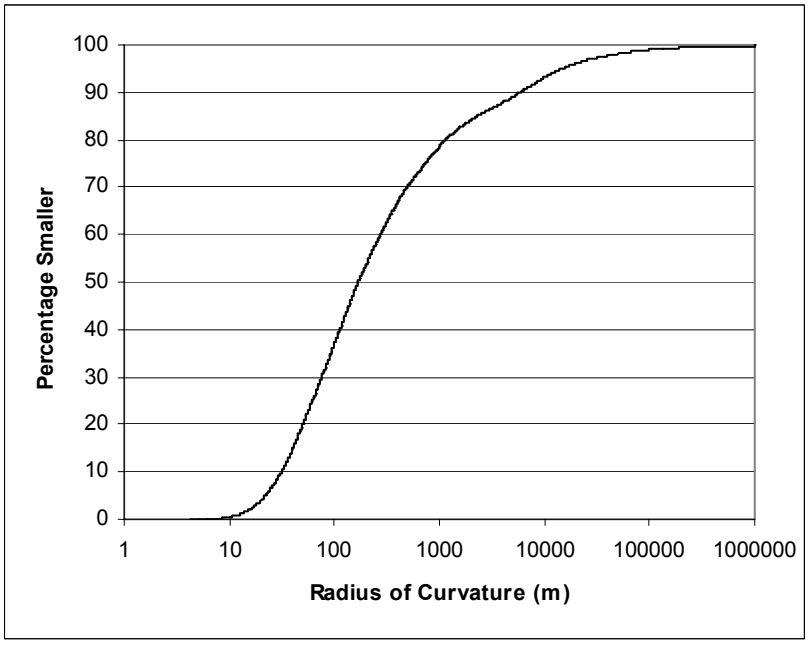

Figure 3.14. Distribution of radius of curvature for the Lower Venoge River

This new sinuosity-based method was programmed in the Delphi® programming language to analyze a point file in text format issued from a digitized river centerline. The analysis was done on the Lower Venoge from the start of zone 1 (figure 3.15) to its outlet. Table 3.2 shows the characteristic lengths for the 1996 and 1839 Lower Venoge River which are derived from the information in figure 3.16. It is somewhat surprising to see that the sinuosity of the Lower Venoge River has changed little from 1839 to 1996 with respect to the upstream channelization. The multibend characteristic length is shown to be longer though in 1996. The 1839 multibend characteristic length is similar to the freely meandering Roujarde alluvial zone so it is assumed that the channelization of the Lower Venoge caused the change in the multibend characteristic length. The analysis was also done for the Roujarde alluvial zone (figure 3.15), the most freely meandering of the alluvial zones. This zone shows simple bends which are shorter compared to the entire Venoge, although the compound and multibend lengths are comparable to the natural 1839 state. The sinuosities though are much greater. The greater sinuosity, especially for the multibends, reflects the space the Venoge has to move laterally in the Roujarde area. In other sections of the Venoge valley, the river is more confined by the valley side walls. Based on the sinuosity of 1.2 and the length z of 4.5w for the Roujarde zone, the mean wavelength, L, is 7.5w. This is lower than the value suggested by Richards (1982 in Thorne, 1997) of L=12.34w for a meandering river, but is in line with a sinuosity of 1.2 (Chorley et al., 1984 in Thorne, 1997).

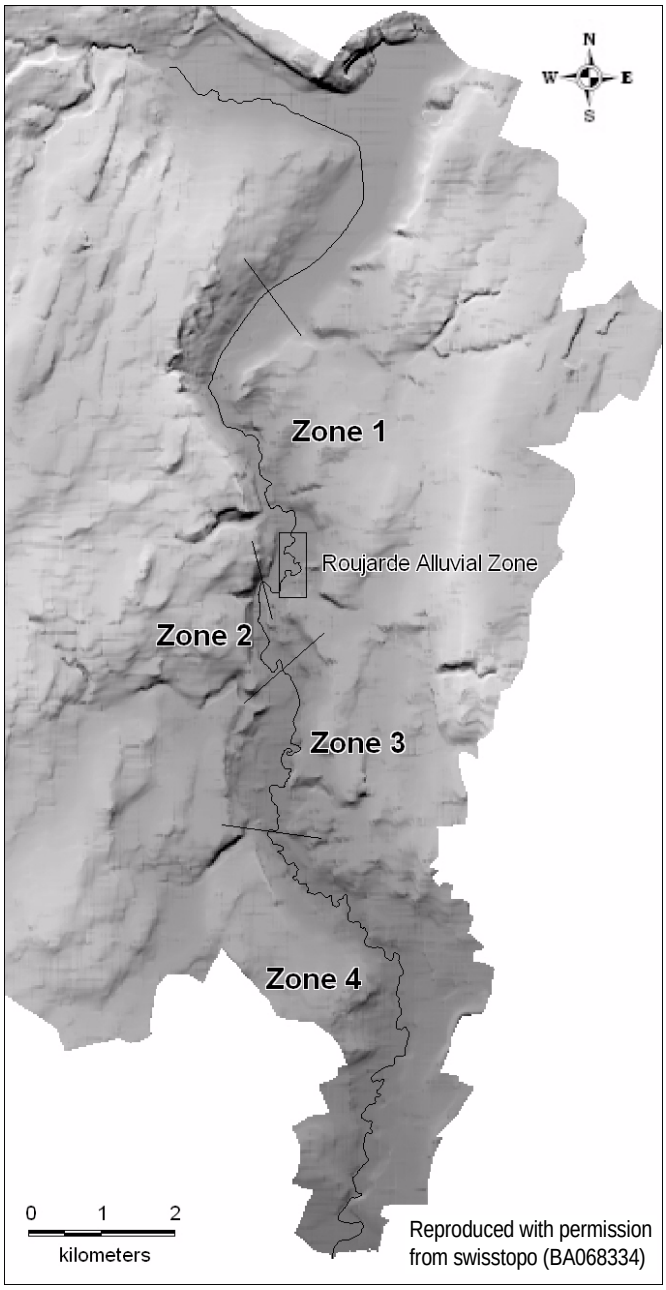

Figure 3.15. A view of the sinuosity of the Lower Venoge River. Background: DTM25 © 1995, Swisstopo.

	1996						1839	
	Lower Venoge River		Zone 1 to Lake		Roujarde Alluvial Zone		Lower Venoge River	
	length (m)	sinuosity	length (m)	sinuosity	length (m)	sinuosity	length (m)	sinuosity
simple	100-120	1.11	100-120	1.15	80-90	1.19	120-140	1.15
compound	260	1.24	260	1.33	230	1.55		
multibend	560	1.44	560	1.53	460	1.88	460	1.41

Table 3.2. Lower Venoge River sinuosity and characteristic bend lengths

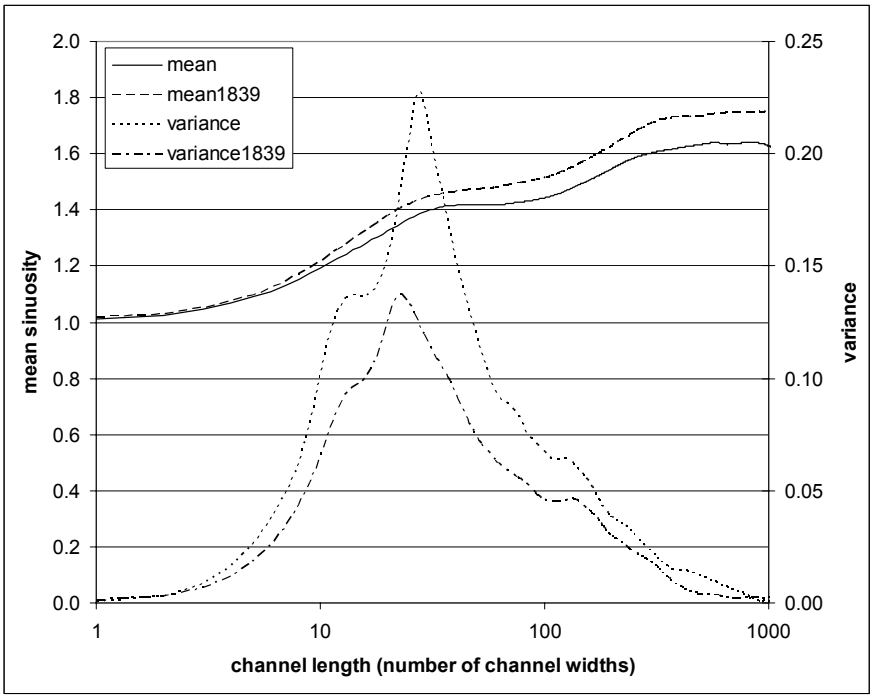

Figure 3.16. Analysis of mean sinuosity and its variance on the Lower Venoge River. Mean channel width is considered to be 20 meters.

3.7.3 Longitudinal profile

The longitudinal profile is an extremely important feature in geomorphological analysis. It is often the breaks in slope that cause the aggradational or degradational tendency of a stream. Its form will also give an idea of its equilibrium status. As can be seen in figure 3.17 (or in more detail in figure 4.17), the Lower Venoge River has a concave form with the only significant slope breaks being those imposed by instream weirs. This concave shape indicates most likely a stable slope, which is largely confirmed by the few changes in the thalweg elevation from cross sections taken in 1996 and 2004.

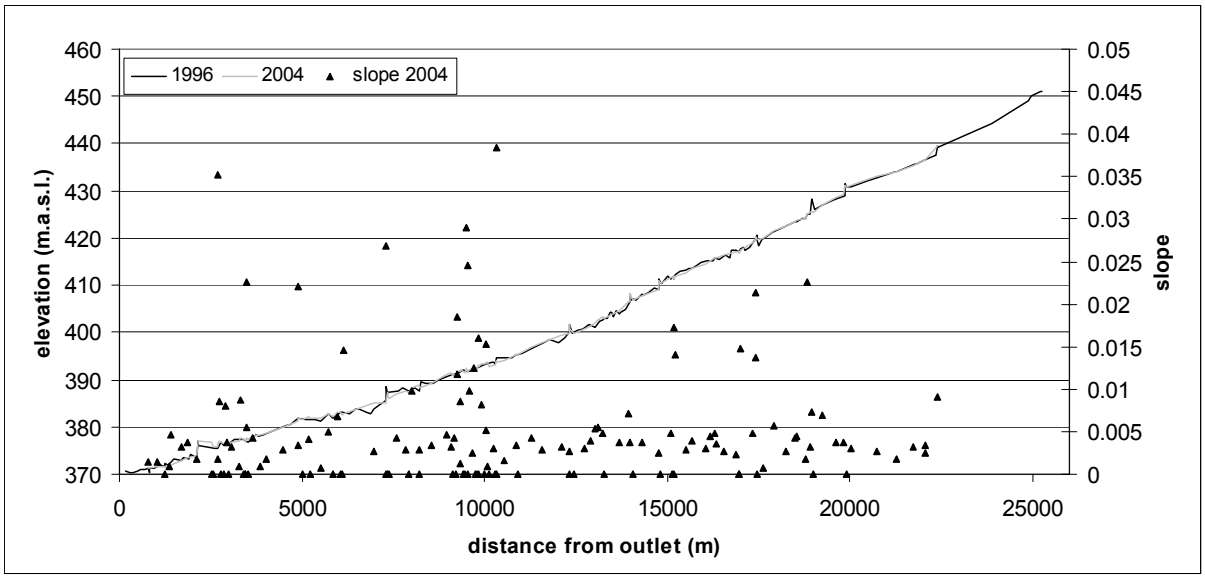

Figure 3.17. Longitudinal profile of the Lower Venoge River

3.7.4 Cross section characteristics

Cross section characteristics are usually expressed in terms of the bankfull channel width and depth. At-a-station hydraulic geometry is often used to express the width, depth, and velocity variation with respect to discharge: $W = aQ^b$, $D = cQ^f$, and $U = kQ^m$ (Leopold and Maddock, 1953), in which *a*, *b, c*, *f*, *k*, and *m* are the coefficients of the power laws. Leopold and Maddock (1953) also introduced the idea of downstream hydraulic geometry suggesting that downstream geometry (*W, D,* and *U*) can be determined based on the evolution of the mean or bankfull discharge. There is considerable variability in the at-a-station hydraulic geometry (HG) coefficients, and this even for the same stream reach. This has driven various authors (Jowett, 1998, Lamouroux and Capra, 2002, in Stewardson, 2005) to make attempts at defining reach hydraulic geometry based on reach average values. Stewardson (2005) concludes that hydraulic geometry relations using reach averaged width and depth, as well as the coefficient of variation of width and depth and velocity provide an efficient description.

Reach averaged width and depth as well as the standard deviation were determined for the four zones shown in figure 3.15 and are given in table 3.3. These results were developed from HEC-RAS simulations using cross sections from the HYDRAM Venoge study (Lance et al., 1997) and an initial HEC-RAS project developed during a postgraduate study (Rakotondranaly, 2001). As can be seen in table 3.3, bridge cross sections were excluded in the estimation of a reach averaged width and depth. The results of table 3.3 also excluded cross sections which had overbank flow. Four flows approximating the 0.5, 0.75, 1, and 2 year return period flows were simulated. Figures 3.18 and 3.19 graphically show the reach averaged widths and depths of table 3.3 and show possible HG relations fixing the b and f coefficients at 0.5 and 0.37 (Hey, 1997), respectively. It can be seen that zone 4 of the Lower Venoge River distinguishes itself from the three other zones.

zone	number excluding bridges	number used excluding overbank flow	Q (m3/s)	avg width (m)	standard deviation width	average hydraulic depth (m)	standard deviation depth
		25	23.1	18.9	6.8	1.10	0.31
		21	26.9	17.5	5.4	1.22	0.33
		20	30.8	17.2	4.2	1.30	0.34
1	31	19	36.2	18.1	4.7	1.37	0.37
		18	24.9	16.9	6.7	1.28	0.38
		17	29	17.7	7.1	1.34	0.39
		17	33.2	18.5	7.3	1.39	0.37
2	21	16	39	19.3	7.4	1.46	0.37
		16	27.6	19.8	8.3	1.33	0.40
		15	32.2	19.2	5.6	1.42	0.44
		12	36.8	19.1	4.4	1.45	0.52
3	22	12	43.2	20.0	4.8	1.54	0.53
		54	29.3	22.2	7.7	1.51	0.33
		52	34.2	23.6	8.0	1.57	0.32
		45	39.1	25.3	8.8	1.62	0.32
4	70	29	46	26.4	8.0	1.66	0.32

Table 3.3. Average width of 4 zones of the Lower Venoge River (c.f. figure 3.15). Results were developed from HEC-RAS simulations using 1996 cross section data.

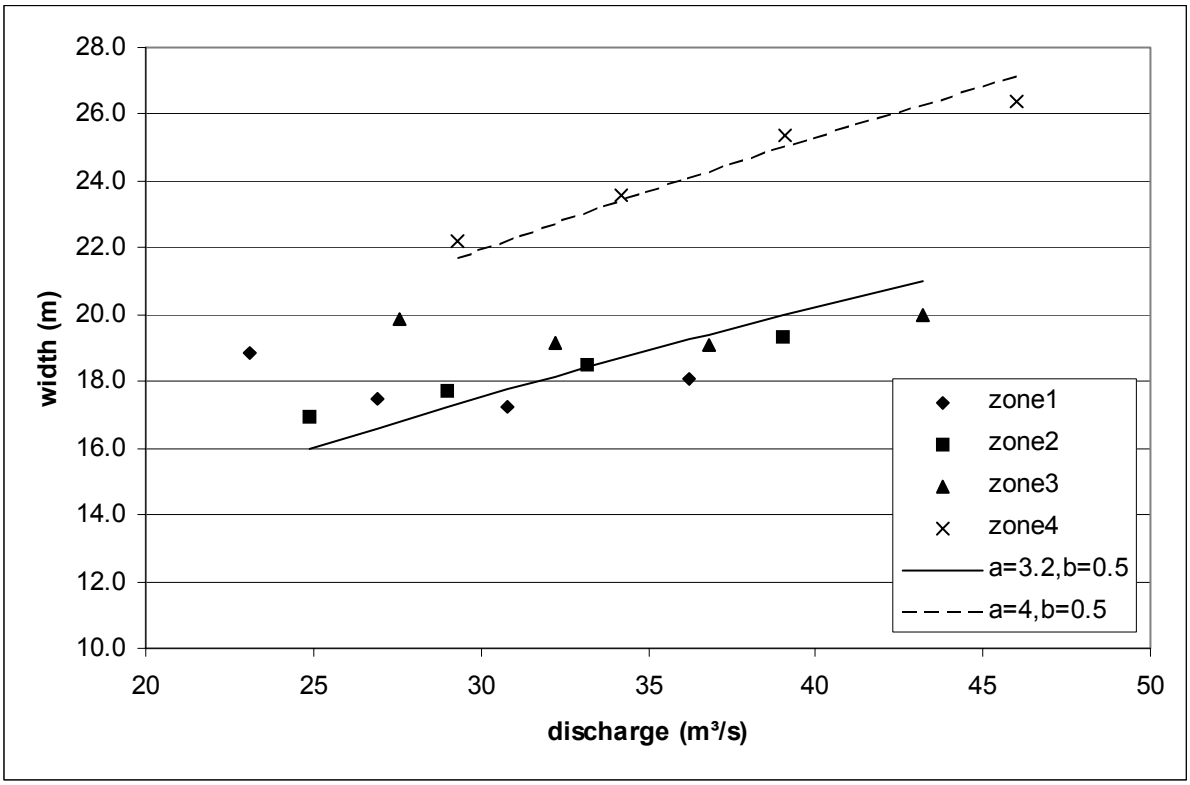

Figure 3.18. Reach averaged width for four zones of the Lower Venoge River at discharges approximating the 0.5, 0.75, 1, and 2 year return period flows. Lines show possible parameters for the relation $W = aQ^b$.

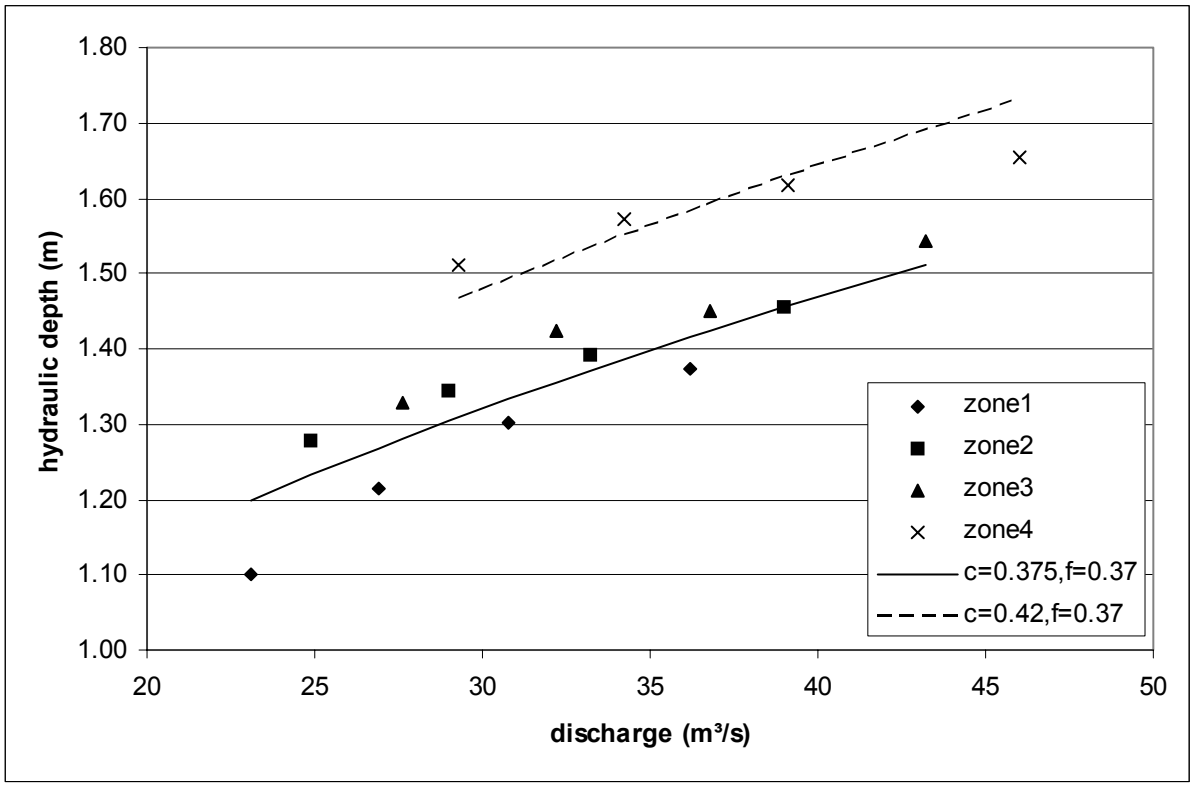

Figure 3.19. Reach averaged depth for four zones of the Lower Venoge River at discharges approximating the 0.5, 0.75, 1, and 2 year return period flows. Lines show possible parameters for the relation $D = cQ^f$.

Chapter 4

Venoge River Data for Streambank Erosion Modeling

4.1 Introduction

Streambank erosion modeling is a complex natural process that involves many parameters. Some data were readily available for the Lower Venoge River, but other data had to be collected. This chapter will explain how the experimental erosion zone was determined, what data was available, and the data that was collected to characterize the streamflow and streambank erosion, cross sections, bank and bed sediments, and boundary conditions of the study reach.

4.2 Experimental setup

An initial survey of the Lower Venoge River (from Lussery to the lake) was undertaken to determine the actively eroding banks, note the position of bank protection works, and determine a zone where erosion could be monitored (figure 4.1). Observations indicated that the alluvial zone "Iles de Bussigny" (islands of Bussigny) would work well for erosion monitoring as well as a zone relatively free to meander near the town of Denges (figure 4.2). Significant erosion occurs in the alluvial zones of the Roujarde and the Lovateire, but these zones are less accessible and farther away. The study reach was thus determined to be from the Moulin de Choc, Bussigny to the reach just downstream from Denges. This zone is ideal in that it will provide three different type of zones for the erosion modeling. The Bussigny islands alluvial zone is free of bank protection and moving frequently. The intermediate zone is mostly fixed by bank protection. It will be interesting to see how the streambank erosion modeling will handle a zone with

minimal data. The third detailed erosion monitoring zone at the end of the study reach is also interesting because of the freely eroding banks which are mixed in between some banks that are protected.

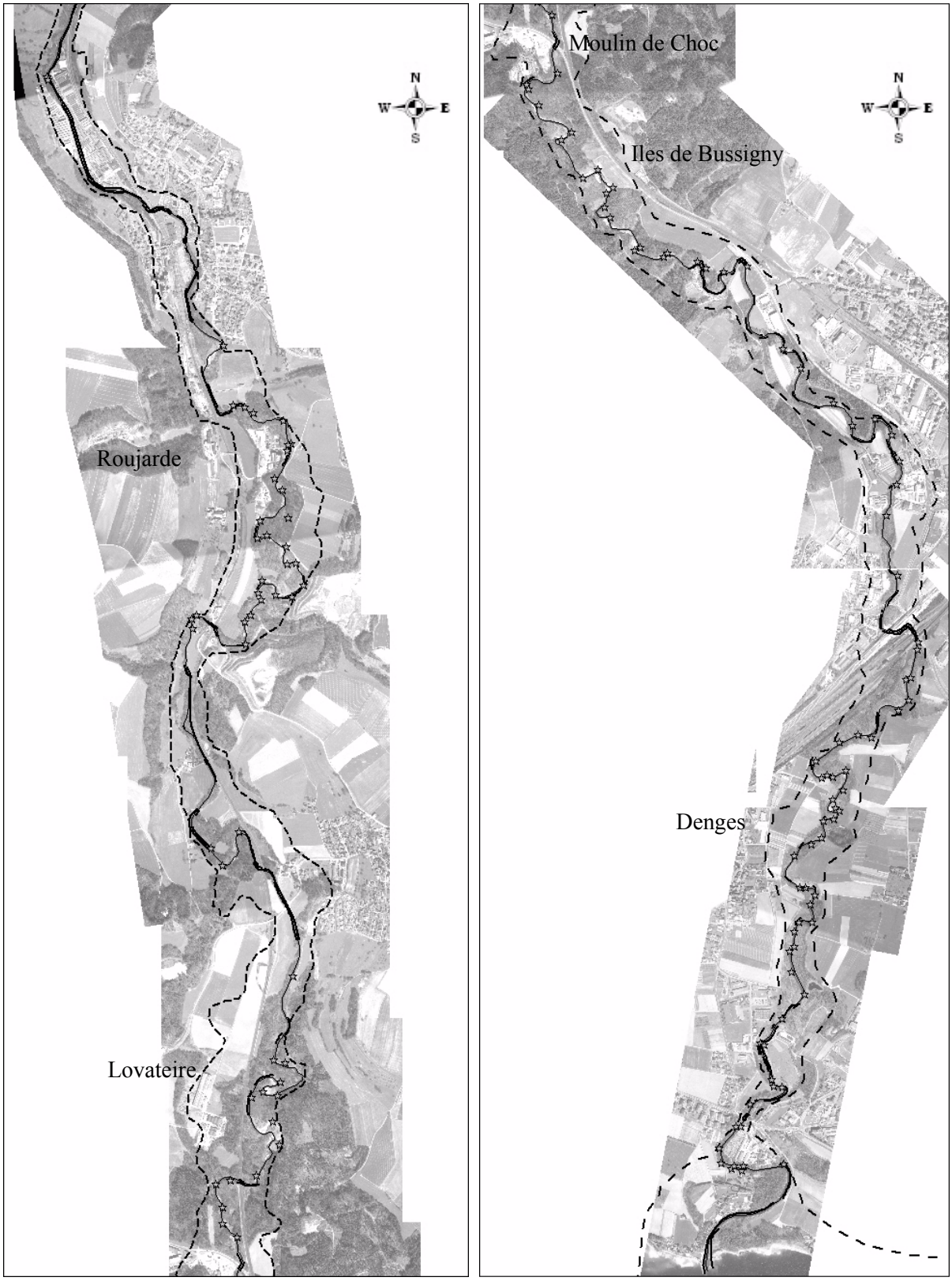

Figure 4.1. Erosion scars (stars) observed along the Lower Venoge River. Solid bold lines indicate bank protection and the dashed line indicates the line approximately 5 meters above the river.

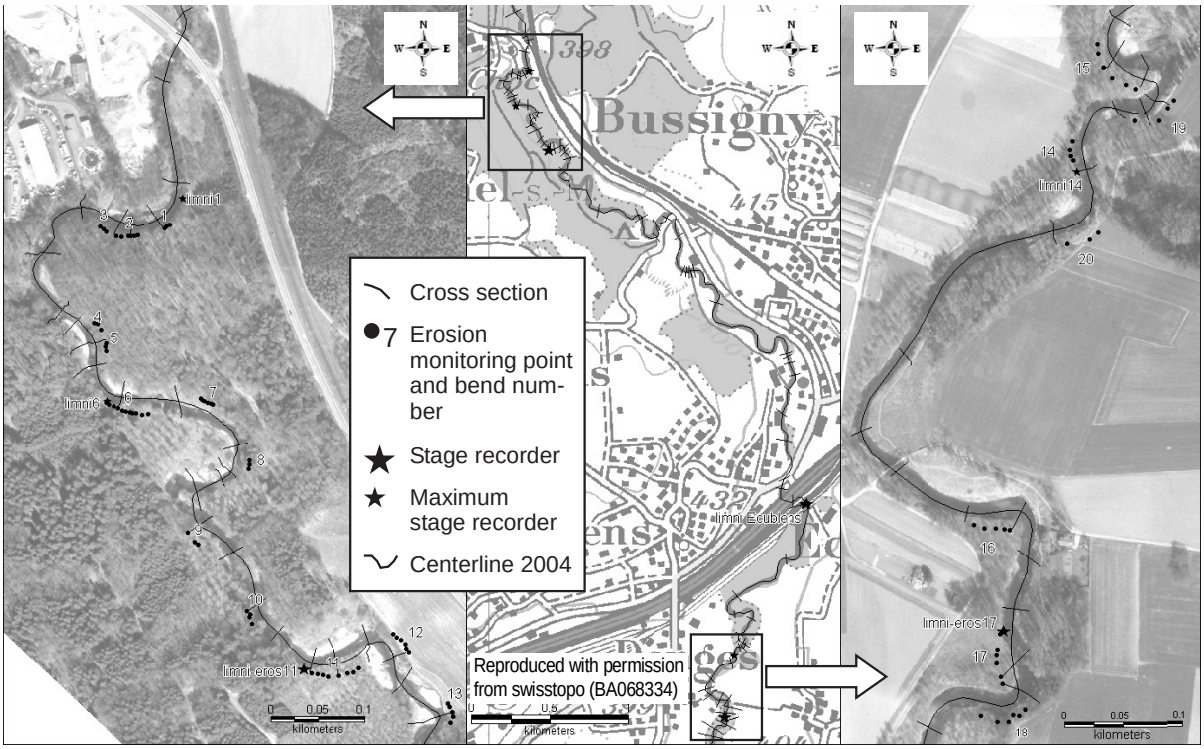

Figure 4.2. Study reach, new cross sections, water level measurements, and bends where erosion was monitored. Center background map: CP100 ©1997, Swisstopo.

4.2.1 Erosion monitoring

Due to the limited knowledge concerning the erosion of the Venoge, especially on the processes occurring, it was decided that erosion monitoring should be undertaken. A review of possible methods to use was undertaken before choosing the methods to be applied.

4.2.1.1 Possible methods

A review of possible methods for "the measurement of river bank erosion and lateral channel change" was done by Lawler in 1993. A summary of his review with some additional comments based on recent advances is given here.

Measurement techniques can be divided into three classes based on the timescale that is measured (Lawler, 1993):

1. long timescale (10-10’000 years): sedimentological evidence, botanical evidence, and historical sources
2. medium timescale (0.5-20 years): planimetric resurvey and repeated cross-profiling
3. short timescale (event-10 years): erosion pins, the Photo-Electronic Erosion Pin (PEEP) system, bank profiling, and terrestrial photogrammetry and laser scanning

Since the objective of the streambank erosion monitoring is to use the data for the calibration of erosion and bank failures, it is necessary to use methods adapted to a short timescale. The following paragraphs give details on short timescale methods:

1. Erosion pins: Lengths of rod are inserted into the bank leaving a small portion visible. Measurements are made before and after discharge events or on a certain schedule. Measurements are made with a caliper or ruler depending on the precision required. The frequency of the measurements depends on the purpose of the study. Pins are usually in lengths of 25-50 cm with a diameter of 2 - 6 mm. They should be non-rusting and strong enough to resist bending due to debris flow and/or installation in hard material. The advantages of the system are its suitability in a wide range of fluvial environments, its simplicity, cheapness, and the precision possible. The disadvantages include the representativeness of point measurements for spatial erosion assessment, bank swelling or contraction that can causes difficulties in reading interpretation, pin movement or loss due to dislodging by debris or mass failures, and the effect of the pins on the bank conditions (turbulence around pins, reinforcement in cohesive soils, disruption of gravel imbrication). Erosion pins must be used in a network to produce meaningful measurements. These networks should have a longitudinal spacing of 1-5 meters and use two or more pins in a vertical profile (Thorne's recommendation (1981) in Lawler, 1993) to capture the spatial variations of erosion.
2. PEEP sensor: Lawler et al. (1997) refer to the PEEP sensor as a "self-reading erosion pin". It is a "relatively simple optoelectronic device consisting of an array of photovoltaic cells (photodiodes) connected in series and enclosed within a transparent acrylic tube. It outputs an analogue millivolt signal directly proportional to the length of the tube which is exposed to light" (HydroScientific, 1999) (figure 4.3). To eliminate the problem of varying luminosity during the day and also due to turbid water conditions, the sensor uses reference photodiodes that are placed at the beginning and end of the measurement zone. Using the outer reference photodiode measurement, the Photovoltaic Ratio, *Rpp* (Hydroscientific, 1999), can be calculated:

$$Rpp(\%) = (V_{cs}/V_{rc}) \times 100 \qquad \textit{Eq. 4.1}$$

   where V_{cs} is the voltage of the cell series and V_{rc} is the outer reference cell voltage. The PEEP user guide suggests then the use of the linear regression formula:

$$L = c + d \times Rpp \qquad \textit{Eq. 4.2}$$

   to calculate the exposed length, L, in mm of the sensor. Sensors come in two different lengths, 50 cm and 66 cm. The user guide suggests the calibration of the coefficients c and d in situ. Otherwise, factory values of c and d can be used. Besides the photodiodes, there are also thermistors incorporated in recent versions of the sensor (figure 4.3) so that important erosion or mass failure can be detected during the night. This detection works when the inner thermistor registers a different temperature value due to the soil around it. The advantage of such a system is of course the information that can be gained on the erosion process by following it continually. The disadvantage of the system is the installation necessary and the possible loss of the apparatus in the case of a large bank failure.
3. Bank profiler: A third option mentioned by Lawler (1993) as a medium timescale option, the bank profiler (figure 4.4), could also be used at a shorter time scale for rapidly eroding banks. The horizontal and vertical stadia rod provide datums which can be used to measure down and over to

record the bank position. The difference in bank position at a certain depth will give the erosion at that depth. To overcome the inaccuracies possible due to poor positioning of the horizontal stadia rod, Lawler (1993) suggests using a graduated profile frame which can be inserted into receiving sockets set in the bank. To ease the vertical and horizontal measurements, he then suggests the use of a double rack and pinion system for the measuring rod. The advantages of this type of system is that no flow disturbance is created and that there is no risk of pin loss. The disadvantage of course is the loss in accuracy, although this can be largely overcome with the relocatable bank profiler of Lawler. Another disadvantage that can occur can be the difficulties associated with maintaining the datums. Finally, the measurements are more time-consuming than erosion pins and the profiling equipment is more cumbersome for transport.

4. Terrestrial photogrammetry and laser scanning: These two measurement techniques are grouped together because the desired output, a DTM of the bank, is the same. Terrestrial photogrammetry has been used in a few cases already (Lawler, 1993), but no terrestrial laser scanning examples for measuring bank erosion were found in literature. Airborne laser scanning data has already been used for determining bank erosion (Thoma et al., 2005), but would not be practical for the event scale nor for precise measurements of erosion at the bend length. Laser scanning has the advantage of the number of points that can be obtained very quickly. With an appropriate filter, the bank vegetation could be removed leaving the points that can be interpolated to produce a DTM of the bank. The disadvantage of the system is the cost of the laser scanner and the setup time necessary for installing precise reference points where the scanner tripod can be setup. In some cases, vegetation and trees might make it nearly impossible to implement, but this is the case for all of the methods.

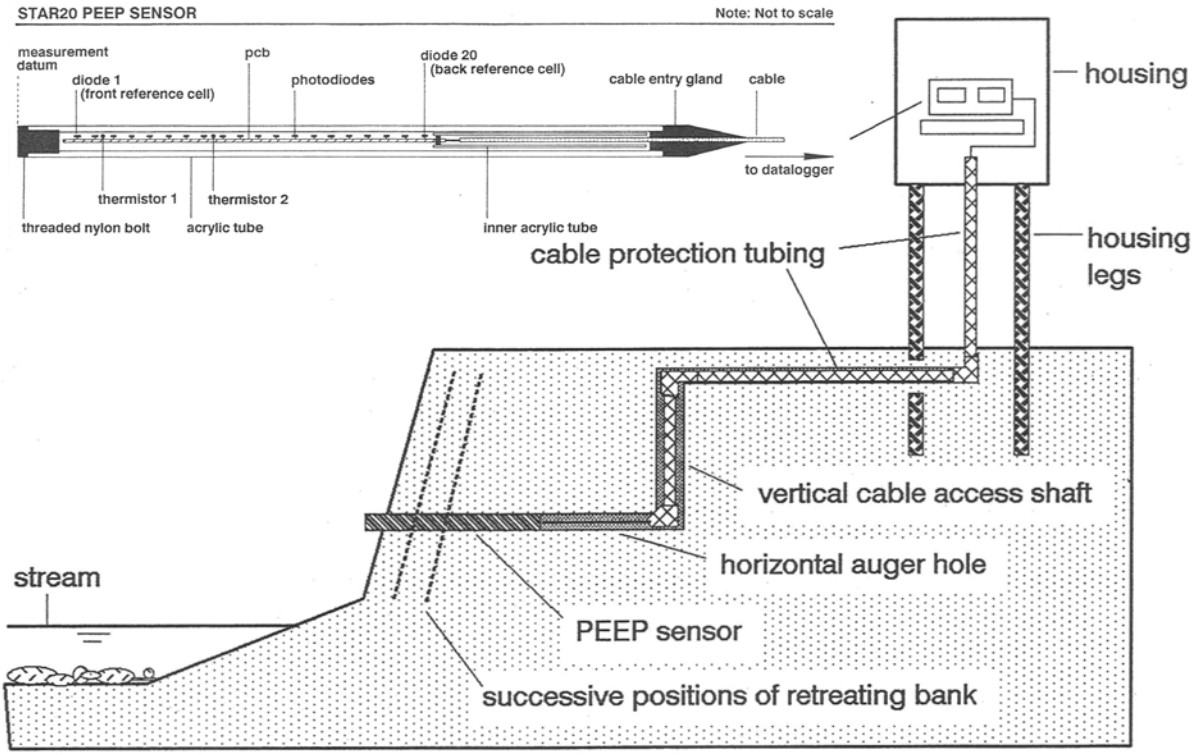

Figure 4.3. PEEP sensor and its typical installation for measuring bank erosion (from the PEEP user guide (HydroScientific, 1999))

4.2.1.2 Chosen methods

Erosion pins were chosen due to their simplicity of use. Knitting needles, as suggested by Lawler (1993) of 40 and 50 cm lengths were used to begin with. The heads on the needles, which Lawler found practical for numbering, were found to be impractical because of the added difficulty for measuring and also due to the heads busting when the needle had to be hammered into the bank. Inox rods 50 cm long of 5 mm diameter proved to be more practical.

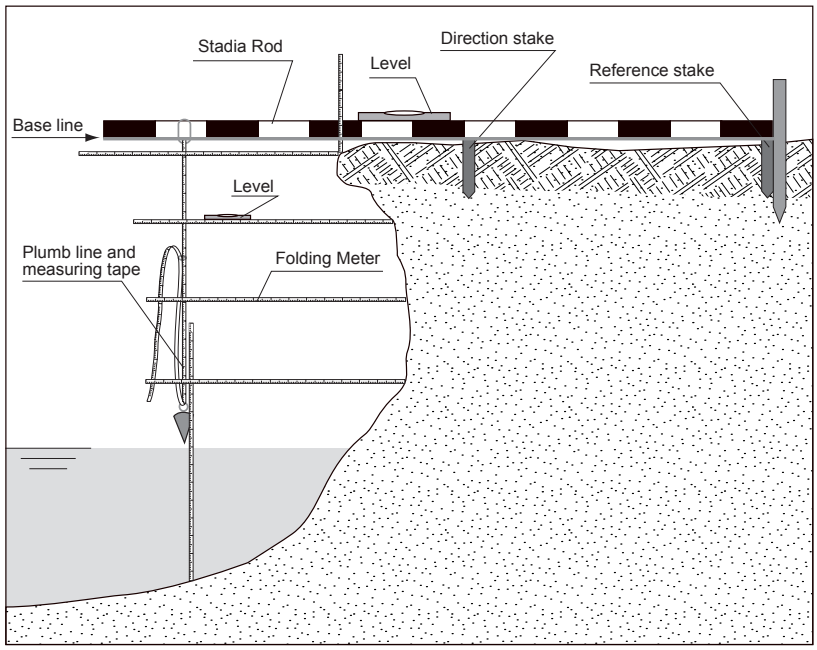

Figure 4.4. Bank profiling system used for the Lower Venoge study

Two to four erosion pins were put in each vertical profile and a minimum of three vertical profiles were used for each measurement group. Each measurement group is called a bend, although sometimes a real bend encompasses two or three erosion monitoring bends. The twenty erosion monitoring bends can be seen in figure 4.2. One hundred and eighty pins were installed in the 12 bends in the Bussigny reach and 120 were installed in the Denges reach. Installation of the 300 pins was done on November 11, 12, 19, and 20 of 2003. Figure 4.5 shows a small bend of three verticals each with 3 pins. The pins were only possible to find by putting marker stakes on the top of the bank.

Fortunately, a 15 year return period flood occurred on January 15, 2004, wiping out nearly half of the erosion pins. This allowed for the bank profiling method to be adopted where necessary. Bank profiling was done for all measurement points during the course of the spring of 2004 in the case of future pin losses so that pins could be reinstalled if necessary. The bank profiling method adopted was less precise, but was suitable for measuring mass wasting. The combination of using pins in slowly eroding bends and the bank profiler in bends where rapid change was occurring due to mass wasting proved to be sufficient. Figure 4.5 shows how the bank profiling system was setup. The first operator (he is not in place in figure 4.5 because he is taking the picture) assures the level based on a reference stake that is at ground level. A second stake, closer to the bank, that is also pounded to ground level gives the direction of the measurement. The second operator then measures down the plumb line a specified distance (the same from visit to visit) and measures over to read a distance indicating the bank position.

Besides the erosion pins and the bank profiler, two PEEP sensors were installed in the spring of 2004 (location of big stars (together with stage recorder) in figure 4.2). Their installation was very difficult due to roots and gravel encountered during boring of the horizontal and vertical conduits. Their installation was also complicated by the need to place the datalogger in a safe place, to avoid a bank failure that might drop the datalogger into the river and destroy it, yet in a place that erodes enough to

make it worth the installation. The datalogger was also used to record water depths from a submersible pressure transducer.

Figure 4.5. Erosion monitoring on the Lower Venoge River. Bottom shows a small monitoring bend (pin locations marked by arrows). Upper left shows the pin installation. Upper right shows the bank profiler.

4.2.2 Flow monitoring

Besides the erosion monitoring, maximum stage recorders and continuous stage recorders were used to monitor flow depths (small and big stars in figure 4.2 respectively). The planned use of the water depth information resulting from these recorders is for the calibration of Manning coefficients to ensure that mean velocities, and indirectly mean shear stresses, are relatively correct throughout the detailed study area.

Maximum stage recorders were fabricated in-house by the HYDRAM technician, Alex Amiguet. A metallic ruler is suspended by the cap of the galvanized tube. On this ruler is a red tape, which loses its color as water touches it. The cap of the stage recorder tube was surveyed so that its position and elevation were known. The resulting measurements could then be transformed to an absolute water surface elevation. The red tape was changed of course after each high flow event.

Continuous stage recorders used submersible pressure transducers and were connected to HydroMadd dataloggers. The pressure transducer was placed in an appropriate galvanized tube and its bottom rested on a cross at the bottom of the tube. The elevation of the cross was determined by surveying, allowing the resulting measurements to be transformed to absolute water surface elevation. Recording was done every 15 minutes.

Besides the installed stage recorders, the federal continuous stage recorder data for the station of Ecublens, Les Bois (figure 4.2), was available and extremely helpful. A rating curve for this station is maintained by the National Hydrological Service (SHN) of the Swiss Federal Office for Water and Geology (FOWG). Flow, water level, and temperature evolution can be followed on the internet as it is updated generally every two hours (http://www.bwg.admin.ch/service/hydrolog/f/2432.htm). Digital data was available from the SHN.

4.2.3 Measured values

4.2.3.1 High flows and stage recorder values

The continuous stage recorders, limni11 and limni17, recorded water depths from 26.03.2004 to 14.08.2005. Holes in the measured values occurred during the following periods: 01-03.05.2004, 19-21.05.2004, 15.06.2004-02.07.2004, 18-20.07.2004, 15-30.09.2004, 19.11.2004-21.12.2004, 06-20.01.2005, 28.05.2005-17.06.2005, and 03.07.2005-29.07.2005. Besides those measurement holes, limni17 measurements had another hole during the period 03-17.08.2004 and measurements deviated from the calibrated values during the period 01.03.2005-17.06.05.

The high flow events during the erosion monitoring period are given in table 4.1. The event length and volume are based on 9 m^3/s starting and ending discharges. The high flow events of 14.01.2004 and 26.10.2004 were particularly strong and can be evaluated at 11 and 4 year return periods, respectively, according to the Gumbel distribution shown in figure 5.13. The hydrograph of the 14.01.2004 high flow event is shown in figure 5.15, while that of the 26.10.2004 event is shown in figure 4.6. Due to the

relatively small discharge inputs between the limni11, limni17, and the Ecublens stage recorders, approximate rating curves for limni11 and limni17 could be produced using the Ecublens discharges of the 26.10.2004 event (figure 4.6).

Start date	Q peak (m^3/s)	Event length (h)	Volume (m^3)	Date peak	Erosion measuring date	Note
					11,12,19,20.11.2003	installation pins
28.11.2003	4.48			28.11.2003	04.12.2003	
12.01.2004	77.793	256.6	2.36E+07	14.01.2004	28.01.2004	followed event 14-19.01.2004
					11.02.04-10.03.04	change of pins to stadia rod
14.03.2004	12.157	20.0	7.80E+05	14.03.2004	18.03.2004	
20.03.2004	11.169	51.3	1.92E+06	21,22.03.2004	24.05.2004	snow melt; two peaks
16.07.2004	10.908	0.3	9.73E+03	16.07.2004		
24.07.2004	10.495	0.5	1.68E+04	24.07.2004	25.07.2004	
19.08.2004	19.237	38.1	1.93E+06	20.08.2004	30.08.2004	
19.10.2004	14.655	43.9	1.92E+06			
26.10.2004	61.412	139.5	1.11E+07	26.10.2004	09.11.2004	followed event 26-29.10.2004
19.12.2004	25.253	35.1	1.92E+06	20.12.2004	17.01.2005	
12.02.2005	22.334	69.3	3.96E+06	13.02.2005	28.02.2005	
24.03.2005	14	129.5	4.78E+06	27.03.2005	11.04.2005	snow melt
24.04.2005	20	126.0	6.05E+06	25.04.2005	26.09.2005	

Table 4.1. High flow events during the erosion monitoring period. Discharge information is derived from the Ecublens stage recorder.

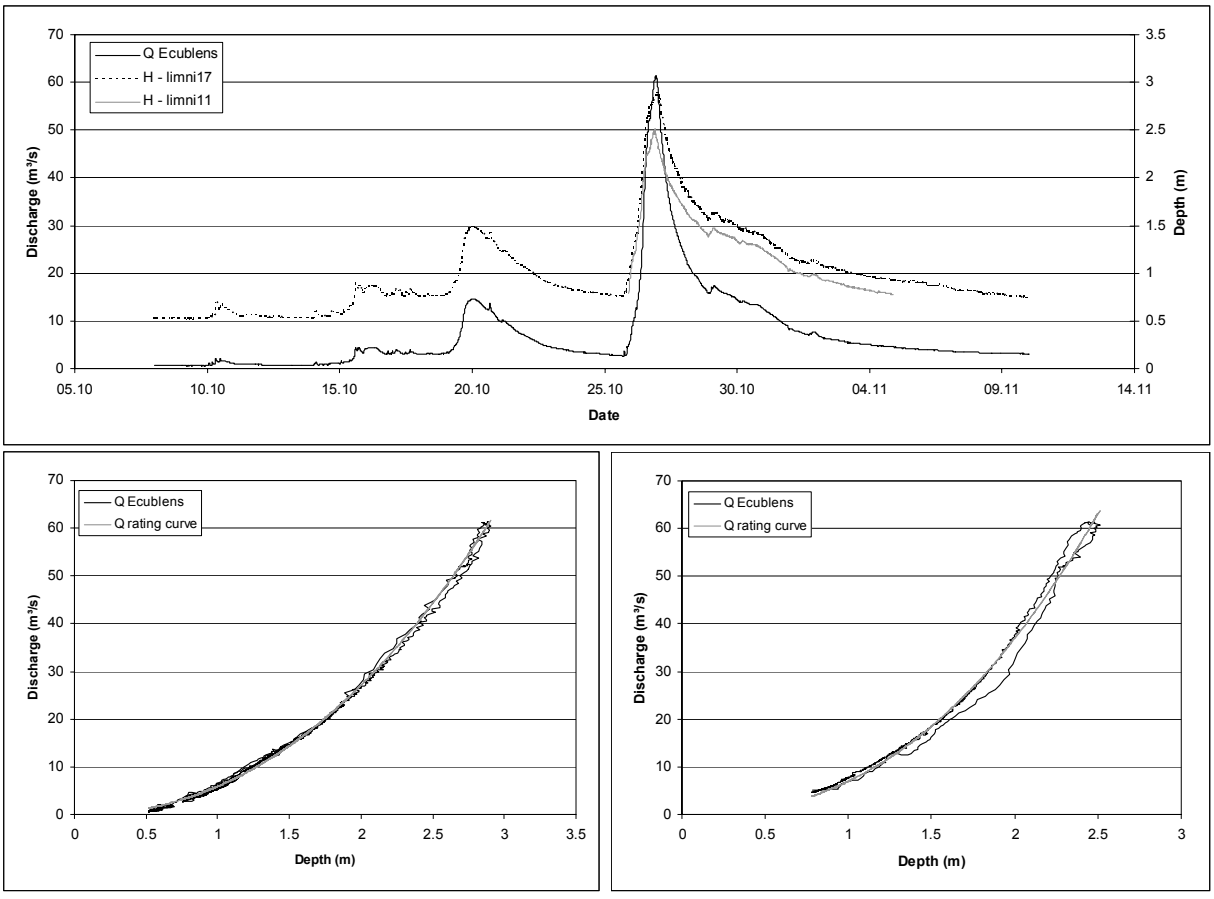

Figure 4.6. October 26, 2004 high flow event. Rating curves for the limni17 (left) and limni11 (right) based on the Ecublens discharges.

The maximum stage recorders also provided important water depth readings. Those readings are shown in figure 4.7. It was possible with the maximum stage recorders to record not only the maximum event values, but also to measure the water surface at the time of visit. This extended considerably the number of measurements, especially for the stage recorders that were placed relatively high and recorded only two or three high flow events.

The stakes marking each erosion measuring point also served as maximum stage recorders. High water marks during the October 26, 2004 flood were found on many of the stakes and their water surface elevations could be determined by the reference stake elevations. Besides the October 2004 high water marks, some high water marks were available from the January 2004 flood as well as others from the HYDRAM Venoge study (Lance et al., 1997). Those values are given in table 4.2.

distance to outlet (m)	point id	discharge	wse 2004	date	max water depth 1996 report	thalweg 1996 report	wse 1996 report
10323	360	50			2.5	394.76	397.26
10282	361	55			3.6	393.26	396.86
10104	limni1	57	396.365	26.10.2004			
10053	2.1	57	396.14	26.10.2004			
9804	4.1	60	395.61	26.10.2004			
9728	limni6	60	395.49	26.10.2004			
9635	7.1	60	395.18	26.10.2004			
9625	7.4	60	395.03	26.10.2004			
9583	DELAISSE1	78	395.014	14.01.2004			
9549	8.3	60	395.21	26.10.2004			
9269	limni-eros11	60	394.31	26.10.2004			
9087	DELAIS3	78	393.898	14.01.2004			
8213	371	55			4.6	387.64	392.24
7771	390	50			2.8	388.19	390.99
7313	412	55			1	388.57	389.57
7297	413	60			3.5	385.62	389.12
5353	460	70			4.4	381.47	385.87
5241	461	50			3.5	381.65	385.15
4910	limni Ecublens	60	384.47	26.10.2004			
3510	15.2	60	381	26.10.2004			
3330	limni14	60	380.65	26.10.2004			
3275	20.2	60	380.45	26.10.2004			
3005	470	55			3.7	376.28	379.98
2963	471	60			3.3	376.93	380.23
2859	16.4	60	379.93	26.10.2004			
2734	limni-eros17	60	379.74	26.10.2004			

Table 4.2. Measured high water marks for the study reach. 1996 report values come from the HYDRAM Venoge study (Lance et al., 1997).

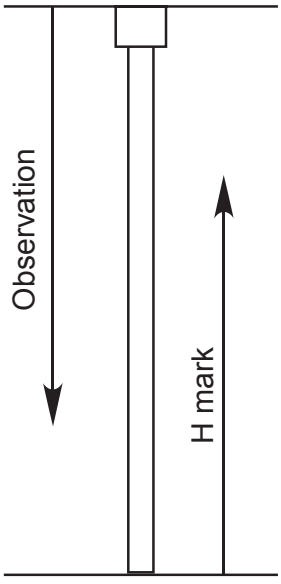

Maximum Stage Recorder Limni1

top tube	cap	top ruler	ruler	Elevation 0
396.406	0.045	396.361	1.500	394.861

time of visit	obser-vation (m)	*WSE (m)*	*Ecublens Q*	Date Qmax	H mark (m)	*WSE mark (m)*	*Ecublens Qmax*
15.04.04 14:48	1.88	*394.53*	*2.4*				
21.05.04 08:44	1.98	*394.43*	*1.3*				
02.06.04 10:45	1.60	*394.81*	*4.7*				
15.06.04 13:51	2.04	*394.37*	*0.8*				
19.07.04 14:20			*0.5*	16.07.04	0.16	*395.02*	*10.9*
17.08.04 11:22	1.80	*394.61*	*3.1*	24.07.04	0.17	*395.03*	*10.5*
30.08.04 13:30	1.90	*394.51*	*2.4*	20.08.04	0.63	*395.49*	*19.2*
26.10.04 14:20	0.25	*396.16*	*47.2*				
27.10.04 14:30	0.62	*395.79*	*30.9*				
28.10.04 14:20	1.00	*395.41*	*18.2*	26.10.04	1.50	*396.37*	*61.4*
03.11.04 13:10	1.57	*394.84*	*5.3*				
21.12.04 15:44	1.46	*394.95*	*7.2*	20.12.04	0.79	*395.65*	*25.3*
31.01.05 10:04	1.83	*394.58*	*2.7*				
22.02.05 16:15	1.75	*394.66*	*3.6*	13.02.05	0.70	*395.56*	*22.3*
23.03.05 14:00	1.40	*395.01*	*8.3*		0.10	*394.96*	
05.04.05 12:25	1.74	*394.67*	*3.7*	27.03.05	0.41	*395.27*	*14.0*
25.04.05 12:30				25.04.05	0.63	*395.49*	*20.0*
29.04.05 12:30	1.31	*395.10*	*8.9*	29.04.05	0.19	*395.05*	*8.90*
12.05.05 13:15	1.86	*394.55*	*2.9*				

Maximum Stage Recorder Limni6

top tube	cap	top ruler	ruler	Elevation 0
395.997	0.045	395.952	1.500	394.452

time of visit	obser-vation (m)	*WSE (m)*	*Ecublens Q*	Date Qmax	H mark (m)	*WSE mark (m)*	*Ecublens Qmax*
15.04.04 15:00			*2.4*				
21.05.04 08:54	2.49	*393.51*	*1.3*				
02.06.04 10:30	2.18	*393.82*	*4.5*				
30.08.04 15:15			*2.3*	20.08.04	0.09	*394.54*	*19.2*
28.10.04 15:00	1.61	*394.39*	*17.9*	26.10.04	1.04	*395.49*	*61.4*
22.02.05 15:50	2.30	*393.70*	*3.6*	20.12.04	0.24	*394.69*	*25.3*

Maximum Stage Recorder Limni14

top tube	cap	top ruler	ruler	Elevation 0
380.624	0.045	380.579	1.500	379.079

time of visit	obser-vation (m)	*WSE (m)*	*Ecublens Q*	Date Qmax	H mark (m)	*WSE mark (m)*	*Ecublens Qmax*
15.04.04 16:00			*2.3*				
21.05.04 09:36	2.20	*378.43*	*1.3*				
02.06.04 09:40	2.00	*378.63*	*3.3*				
28.10.04 16:30	1.41	*379.21*	*17.3*	26.10.04	1.57	*380.65*	*61.4*
22.02.05 15:20			*3.5*	20.12.04	0.50	*379.58*	*25.3*

Figure 4.7. Maximum stage recorder measurements. Top left shows recorder limni6.

4.2.3.2 PEEP

The PEEP measurements have the same measurement periods and missing value periods as that of the accompanying stage recorder. Before installation, laboratory and field calibrations were conducted. The

laboratory calibrations gave calibrated *c* and *d* values (equation 4.2) very different than those suggested in the PEEP manual (HydroScientific, 1999). After in situ calibration (figure 4.8), it was clear that the laboratory luminosity played a role in the poor laboratory calibration. The in situ calibration for the two PEEP sensors gave a good linear fit, and *c* and *d* values are similar to those of the PEEP manual.

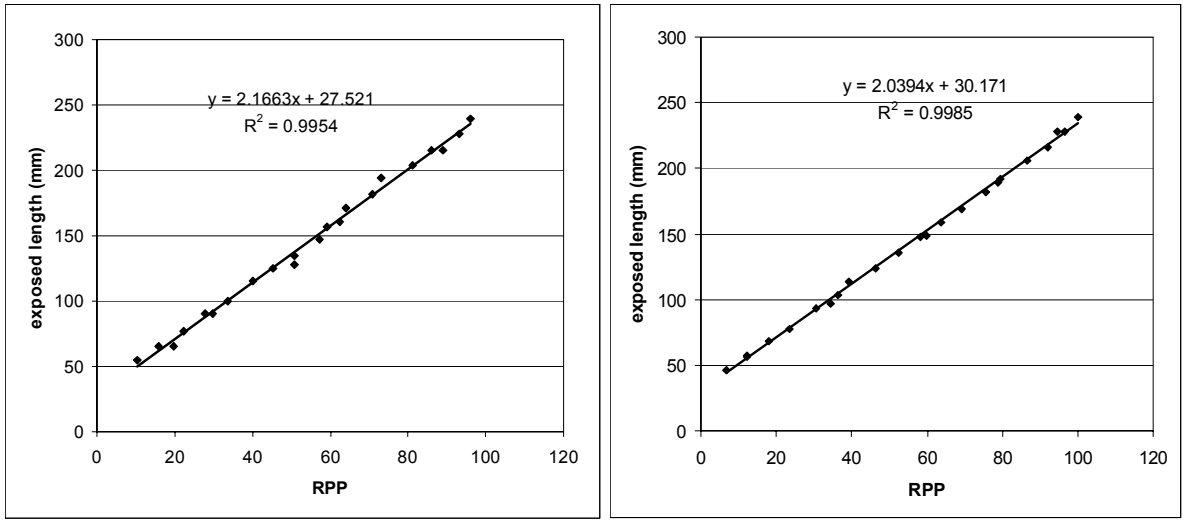

Figure 4.8. In situ calibration of the PEEP sensors during overcast conditions. Eros11 is shown to the left and Eros17 to the right.

Typical measured values from the PEEP sensor are shown in figure 4.9. It is clear that the calculated exposed length varies too much throughout varying daily luminosity and is not practical for identifying precisely the evolution of fluvial erosion. It can be helpful though to determine the moment of a mass failure. A mass failure at the Eros17 sensor was detected on 27.04.2005. What could be assumed to be fluvial erosion by an erosion pin is clearly a small mass failure because the water level is below the sensor level and the length quickly jumps from approximately 56 mm to 125 mm. This sensor was installed among grass and tree roots. It is assumed that the root reinforcement to the soil failed causing the 6 cm mass failure. The final exposed length when demounted on 14.11.2005 was 15 cm on top and 18 cm on the bottom. The last calculated exposed length was 15 cm in August 2005 corresponding correctly to the observed value. The difference between the top and bottom exposed length would suggest a buttressing type added stability to the bank. The middle erosion pin of bend 17.1 is approximately 1 meter downstream. A 6.5 cm "failure" occurred between 17.01.2005 and 28.02.2005 and then a 3 cm "failure" between 28.02.2005 and 11.04.2005. The 9-10 cm of erosion occurred at both spots, but at different times, confirming the important spatial variability of erosion and mass failure as reported by Lawler (1993).

The Eros11 PEEP sensor showed deposition during the measuring period. As the deposition seems to have occurred during several events, it is difficult to determine from the measured values the exact timing of the deposition. The initial exposed value was 65 mm and the final calculated value was 36 mm in August 2005. The sensor was found completely covered when demounted on 14.11.2005.

The experiences with the PEEP sensors allow the following conclusions:

- the PEEP sensor is difficult to install, especially in rooty, gravelly soils
- the installation process will most likely weaken the neighboring soil matrix during boring

- luminosity variation causes variation in the calculated exposed length which makes it nearly impossible to detect fluvial erosion
- when submerged the calculated exposed length was incorrect
- the sensor is useful for detecting mass failures

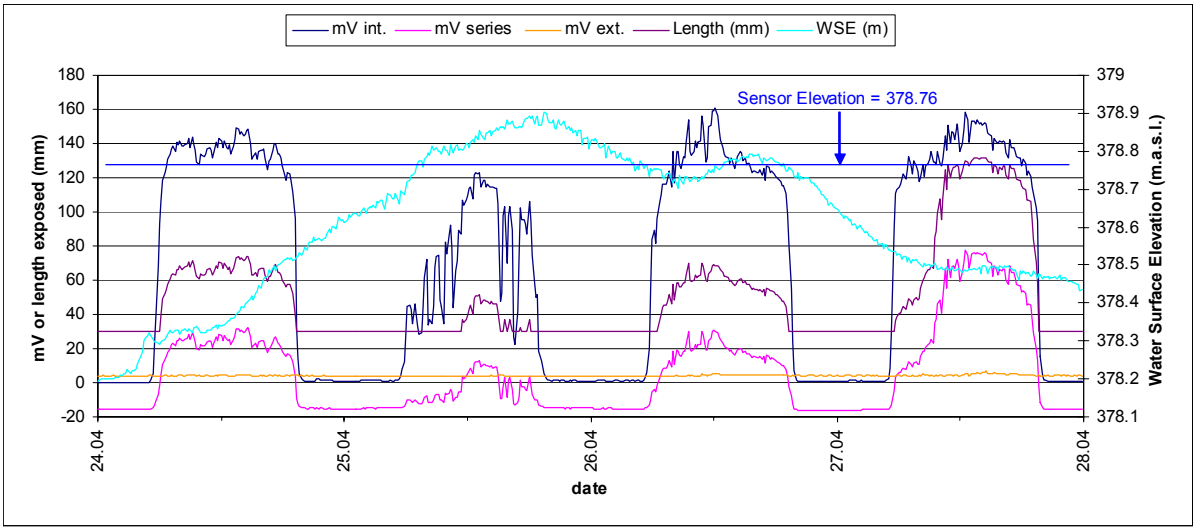

Figure 4.9. The small mass failure of the 17.1 erosion monitoring point measured by the Eros17 PEEP sensor on April 27, 2005.

4.2.3.3 Erosion pin and bank profiler

The erosion pin and bank profiling measurements were very time consuming. Three hundred measurements took between 2 and 2.5 days for two technicians. Installation of the 300 pins took 4 days and initial bank profiling of the 300 measurement points took also 4 days for two technicians.

The field notebooks and EXCEL note keeping evolved as the situations encountered became increasing complex. The first field book (left extract, figure 4.10) was designed simply for noting the erosion pin measurements. After the January 14, 2004 flood, bank profiling was begun for actively eroding banks resulting in a second field book in which lines necessary for the bank profiling were incorporated (middle extract, figure 4.10). Finally, a third field book was necessary to better track reference stake and baseline changes (right extract, figure 4.10). The meaning of the different measurements are shown in figure 4.11. This third system assumed no reference stake *y*, rod/stake *y*, and bank top *y* changes. These changes did occur though occasionally and had to be handled case by case. An improved note keeping system is shown in figure 4.11 in which boxes are available for all possible *x, y* measurements. Notice also that arrival and departure measurement boxes are available. This is necessary in the case of reference stake movement and for erosion pin changes when they must be pounded in or partially pulled out depending on the erosion/deposition evolution. Notice that erosion pin measurements can easily be noted on the bank profiling field book (as seen for bend 2.2 in the right table in figure 4.10). In the *x* column, the erosion pin length is noted. Other measurement boxes are left empty.

2.2		
Date	11.11.03	04.12.03
top	2	2
bottom	2	2.2
2.3		
Date	11.11.03	04.12.03
top	2	2
mid top	2	2
bottom	2	2.6

Date	depth	10.03.04
2.2	remarque:	
bank top	-23	111
top	-50	5.5
bottom	-100	4
2.3	remarque:	
dist. meas.	0	270
bank top	-70	180
top	-90	70
mid top	-130	61
bottom	-160	89
bed	-260	260

Date	depth	30.08.04
2.2	remarque:	
dist. mes.		
rod/stake		
ref x		
bank top	-23	235
top	-50	5.5
bottom	-100	24
bed	-200	
2.3	remarque:	
dist. mes.		270
rod/stake		0
ref x		0
bank top	-61	190
top	-90	72
mid top	-130	51
bottom	-160	88
bed	-260	273

Figure 4.10. Evolution of the erosion measurement field book due to the complex situations encountered.

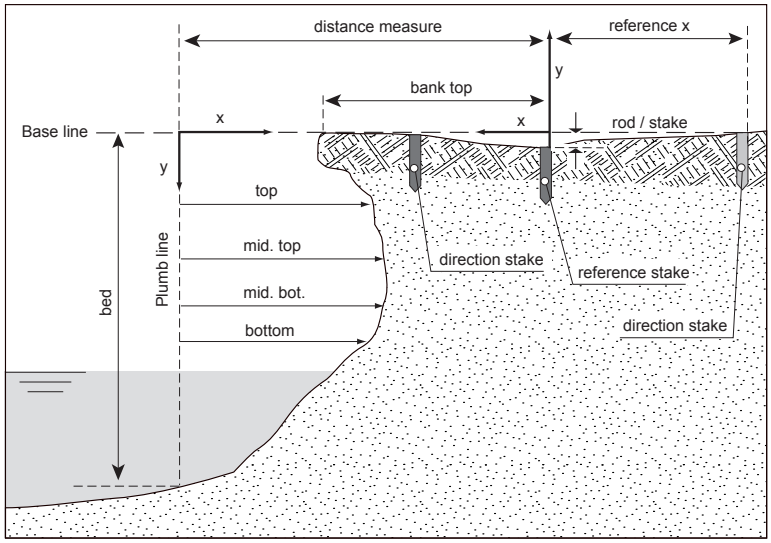

	date	
	arrival	depart.
dist. mes.		
rod/stake		
ref x		
bank top		
top		
mid top		
mid bot		
bottom		
bed		

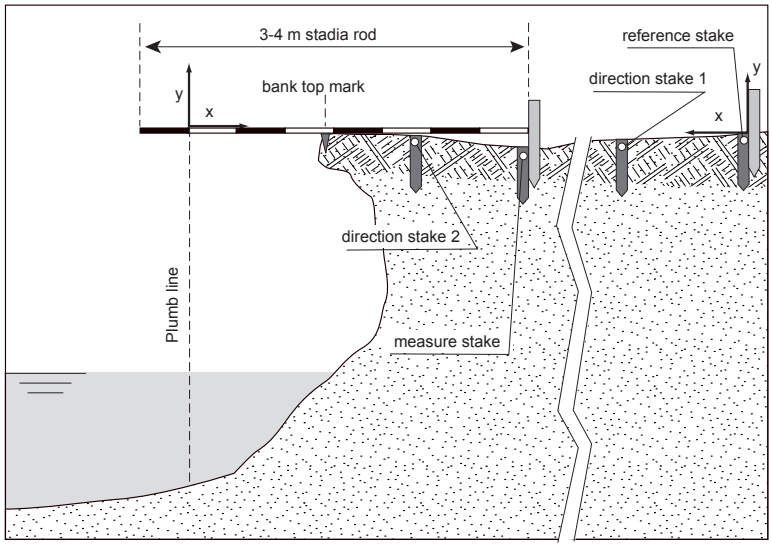

	date			
	arrival		depart.	
	x	y	x	y
meas stake	reference system 1			
meas stake	reference system 2			
bank top				
top				
mid top				
mid bot				
bottom				
bed				

Figure 4.11. Bank profiling measurement system used (top) and recommended (bottom)

The complete bank retreat measurements are reported in appendix 6. The cumulative bank top position changes are given in table 4.3 and that of the bottom position changes are shown in table 4.4. Notes on bank erosion and bank mass failure are included in table 4.3.

As is expected and witnessed in tables 4.3 and 4.4 is that erosion and bank failures are not directly correlated with maximum discharge or the volume of the flood. This is assumed to be largely due to the predisposition of a bank to fail (basal sediment condition and bank soil-vegetation heterogeneities) as well as the flow conditions which change due to the influence of neighboring failed bank soil and vegetation. It is expected to find correlation between the event flood volume and discharge and reach bank erosion. Correlation of reach bank erosion, represented by the sum of all of the average measured profile erosion, is compared against maximum event discharge, flood volume (based on 9 m³/s start and end), and the product of Qmax and flood volume (figure 4.12). The graphs show important variability for the lower discharge events, but that the linear relationship relating erosion and the product Qmax-flood volume explains quite well the quantity of bank erosion. The number of bank failures is also well correlated with the product Qmax-flood volume.

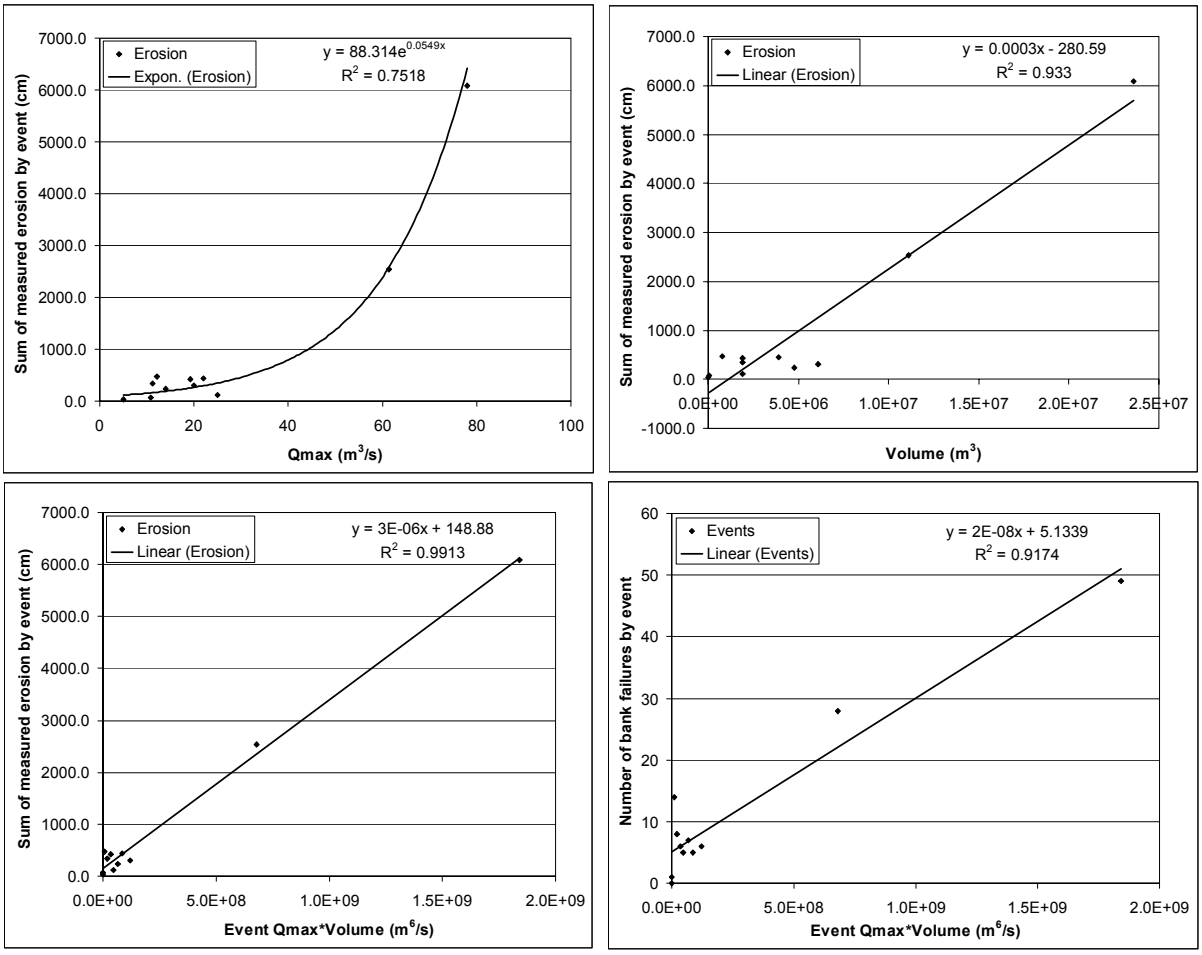

*Figure 4.12. Relationship of event erosion compared to maximum event discharge, flood volume, and Qmax*flood volume, and bank failures compared to Qmax*flood volume*

The bank mass failures observed on the Lower Venoge monitoring sites are slab (block) failures, soil falls, planar slides, and cantilever failures (table 4.3). Slab failures and soil falls are the most common. They occurred or could occur on all of the monitored bends except for bend 18, where there was planar

sliding of the upper glacial till on a fine silt layer. Soil fall and slab failures are difficult to distinguish between because it is unknown to what degree the toe is being undercut before failure. Bank failure mechanisms other than slab failures are noted in table 4.3. Cantilever failures are also frequent, but serious cantilever failures due to trees toppling into the river are a minority of the failures simply due to the frequency of tall trees near the banks.

Figure 4.13. "Carpet" of the soil-root system left after a soil fall

The most frequent bank mass failure mechanism observed was that of slab failure underneath a vegetated surface (figure 4.13). If the root reinforcement of the vegetated surface was sufficient, a "carpet" of the vegetated surface would remain after slab failure to protect the upper part of the bank. This sometimes caused negative bank retreat measurements for the top measurement zone. The sequence of events was often the following: toe erosion, slab failure accompanied by the incomplete fall of the vegetation zone producing a "carpet" protection of the upper bank, failure of the upper bank "carpet" after weakening of the soil-root system by subaerial processes or fluvial erosion. The failed sediments of the bloc failure and upper bank "carpet" mostly deposit at the bank toe and must be eroded away before a new slab failure can occur.

Figure 4.14. Observed tension cracks at bend 3.3 during the drawdown of the October 26, 2004 flood

Another process observed in the slab failures was that of tension cracking (figure 4.14). Tension cracking was only observed during high flows or during the following days. The tension cracking occurred close to the bank and multiple tension cracks occurred. It is assumed these tension cracks are critical in determining the width of the slab that fails. It is also assumed that the tension cracking will increase infiltration promoting a more rapid failure (Abramson et al., 2002).

Banks are considered to have failed if the bank top measurement exceeded 20 cm (table 4.3). Twenty centimeters was decided as the criteria because of measurement uncertainty associated with the bank top measurement. Slab failures caused bank top retreat of 20 to 250 cm, while tree toppling cantilever caused

bank retreat of up to 350 cm. Of course the bank retreat amount in such a case depends on the rooting system of the tree. Bank overhang was observed to be as much as 85 cm.

The tree cantilever failures bring up the question of the effect of vegetation on bank stability. Vegetation has positive and negative effects on bank stability. Those effects are relatively well documented (ASCE, 1998a, Abramson et al. 2002). An indirect effect of tree cantilever failures, though, is that of the failure on the flow field. A tree cantilever failure was observed at bend 7.2 on 30.08.2004 (table 4.3 and figure 4.15). Rapid bank retreat occurred throughout bend 7 during the preceding year. No bank retreat occurred during the year after the failure despite the important 26.10.2004 high flow. There is no question of the positive effect of the bend 7.2 tree cantilever on the reduction the eroding shear stresses. Daniels and Rhoads (2004) measured the effect of outer bend woody debris on the flow field and showed that the maximum turbulent kinetic energy shifted away from the outer toe.

Figure 4.15. Tree cantilever failure of bend 7.2

The observed Lower Venoge bank retreats are largely fluvial erosion dominated. The slab failures seem to be very small and possibly multiple during a single event. It is the rate of erosion of the bank toe and the basal sediments that seem to dictate the bank retreat rate. The erosion rate of the monitored bends is evident with the bottom erosion measurement. As can be seen in table 4.4, some bends will quickly evacuate basal sediments while others do not have sufficient shear stresses to evacuate them.

Piping is another form of erosion. Soil water exfiltration was seen in bends 9 and 10 and some piping is assumed to have occurred in these bends although it is assumed that no significant erosion occurred because of the piping. The exfiltration in these banks reflects the sometimes saturated nature of these banks which is probably more important than the piping itself.

date / bend	04.12.03	28.01.04	18.03.04	24.05.04	26.07.04	30.08.04	09.11.04	17.01.05	28.02.05	11.04.05	26.09.05	notes
1.10	0.00	0.00	0.00	0.00	0.00	0.00	0.00	0.00	0.00	0.00	0.00	
1.20	0.00	0.00	0.00	0.00	0.00	0.00	0.00	0.00	0.00	0.00	0.00	
1.30	0.00	0.00	0.00	0.00	0.00	0.00	0.00	0.00	-6.00	-6.00	-6.00	
2.10	0.00	0.00	0.00	0.00	0.00	0.00	3.00	3.00	3.00	3.00	3.00	
2.20	0.00	0.00	0.00	0.00	-2.00	-20.00	-7.00	46.00	46.00	46.00	46.00	
2.30	0.00	0.00	0.00	0.00	-10.00	-10.00	-10.00	-10.00	-10.00	-10.00	-10.00	
2.40	0.00	31.00	31.00	36.00	36.00	36.00	36.00	38.00	41.00	46.00	46.00	
2.50	0.00	83.00	83.00	83.00	83.00	83.00	83.00	83.00	83.00	83.00	83.00	
2.60	0.00	83.00	83.00	83.00	83.00	83.00	88.00	88.00	88.00	93.00	103.00	
3.10	0.00	124.00	124.00	127.00	127.00	128.00	143.00	147.00	147.00	147.00	147.00	
3.20	0.00	132.00	137.00	142.00	142.00	142.00	142.00	142.00	137.00	137.00	137.00	
3.30	0.00	175.00	175.00	175.00	175.00	175.00	278.00	313.00	313.00	313.00	313.00	
4.10	0.00	0.00	0.00	5.00	5.00	5.00	88.00	88.00	88.00	88.00	88.00	
4.20	0.00	0.00	65.00	65.00	65.00	65.00	110.00	110.00	110.00	110.00	110.00	
4.30	0.00	0.00	0.00	-10.00	-10.00	0.00	35.00	35.00	35.00	50.00	50.00	
5.10	0.00	96.00	111.00	106.00	106.00	106.00	134.00	136.00	131.00	173.00	177.00	
5.20	0.00	9.00	9.00	9.00	9.00	9.00	9.00	9.00	9.00	9.00	9.00	
5.30	0.00	4.00	4.00	4.00	4.00	4.00	4.00	-1.00	-4.00	-4.00	-4.00	
6.10	0.00	0.00	8.00	18.00	18.00	18.00	18.00	18.00	18.00	18.00	43.00	
6.20	0.00	0.00	0.00	15.00	15.00	15.00	15.00	0.00	35.00	35.00	70.00	
6.30	0.00	90.00	95.00	90.00	95.00	95.00	125.00	165.00	165.00	175.00	175.00	
6.40	0.00	127.00	135.00	130.00	130.00	130.00	130.00	133.00	135.00	140.00	200.00	
6.50	0.00	81.00	81.00	96.00	96.00	96.00	96.00	96.00	96.00	96.00	116.00	
6.60	0.00	157.00	162.00	162.00	162.00	162.00	232.00	277.00	277.00	282.00	282.00	
6.70	0.00	160.00	160.00	160.00	160.00	160.00	380.00	380.00	380.00	380.00	380.00	
6.80	0.00	160.00	165.00	175.00	175.00	175.00	247.00	247.00	252.00	270.00	270.00	
6.90	0.00	144.00	144.00	144.00	144.00	144.00	159.00	159.00	259.00	259.00	259.00	
6.91	0.00	91.00	91.00	96.00	96.00	96.00	121.00	121.00	121.00	121.00	121.00	
6.92	0.00	67.00	72.00	82.00	82.00	82.00	92.00	127.00	132.00	132.00	132.00	
7.10	0.00	104.00	169.00	204.00	204.00	314.00	319.00	314.00	324.00	329.00	329.00	
7.20	0.00	190.00	231.00	281.00	281.00	501.00	506.00	516.00			521.00	block failure, tree cantilever
7.30	0.00	129.00	154.00	249.00	249.00	254.00	254.00	254.00	256.00	254.00	264.00	
7.40	0.00	79.00	99.00	141.00	141.00	134.00	134.00	144.00	154.00	154.00	154.00	
7.50	0.00	204.00	243.00	253.00	253.00	253.00	248.00	253.00	253.00	258.00	258.00	
7.60		200.00	275.00	281.00	281.00	281.00	281.00	290.00	290.00	290.00	290.00	
8.10	0.00	10.00	10.00	15.00	15.00	15.00	70.00	70.00	70.00	85.00	85.00	
8.20	0.00	0.00	10.00	10.00	10.00	10.00	10.00	5.00	5.00	60.00	75.00	
8.30	0.00	183.00	183.00	183.00	183.00	183.00	183.00	183.00	183.00	183.00	209.00	block failure, tree cantilever
9.10	0.00		150.00	150.00	150.00	150.00	380.00	380.00	380.00	380.00	380.00	piping, block failure, tree cantilever
9.20	0.00		150.00	148.00	148.00	148.00	148.00	150.00	150.00	145.00	145.00	
9.30	0.00		150.00	152.00	152.00	152.00	152.00	152.00	152.00	152.00	152.00	
10.10	0.00	0.00	0.00	0.00	0.00	0.00	3.00	3.00	3.00	3.00	3.00	
10.20	0.00	4.00	4.00	4.00	4.00	4.00	4.00	4.00	4.00		-11.00	
10.30	0.00	13.00	13.00	13.00	17.00	17.00	1.00	1.00	1.00		1.00	
10.40	0.00	23.00	123.00	123.00	138.00	163.00	262.00	263.00	263.00	263.00	263.00	sandier, piping, block failure
11.10	0.00	0.00	0.00	0.00	0.00	0.00	15.00	15.00	15.00	15.00	15.00	
11.20	0.00	85.00	85.00	93.00	93.00	93.00	93.00	90.00	90.00	90.00	90.00	
11.30	0.00	1.00	1.00	3.00	3.00	3.00	3.00	58.00	58.00	58.00	58.00	
11.40	0.00	0.00	0.00	0.00	0.00	0.00	0.00	0.00	0.00	0.00	0.00	
11.50	0.00	100.00	100.00	105.00	105.00	105.00	105.00	108.00	248.00	248.00	258.00	
11.60	0.00	125.00	131.00	133.00	133.00	133.00	290.00	290.00	290.00	290.00	290.00	
11.70	0.00	132.00	132.00	135.00	180.00	132.00	132.00	140.00	132.00	135.00	135.00	
11.80	0.00	132.00	132.00	127.00	134.00	134.00	134.00	134.00	136.00	132.00	132.00	
12.10	0.00	0.00	0.00	-1.00	-1.00	-1.00	-5.00	-11.00	-5.00	4.00	4.00	
12.20	0.00	0.00	0.00	0.00	0.00	0.00	92.00	90.00	90.00	113.00	113.00	
12.30	0.00	160.00	160.00	165.00	165.00	165.00	285.00	295.00	300.00	307.00	307.00	
12.40	0.00	150.00	155.00	160.00	160.00	160.00	215.00	220.00	225.00	225.00	250.00	
12.50	0.00	212.00	209.00	235.00	235.00	235.00	302.00	300.00	355.00	365.00	364.00	
12.60	0.00	245.00	245.00	235.00	235.00	235.00	313.00	313.00	370.00	370.00	380.00	
13.10	0.00	0.00	0.00	0.00	0.00	0.00	0.00	-8.00	-8.00	-8.00	-8.00	
13.20	0.00	0.00	0.00	0.00	0.00	0.00	35.00	40.00	50.00	63.00	63.00	
13.30	0.00	0.00	0.00	0.00	0.00	10.00	120.00	118.00	117.00	125.00	125.00	
13.40	0.00	0.00	0.00	0.00	0.00	0.00	40.00	38.00	75.00	80.00	85.00	
13.50	0.00	0.00	0.00	1.00	1.00	1.00	1.00	1.00	11.00	11.00	11.00	
14.10	0.00	0.00	0.00	0.00	0.00	0.00	0.00	0.00	0.00	0.00	0.00	
14.20	0.00	0.00	0.00	0.00	0.00	0.00	0.00	0.00	0.00	0.00	0.00	
14.30	0.00	0.00	0.00	0.00	0.00	0.00	0.00	0.00	0.00	0.00	0.00	
14.40	0.00	0.00	0.00	0.00	0.00	0.00	0.00		0.00			
15.10	0.00	115.00	115.00	125.00	125.00	125.00	125.00	125.00	125.00	135.00	140.00	
15.20	0.00	80.00	90.00	90.00	90.00	90.00	105.00	110.00	110.00	110.00	115.00	
15.30	0.00	70.00	90.00	95.00	95.00	95.00	390.00	390.00	385.00	385.00	395.00	block failure, tree cantilever
15.40	0.00	55.00	55.00	45.00	45.00	45.00	131.00	130.00	130.00	130.00	130.00	
15.50	0.00	78.00	78.00	78.00	78.00	78.00	88.00	88.00	93.00	93.00	93.00	
15.60	0.00	40.00	40.00	42.00	42.00	42.00	42.00	52.00	37.00	37.00	37.00	
16.10	0.00	0.00	0.00	0.00	0.00	0.00	0.00	0.00	0.00	0.00	0.00	
16.20	0.00	87.00	87.00	92.00	92.00	92.00	122.00	122.00	127.00	127.00	127.00	
16.30	0.00	80.00	80.00	80.00	80.00	80.00	80.00	85.00	80.00	80.00	80.00	
16.40	0.00	92.00	92.00	97.00	97.00	97.00	137.00	137.00	137.00	137.00		
16.50	0.00	0.00	0.00	3.00	3.00	3.00	3.00	13.00	8.00	28.00	28.00	
17.10	0.00	0.00	0.00	1.00	1.00	1.00	1.00	1.00	1.00	1.00	1.00	
17.20	0.00	0.00	0.00	0.00	0.00	0.00	0.00	5.00	5.00	5.00	5.00	
17.30	0.00	46.00	46.00	56.00	56.00	211.00	211.00	211.00	211.00	211.00	211.00	
17.40	0.00	92.00	127.00	157.00	157.00	287.00	287.00	287.00	287.00	312.00	312.00	
17.50	0.00	200.00	200.00	200.00	200.00	200.00	557.00	560.00	560.00	560.00	560.00	block failure, tree cantilever
17.60	0.00	215.00	240.00	230.00	235.00	435.00	555.00	555.00	560.00	575.00	580.00	block failure, tree cantilever
18.10	0.00	50.00	50.00	50.00	50.00	50.00	50.00	50.00	50.00	50.00	50.00	
18.20	0.00	0.00	0.00	2.00	15.00	15.00	15.00	15.00	5.00	5.00	5.00	
18.30	0.00	50.00	50.00									sliding
18.40	0.00	0.00	0.00	0.00	0.00	0.00	0.00					
18.50	0.00	0.00	0.00	0.00	0.00	0.00	0.00	0.00	0.00	0.00	0.00	
18.60	0.00	0.00	0.00	0.00	0.00	0.00	0.00	0.00	0.00	0.00	0.00	
18.70	0.00	0.00	0.00	20.00	20.00	20.00	20.00	20.00	20.00	20.00	20.00	
19.10	0.00	0.00	5.00	9.00	9.00	9.00	9.00	9.00	9.00	9.00	9.00	
19.20	0.00	0.00	0.00	35.00	35.00	35.00	35.00	35.00	35.00	35.00	35.00	
19.30			0.00	0.00	0.00	0.00	5.00	5.00	20.00	40.00	40.00	
19.40	0.00	0.00	0.00	0.00	0.00	0.00	3.00	3.00	2.00	2.00	2.00	
20.10	0.00	0.00	0.00	0.00	0.00	0.00	0.00	0.00	0.00	0.00	0.00	
20.20	0.00	62.00	62.00	62.00	62.00	62.00	72.00	72.00	72.00	72.00	72.00	
20.30	0.00	0.00	0.00	10.00	10.00	10.00	3.00	3.00	3.00	3.00	3.00	

Table 4.3. Measured cumulative bank top change from November 2003 - September 2005. Shaded cells indicate bank failures (>20 cm). Maximum change was 580 cm.

bend \ date	04.12.03	28.01.04	18.03.04	24.05.04	26.07.04	30.08.04	09.11.04	17.01.05	28.02.05	11.04.05	26.09.05
1.1	0.00	-3.00	-2.80	-2.80	-2.80	-7.50	-6.00	-7.00	-9.00	-8.00	-9.00
1.2	0.00	2.00	1.00	0.00	-1.00	-2.00	-2.00	-2.00	-4.00	-1.50	-1.50
1.3	0.00	2.50	3.00	1.40	0.00	-0.50	-3.00	-4.00	-3.50	0.50	3.50
2.1	0.00	1.00	3.00	1.50	1.50	1.50	1.50	1.50	2.50	8.00	9.00
2.2	0.00	2.30	2.80	2.80	2.80	60.30	61.30	61.30	65.00	69.00	72.00
2.3	0.60			7.60	-0.40	-0.40	1.60	1.60	16.60	9.60	9.60
2.4	1.00			1.00	4.00	13.00	60.00	69.00	73.00	79.00	85.00
2.5	0.00			58.50	50.00	46.00	61.00	45.50	55.00	59.00	67.00
2.6	0.00		72.00	74.00	58.00	54.00	81.00	73.00	73.00	73.00	80.00
3.1	0.00		117.00	120.00	120.00	118.00	124.00	123.00	124.00	127.00	132.00
3.2	0.00		104.00	102.00	102.00	102.00	102.00	104.00	108.00	108.00	108.00
3.3	0.00		173.00	173.00	173.00	173.00	272.00	259.00	259.00	259.00	259.00
4.1	0.00	1.00	43.00	43.00	43.00	62.00	35.00	26.00	43.00	47.00	62.00
4.2	-1.50	-14.00		17.00	22.00	12.00	30.00	11.00	15.00	23.00	23.00
4.3				-76.00	-76.00	-76.00	-79.00	-73.00	-73.00	-73.00	-69.00
5.1	-0.50		109.50	105.50	114.50	114.50	140.50	138.50	127.50	153.50	154.00
5.2	0.00	2.50	2.50	2.50	-0.50	-0.50	-0.50	89.50	89.50	91.50	91.50
5.3	0.00	2.00	2.00	2.00	0.50	-3.00	1.50	3.00	3.00	20.50	-25.50
6.1	0.00	2.50		1.50	5.50	5.50	11.50	-0.50	9.50	29.50	35.50
6.2	0.00	8.00	51.00	10.00	10.00	10.00	17.00	4.00	35.00	30.00	30.00
6.3	0.00	90.00	93.00	93.00	99.00	95.00	126.00	129.00	153.00	160.00	178.00
6.4	0.00	127.00	139.00	149.00	149.00	149.00	163.00	172.00	200.00	212.00	221.00
6.5	0.00	81.00	57.00	75.00	80.00	80.00	106.00	113.00	132.00	132.00	140.00
6.6	0.00	157.00	159.00	159.00	159.00	153.00	325.00	209.00	209.00	224.00	224.00
6.7	0.00	160.00	189.00	189.00	176.00	163.00	116.00	116.00	covered	covered	covered
6.8	0.00	160.00	156.00	188.00	170.00	170.00	245.00	240.00	232.00	216.00	216.00
6.9	0.00	144.00	132.00	163.00	138.00	132.00	208.00	208.00	204.00	214.00	covered
6.9	0.00	91.00	80.00	80.00	80.00	80.00	184.00	184.00	153.00	121.00	158.00
6.9	0.00	68.00	65.00	65.00	65.00	59.00	146.00	117.00	107.00	112.00	150.00
7.1	0.00	104.00		217.00	217.00	269.00	269.00	269.00	282.00	282.00	269.00
7.2	40.00	230.00		312.00	356.00	418.00	427.00	420.00			428.00
7.3	0.00	129.00	130.50	202.50	207.50	205.50	206.50	206.50	206.50	209.50	209.50
7.4	0.00	79.00		130.50	137.00	137.00	130.00	130.00	140.00	157.00	163.00
7.5	0.00		232.00	232.00	232.00	232.00	229.00	224.00	224.00	235.50	244.00
7.6		200.00	230.00	230.00	230.00	230.00	231.00	231.00	231.00	237.00	237.00
8.1	0.00		0.00		0.00	0.00	41.00	41.00	46.00	46.00	46.00
8.2	0.00	8.00	8.00	13.00	10.00	10.00	69.00	77.00	77.00	74.00	74.00
8.3	0.00		181.00	176.00	172.50	171.50	171.00	170.00	167.50	175.50	
9.1	0.00		142.00	135.00	140.00	140.00	140.00				
9.2	-3.50		155.50	152.50	145.50	150.50	169.50	231.50	167.50	163.50	227.50
9.3	-1.00		65.00	65.00	70.00	61.00	68.00	68.00	68.00	57.00	73.00
10.1	0.00	4.00	6.00	7.50	13.50	31.50	34.50	35.50	35.50	39.00	42.00
10.2	0.00	0.60	0.60			1.60	2.10	3.10	3.60	7.10	7.10
10.3	-0.90	1.00	1.00	0.00	0.00	0.00	0.00	2.00	3.00	7.00	17.00
10.4	0.00	3.50	103.50	158.50	158.50	158.50	168.50	185.50	200.50	193.50	191.50
11.1	0.00	4.00	4.00	2.00	2.00	0.50	84.00	64.00	67.00	85.00	54.00
11.2	-0.50	28.00	-47.00	-47.00	-47.00	-47.00	-49.00	-49.00	-49.00	-42.00	-45.00
11.3	0.00	40.00	40.00	30.00	34.00	34.00	39.00	54.00	37.00	58.00	46.00
11.4	0.00	3.50	5.00	5.00	6.50	6.00	8.00	5.00	74.00	89.00	53.00
11.5	0.00	100.00		98.00	102.00	102.00	97.00	107.00	175.00	219.00	224.00
11.6	0.00	125.00	129.00	129.00	126.00	133.00	218.00	255.00	262.00	256.00	262.00
11.7	0.00	132.00	132.00	126.00	174.00	128.00	126.00	133.00	111.00	98.00	133.00
11.8	-1.50		121.50	121.50	118.50	122.50	116.50	115.50	110.50	113.50	113.50
12.1	0.00	0.00	1.50	2.70	10.00	14.00	17.00	30.00	35.00	36.50	41.50
12.2	0.00	35.00	38.00	38.00	36.00	38.00	161.00	164.00	170.50	168.00	173.50
12.3	0.00	180.00	183.00	166.00	176.00	137.00	291.00	304.00	296.00	301.00	318.00
12.4	0.00		138.00	125.00	130.00	130.00	235.00	235.00	235.00	235.00	246.00
12.5	0.00		205.00	205.00	187.00	202.00	323.00	303.00	331.00	340.00	340.00
12.6	0.00	245.00	224.00	224.00	218.00	224.00	307.00	307.00	325.00	316.00	349.50
13.1	0.00	0.00	1.00	1.00	1.00	7.00	23.00	27.00	27.00	27.50	27.50
13.2	0.00	1.00	1.00	2.00	2.00	3.00	68.00	62.00	74.00	75.00	78.00
13.3	0.00	3.00	29.50	44.50	50.00	52.50	11.00				103.00
13.4	-1.00	11.50	24.50	25.50	25.50	57.00	30.50	54.50	77.50	83.50	88.50
13.5	0.00	3.00	5.50	13.00	12.00	12.00	12.00	14.00	28.50	36.00	36.50
14.1	0.00	2.00	4.00	4.00	4.00	4.00	4.00	4.00	8.00	8.00	16.00
14.2	0.00	1.50	1.50	-0.50	1.00	1.00	1.50	1.50	1.50	1.50	6.00
14.3	0.00	-1.00	6.00	4.00	4.00	9.00	20.00	20.00	21.00	21.00	21.00
14.4	0.00	3.00	4.50	6.50	6.00	6.00	10.50	8.50	15.00	18.50	20.00
15.1	0.00	115.00	113.00	108.00	108.00	101.00	107.00	113.00	113.00	105.00	153.00
15.2	0.00	80.00	97.00	81.00	71.00	71.00	58.00	58.00	45.00	57.00	83.00
15.3	0.00	70.00		80.00	80.00	80.00	48.00				
15.4	0.00	55.00		57.00	53.00	37.00	55.00	55.00	55.00	61.00	35.00
15.5	-1.00	77.00		61.00	67.00	61.00	68.00	98.00	112.00	132.00	135.00
15.6	0.00	11.00		1.00	-6.00	-7.00	34.00	34.00	36.00	46.00	46.00
16.1	-2.00	9.00	5.00	5.00	4.00	3.00	3.50	3.50	3.50	7.50	7.50
16.2	0.00	87.00	91.00	91.00	97.00	84.00	89.00	89.00	94.00	86.00	92.00
16.3	0.00	80.00		76.00	76.00	56.00	75.00	75.00	75.00	75.00	95.00
16.4	8.00	99.00		100.00	100.00	100.00	106.00	103.00	118.00	124.00	
16.5	8.00	38.00		51.00	41.00	41.00	40.00	40.00	74.00	74.00	60.00
17.1	0.00		2.00	2.00	0.00	0.00	2.00	2.00	6.50	6.50	5.50
17.2	0.00	15.00	34.50	34.00	34.00	59.00	61.00	57.00	75.50	75.50	77.00
17.3	0.00	38.00		48.00	62.00	87.00	87.00				
17.4	-3.00	89.00		238.00	245.00	206.00	208.00	213.00	226.00	214.00	235.00
17.5	0.00			200.00	200.00	212.00	210.00				444.00
17.6	0.00			248.00	249.00	250.00	459.00		489.00		
18.1	0.00	5.00		4.00	5.00	-0.20	0.50	0.50	-2.50	-2.50	-2.50
18.2	0.00	12.00	11.50	9.00	9.00	9.00	7.50	7.50	5.00	5.00	5.00
18.3	-3.00	47.00									
18.4	-1.00	-10.00			-9.50	12.30	19.80				
18.5	0.50	9.00		9.20	-1.00	-4.20	7.50	9.00	11.50	12.00	14.00
18.6	0.00	9.00	12.50	12.00	11.50	11.00	12.50	12.50	19.00	26.00	28.00
18.7	0.00	18.00		-1.00	0.00	0.00	4.00	3.00	13.00	17.00	19.50
19.1	0.00	0.50	2.00	2.00	2.00	2.00	2.50	2.50	1.50	4.50	4.50
19.2	0.00	14.20	14.20	13.70	12.20	11.60	18.20	16.20	16.70	21.20	21.70
19.3			-1.00	20.00	-3.00	1.50	29.00	4.00	66.00	44.00	53.00
19.4	-1.00	-0.50	-4.50	-3.00	-3.50	-5.90	-5.90	-5.40	-6.40	-5.40	-6.40
20.1	0.00	-7.50	-7.50	-7.50	15.50	27.00	20.50	24.50	22.20	24.00	28.00
20.2	-3.50	12.00	13.50	16.00	14.00	12.50	12.00	11.00	11.50	13.50	14.50
20.3	0.00	2.50		3.00	8.00	19.50	25.50	27.00	27.50	26.00	23.50

Table 4.4. Measured cumulative bank bottom changes from November 2003 - September 2005. Maximum bottom erosion was 444 cm.

4.3 Historical and remotely sensed channel data

4.3.1 Available data

4.3.1.1 Historical maps

Lance and Consuegra (1998) investigated the list of available historical maps during the HYDRAM Venoge Study. In the cantonal archives (1:50'000 scale) and those of the Federal Office of Topography (Swisstopo) (1:25'000), maps from 1839, 1849, 1882, 1892, and 1945 are available. The current 1:25'000 maps of Swisstopo were first mapped in 1952 (map 1242 Morges) with a latest impression in 2000 (content 1998) and in 1955 (map 1222 Cossonay) with a latest impression in 1999 (content 1997) (Swisstopo Status, 2005). The different revisions of these maps are of course available at Swisstopo. The Vaud canton has a map at the 1:10'000 scale. The last revision of the digital maps was December 1990.

4.3.1.2 Remotely sensed data

An impressive quantity of remotely sensed data[1] for the Lower Venoge River is available. Aerial photos were taken in 1964 by the EPFL laboratory of photogrammetry as well as April 15, 1996. More photos were taken by the Swiss railways (SBB) in March 1994. Besides these dates, photos were also taken in 1933, 1957, and 1974 (Lance and Consuegra, 1998), although their sources are unknown. Other photos of the Venoge exist and are available at the Swiss Federal Office of Topography (Swisstopo). In their recent campaign of orthophoto coverage of Switzerland in its entirety, called SwissImage, they produced orthophotos of the entire Venoge catchment in 1998. These orthophotos were made available by the Vaud Canton for this thesis.

Unfortunately, for the orthophotos of 1964, 1994, and 1996, no quality information was found concerning the ortho-rectification of the photos. Concerning the orthophotos SwissImage, they have a quality of 1 meter precision (under smooth relief conditions) with pixel sizes of 50 cm.

Besides the photogrammetric data available, recent advances in airborne laser scanning using LIght Detection And Ranging (LIDAR) technology have permitted high resolution digital terrain models to be developed. It was possible to buy from Swisstopo, the laser elevation points issued from their 2001-2002 flights over the Lower Venoge River. Two data sets were available: the MNS-MO - the surface model points, as well as the MNT-MO, the actual terrain points. The surface model points are the original LIDAR points. To take out points that represent objects (vegetation, buildings,...), and not the actual land elevation, filters are employed resulting in the terrain model points of the MNT-MO. There are typically 1-2 points per square meter for the surface model points. MNS-MO precision is advertised as 1.5 meters

1. Remotely sensed data is defined by Burrough and McDonnell (1998) as: "the collection of data about an object without coming into contact with it." In this broader sense, aerial photography is considered in this research as remotely sensed data.

standard deviation in wooded areas and 0.5 meters in open areas, and 0.5 meters for the MNT-MO (Swisstopo MNS, 2005).

Processing the LIDAR point data proved difficult. Modern Geographical Information Systems (GIS) are not necessarily equipped to handle the volume of point data supplied. This was true for the software, Mapinfo® Professional®, in combination with the spatial analysis tool, Vertical Mapper®. LIDAR data points are delivered by tile (size of 3 by 4.125 km) and this was approximately the size that was reasonable for processing in the GIS. Points from adjacent tiles were added to the tile in question before interpolation of the points. This was necessary to provide an overlap between tiles. A DTM and DSM (Digital Surface Model) was then created with each set of extended tile points with the Inverse Distance Weighting interpolation algorithm available in the Vertical Mapper® software (Northwood, 2001). Although the algorithm is labeled as an interpolation program, it is used here more as an aggregation algorithm (Metzger, 2003) due to the original point density of 1 - 2 points per square meter compared to the one meter resolution DTM/DSM to be produced. For the DSM, the IDW was carried out using an exponent of 2 for the exponential distance weighting and the nearest 10 points were used in a radius of 10 meters. For the DTM, an exponent of 2 was also used although the first 25 points encountered in a radius of 250 meters were used. A lower radius and number of points for the DSM was used to avoid too much smoothing. After the creation of each separate DTM/DSM, their edges were trimmed of 100 meters to cutoff any border effects and then the 6 tiles which make up the Lower Venoge stream corridor were spliced together averaging any overlapping points. As a result, a DTM and DSM of the Lower Venoge River stream corridor were obtained.

Besides the high resolution DTM and DSM that were developed, the MNT25 (DTM at 25 meter pixel size) was also available from Swisstopo. This DTM is developed from the elevation contours of the 1:25’000 national topographic map and the advertised precision is 1.5 meters (Swisstopo MNT25, 2005).

4.3.2 Derived information

4.3.2.1 Lower Venoge River centerline

The first application for the historical and remotely sensed data was the development of the Lower Venoge River centerline. The centerlines for the 1996 Lower Venoge as well as the 2004 Lower Venoge were desired because of the cross sections achieved approximately during these periods. As simple as the task might seem, it proved itself to be much more difficult. Digital river data is available from the Vaud canton as well as from Swisstopo (Vecteur25), but this data was not considered because of the precision necessary. Using the available maps to reference the river centerline was also avoided due to the map scale or the year of revision of the maps. Quality issues of the 1996 ortho-rectification were raised when planimetric differences of up to 4 meters were found in places compared to the Swissimage 1998 orthophotos. To produce the 1996 centerline, it was finally decided to base it on the 1998 Swissimage orthophotos and where significant channel change was obvious between the 1996 and 1998 photos, the 1998 line was changed in those places to produce the 1996 channel centerline. Producing the

1998 centerline was not always easy though because of the vegetation that appears in the Swissimage orthophotos (based on summer aerial photos).

The task was even more complicated for the 2004 centerline because there are no more recent orthophotos than those of 1998. To approximate the channel centerline changes that needed to be incorporated into the 1998 centerline to make the 2004 centerline, the LIDAR DTM and 2004 cross section (cf. §4.4) were used. Figure 4.16 show the most important channel changes during the course of 1996-2004 for the study reach.

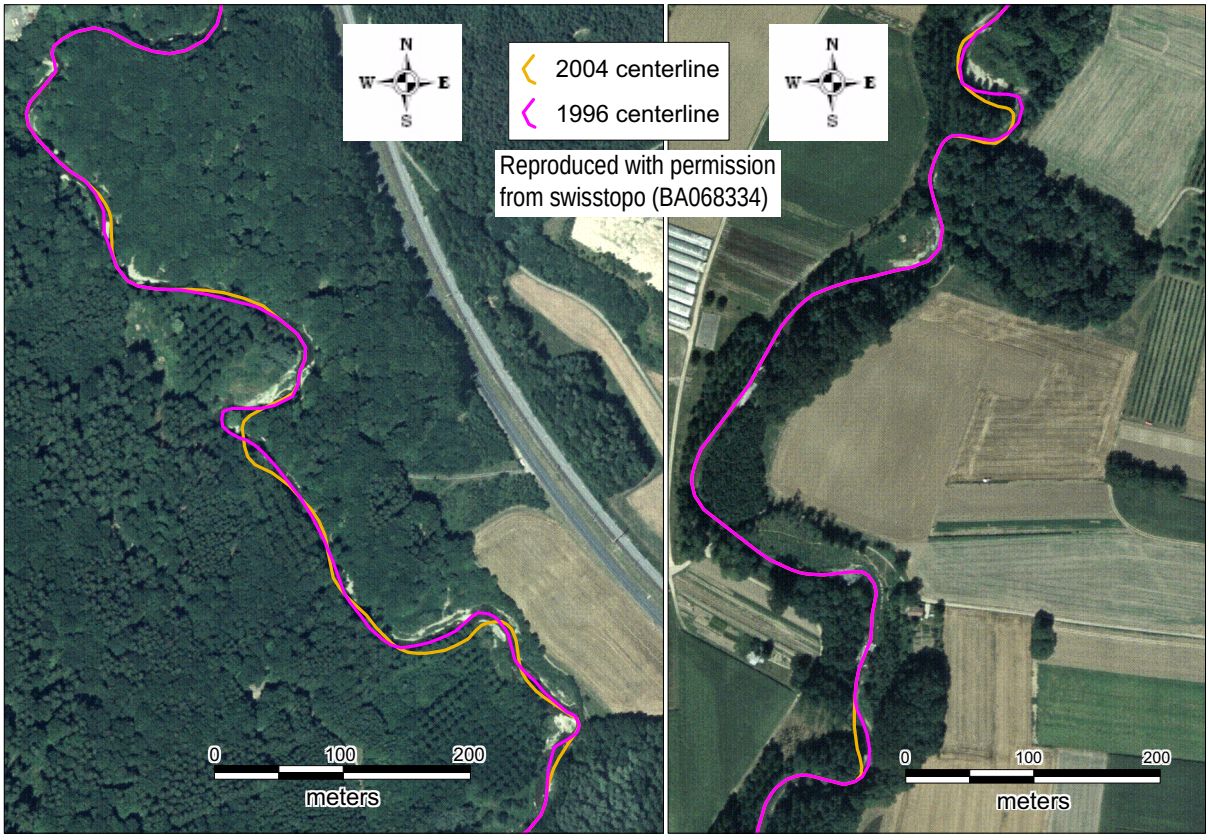

Figure 4.16. Channel centerlines determined with 1998 orthophotos and 2001/2002 LIDAR data and 2004 cross sections. Background images: SWISSIMAGE © 1998, Swisstopo (DV012716).

4.3.2.2 Channel migration and erosion estimates

It is often cited in literature of the possibility to estimate erosion based on two sets of aerial photos (preferably orthophotos). Lawler (1993) includes using historical sources for medium timescale measurement of river bank erosion. He warns of the following problems that must be considered with the use of historical information: "assumption of continuity and/or linearity in channel, change of time - representativeness of temporal sampling, survey errors/plotting errors/map distortion, confusion over map revision, change in channel definition criteria between two surveys, misleading information, and possibility of contradictory evidence". Although the problems Lawler cites are important and could completely negate the use of a historical source, it is still possible to glean significant information from them.

Lance and Consuegra (1998) were able to make general conclusions on the bank erosion, channel changes and stream corridor width of the Lower Venoge River by analyzing the different historical maps and orthophotos available to them. Concerning the study reach of this thesis, they concluded the following:

- the meander near km 10 (see appendix 2 for locations), progressed very little according to the historical maps (1850-1950), but seems to be progressing more rapidly in the last 30 years, most likely due to the industrial zone implanted on the raised right bank,
- from the "Abbaye" weir (km 7300) to the federal stage recorder weir (km 4900), the river planform has changed very little. The channel is deeper in this section.
- from the federal stage recorder weir (km 4900) to the football field (km 4100) the river planform has changed little in the last century because of bank protection works although the river will probably regain ground as the bank protection works will not be maintained. From the football field down to the "Valeyre" weir (km 2150), bank failures are important and seem to be occurring more frequently than in the last century. New meanders are developing.

The use of the aerial photos and the LIDAR DTM was already seen in section 3.7.1 to help classify the Lower Venoge River type and to better understand the meander cutoffs that have occurred in the last forty years.

It is of primary interest for this study to evaluate the use of the aerial photos for a quantitative assessment of mean annual erosion. Due to the fact that Swissimage orthophotos are taken in the summer, nearly all of the study reach banks in the 1998 orthophotos are covered by vegetation. At some places, vegetation completely masks the river channel. As mentioned above, the 1964 and 1996 orthophotos have accuracy problems. Thus only along river reaches where there is another fixed reference on the map, and the bank is relatively visible, is it really possible to use the 1964 and 1996 orthophotos to evaluate relatively precisely (±1 meter). Due to the very partial information that could be obtained with the aerial photos, it was decided not to try to estimate annual erosion rates over the entire study reach.

4.4 Channel topography

Probably one of the greatest hurdles to overcome in streambank erosion modeling is that of the topographic data of the stream channel. Banks shapes and slopes can vary significantly even over tens of meters, due to soil and vegetation heterogeneities. Lane et al. (1994) estimated bedload transport rates and aggradational and degradational zones of the stream bed by repeated tacheometric surveying. They concluded that bed cut and fills could be estimated to 20% of the correct value with cross section spacing of 2 meters. Although their study on bedload transport is a different context, it does reflect the spacing necessary to define changes in the channel bottom accurately. This amount of cross section data is impractical for a long stream reach.

High resolution LIDAR can provide a very accurate DTM. Its application in the river environment has been investigated and it has been found though to be accurate only in exposed, unvegetated channels (Charlton et al., 2003). Accuracy suffers also on steep slopes because the ground surface becomes greater than the horizontal projected surface reducing the number of points per surface area. LIDAR surveying

usually uses an infrared frequency for measurement. This frequency will not penetrate water. Thus, when riparian vegetation is sparse, it is possible to pickup the channel water surface. Other LIDAR techniques, such as the Scanning Hydrographic Operational Airborne Lidar Survey (SHOALS), have been developed using other frequencies so bathymetry can be detected (Irish and Lillycrop, 1999). The SHOALS system and other related remote sensing techniques show the future for obtaining high definition channel topography. Until these methods become widespread, proper interpolation methods need to be used to approximate the channel bottom to be combined with a high resolution DTM issued from LIDAR.

Many cross sections of the Lower Venoge River were surveyed in 1995-1996 during the HYDRAM Venoge study and during a fieldwork campaign of EPFL environmental engineering students. A comparison of those cross sections with cross sections surveyed in 2004 during this thesis permits an evaluation of the stability of the thalweg. Cross section density is insufficient in these two measuring campaigns to provide accurately interpolated meander scour holes throughout the study reach. A new interpolation method is presented to improve interpolated cross sections.

LIDAR data was available for this thesis. In areas of significant riparian vegetation and steep streambanks, LIDAR terrain point density suffers and a poor topographic representation results. A linear interpolation method is presented to improve river representation in a LIDAR derived DTM. This method interpolates linearly between channel LIDAR points in the streamwise direction. This linear interpolation could also be applied to integrate real cross section data into the DTM. The improved DTM could be very significant for developing a regional erosion model as described in chapter 2.4.1.

4.4.1 Cross section data

During the 1996 HYDRAM Venoge study, 98 cross sections were surveyed in the Lower Venoge River from kilometer 0.7 to 27. Cross sections locations were primarily at hydraulic structure locations and in urban areas. From kilometers 0 to 22.5, it was decided to reprofile some of the 1996 cross sections and add other cross sections in areas insufficiently covered in 1996, especially in the areas of erosion monitoring. One hundred and fifty-five cross sections were surveyed in 2004. After the 2004 survey, other cross sections from the EPFL environmental engineering students fieldwork campaign in 1996 were found in the archives. One hundred and five new cross sections were added to the 98 cross sections to give a total of 203 for 1996. No x-y reference points were found for the 1996 fieldwork campaign cross sections so their exact location is unknown. The majority of the locations of the cross sections could be estimated though from paper maps found in archives.

The measured cross sections allowed for detailed longitudinal profiles to be plotted (figure 4.17). These plots show that during the eight year period little bed elevation movement occurred. The bed of the Lower Venoge River seems to be stable, except the reach from kilometer 7.3 to 7.7 seems to have degraded. In a personal communication, Bujard (2005) related the history of the "Abbaye" weir. It failed during the March 9, 2001 high flow. To combat the regressive erosion that was occurring after this failure, a temporary reparation was done in October 2002. Large boulders were put in place to simulate the effect of the old weir. Two other areas have possibly changed their bed elevations: downstream from the Abbaye weir, and in the vicinity of kilometer 12. Due to insufficient cross sections and uncertainties

in the exact location of some of the 1996 cross sections in these areas, it is impossible to confirm the bed movement. It is possible in both locations that the low points from 1996 all come from scour holes and the high points of 2004 come from riffles, although the thalweg values downstream from the "Abbaye" weir seem too big to be explained simply as scour holes.

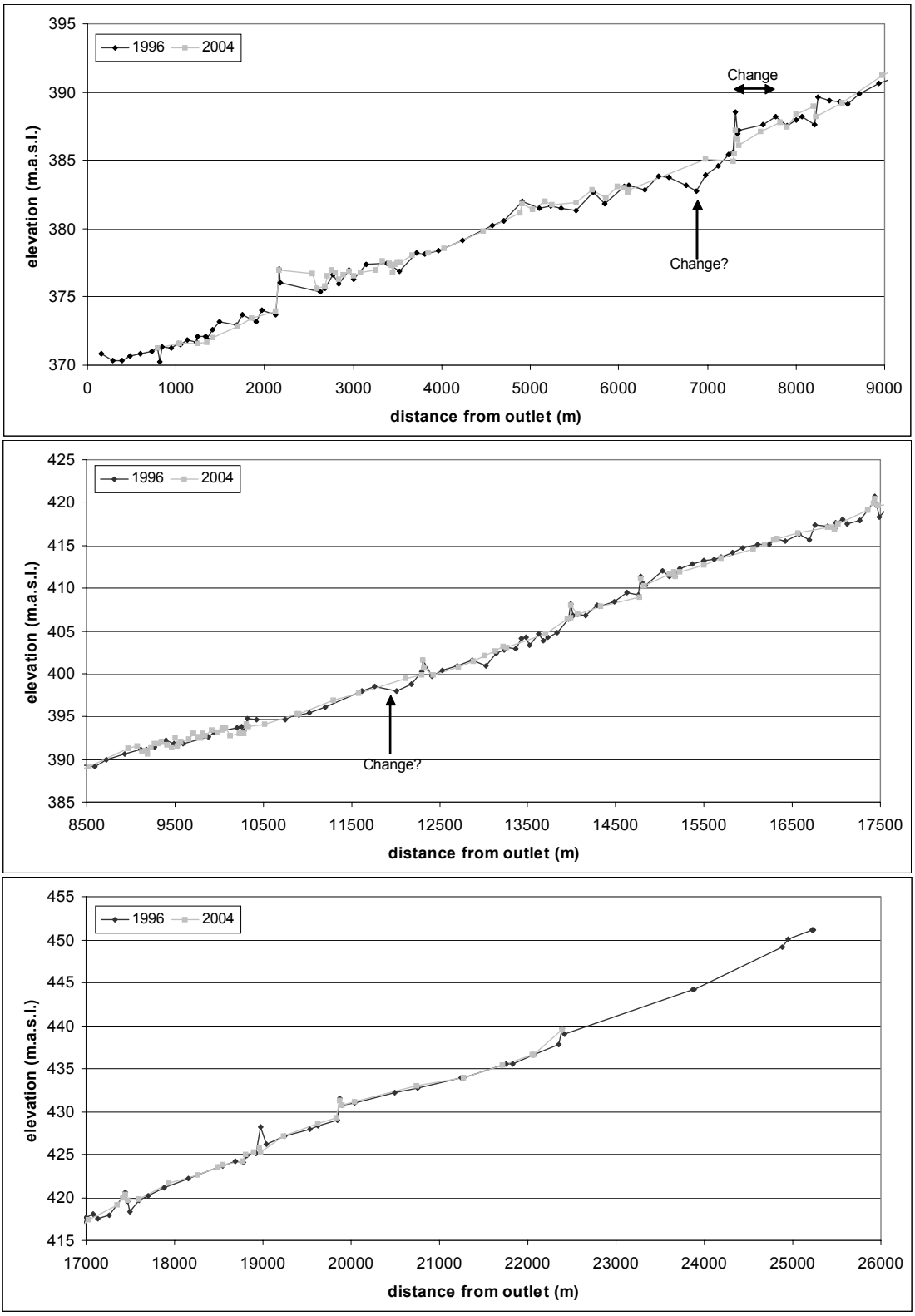

Figure 4.17. Longitudinal profiles of the Lower Venoge River based on cross sections from 1996 and 2004. Points indicate cross section locations.

1996 profile id	channel width (m)	km 2004	channel width (m)
360	24	10.336	26
6012	23	9.413	24
6011	25	9.262	27
6010	24	9.158	24
6009	30	9.126	27
370	22	8.228	21
381	21	8.002	16
400	21	7.602	19
430	19	6.117	19
440	18	5.702	18
450	20	5.515	15
8007	26	3.5	26
470	16	3.005	19
9001	19	2.841	25
9002	22	2.752	16
9003	19	2.682	26
average	21.81		21.75

Table 4.5. Comparison of 1996 and 2004 cross section widths

Besides the evaluation of the stability of the longitudinal profile, cross sections were analyzed in the study reach to see if average channel width was changing. It was possible to compare 16 cross sections for channel width changes. Some of the cross sections are not exactly at the same place so it is normal to expect some difference. Table 4.5 shows that on average cross section width has not changed. Some cross sections have changed though because of the dynamic nature of the river. Other differences are due most likely to slight location differences.

The locations of the 2004 cross sections that will be used for the erosion modeling are seen in figure 4.2. The CCHE1D model asks for cross section data in a text file format. It is possible, though, to avoid the text export with careful preparation of the GIS cross section database. To help in the cross section database preparation, a cross section tool was programmed. As will be seen in this section, the cross section tool became much more than simply a viewer. The interface of the cross section tool is shown in figure 4.18. Most all GIS's will open and work with dbf files. The strategy for the 2004 surveying was to do it in 3D coordinates rather than by leveling. GPS points were implanted during the spring of 2004. Tacheometric (Total Station) surveying was then performed using the GPS points as base points. These points were then imported into Mapinfo Professional® and saved as a dbf file. These dbf points are not possible to visualize rapidly without some programming in Mapinfo®. Rather than being dependant on a GIS software, it was decided to program in Borland® Delphi®.

CCHE1D needs the cross sections to be ordered according to a cross section identifier and according to its position from left to right. Once the dbf points have been identified by cross section via manipulation in a GIS, and the leftmost point has been indicated as the first cross section point, it is possible with the cross section tool to calculate the cross section transverse distance, *cp_w*, and its cross section position index, *cp_posidx*. Once this has been done, it is easy with the viewer to visualize where the bank top and bank toe are located and to check the appropriate boxes in the database spreadsheet to assign them.

Other capabilities were also added to the cross section tool. Unnecessary points can be removed from the cross section by running the smoother and points can also be added. Parts of the cross section can be labelled as the left overbank, left bank, main channel, right overbank, or right bank. This labelling will be used in other routines in the cross section tool and is helpful for other GIS manipulations.

If cross sections are numerous enough and correctly spaced, a linear interpolation of cross section points from one cross section to the next will give a sufficient approximation of the channel topography. As mentioned in chapter 2.4.2, nodes for the CCHE1D calculations are selected in a GIS. If these nodes are in dbf format, necessary for CCHE1D, they can be opened in the cross section viewer with the "Node Points" tab. This part of the cross section tool allows the user firstly to recalculate the x-y coordinates of

cross sections to straighten the points in a perpendicular fashion around the channel centerline if desired, although it is not absolutely necessary. Secondly, cross sections can be linearly interpolated. This interpolation is based on master chords that run from a definition point on one cross section, such as the left bank top, to the corresponding definition point on the next cross section (figure 4.19). This interpolation scheme is similar to the scheme used in HEC-RAS (USACE, 2002), although HEC-RAS uses a thalweg master chord rather than two toe master chords.

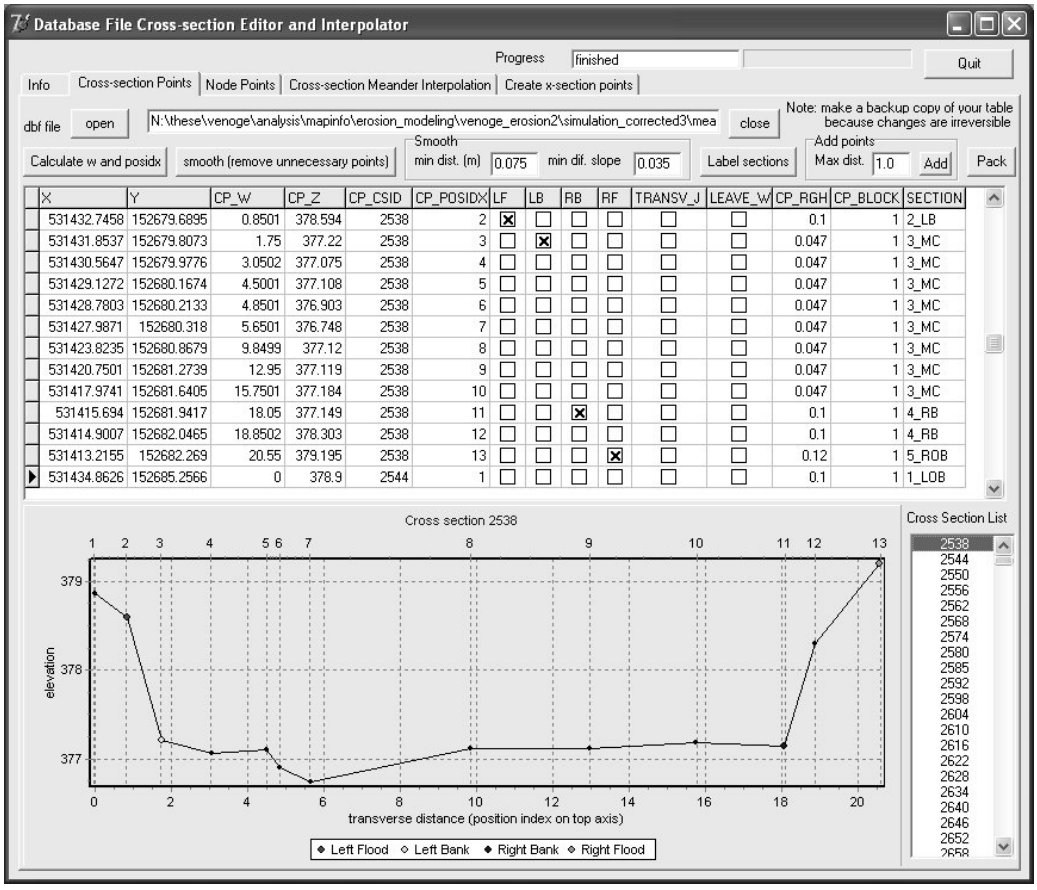

Figure 4.18. Database file cross section tool for viewing cross sections in dbf format. The tool interpolates cross sections linearly and with respect to bend curvature. The tool can also interpolate and smooth LIDAR topographic points to estimate channel geometry.

The interpolation of the cross sections based on node locations ensures a cross section at each node location for CCHE1D. The CCHE1D model needs two other information for the cross section points. A roughness value, *cp_rgh*, that of Manning, must be specified for every point, as well as an effective flow logical value, *cp_block*, which if set to "0" means that no flow will be calculated from that cross section point to the next transverse point. In the case of the Venoge study reach, effective flow was only set to "0" for bridge pillars. These values are updated in Mapinfo Professional® via Manning and ineffective flow polygons as shown in figure 4.20.

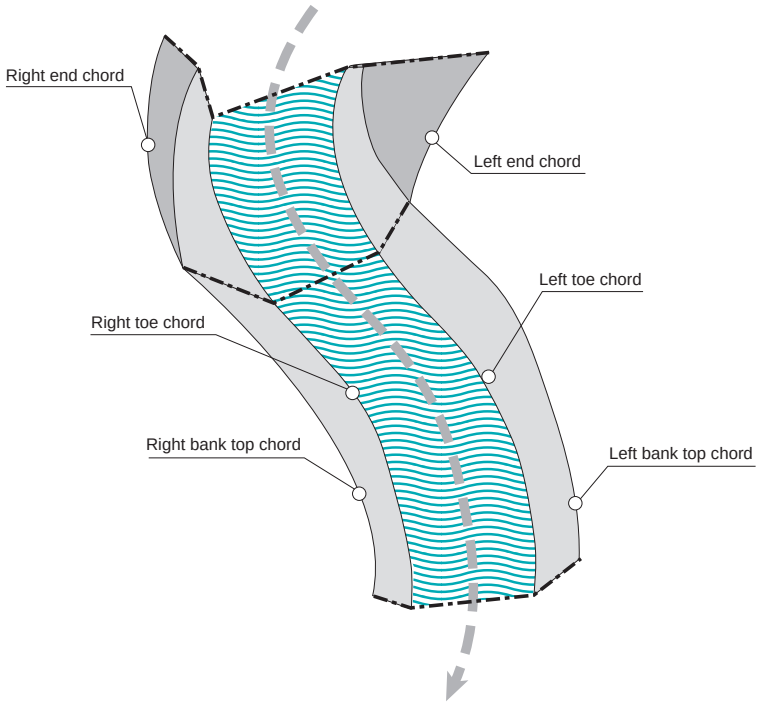

Figure 4.19. Linear cross section interpolation based on master chords between cross section definition points

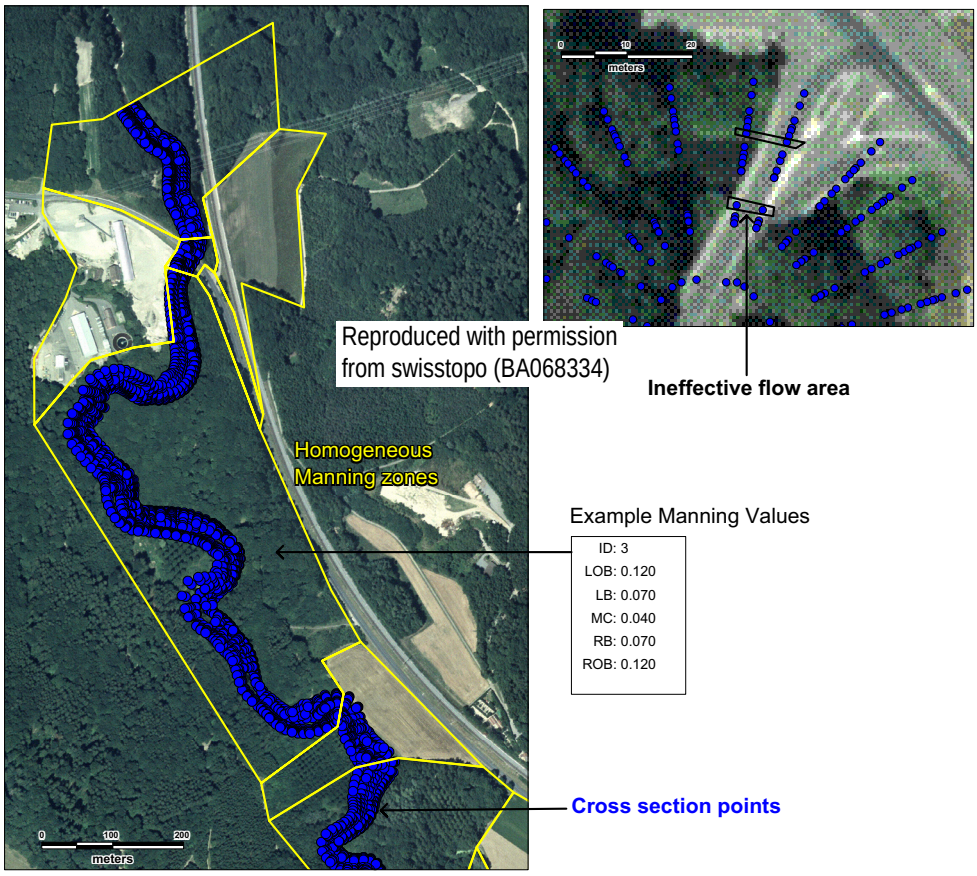

Figure 4.20. Attribution of Manning values and ineffective flow areas to cross section points within a GIS. Background images: SWISSIMAGE © 1998, Swisstopo (DV012716).

4.4.2 Interpolation in meanders

4.4.2.1 Development

The number of cross sections necessary to roughly describe a channel bottom would be one for each riffle and one for each scour pool. With Lower Venoge River wavelength roughly in the 100-160 meter range, this would mean a cross section every 25-40 meters. Because of erosion and depositional complexities that occur due to flow complexities, bed changes between a riffle and a scour pool will not follow a linear interpolation between the riffle cross section and the bend cross section. This is the reason for Lane et al.'s (1994) recommendation of 2 meter spacing for an 80% accuracy in calculating cuts and fills. For the erosion modeling, a cross section for every riffle and scour pool is probably sufficient, but finding the deepest scour hole can be time consuming as for many rivers it requires the use of a boat.

Cross section surveying of the Lower Venoge River in 2004 is sufficiently dense in the bends that are monitored for erosion, but elsewhere is insufficient. For this reason, it was decided to explore the possibilities of interpolating cross sections with respect to channel curvature. A theoretical "model of equilibrium bed topography for meander bends with erodible banks" has been proposed by Darby and Delbono (2002), but it was chosen here to follow a calibration approach that is much simpler to program. The bend scour pool location is related to the zone of maximum outer bend shear stress. The location of that maximum shear stress and maximum migration rate have been estimated via the use of weighting upstream migration rates by the equation 2.15. It is proposed that by weighting upstream curvature, it will be possible to estimate the radius of curvature that can be used with equation 2.5 to estimate bed topography. The equation for bed topography then is:

$$\frac{h}{h_m} = a\left(\frac{r_w}{r_{cw}}\right)^K \qquad \textit{Eq. 4.3}$$

where h is the water depth, h_m is the mean cross section water depth, r_w is the weighted radius of curvature at a cross section bottom point, r_{cw} is the weighted radius of curvature at the channel centerline, and a and K are calibration coefficients. The coefficient a is introduced because it is observed that at the channel bottom center in bends the flow depth is often slightly lower than h_m. An a value in the 0.75 to 1 range permits this adjustment. Inspired by equation 2.15, the weighted curvature, c_1, can the be estimated by the following equation:

$$c_1(s) = \left[\int_0^\infty c_0(s-\zeta)G(\zeta)d\zeta\right]\left[\int_0^\infty G(\zeta)d\zeta\right]^{-1} \qquad \textit{Eq. 4.4}$$

where $c_0(s\text{-}\zeta)$ is the channel centerline curvature at a distance of ζ upstream from point s and $G(\zeta)$ is the weighting function. Curvature and radius of curvature are related by $c = 1/r_c$. It is proposed to use the same exponential decay weighting function as in equation 2.16 that uses the decay parameter α.

As the bankfull discharge is considered to be approximately the formative channel discharge, and the bankfull discharge is often between a one and two year return period (Bravard and Petit, 1997), the mean

flow depth, h_m, can be based on the maximum water surface elevation of the simulation of the one year return period flood (or the steady flow simulation of the one year return period maximum discharge).

The values of α, *a*, and *K* need to be evaluated for each node. It is possible to linearize equation 4.3 permitting a linear regression to be performed to find an optimal *a* and *K* compared to a measured cross section and that for a given α. Upper and lower bounds for these three parameters should be set to avoid unrealistic values. For the study reach, ranges of realistic values are 5-50 meters, 0.75-1, and 1-5 for 1/α, *a*, and *K*, respectively. The coefficient of determination can then be used to judge the fit of the linearized form of equation 4.3 to the cross section bottom data. Toe points are removed from the linear regression fit because toe geometry is variable depending on the status of basal sediments. To avoid bias due to poorly distributed bottom points, the linear regression and coefficient of determination is based on evenly spaced interpolated bottom points. The values of α, *a*, and *K* giving the best coefficient of determination are then written to the node database. Node points in between real cross sections are given estimations of the three variables according to a linear interpolation of 1/α, *a*, and *K* between the upstream and downstream real cross sections. The interface for determining these values in the cross section tool is shown in figure 4.21.

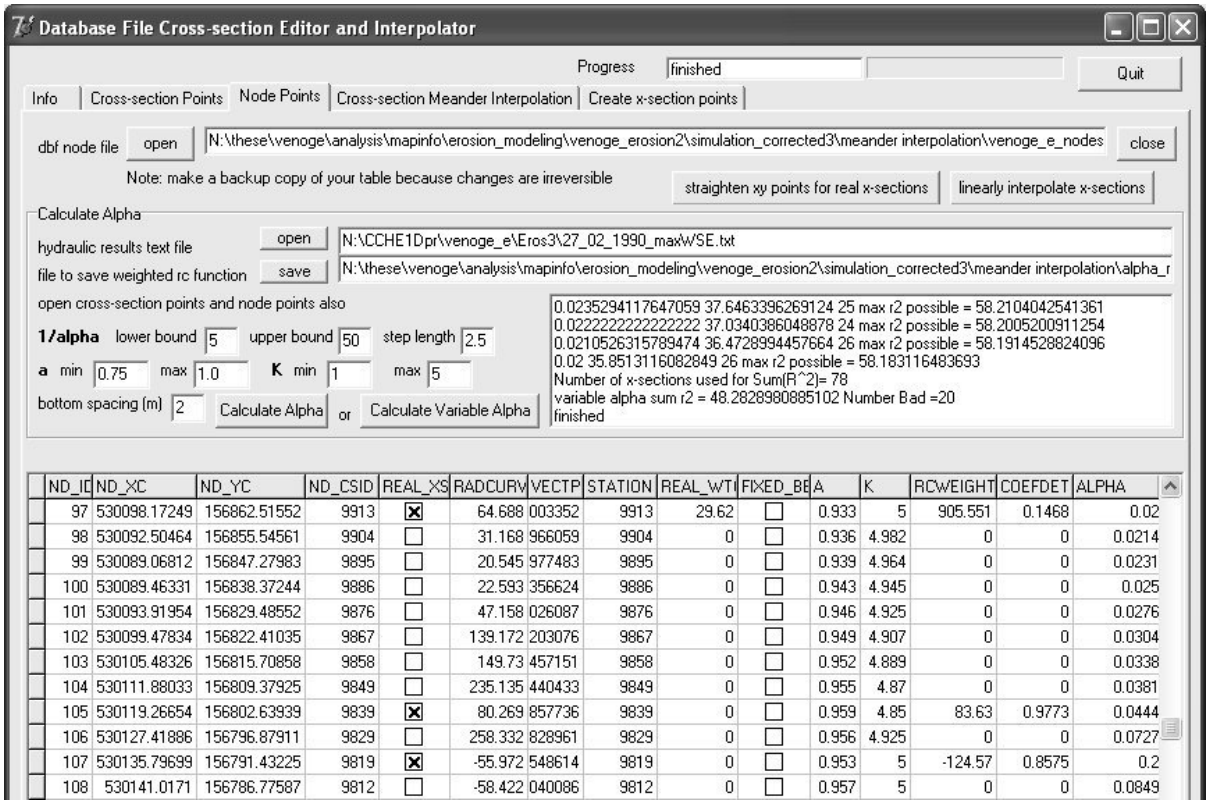

Figure 4.21. Calculation of α, a, and K values based on measured cross sections

The cross section tool also allows a text file to be saved containing calculated channel curvature values at measured cross sections as a function of the value of α. This output is useful to determine if the step of the 1/α value was sufficient. Several distributions of curvature as a function of the inverse of alpha are shown in figure 4.22. It can be noticed that channel curvature is sometimes maximized at values of the inverse of alpha greater than 5. This response is of course to be expected and allows for a scour hole to be located downstream from the bend apex.

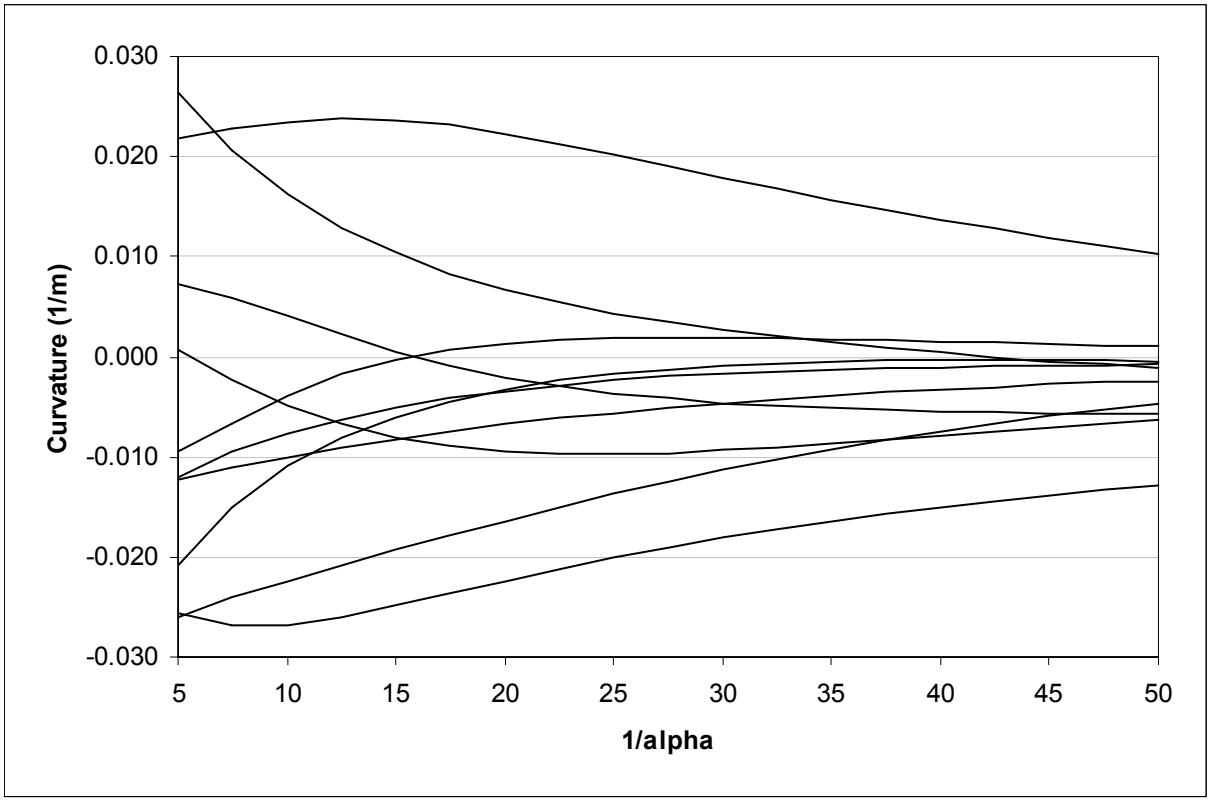

Figure 4.22. Ten examples of the influence of the parameter alpha on the upstream weighted curvature

4.4.2.2 Procedure

The procedure then to interpolate cross sections with respect to meander curvature using the model CCHE1D and the cross section tool then is the following:

1. Prepare nodes for CCHE1D as indicated in chapter 2.4.2.
2. Linearly interpolate the cross sections with the cross section tool.
3. With the linearly interpolated cross sections, run a CCHE1D calculation with fixed bed and banks to calculate the maximum Water Surface Elevation (WSE) at each node.
4. Open the linearly interpolated cross sections, the cche1d nodes, and a text file containing the WSE results for each node.
5. Calculate optimum α, a, and K values using the cross section tool.
6. For poorly fitted cross sections or zones where cross sections are sufficient, check "fixed_bed" in the node database file to keep the originally interpolated cross sections.
7. Interpolate with respect to curvature using the cross section tool.
8. Pack the cross section table to eliminate deleted bottom points.
9. Recalculate transverse distance, *cp_w*, and the position index, *cp_posidx*.
10. Compare real cross sections with fitted ones.

The above procedure has been done in connection with the model CCHE1D, although any other 1D hydraulic model could be used to calculate the WSE's.

4.4.2.3 Results

The meander interpolation procedure was applied to the 82 cross sections that make up the erosion modeling study reach. Four of those cross sections are related to the weir in the middle of the study reach. They were excluded from bed topography fitting. The sum of the coefficient of determination (R^2) is output for each cross section linear regression. If the weighted channel curvature forces a bed slope opposite of that observed, the fit is considered bad and the R^2 is zero in this case. The cross section tool allows two modes for calculating optimum α, a, and K values. Alpha can be fixed for the entire zone or it can be variable. For the case when alpha must remain constant throughout the reach, an optimum at α=0.05 was found with a sum of the R^2 = 41.3 and 24 bad fits out of 78 cross sections (figure 4.23). The cross section tool also outputs the sum of the coefficients of determination without respect to any constraints to give an impression of how well the model of bed topography performs. This unconditioned sum of the R^2 = 58.5. When alpha is allowed to be variable, the sum of the R^2 = 48.2 and there are 20 bad fits. Using a variable alpha does improve the result significantly. With a result of 48 out of the 59 possible for the 78 cross sections, the bed topography model used here is capable of reproducing the majority of the bed slopes. Examples of different bed fits are shown in figure 4.24. The top two figures show well the basal sediments at the toe, while the basal sediments seem to have been eroded away in the bottom cross section. The top cross section bed fit is probably a good estimation of the cross section when basal sediments have been eroded away.

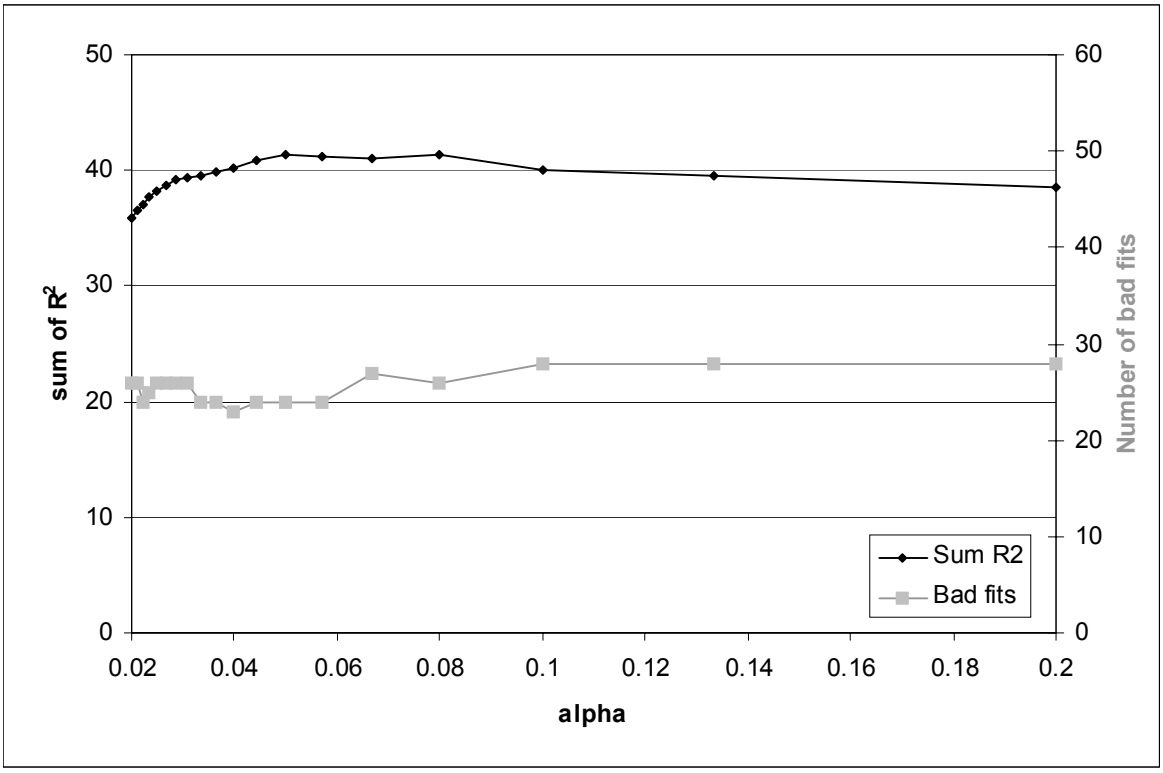

Figure 4.23. Results of the search for optimum parameters for the bed topography model applied to the Venoge study reach

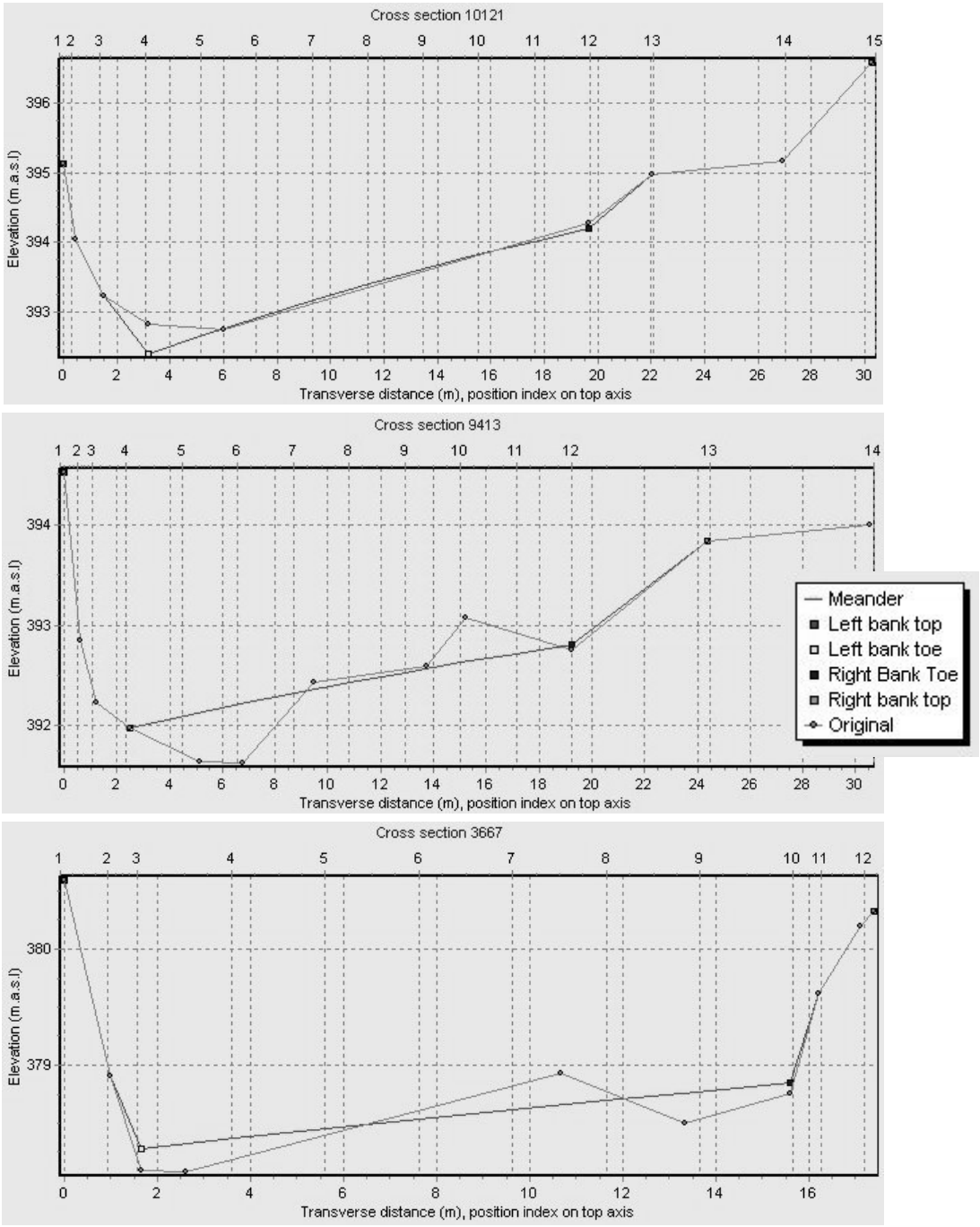

Figure 4.24. Examples of best fit calculated channel bottoms. R^2 values are 0.99, 0.63, and 0.36 for the top, middle, and bottom cross sections, respectively.

To avoid poor interpolations, areas where poor fits occurred were marked "fixed_bed" in the nodes database and original linearly interpolated cross sections were maintained in these zones. Although, it is sure that some of the cross sections interpolated with respect to channel curvature will overestimate or underestimate some bend scour holes, it will in the majority of cases help to correct very poor linear interpolations as shown in figure 4.25. More objectively, real cross sections that were not included in the parameter estimation should be compared to linear and meander interpolated cross sections to quantify the improvement brought by the new interpolation method. Real cross sections measured in 1996 are

compared with the linear and meander interpolated cross sections of 2004 (figure 4.26). This comparison is permitted in that the channel bed elevation seems relatively stable in this zone according to the longitudinal profile comparison (figure 4.17). The positioning of some of the 1996 cross sections is uncertain though and this can be very critical. Sometimes the improvement when compared to the linear interpolation is small, but often the meander interpolation places the most appropriate cross section just upstream or downstream because the weighted radius of curvature evidently did not respect a linear interpolation of the meander interpolation parameters. This means that upstream influence is extremely variable and/or the digitization of the channel centerline does not accurately reflect the flow curvature. The fact that interpolated cross sections are displaced too much upstream or downstream is important. It can be suggested for cross sections that have been meander interpolated, erosion results should be considered to apply to the upstream and downstream nodes (possibly several nodes in each direction if the displacement is long or if the node spacing is close).

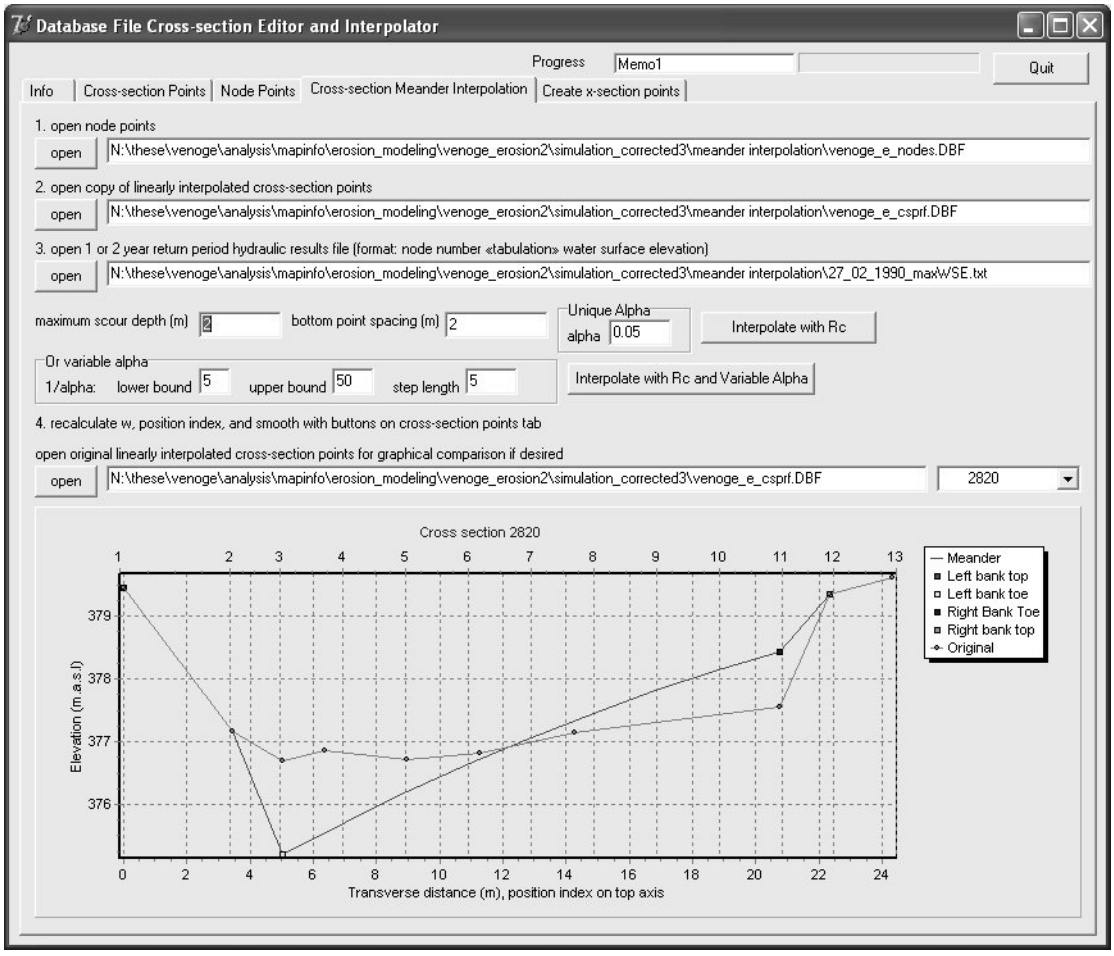

Figure 4.25. The meander interpolation method can significantly improve interpolated cross sections in bends such as this one.

To complete the verification of the meander interpolated cross sections, a simulation of the one year return period discharge was done with the new cross sections. Average absolute WSE difference was 1 cm and the maximum difference was 9 cm. This amount of difference is accepted for this study, although the source of the difference should be investigated. It could be linked to the lower limit of *a* being too low or more likely to higher point bar elevations that reduced effective flow capacity.

Station (m)	Meander scour elevation, side	Linear scour elevation, side	Improvement (cm)	1996 real scour elevation, side	1996 id	Comment
8937	391.2F					
8930	390.9R	391.2L	30	390.65F	6007	
8728	390.2R					
8721	390.3R	390.2R	5	389.9L	6005	1996 profile most likely at 8707
8707	390.2L	390.1R	50			
8588	390.0F	389.6R	40	389.1C	6004	
8581	389.3R					
8488	389.2R	389.2R	0	389.3R	6003	
8498	389.3R					
8247	387.7L	388.3C	-60	389.6C	370	
8238	388.6F	388.2C				
8213	388.2L	388.7L	50	387.6L	371	
8221	387.6L	388.5C	90			
8070	388.7R	388.6L	50	388.2R	380	

Figure 4.26. Comparison of some 1996 measured cross sections with linear and meander interpolated cross sections. Improvement is based on the difference of outer bend elevation between linear and meander cross sections. F=flat, R=right, L=left, and C=center.

4.4.3 LIDAR and river topography

Airborne laser scanning has the potential of providing significant river topographic information. A DTM derived from a non-water penetrating laser scan has the potential to accurately describe the water surface, exposed bars, and channel banks if the last return laser point density is sufficient. This is usually not the case for most airborne laser scans due to the effect of significant riparian vegetation. For the Lower Venoge stream corridor, the average point density is around 1 point per square meter while the density in the radius of 30 meters around the channel centerline is on average 1 point per 2 square meters. Although, 1 point/2 m² may seem quite good, there are patches where the density is much less than this causing poor river representation for most interpolation methods. Typical laser river cross section interpolation problems are: widening, constriction, and bed raising (figure 4.27 shows examples from the Lower Venoge River). Of course, the LIDAR derived DTM river topography will depend on the interpolation method employed. Most GIS packages do not offer a polyline interpolation method which is assumed to be necessary to improve the channel topographic description.

For an accurate description of the river topography, accurate bathymetric measurements must be made, by appropriate laser scanning, tacheometric surveying, or sonar sounding, to be combined with standard airborne laser scanning. Such combined surveys are rare. The next best possibility is to combine surveyed cross sections with LIDAR topographic points. For such a method to give good results, a linear streamwise interpolation method must densify the channel points before integration with the non-channel airborne laser scanned last return points. Such a streamwise linear interpolation method is elaborated here and the procedure for the integration of the points with a LIDAR derived DTM is explained.

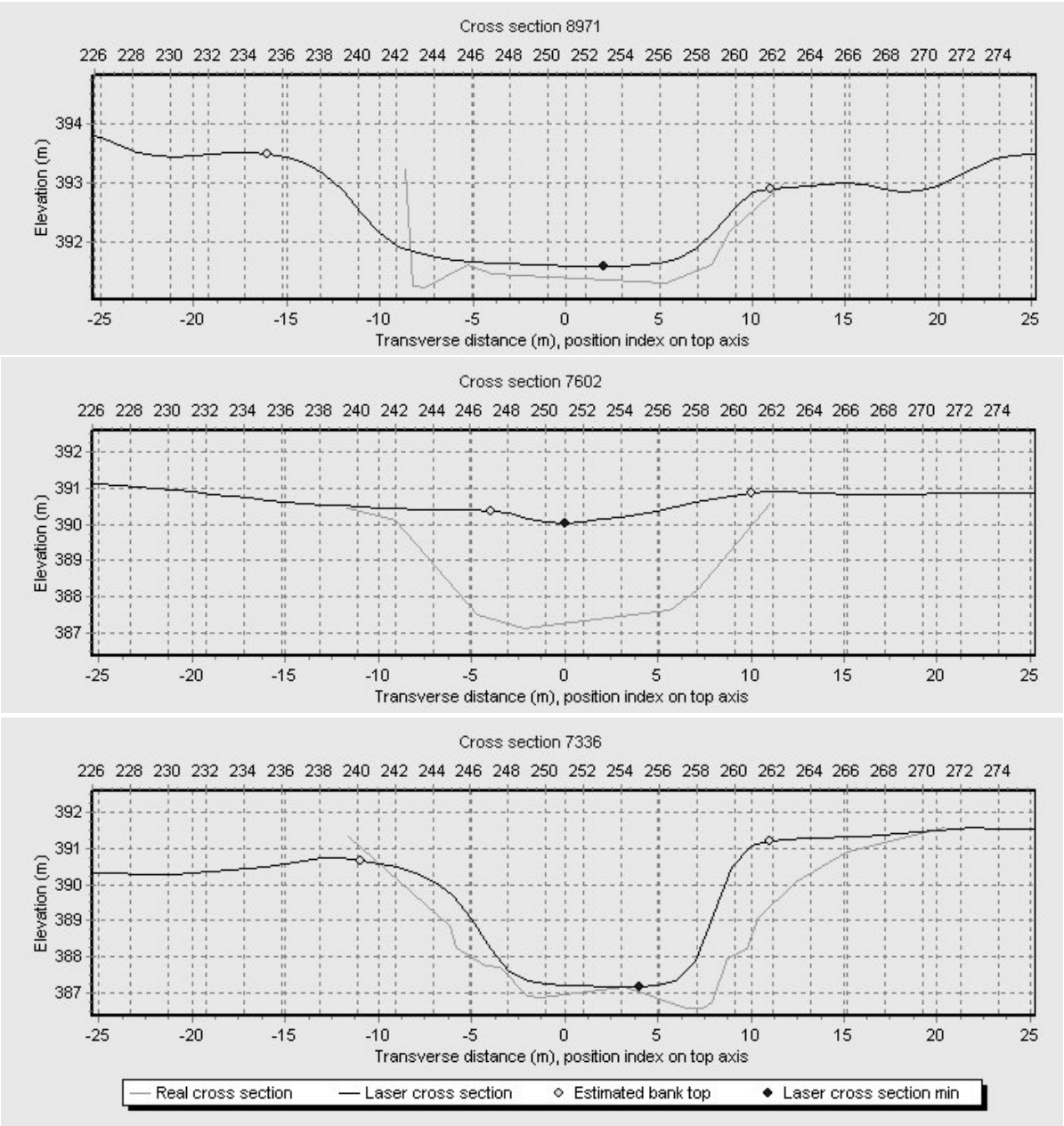

Figure 4.27. Examples from the Lower Venoge River comparing cross sections extracted from a LIDAR derived DTM and surveyed cross sections showing the interpolation problems of widening (top), bed raising (middle), and constriction (bottom).

4.4.3.1 Linear streamwise interpolation

Linear and meander based cross section interpolations have been explained in the previous sections. These methods are, of course, appropriate methods of interpolation, but require a certain effort in defining cross section geometry and performing hydraulic modeling before the interpolations can be run. To avoid these preliminary tasks, it is proposed here to linearly interpolate cross section points based on real upstream and downstream points that are at a given perpendicular distance to the channel centerline.

Such a method can be applied to the original channel LIDAR last return points or based on surveyed cross section data.

The cross section tool was extended to perform this linear streamwise interpolation. Cross section points can be created according to channel centerline node points at regular transversal spacing to an equal width on each side of the channel node point. These points (called laser cross section points here) are easily mapped in a GIS (figure 4.28). Surveyed cross section points and/or original LIDAR river points can then be attributed to the laser cross section points (figure 4.28). After this step, the points can then be opened again by the cross section tool to perform the interpolation. This interpolation is performed in two steps: first, cross section points are interpolated transversely such that any null value point that is surrounded by non-null points is interpolated, and secondly, interpolation proceeds by cross section position index in the streamwise direction (shown by the example interpolation line in figure 4.28).

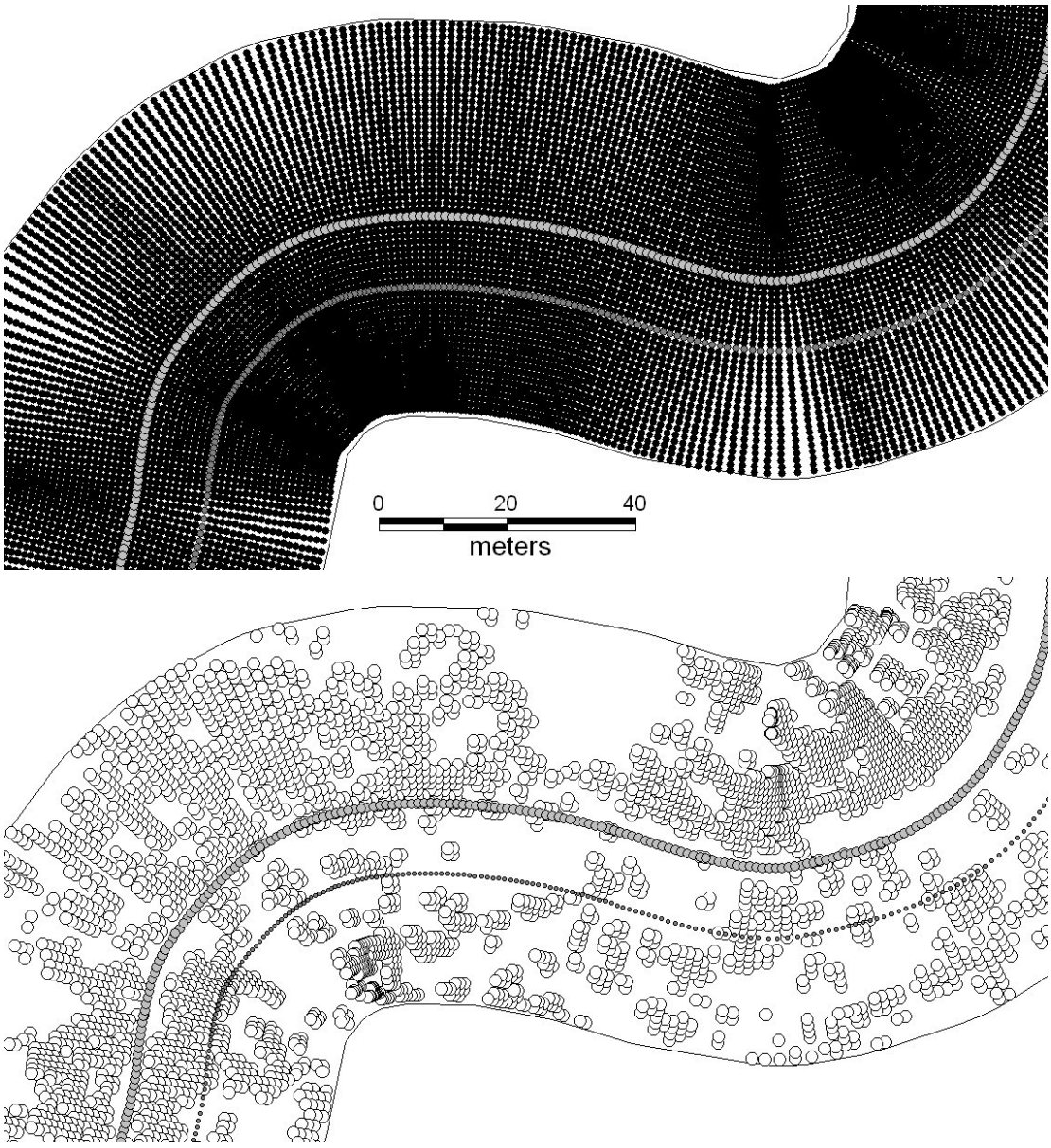

Figure 4.28. Top - Created cross section points (black) around the channel centerline (light grey). Dark grey circles show an interpolation line. Bottom - White circles show points that were attributed a laser point that will be used to interpolate elevation values onto points having a null elevation.

This streamwise interpolation causes poor original laser points to propagate their error downstream. This is often seen by abnormal bumps in the cross section. A smoothing algorithm can be applied to remove these bumps. The algorithm was programmed to use only local minimums for the channel bottom and all intermediate points are interpolated between the local minimums. The channel bottom is defined as the elevation halfway vertically between the channel minimum and the lower of the starting and ending laser cross section points. After this bump removal, an additional smoothing is run based on a moving average over three points except for the minimum point that is preserved.

4.4.3.2 Creation of a DTM with streamwise interpolated cross section points

The procedure for the creation of a DTM based upon the streamwise interpolated cross section points is then the following:

1. Laser cross section points are created such that the perpendicular cross section length is two times that of the maximum estimated river width.
2. Laser points (or surveyed cross section points) are attributed to laser cross section points. For the Lower Venoge River, any original laser point within 1 meter of the laser cross section point was attributed to that point. Points are averaged if several points are within the attribution radius.
3. Laser cross section points are then interpolated and smoothed in the cross section tool.
4. A DTM as well as a grid of the slopes of the linearly interpolated laser cross section points are made. For the Lower Venoge River, an Inverse Distance Weighted (IDW) interpolation was performed based on exponential weighting of 2 on the five closest points to create the DTM. A slope model can then be derived from the DTM in a GIS (figure 4.29).
5. The channel area is digitized from the slope model.
6. All laser points are opened and the channel area points are deleted.
7. Laser points without the channel area are interpolated.
8. The DTM produced in step 4 is trimmed according to the digitized channel area of step 5 and this river channel DTM is spliced onto the DTM of step 7 to produce the final DTM.

The above procedure was adapted slightly for the Lower Venoge stream corridor because the DTM had already been developed for the Lower Venoge without any special river interpolation (c.f. section 4.3). In this case, step 7 involves the following before performing step 8:

7. All laser points are interpolated together. For the Lower Venoge stream corridor, an IDW interpolation based on exponential weighting of 2 on the 25 closest points was used to create the DTM.

7a. A grid of the river banks without the channel is created. For the Venoge, this was done over a distance of two times the estimated maximum river width.

7b. This grid is maximized onto the grid created in step 7.

4.4.3.3 Results

Due to differences in dates of cross sections and the LIDAR points, and also due to an insufficient spacing of cross sections in some areas, it was chosen to interpolate LIDAR channel points streamwise instead of surveyed cross section points. A DTM was created upon the steps elaborated in the previous subsection. Although some artifacts remain from the linear interpolation and smoothing algorithms, the bank outline is significantly better in most areas. Comparison of the river integrated DTM and the non-river DTM shows a difference in channel volume of 119'260 m³, giving an average change in depth of 0.2943 m. The channel surface area is 405'208 m² for the downstream 18'488 m of length giving an average channel width of 21.92 m.

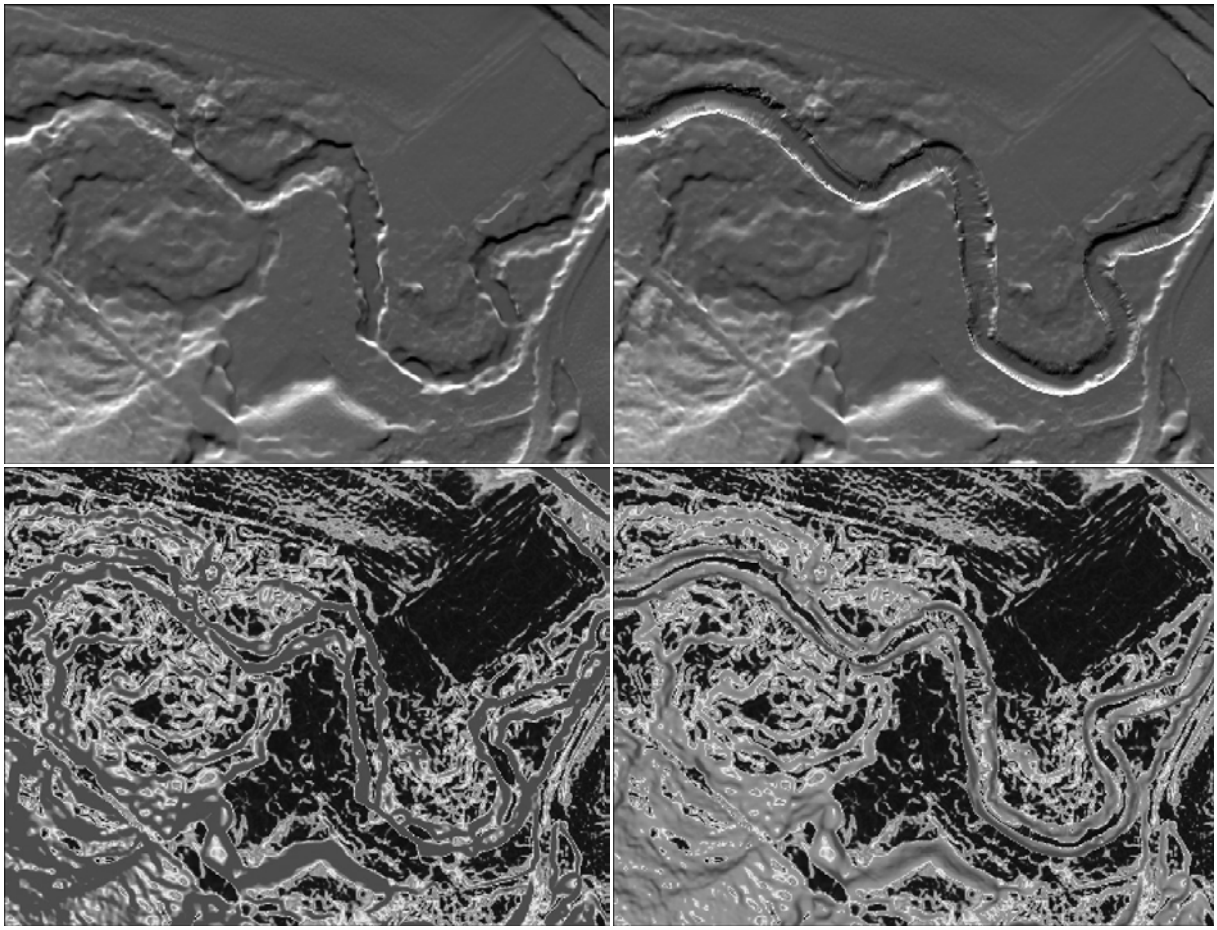

Figure 4.29. Comparison of the LIDAR derived non-river integrated DTM (top left) and corresponding slopes (bottom left) and the river integrated DTM (top right) and corresponding slopes (bottom left). LIDAR points come from DTM-AV ©2004, Swisstopo (DV043683).

4.4.3.4 Possible future developments

The improved channel definition obtained with the river integrated LIDAR DTM and the cross section interpolation methods leads to the following possible future developments:

1. Using the LIDAR DTM based only on LIDAR points, a relatively good water surface elevation indicative of the energy slope can be obtained. This was tested for the Lower Venoge and the results

seem good although more detailed survey data would be necessary to validate it (figure 4.30). The LIDAR DTM water surface longitudinal profile has significant noise. The profile was smoothed by the following procedure: the upstream elevation was used as the starting elevation, and then going downstream, the next downstream water surface point was not added to the longitudinal profile until its vertical difference was at least 50 cm. This was continued until the outlet. The longitudinal profile minimum was used as the outlet value. A good energy slope estimation could be very important for a regional streambank erosion model (see chapter 2.4.1).

2. Bank tops are much more clearly defined (figure 4.29). Either by manual digitization or by automatic detection, bank tops can be delimited. This would permit the bank height to be estimated from the LIDAR DTM which is an important variable in bank failure probability. Bank slopes could also be approximated. Again this bank information could be used in a regional streambank erosion model.
3. Cross section data that is from a different date than that of the LIDAR data and in an insufficient quantity is more frequent than the contrary and thus a procedure to properly integrate such survey data with a LIDAR DTM should be developed. Special attention needs to be taken when channel migration has occurred or when the bank heights and channel widths are significantly different than the interpolated cross sections. Such an integration method could be significant for streambank erosion modeling because it would improve the bank height definition of interpolated cross sections.

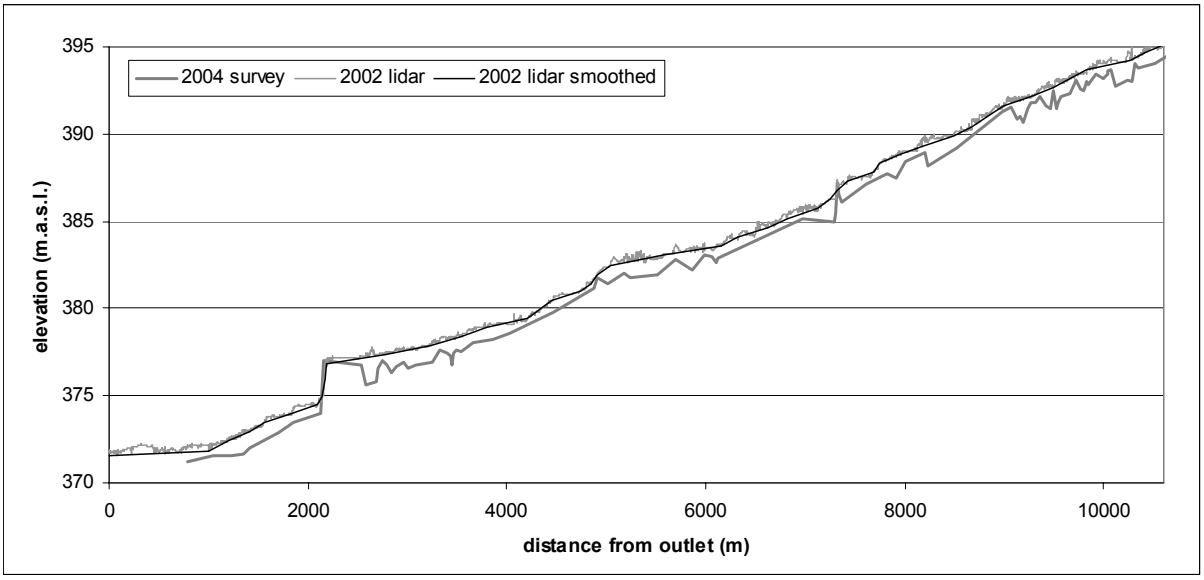

Figure 4.30. Approximation of the longitudinal water surface elevation profile with LIDAR data and comparison with the thalweg based on surveyed cross sections. LIDAR data from DTM-AV ©2004, Swisstopo.

4.5 Bed

4.5.1 Necessary input data

The bed data needed for use in a mobile bed hydraulic model are porosity, depth to bedrock, and the Grain Size Distribution (GSD) of the subpavement. Besides these data, the CCHE1D model uses a logical variable, a non-erodibility variable, that can be turned on if a river bottom should not be eroded. No bedrock exposure was found along the study reaches, so the depth to bedrock can be assumed to be great and a very large value will be used in the model to allow unlimited degradation. The non-erodibility option will be used only in the vicinity of the "Abbaye" weir. Rather than try to estimate an appropriate GSD for this improvised, large boulder weir, it was decided to consider the bed to be non-erodible at the brink down to its base. Concerning bed porosity, the tests necessary to determine it regularly along the reach would be too time consuming as important volumes of bed sediment would have to be analyzed. Values in literature range from 0.25 to 0.45 with more typical values being in the 0.30-0.40 (Church et al., 1987). It was decided to use the standard porosity value of 0.4 used in previous studies done with the CCHE1D model.

4.5.2 Grain size distribution

The Grain Size Distribution (GSD) of the bed sediment is of course a very important input data for the determination of the bedload transport. With the concave longitudinal profile of the Lower Venoge River it is to be expected that the average grain size will diminish as one progresses downstream. Thus, an appropriate sampling method will need to be employed to detect the significant changes in this downstream fining. The sampling method must also take into account that the subsurface needs to be sampled, which is not the same as the surface layer due to armoring.

4.5.2.1 Sampling techniques

There are numerous possibilities available for the determination of the GSD of a gravel bed river, which were initially described by Kellerhals and Bray (1971) and more recently by Petrie (1998):

1. Volume sampling: This method involves extracting a volume from the subsurface layer for sieve and gravelometric analysis. Church et al. (1987) calculated sample sizes based on the percentage of the weight of the largest stone compared to the sample weight. They calculated for a 10 cm maximum diameter (approximate Venoge study reach d_{max}) that the 0.1% criteria would necessitate a sample size of 1400 kg. They show also that the 0.1% criteria is similar to the ISO low precision standard 4364-1977(E). Fehr (1987) suggests that a volume analysis needs a size of $2.5 \times d_{max}$ where d_{max} is in m and the estimated volume is in m³. To calculate the GSD, the proportion of sediment in predefined classes is calculated by dividing the class weight by the total weight.
2. Grid sampling: This method involves placing a grid on the surface and sampling grains located on

each grid point. The b-axis, the middle dimension of the ellipsoid, is measured. Various grid spacing techniques exist: Wolman pacing (1954), using a wire grid, or using a survey tape at regular spacing. The grid spacing can be variable within an isotropic reach. The main criteria to respect is to avoid bias in selecting grains. It is easier to select larger grains that are more visible. The biggest problem with grid sampling is that there will be a truncation limit at approximately 1 cm because of the grain size one can reasonable pickup with his/her hand. Various authors (Hey and Thorne, 1983; Wolman, 1954; Kondolf, 1997; Fripp and Diplas, 1993; Rice and Church, 1996) have proposed sample sizes in the range of 40 - 1200 stones based on their replicate sampling tests, and the parameter and accuracy sought. Recently Petrie and Diplas (2000) made an important advancement in determining sediment sampling accuracy. They applied binomial and multinomial distributions for the quantification of the number of stones to be sampled for a given confidence interval for a given diameter (binomial) or for a given number of classes (multinomial). For example a confidence interval of 95% with a bounds of ±10 percent finer on an analysis using 10 classes would need a sample of 190 stones.

3. Areal sampling: It involves picking up all exposed surface grains in a given area for the determination of the GSD. The proportions of each class can then be determined by weighing or counting the grains. Usually this is done by weighing because a small grain size limit can be obtained according to the pickup procedure. The pickup procedures usually involve adhesives: clay, wax, or tape; or use spray paint to help in hand removal. Clay is often used because it can be used underwater. There is unfortunately an upper size limit to what the adhesives can pickup which is approximately a diameter of 4 cm. Analysis of photos is also possible, but is not recommended due to the b-axis being hidden at times.
4. Transect sampling: This method is similar to grid sampling in that it involves picking up stones from the surface, but is done by laying down a line (usually a tape measure) and then removing every surficial stone that lies under the line. The Fehr (1987) method is often used in Switzerland, although the method is rarely cited in scientific bed sampling literature. It recommends the pickup of a minimum of 150 stones.

Very little advance has been shown in the scientific literature concerning methods to combat the excessively large volumes needed to accurately describe the subpavement. The recent work of Petrie and Diplas (2000) needs to be mentioned again here because they extended the multinomial analysis to give sampling accuracy estimates not only for grid sampling but also for volume and areal sampling. In this sense, the sampling operator can determine the quantity to sample for the desired accuracy. Work still needs to be done to attack the problem of determining the GSD for the subpavement of a gravel bed river. The only real practical method developed in scientific literature seems to be the hybrid method suggested by Fripp and Diplas (1993) and revisited by Rice and Haschenburger (2004). This method involves determining the upper curve of the GSD by a truncated grid sample and the lower part of the curve by a truncated volume sample. Rice and Haschenburger (2004) postulate that the grid-by-number and the volume-by-weight distributions overlap in the middle of the GSD and this provides the necessary information to combine these two informations to form the total GSD. The other practical method, and much quicker than the hybrid method, is that of Fehr (1987). The Fehr method is quicker because no subpavement measurements are made. The distribution of fines in the total GSD is assumed to follow a Fuller curve in which the percent finer is equal to the value $\sqrt{d/(d_{max})}$.

4.5.2.2 Analysis techniques

To determine the GSD, it is necessary to determine the proportion of grains in each predefined size class. The number of classes depend on the size range to be covered. Fehr (1987) suggests classes that increase by a factor of $\sqrt{2}$. Others use classes that increase by the phi, $D = 2^{-\phi}$, or half phi ranges. The proportion of grains in each class can be determined by different analysis techniques: frequency-by-number, frequency-by-volume, frequency-by-area. Frequency-by-number involves counting the number of particles in a size class compared to the total population to determine the class proportion. Frequency-by-volume compares the class volume to the total volume. Volume is usually substituted by weight which is valid for particles with the same specific gravity. Frequency-by-area determines the class proportion by comparing the projected area of the class sediments to the total projected area.

4.5.2.3 Equivalence of sampling methods

Depending on the sampling method, the most common are volume-by-weight and grid-by-number and area-by-weight, a conversion may be necessary. The standard is to express sampling results in a volume-by-weight equivalent. Kellerhals and Bray (1971) laid the foundation for this standard. Their analysis of different sediments (represented by blocks) in a cube allowed them to determine the conversion formulas between the different sampling methods. Their conversion formula can be expressed generally by the formula (Petrie, 1998):

$$p(V-W)_i = \frac{p(S)_i D_i^x}{\sum (p(S)_i D_i^x)} \qquad \textit{Eq. 4.5}$$

where $p(V\text{-}W)_i$ is the proportion by volume-by-weight of the sediment in class i, $p(S)_i$ is the fraction of class i to be converted, D_i is the sieve diameter for size fraction i, and x is the conversion exponent. The conversion exponents proposed by Kellerhals and Bray are 0 for grid-by-number, -3 for grid-by-weight, 2 for area-by-number, and -1 for area-by-weight. Diplas and Sutherland (1988) used a modified Kellerhals and Bray cube which included blocks that represented porosity to show that the exponent for area-by-weight (when using wax as a pickup adhesive) varies in the range of -0.4 to -0.5 depending on the porosity. The value of -1 from Kellerhals and Bray should be used for area-by-weight conversions when using tape as an adhesive. No conversion exponents for line-by-number were found except for that proposed by Fehr which is 0.8.

4.5.2.4 Fehr conversion of pavement GSD to subpavement GSD

Fehr (1987) converts a line-by-number sample to a volume-by-weight sample using equation 4.5 with the conversion exponent of 0.8. He suggests that particles less than 1 cm should not be picked up. To estimate the fines that were not picked up, he proposes a correction of the GSD with the formula:

$$p_i c = 0.25 + 0.75 \times \sum_{1}^{i} p(S)_i \qquad \textit{Eq. 4.6}$$

where p_ic is the corrected cumulative proportion smaller than the class D_i. This GSD still does not represent correctly the fine distribution of the subpavement according to Fehr and he proposes that the fine part of the GSD should be replaced by a Fuller curve. He introduces the Fuller curve in the GSD by looking for the point on the curve that has a slope that coincides with the Fuller curve. The GSD that is finer than this point is replaced by the Fuller curve.

4.5.2.5 GSD's of the Lower Venoge River

The Fehr method was chosen for determining the GSD of the subpavement of the Venoge. Although, time will not allow this method to be compared in more depth to the hybrid method of Rice and Haschenburger (2004), this should be done to validate the Fehr method and an accuracy quantification should be done following the recommendations of Petrie and Diplas (2000).

Before the exact length of the Lower Venoge study reach was determined, line samples were collected from the zone of Lussery (km 22.5) down to km 1. A survey tape was laid on the ground and all grains falling below the tape edge and greater than 1 cm were measured for the b-axis dimension with a folding ruler (figure 4.31). The sampling was usually stopped at 150 stones. All sizes were recorded, and the values were assigned to classes following the suggestion of Fehr, applying a factor of $\sqrt{2}$; the first class starts at 1 cm, followed by 1.41, 2, 2.83 and so on. Forty-eight samples were collected on the Lower Venoge and 8 were collected on the four tributaries: Ruisseau de Molomba, Sorge, Vaube, and Arena.

Figure 4.31. The author performing a line sample on the Vaube tributary of the Venoge

Figure 4.32 shows an example of the results of a Fehr line analysis. The p_ic curve shows the distribution after correction with equation 4.6. The p_iFu curve shows the Fuller curve calibrated according to the appropriate intersection point of the p_ic curve. The resulting GSD is that of the p_iv curve.

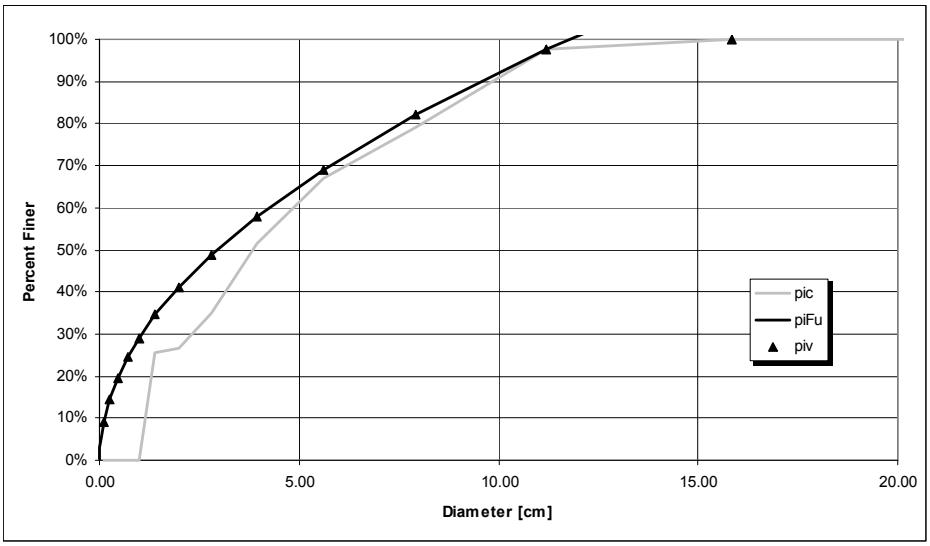

Figure 4.32. Example of a GSD determined with the Fehr line-by-number analysis on the Lower Venoge River

The GSD's (in terms of the class fraction) of the 56 samples are given in appendix 3. Figure 4.33 shows the results of the GSD's in terms of their characteristic diameters.

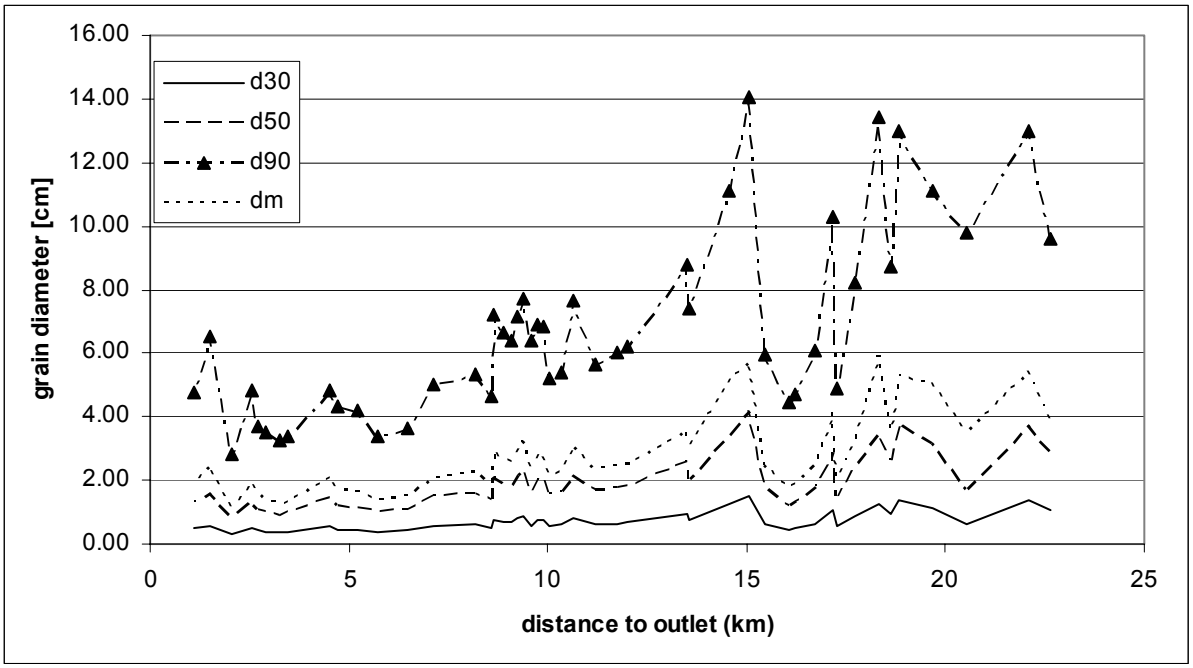

Figure 4.33. Evolution of the characteristic diameters of the bed sediment of the Lower Venoge

4.6 Bank

4.6.1 Input data and methods

The input data required by the CCHE1D model to describe streambanks are: bulk density (N/m^3), critical shear stress, τ_c (kPa), porosity (-), shear stress coefficient (-), cohesion (Pa), friction angle (°), specific gravity and the particle size distribution. The bulk density is interpreted to be the saturated unit soil weight as this is the weight that will typically be involved in mass failures. Values for cohesion and friction angle are the effective cohesion and effective friction angle. More or less attention can be given to certain parameters depending on the importance and type of bank failures and the type of streambank erosion simulations to be run.

Bank classification methods

At present, streambank erosion numerical modeling has been applied mostly to short reaches and consequently authors have used time consuming point measurements for determining the above listed bank parameters. It would seem necessary, though, to go towards a field inspection type of bank classification for streambank erosion modeling to be more practical for long reaches. It is assumed that each of the above parameters has a given distribution and that the mean values of those distributions can be used to represent the parameters throughout a reach with the same classification. Optimally, uncertainty analysis in streambank erosion modeling would employ Monte-Carlo analysis to sample the entire distributions.

In the Venoge case study, bank classification is based on the Unified Soil Classification System (USCS) as described in the Swiss standard SN 670 008a (VSS, 1997a). This classification involves the determination of the particle size distribution, Atterberg limits (liquid limit and plastic limit to determine the plasticity index), and organic content. Their determination are standard laboratory analyses and are described in many books (e.g. Terzaghi et al., 1996 and Mandal and Divshikar, 1995) and standards, so they will not be discussed here. Besides the USCS classification tests, porosity, natural unit weight, and water content were also determined by laboratory analysis.

Three levels of bank description were carried out on the Lower Venoge River:

1. USCS laboratory classification along with classification criteria suggested by Terzaghi et al. (1996) as well as pocket shear vane and penetrometer tests
2. USCS field classification, laboratory particle size distribution, and pocket shear vane and penetrometer tests
3. USCS field classification and pocket shear vane and penetrometer tests

The initial values of the parameters to be used will be based on typical values used in other streambank erosion studies (Darby, 2005 and Simon et al., 2002) and from index properties (Vss, 1999b) based on soil classification. Those values are given in table 4.6.

Description	Friction angle (°)	typical friction angle (°)	Cohesion c' (kPa)	typical cohesion c'	Saturated unit weight (N/m^3)	Matric suction friction angle (°)
Gravel	45-35	35	0	0	20000	10
Sand	40-30	37	0	0	18000	15
Sandy Silt	35-30	35	0-10	2.5	18000	15
Silt	35-25	30	0-10	5	18000	15
Soft clay	32-20	28	0-20	10	16000	15
Stiff clay	30-10	25	10-30	15	18000	15

Table 4.6. Cohesion and friction angle values as well as initial values used according to soil classification

Another possible method would be to rank banks according to their stability and erodibility. In the project SAFER, this was done for the stability of the streambanks of the Enrick River (table 4.7 and appendix 4). Point measurements are made at various places along the different bank types to estimate the parameters' distributions.

Bank type	Stability
Bedrock	Very High
Tree lined bank	High
Fine grained bank	High
Rip-rapped bank	High
Walled	High
Point bar	Moderate - High
Vegetated valley-side slope	Moderate but vulnerable to large floods.
Composite bank	Low- moderate
Cobble bank	Low
Eroding valley-side slope	Low –Frequent failures during high flows.

Table 4.7. Bank types and stability as evaluated in the SAFER project on the Enrick River (Jacobs Babtie, 2005)

Although the specific point measurements for determining effective cohesion, effective friction angle, and critical shear stress were not used for the Venoge, they will be presented here for completeness. Optimally, such point measurements should be used to provide the parameter distributions for bank types rather than deriving parameter distributions from index properties based on soil classification.

Point measurements for critical shear strength

While the critical shear stress of non-cohesive sediments is relatively well known by the work done by Shields and others and can be approximated by $\tau_c(N/m^2) \cong D_{50}(mm)$ (Briaud et al., 2001), the estimation of the critical shear stress of cohesive sediments is more complicated. Numerous soil properties have been shown to influence the erodibility of a cohesive soil such as antecedent moisture, clay mineralogy and proportion, density, soil structure, organic content, as well as pore and water chemistry (Grissinger, 1982). Various test procedures for determining critical shear stress are reported by Grissinger (1982), but recent literature has given most of its attention to three in situ measuring apparatus. They are the submerged jet apparatus (Hanson and Cook, 2004), the Erosion Function

Apparatus (EFA) tested for scour rate predictions (Briaud et al., 2001), and the cohesive strength meter (CSM) tested for measuring the in situ erosion shear stress of intertidal sediments (Tolhurst et al., 1999). The first two apparatus will be briefly described because they have been used specifically in the context of stream erosion.

The submerged jet test has been used in many studies (e.g. Hanson and Simon, 2001 and Simon and Thomas, 2002) and is described in detail by Hanson (2004). The principle behind the test is to erode a material with a jet of the eroding agent (water in our case). The critical shear stress is determined from the equilibrium scour depth. For a given jet velocity, scour will continue until the equilibrium scour depth is reached. The scour depth data versus time used with the Blaisdell et al. (1981 in Hanson, 2004) formulas permit the calculation of the critical shear stress. Once the critical shear stress, τ_c (Pa) has been determined, the erodibility coefficient, k_d (m³/N-s), can then be determined by the excess shear stress erosion rate formula:

$$\varepsilon_r = k_d(\tau_e - \tau_c) \qquad \textit{Eq. 4.7}$$

where τ_e is the effective hydraulic stress (Pa) and ε_r is the erosion rate (m/s) which is known from the scour depth versus time data.

The EFA is not an in situ test, but rather uses an intact soil sample in the laboratory apparatus. The principle behind this test is to push a cylindrical soil sample perpendicularly into a rectangular pipe of flowing water. The flow velocity for the pipe is controlled so the eroding shear stress is known from hydraulic pipe formulas. The erosion rate is determined by pushing 1 mm of the soil sample into the flowing water and measuring the time needed to erode it. This is done at several flow velocities permitting the plotting of the shear stress versus erosion rate curve. The critical shear stress is determined by the first velocity that is able to erode the sediment and the erodibility coefficient is then determined with equation 4.5 by plotting the excess shear stress versus the erosion rate (Briaud et al., 2001).

Point measurements for effective cohesion and friction angle

The determination of effective cohesion and friction angle by soil shear box tests and triaxial compression tests is well known and presented in many textbooks (e.g. Mandal and Divshikar, 1995, Terzaghi et al., 1996, and Selby, 1993). The triaxial test is preferred because of its versatility in performing drained, undrained, or consolidated undrained tests. These test methods won't be described further because their cost essentially negates their use over a long stream reach.

The Iowa Borehole Shear Tester (BST) is the in situ measuring device that has been used frequently in streambank failure studies (e.g. Simon et al., 2002 and Simon et al., 2000). The BST is inserted into a borehole. The head consists of a piston that can expand to apply a normal stress to the shear plates. Transducers in the shear plates measure the pore-water pressure. An upward shearing stress is applied to the plates. Thus, the normal and shearing stresses are known as well as the pore-pressures so that the apparent cohesion and the resulting effective cohesion and effective friction angle can be determined. Many tests can be done in the same borehole at different depths in the borehole and at different normal stresses. The BST is the preferred device for determining the soil strength parameters because it is applied to the soil in its natural state and at natural pore-pressures (Selby, 1993). Saturated tests can also be performed by filling the borehole with water.

Pocket shear vane and penetrometer tests (figure 4.34) can be used to gain a rough idea of the soil strength. A shear vane has four rectangular blades on a rod which are set at right angles to each other. The shear vane test indicates total stress and is dependant on the moisture content at the time of the test so that the test result can not be used directly to determine the effective cohesion and friction angle. Pocket penetrometers have a rod that can be pushed into the soil. The force needed to insert the penetrometer rod into a soil a preset distance is recorded. The penetrometer reading is a useful indicator of bulk density, but is not a reliable indicator of shear strength. Shear vanes are most suitable in fine-grained soils and care must be taken with both of the instruments not to use them in soils with roots, clasts, or strongly developed soil structure (Selby, 1993).

Field shear boxes can also be used, but are much more time consuming than the BST measurements. Notably, the field shear box test has been used by Wu et al. (1988) to determine the contribution of roots to the shear strength of soils.

Figure 4.34. Pocket penetrometer (left) and shear vane (right) used during the Lower Venoge bank investigations

Bank classification methods and soil strength parameters

Various authors (Briaud et al., 2001, and Hanson and Simon, 2002) have shown that no correlation exists between USCS soil classes and soil strength properties. Thus, there is a real dilemma of how to practically determine the soil strength parameters for streambank erosion hazard modeling. Point measurements are too timely and costly to be performed over a large area, but bank classification based on soil type has failed up to date. It is hypothesized that even with a large number of point measurements, bank heterogeneity is such that soil strength parameter calibration will be needed regardless. Concerning the bank toe critical shear stress, one value is certainly not enough as the value for the original bank toe sediment is probably different than that of failed basal sediments. Therefore, it is hypothesized that more time should be devoted to understanding and observing erosion and failure processes than for performing point measurements. Model parameters can be adjusted or calibrated to try to mimic the observed erosion and failure processes.

4.6.2 Bank classification and results

As mentioned in the previous section, three levels of investigation were done on the Lower Venoge River. Level 1 investigation was carried out on each erosion monitoring bend, while level 2 investigations were carried out at a 1 kilometer interval and level 3 investigations at a 500 meter interval. Sampling was mostly done on bend exteriors to avoid sampling of sandy bend interior deposits. Figure 4.35 shows the locations of the sampling and the type of investigation performed.

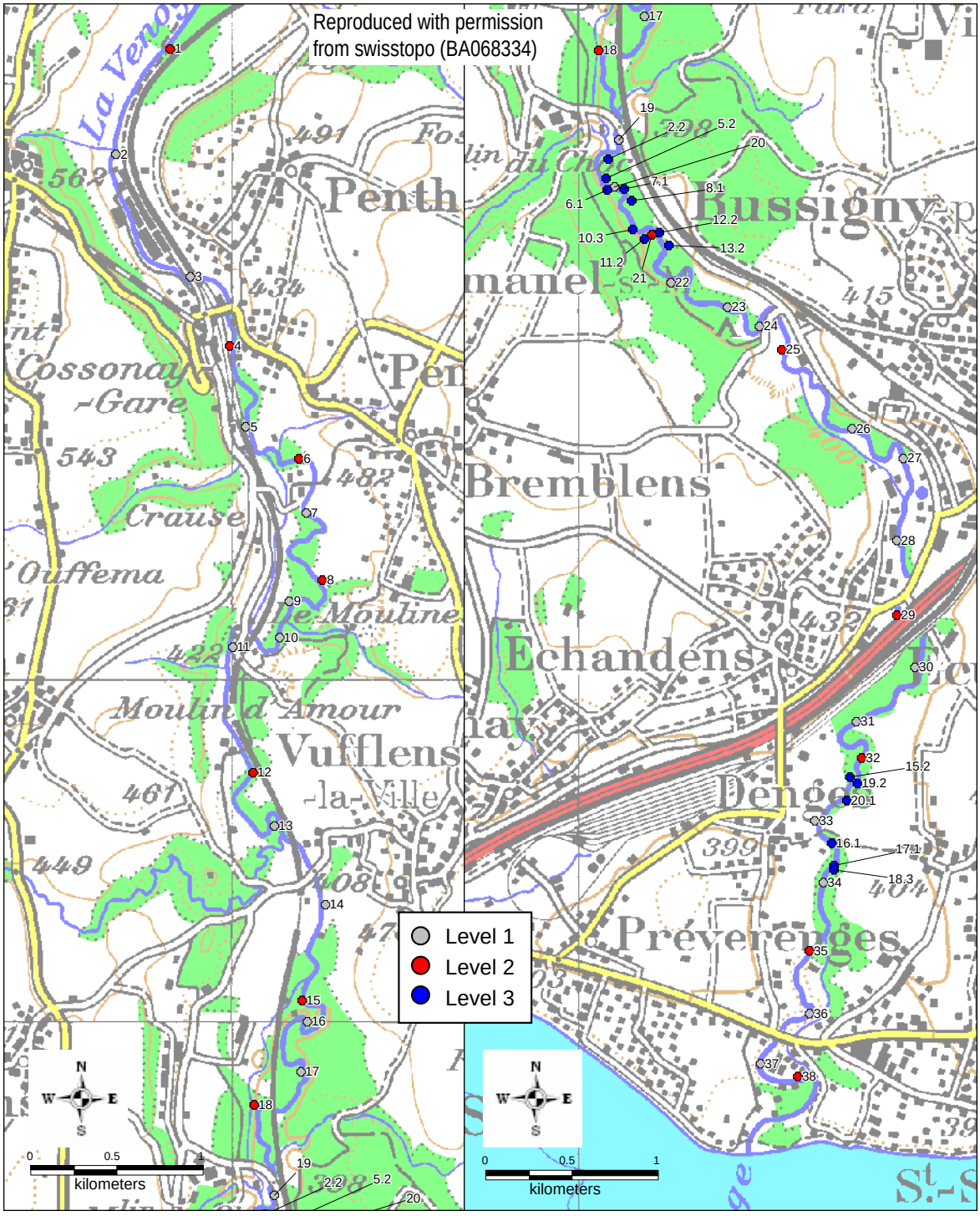

Figure 4.35. Bank sampling locations and the level of investigation (Background maps: CP100 ©1997, Swisstopo)

Table 4.8 shows the bank soil properties that were collected in the level one investigations and how they are determined and the possible values for qualitative testing. Table 4.9 shows the principal results for the monitored bends. It can be noticed that complete level one investigation was not possible of course for non-cohesive soils: shear vane, penetrometer, atterberg tests, and intact soil sampling are not possible. Some layers were not completely tested because of their limited thickness.

	bend/layer	
	thickness	
	representative of	
	photo number	
1. Color		Munsell chart
2. Odor		strong, medium, weak, none
3. Texture:	A. appearance after fracture	granular, dull, smooth, glossy
	B. feeling to fingers	floury, smooth, gritty, sharp
4. Grain properties:	A. form of particles	angular, subangular, subrounded, rounded, well rounded
	B. mica content	high, medium, low, none
	C1. type of organic matter	fibers, twigs, leaves, …
	C2. State of organic matter	visible, slightly visible, decomposed
5. Dry crushing strength		very high, high, medium, low, very low
6. Dilatancy		fast, slow, none
7. Toughness	at plastic limit	high, medium, low, none
8. Ribbon	length	short, medium, long
9. Stickiness		strong, medium, weak, none
10. Porosity (-)		laboratory analysis
11. Moisture content (%)		laboratory analysis
12. Natural unit weight (g/cm3)		laboratory analysis
13. Dry unit weight (g/cm3)		laboratory analysis
14. Unconfined compressive strength, qup (kN/m2):		field test
Unconfined compressive strength after remolding, qur (kN/m2):		field test
Sensitivity, qup/qur		calculation
15. Shear vane result (kN/m2)		field test
16. Liquidity limit, wl (%)		laboratory analysis
17. Plasticity limit, wp (%):		laboratory analysis
Plasticity index (%):	Ip=wl-wp	calculation
18. Particle sizes (mm):	Dmax	
	D90	laboratory analysis
	D60	laboratory analysis
	D50	laboratory analysis
	D30	laboratory analysis
	D10	laboratory analysis
	dm	calculation
	% Gravel	laboratory analysis
	% Sand	laboratory analysis
	% Silt	laboratory analysis
	% Clay	laboratory analysis
	Cud (d60/d10)	calculation
	Ccd (d30^2/(d10*d60))	calculation
19. Carbonate content:	Reaction to HCl	strong, medium, weak, none
Comments:		
Field classification USCS of the fines		
Laboratory Classification USCS:		
Classification name		

Table 4.8. Field and laboratory tests performed in the detailed level 1 of bank investigation for the classification of the bank soil. The right column indicates the method or possible values.

id	bend/ layer	thickness (cm)	10. Porosity (%)	11. Moisture content (%)	12. Natural unit weight (g/cm³)	13. Dry unit weight (g/cm³)	14. Unconfined compressive strength, qup (kN/m²)	15. Shear Vane result (kN/m²)	16. Liquidity limit, wl (%)	Plasticity index (%)	Particle size distribution				19. Carbonate content	Laboratory Classification USCS	Classification name
											% Gravel	% Sand	% Silt	% Clay	Reaction HCl		
83	2.1	0-30	63.3	28.0	1.2	1.0	56.7	42.3	27.4	7.2	0.5	53.0	29.2	17.2	strong	SC	clayey sand
84	2.2	30-50	48.3	13.5	1.6	1.4	92.1	56.2	19.8	3.2	0.6	60.5	27.3	11.6	strong	SM	silty sand
85	2.3	50-80	52.0	14.6	1.5	1.3	80.0	74.0	26.0	5.0	0.7	50.7	35.1	13.5	strong	SC-SM	silty, clayey sand
86	2.4	95-130	46.7	17.3	1.7	1.4	12.5	20.3	27.6	6.8	3.6	59.6	25.5	11.3	strong	SC-SM	silty, clayey sand
88	5.2	20-110	60.0	22.8	1.4	1.1	80.4	69.2	27.0	3.6	0.0	20.9	67.8	11.3	strong	ML	silt with sand
89	6	0-20 cm					13.8	23.5							strong		silty sand
90	6.1	20-130 cm	51.3	15.9	1.7	1.4	37.9	35.0	21.2	2.2	0.0	59.6	20.4	20.1	strong	SM	silty sand
91	6.2	130-140 cm						36.0	18.0	0.0	9.1	71.1	14.4	5.3	strong	SM	silty sand
92	6.3	140-fond						0.0			61.7	29.0	7.0	2.4	strong	GP-GM	Poorly graded gravel with silt and sand
93	7.1	10-120 cm	56.0	34.6	1.7	1.2	46.7	43.0	30.0	11.8	0.0	49.5	39.9	10.7	strong	CM(CL)	clayey, sandy silt
94	8	0-60 cm					45.0	40.3							strong		silty sand
95	8.1	60-140 cm	48.7	12.0	1.7	1.4	53.8	43.0	20.3	2.4	0.0	54.7	32.3	13.0	strong	SM	silty sand
96	8.2	140-160 cm													strong		sand with gravel
97	8.3	160-fond	47.7	17.2	1.8	1.4	35.4	27.7			0.2	87.1	9.5	3.1	strong	SW-SM	Well graded sand with silt
98	10.1	0-30 cm					10.4	11.0	29.7	1.4					strong		silt with sand
99	10.2	30-50 cm	71.0	30.7	1.3	1.0	28.3	24.0	42.2	8.3	0.0	23.2	55.5	21.4	strong	ML ou OL	silt with sand
100	10.3	50-190 cm	56.0	19.4	1.8	1.4	41.3	51.2	24.7	3.5	0.0	38.8	58.0	3.2	strong	ML	sandy silt
101	11.1	0-30 cm					21.3	43.5	35.0	4.1					strong	ML	sandy silt
102	11.2	30-240 cm	54.3	19.2	1.7	1.3	42.5	37.7	41.6	18.2	0.0	34.7	52.5	12.8	strong	CM	sandy lean clay
103	12	0-20 cm					110.0	89.8									limon sableux
104	12.1	20-60 cm	58.3	20.1	1.6	1.3	137.1	84.5	46.3	18.3	0.0	10.6	43.1	46.3	strong	ML (limit CM-CH-MH)	silt
105	12.2	60-190 cm	50.3	14.3	1.7	1.4	145.8	90.4			0.0	67.5	19.6	12.9	strong	SM	silty, clayey sand
106	12.3	190-fond	54.0	8.6	1.5	1.4	165.8	0.0			31.7	51.2	8.2	8.8	strong	SC-SM	silty, clayey sand with gravel
107	13.1	0-20 cm	48.3	13.4	1.6	1.4	94.2	37.0			8.3	42.7	35.0	14.0			silty sand
108	13.2	20-fond	49.0	15.0	1.7	1.4	75.0	66.8			0.1	37.1	46.2	16.6			sandy silt
110	15.1	20-60 cm	53.3	12.6	1.4	1.2	50.4	26.8	22.8	4.8	0.0	79.6	16.1	4.2	strong	SC-SM	silty, clayey sand with gravel
111	15.2	60-200 cm	56.7	18.8	1.5	1.2	69.6	54.7	31.2	5.0	0.0	36.4	46.7	16.9	strong	ML	sandy silt
112	16.1	30-fond	54.3	22.3	1.6	1.2	42.1	45.7	25.6	3.6	0.0	41.3	45.2	13.5	strong	ML	sandy silt
113	17.1	10-140 cm	60.0	22.0	1.4	1.1	45.0	36.7	19.8	1.5	0.0	52.5	36.0	11.6	strong	SM	silty sand
114	17.2	140-fond					5.0	11.0	19.6	1.1					strong	SM	silty sand
115	18.1	0-90 cm					21.3	24.7	30.9	9.9					none		sandy silt
116	18.2	90-170 cm						0.0							strong		Silty gravel with sand
117	18.3	170-fond	58.3	28.4	1.7	1.3	54.2	98.8	43.2	13.9	0.0	0.2	87.2	12.6	none	ML	silt
118	19.1	0-50 cm	69.0	17.6	1.5	1.2	88.8	40.0	26.9	3.0	10.1	47.8	37.6	4.5	strong	SM	silty sand
119	19.2	50- fond									74.9	24.1	0.6	0.4	none	GW	well graded gravel with sand
120	20.1	80- fond	83.0	79.4	0.7	1.1	95.0	21.3	31.8	4.7	1.3	35.1	49.1	14.4	strong	ML	sandy silt

Table 4.9. Results of level 1 soil analyses for the monitored erosion bends and their USCS classification

Results of the level 2 and 3 investigations are shown in tables 4.10. For a specific map location, two or three classification tests were done at different levels on the bank. The first test was done on the face of the bank, the second one on or near the top of the bank, and the third one on the top of the bank. Shear vane and penetrometer results are the average of 6 readings conducted on soils after removal of the vegetation layer (approximately 20 cm depth). The apparent cohesion value is the minimum of the shear vane result or half of the penetrometer reading. Of course this apparent cohesion value is dependant on the moisture content of the soil. The frequency of the particle size distributions for the level 2

investigations is evident by the Particle Size Distribution (PSD) column. For the level 2 investigations, three PSD analyses were averaged to obtain the final distribution.

date	id	id map	Shear Vane, su	Penetrometer, qup	Apparent cohesion, cu	roots	PSD	Moisture content (%)	Natural unit weight (g/cm³)	USCS field classification
			kN/m²	kN/m²	kN/m²					
29.03.2004	1	1	38.5	74.2	37.1					
29.03.2004	2		88.2	257.5	88.2					
29.03.2004	3		46.0	146.7	46.0		yes	27.57	1.09	SL
29.03.2004	4	2	24.0	50.0	24.0					
29.03.2004	5		51.0	98.3	49.2					
29.03.2004	6	3	21.5	40.0	20.0	1				S
29.03.2004	7		20.0	118.3	20.0	1				SL
29.03.2004	8	4	21.5	51.7	21.5	1				SL
29.03.2004	9		51.5	126.7	51.5	1	yes	27.34	1.01	LS
29.03.2004	10	5	27.0	52.5	26.3					SL
29.03.2004	11		19.8	61.7	19.8					SL
29.03.2004	12		9.0	42.5	9.0					SL
29.03.2004	13	6	56.0	125.8	56.0					LS
29.03.2004	14		51.2	288.3	51.2		yes	16.40	1.06	SL
29.03.2004	15	7	30.3	73.3	30.3					SL
29.03.2004	16		31.3	95.8	31.3					
29.03.2004	17	8	81.2	253.3	81.2					LS
29.03.2004	18		86.2	242.5	86.2		yes	18.76	1.19	SL
29.03.2004	19	9	37.3	79.2	37.3					LS
29.03.2004	20		68.7	100.8	50.4					LS
19.04.2004	21	10	25.3	56.7	25.3					SL
19.04.2004	22		36.0	101.7	36.0					SL
19.04.2004	23	11	23.7	59.2	23.7					LS
19.04.2004	24		63.3	135.8	63.3					
19.04.2004	25	12	52.7	215.8	52.7					LS
19.04.2004	26		25.2	50.0	25.0		yes	21.35	0.91	SL
19.04.2004	27		19.5	46.7	19.5					SL
19.04.2004	28	13	33.5	52.5	26.3					LS
19.04.2004	29		50.3	111.7	50.3					LS
19.04.2004	30	14	64.0	135.0	64.0					LS
19.04.2004	31		28.8	80.0	28.8	1				SL
19.04.2004	32	15	48.3	75.0	37.5					LS
19.04.2004	33		66.0	114.2	57.1		yes	24.88	0.94	LS
19.04.2004	34	16	28.3	57.5	28.3					SL
19.04.2004	35		18.7	31.7	15.8					S
19.04.2004	36	17	31.2	90.8	31.2					LS
19.04.2004	37		25.5	55.0	25.5	1				LS
19.04.2004	38	18	22.0	35.0	17.5	1				LS
19.04.2004	39		45.8	40.0	20.0	1	yes	32.18	0.88	SL
26.04.2004	40	19	22.0	47.5	22.0	1				S
26.04.2004	41		44.2	63.3	31.7	2				SL

Table 4.10. Results of the level 2 and 3 bank investigations on the Lower Venoge River. Root density is medium with a value of 1 and high with a value of 2. LS is a sandy-silt and SL is a silty-sand.

date	id	id map	Shear Vane, su	Penetrometer, qup	Apparent cohesion, cu	roots	PSD	Moisture content (%)	Natural unit weight (g/cm³)	USCS field classification
			kN/m²	kN/m²	kN/m²					
26.04.2004	42	20	2.5	0.0	0.0					S
26.04.2004	43		10.8	21.7	10.8	1				S
26.04.2004	44	21	66.3	241.7	66.3					LS
26.04.2004	45		22.7	55.8	22.7		yes	15.72	1.30	SL
26.04.2004	46		23.8	35.8	17.9	1				S
26.04.2004	47	22	26.5	45.8	22.9	1				LS
26.04.2004	48		62.7	102.5	51.3	1				LS
26.04.2004	49	23	12.3	29.2	12.3	1				SL
26.04.2004	50		30.2	62.5	30.2	2				SL
26.04.2004	51	24	10.7	29.2	10.7	2				SL
26.04.2004	52		16.0	38.3	16.0	2				SL
26.04.2004	53	25	59.5	96.7	48.3	1				LS
26.04.2004	54		75.7	167.5	75.7	1	yes	22.47	1.01	LS
26.04.2004	55	26	26.2	78.3	26.2	1				LS
26.04.2004	56		23.8	44.2	22.1	1				LS
03.05.2004	57	27	61.3	119.2	59.6	1				LS
03.05.2004	58		32.7	62.5	31.3	1				SL
03.05.2004	59	28	77.0	148.3	74.2	1				SL
03.05.2004	60		61.3	176.7	61.3	1				SL
03.05.2004	61	29	22.7	91.7	22.7	2				SL
03.05.2004	62		25.0	72.5	25.0	1	yes	10.30	0.83	SL
03.05.2004	63		20.0	45.8	20.0					SL
03.05.2004	64	30	21.7	48.3	21.7	1				S
03.05.2004	65		39.2	133.3	39.2	1				LS
10.05.2004	66	31	21.0	30.8	15.4	2				LS
10.05.2004	67		16.8	45.8	16.8	2				LS
10.05.2004	68	32	54.2	116.7	54.2	2				LS
10.05.2004	69		45.0	148.3	45.0	1	yes	15.78	1.12	SL
10.05.2004	70		32.2	104.2	32.2	2				LS
10.05.2004	71	33	41.5	115.0	41.5	1				SL
10.05.2004	72		28.7	104.2	28.7	2				SL
10.05.2004	73	34	43.8	52.5	26.3	1				LS
10.05.2004	74		41.0	95.0	41.0	1				LS
10.05.2004	75	35	24.5	57.5	24.5	1				LS
10.05.2004	76		21.5	65.0	21.5	2	yes	14.46	1.09	SL
10.05.2004	77	36	53.5	81.7	40.8	2				SL
10.05.2004	78		33.7	73.3	33.7	2				SL
10.05.2004	79	37	45.2	58.3	29.2	1				LS
10.05.2004	80		46.3	60.8	30.4	2				LS
10.05.2004	81	38	47.7	67.5	33.8	1				SL
10.05.2004	82		25.0	56.7	25.0	2	yes	28.32	1.02	SL

Table 4.10 (cont.). Results of the level 2 and 3 bank investigations on the Lower Venoge River

In the level 2 PSD's, it was evident that there was little PSD variability (c.f. appendix 5) and that one PSD is sufficient at a location for the level 1 investigations to get a representative bank PSD. All of the determined particle size distributions are shown in figure 4.36. It can be seen in this graphic the majority of distributions are typical of silty sand or sandy silt soils. Only the two left distributions and the two right distributions depart from these typical alluvial soil distributions. The particle size distributions are also shown on textural triangles in appendix 5 to allow a comparison of the Lower Venoge PSD's with those shown in appendix 1.

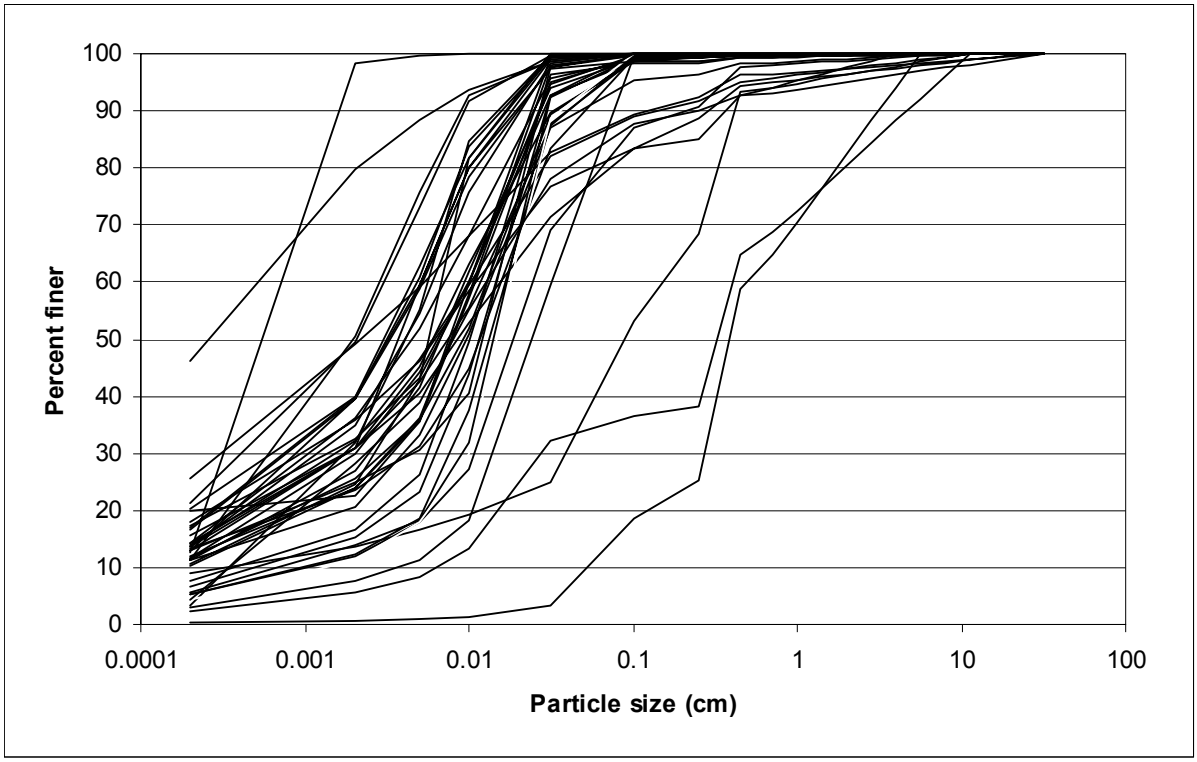

Figure 4.36. Particle size distributions of the Lower Venoge banks

As has been mentioned earlier, it is not expected to find correlations between the USCS soil classes and the soil properties. The initial soil strength parameters to be used in the streambank erosion modeling will be based on the observed soil classes and the typical values given in table 4.6. The soil strength parameters will then be calibrated according to erosion observations and correlations between soil classes and/or shear vane results will be investigated.

The bank analyses served to prepare the bank input for the CCHE1D model. Figure 4.37 shows the soil areas that were estimated according to the point sample results. Further point sampling would be necessary to ensure these soil areas are correct, especially at distances far away from the original sampling points. Figure 4.37 also shows bank protection works. At these locations, subdivisions of the bank soil areas have been made so that non-erodible banks can be incorporated, if desired, in the bank erosion simulations.

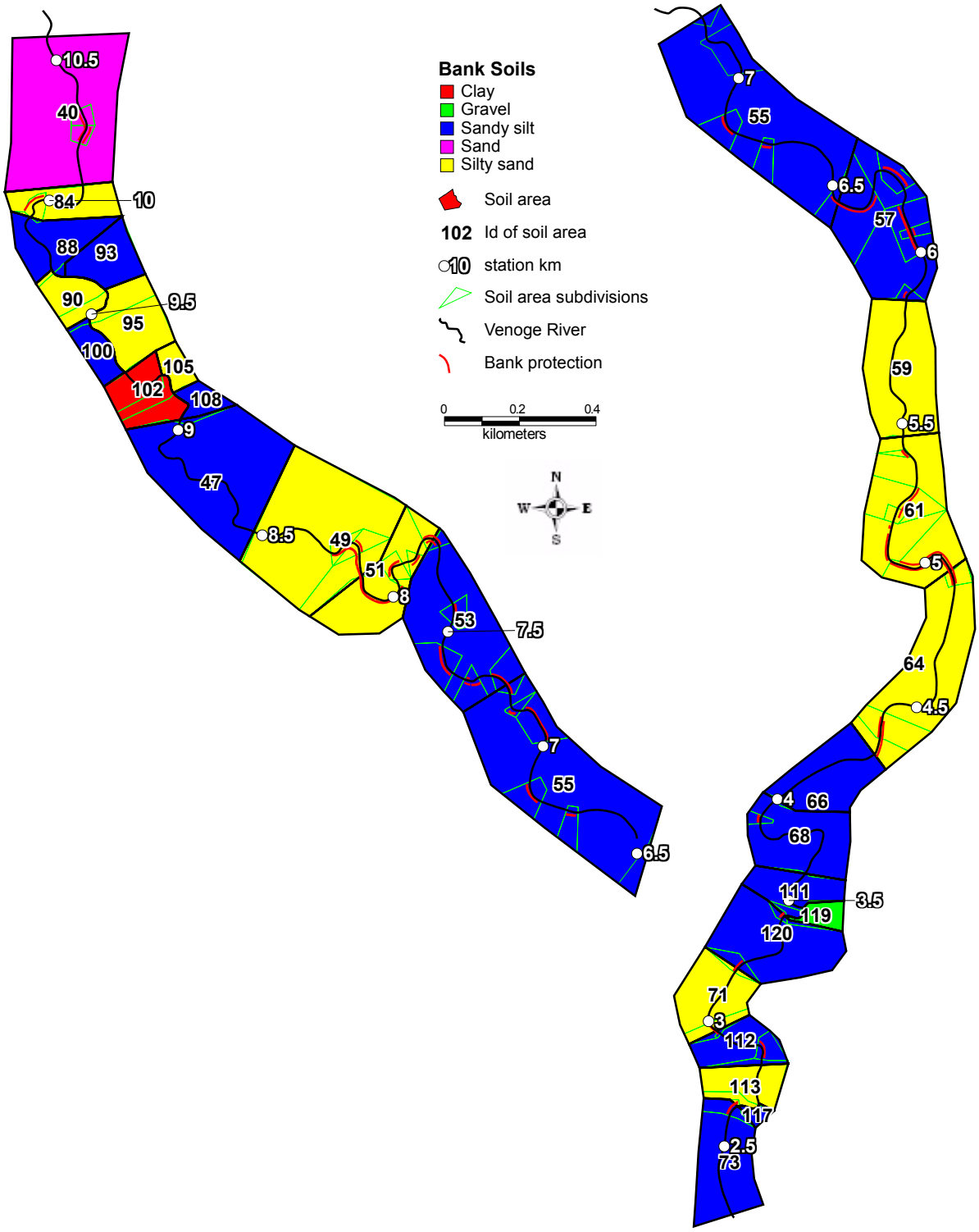

Figure 4.37. Soil areas along the Lower Venoge River according to field investigations to be used in the streambank erosion modeling

4.7 Boundary conditions

Streambank erosion modeling necessarily implies the specification of boundary conditions. The CCHE1D model needs to know sediment and discharge input the length of the study reach as well as the downstream water depth for the subcritical hydraulic calculations of the model. Approximations for these boundary conditions are made for the Lower Venoge River study reach in the following manners:

1. Discharge input will be based on hydrologic modeling which is described in chapter 5. A historical discharge series (Ecublens, Les Bois, figure 4.2) is available which will permit the calibration of the model and the refinement of the simulated discharges.
2. Sediment input is based upon a sediment transport capacity equation. Only three sediment transport curves need to be developed for the Venoge study reach: the upstream Venoge input, and the two main tributaries, the Vaube and the Arena, input, as all other tributary input are small and thus assumed to be clear water. The sediment transport curves (figure 4.38) are based on the Smart and Jaeggi equation (equation 2.3). Channel slopes for the Vaube and the Arena are approximated based on the LIDAR DTM and their average channel dimensions near their outlets were measured at the same time that bed GSD samples were taken.
3. The downstream rating curve (figure 4.39) is approximated with the Manning/Strickler formula.

Sediment and water discharge are input into the CCHE1D model via a text file requiring a given format (Vieira and Wu, 2002). A program was written to prepare this text file. The hydrograph and sediment transport curve and corresponding GSD for each node as well as the starting and ending dates of the high flow events are read by the program. Sediment input is divided into the grain size classes according to the GSD of the bed at the input location.

4.8 Summary and conclusions

The goal of this chapter was to show the data that was collected and measured to be able to simulate streambank erosion and to describe the measurement methods. Erosion scars were observed on the Lower Venoge River from km 22.390 to km 0.789 as shown in figure 4.1. This allowed two detailed zones, km 10.100 to km 9.075 and km 3.510 to km 2.650, to be identified for detailed erosion monitoring. These zones were monitored for erosion from November 2003 through September 2005 and for flow depth from March 2004 through August 2005. The streambank erosion modeling zone was chosen to encompass these erosion monitoring zones going from km 10.516 to km 2.538.

Erosion and failure processes were better understood with the detailed erosion measurements. Bank failures on the Venoge River are mostly soil falls and slab failures. It is very difficult to distinguish between these two failure types because it is unknown to what extent the bank is being undercut before the failure. Cantilever failures occur also, mainly due to vegetative effects, but also due to composite bank stratigraphy. Often soil fall occurs in combination with fluvial toe erosion to undercut highly vegetated banks before a cantilever fail occurs.

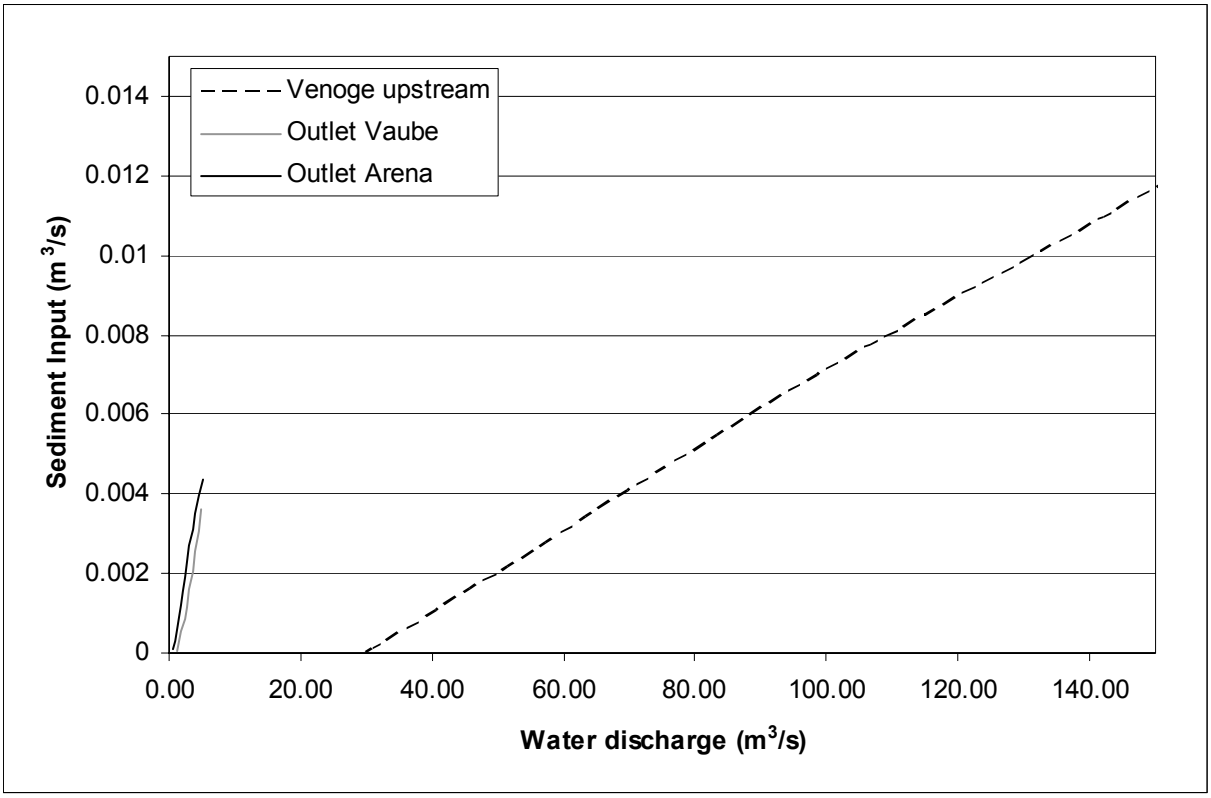

Figure 4.38. Sediment transport curves for the estimation of sediment input into the Lower Venoge River study reach

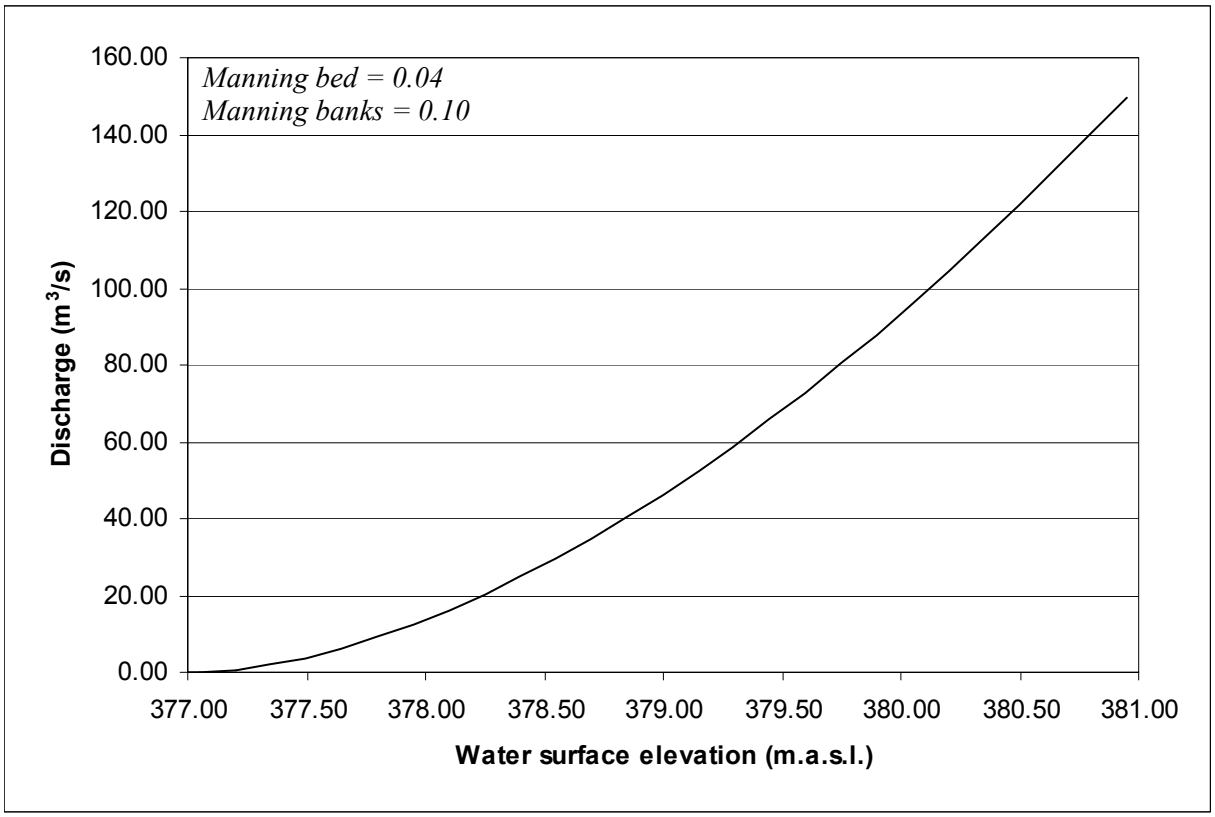

Figure 4.39. Estimation of the downstream rating curve for the Lower Venoge River study reach

Bank retreat rate is determined by basal endpoint control. This is particularly important for the Lower Venoge River where non-cantilever bank failures are small (usually less than 1 meter) and failures can be multiple during a high flow event.

Erosion was monitored with erosion pins, two PEEP sensors, and bank profiling. The PEEP sensors were difficult to install because of the gravel and roots in the alluvial soils. Measurement values also fluctuated too much to be able to correctly measure fluvial erosion. One of the PEEP sensors did record a soil fall that was distinguishable with the measurements. This measurement confirmed that fluvial erosion was not responsible for the retreat recorded at that point and that fluvial toe erosion can cause these small soil falls below a vegetative cover on the bank top.

If erosion is active enough, bank profiling is to be preferred because of the toe measurement that is important. Bank profiling and pin erosion measurements can be used together, though, and the experimental system to do so was explained.

Historical maps, orthophotos, and topographic LIDAR data (surface and terrain) were obtained for the Lower Venoge River. By comparison of this data between each other, it provides valuable information on past channel migration. If two of these data sets provide an accurate description of the channel bank tops, it can provide valuable information on bank retreat rate. The only historical data set that seems to provide this accurate bank line description is the LIDAR data. The historical maps and orthophotos provide piecemeal information, but have accuracy problems or problems with determining the bank lines as is the case for the summer SwissImage orthophotos. The available information was used to determine the Lower Venoge River 2004 centerline.

The channel topographic description is a big hurdle to overcome for streambank erosion hazard modeling. Linear interpolation of cross sections is possible if there is a cross section for at least every riffle and pool, although even more frequent cross sections are necessary if an accurate interpolated bank and bed definition is desired in between surveyed cross sections. This amount of cross sections is never available unless surveyed specifically with sediment transport calculations in mind. Cross sections measured in 1996 on the Venoge River were recovered, but those in the detailed erosion monitoring zones are from leveling without an accurate plan precision. Cross sections in 2004 are georeferenced. Comparison of thalwegs and cross sections for the period 1996 and 2004 in the modeling reach shows definite channel instability in the region of km 7.3 to km 7.7, although it has supposedly been stabilized after the "Abbaye" weir reparation in 2002. A few other zones are possibly instable, but the cross section data in those areas is insufficient to confirm instability. Otherwise, the majority of the 22 kilometers surveyed in 2004 show that the Lower Venoge River is stable.

A cross section tool was programmed to work with GIS cross section database files. This facilitates the transformation of surveyed cross section points into two dimensional (transverse and elevation) cross sections for modeling and is coordinated for the model CCHE1D. This tool can be used to visualize cross sections for calculating transverse cross section distance and position and for defining bank definition points. The tool can interpolate cross sections linearly or based on channel curvature along river centerline points. Interpolated cross sections with respect to channel curvature demands the calibration of bed topography parameters based on surveyed cross sections. The cross section tool does this calibration and uses the parameters to interpolate cross sections with respect to channel curvature. For

reaches with insufficient cross section data (missing riffle or pool cross sections), this interpolation method can be used to interpolate cross sections that are coherent with the channel curvature. Scour holes were found to be displaced upstream or downstream from some surveyed cross sections.

The possibility of improving the channel description in a LIDAR derived DTM was explored. With sufficient cross sections surveyed at the same time as the LIDAR measurements, linearly interpolated or meander interpolated cross sections can replace the original channel LIDAR points. This is usually not the case as is for the Venoge. Streamwise linear interpolation of channel points was programmed into the cross section tool. If sufficient cross sections are available and aligned with the LIDAR data, they can be interpolated with this module and replace the original LIDAR channel points foregoing the more timely linear interpolation procedure. Otherwise, as was done for the Venoge, the original LIDAR channel points can be interpolated with this module. This significantly improved the Venoge channel bank line description, and it is assumed that the DTM channel bottom now reflects the approximate water surface at the time of the LIDAR measurement. The interpolation and smoothing procedure produces some artifacts in the DTM. A more sophisticated interpolation procedure, such as an IDW in the streamwise direction, could help this.

The Fehr line sampling method was used to collect bed grain size data and estimate the subpavement grain size distribution. This method depends on the assumption that the subpavement follows a Fuller curve. The Fehr method should be compared against the hybrid method of Rice and Haschenburger (2004) to verify that the Fuller curve assumption is verified for different types of rivers. More bed samples should also be obtained for the Venoge River and in different locations in a riffle-pool sequence to better understand the sediment facies.

Three levels of investigation of bank soil properties were conducted. The investigated soil properties will be compared against calibrated bank values to determine if they can explain the critical shear stress, cohesion, and friction angles without measuring these values with the specific equipment necessary.

The upstream and tributary sediment input into the river is estimated with the Smart and Jaeggi sediment transport capacity formula and the downstream rating curve is based on uniform flow.

Chapter 5

Hydrologic Modeling for Distributed Discharge Input

5.1 Objectives of the hydrologic modeling

The goal of the hydrologic modeling shown in this chapter is to provide a correct spatial representation of the discharge input (and indirectly an appropriate sediment discharge input) into the river. This is possible with a continuous hydrologic model, HydroRoute, that takes into account the important hydrologic processes. Spatial interpolation of meteorological data is performed to properly generate the model input data. The model is calibrated and the historical period is simulated producing discharge inputs for the Lower Venoge River tributaries. This historical period is used as a basis for preparing three series of 300 years of discharge. These long series will permit the streambank erosion model to predict erosion for extreme hydrologic events.

5.2 Hydrologic model

A continuous hydrologic model is used for the generation of the tributary hydrographs. The model GSM-SOCONT (Glacier and SnowMelt - SOil CONTribution model) developed at the HYDRAM laboratory was available for use. The origin of this model is the model SOCONT developed by Consuegra and Vez (1996) based largely on the GR models (Edijatno and Michel, 1989). The model was adapted for mountain hydrology during several research projects (Schaefli et al., 2005, Hamdi et al., 2005). The GSM-SOCONT model theory was used as the basis for the generation of an object-oriented program called HydroRoute developed by the company SODELO. The HydroRoute model is under development and its use in this

thesis served to test the implementation of the GSM-SOCONT model in the user-friendly, convivial interface proposed by HydroRoute.

HydroRoute can be classified as a semi-distributed conceptual reservoir model. Hydrographs are generated in a lumped fashion for each subcatchment, but the possibility to use many subcatchments within a catchment and then to route them provides a semi-distributed catchment response. The model also incorporates snow storage units, also called bands, which can be multiple for a subcatchment. This permits a refinement in the quantification of the equivalent rainfall that will be routed in the model.

5.2.1 Elements of the HydroRoute model

The hydrologic elements (objects) of HydroRoute (figure 5.1) and their brief description are as follows:

- *Junction*: adds two or more upstream hydrographs to form a single hydrograph.
- *Hydrograph-input*: allows the input of a discharge time series.
- *SOCONT*: transforms a rainfall time series and Potential EvapoTranspiration (PET) time series into a discharge time series through the use of a linear slow reservoir and a nonlinear runoff reservoir.
- *SOCONT-Alpine*: incorporates snow and glacier effects together with the aspects of the SOCONT element. Precipitation, PET, and temperature time series are needed as input. Snow storage units handle the calculation of the equivalent rainfall and snow height, and glacier units can be used to calculate the snowmelt and glacier melt hydrograph contribution. The non-glacier parts of the subcatchment use the same rainfall-runoff transformation as the SOCONT element.
- *Muskingum*: provides the channel routing of hydrographs before addition with downstream hydrographs using the classical formulation (see Chow et al., 1988 for an example).
- *Derivation*: allows for an input hydrograph to be separated into two output hydrographs according to the Q_{in}-Q_{outs} relationship specified by the user.

A model topology can be constructed with the above elements, as shown in the example in figure 5.1. A global parameters window allows global parameters (Tc_1, Tc_2, Tc_3, Tc_4, θ_r) to be specified. Through the parameters' window, the user can indicate the input files, the output variables to be stored, and the parameters specific to the selected element. Another window allows the simulation time, time step, and precision to be specified. It is worthwhile to note here that the model can use input data at variable time steps, even variably spaced, through a new time series format that has evolved from the CODEAU® time series format (De Souza et al., 1994) developed by the HYDRAM laboratory in the last decade. A simulation window allows the user to choose calibration or simulation mode. In calibration mode, the user can search for an optimal parameter set using Monte-Carlo (MC) parameter sets generated by random sampling of uniform parameter distributions or using sweep parameter sets which sample uniform distributions at regular intervals. Calibration parameter sets and the resulting objective function criteria (Nash or Log-Nash of the entire or superior truncated (low flows) or inferior truncated (high flows) hydrograph) can be output to a text file for further analysis. For a "normal" (non-calibration) simulation, the user can store the output time series for visualization within HydroRoute.

The SOCONT-Alpine element is heavily used in the Venoge catchment modeling so the theory behind the snow storage and the rainfall-runoff transformation of it will be discussed in the next two sections.

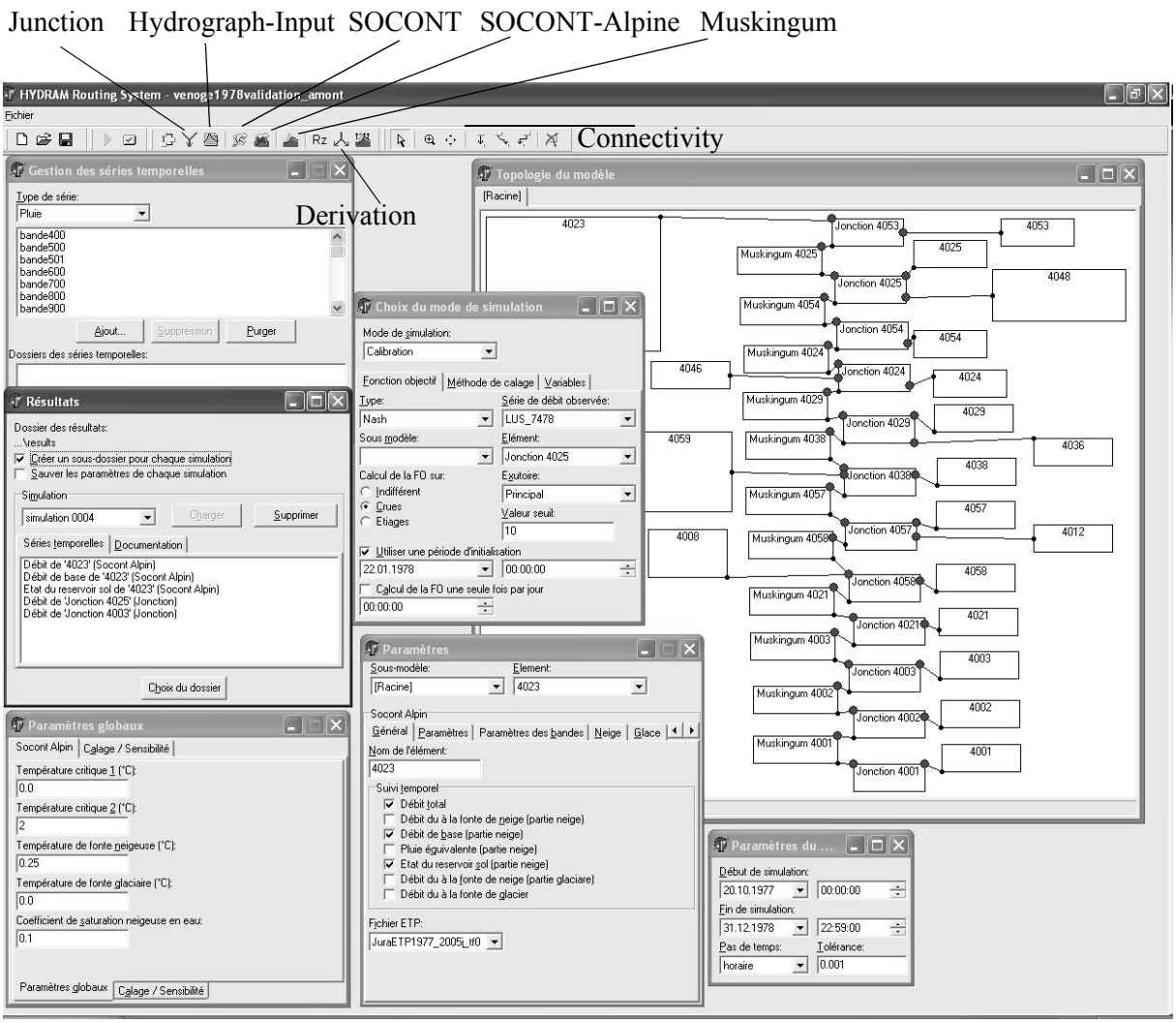

Figure 5.1. Elements of the HydroRoute model and its graphical interface

5.2.2 Snow storage

The flowchart in figure 5.2 illustrates the formulas involved in the transformation of precipitation into rain and snow[1], and the subsequent calculation of the equivalent rainfall at a time t in one snow storage unit of an element SOCONT-Alpine. A subcatchment can have as many snow storage units as the user decides, but precipitation, P, and temperature, T, must be provided for each snow storage unit. Model performance will increase by increasing the number of snow storage units, but only up to a threshold that depends on the catchment elevations (Schaefli et al., 2005). The quantity of precipitation that falls as snow, S, and as rain, Rn, is determined according to the two critical temperatures, Tc_1, and Tc_2. Below Tc_1 all precipitation is snow, while above Tc_2 it is all rain. Between the critical temperatures, a linear transition determines the amount of snow and rain. The quantity of snow is then added to the snow height, H_s. If the temperature is greater than a third critical temperature, Tc_3, indicative of the melting

1. Snow is used here to refer to all solid precipitation.

temperature, the quantity of melted snow, M_S, is calculated. Snowmelt is calculated by a temperature index method using a degree-day factor (mm/h/°C) and a coefficient b_{rn} (h/mm) which increases the degree-day factor in case of rain on snow. The melted snow and rain are added to the snow water, W_S. Snow has a capacity to retain a certain quantity of water. This is represented by the variable, θ_r. If the quantity of water in the snow is greater than this capacity, the quantity that goes over it will be considered to be equivalent rainfall, P_{eq}.

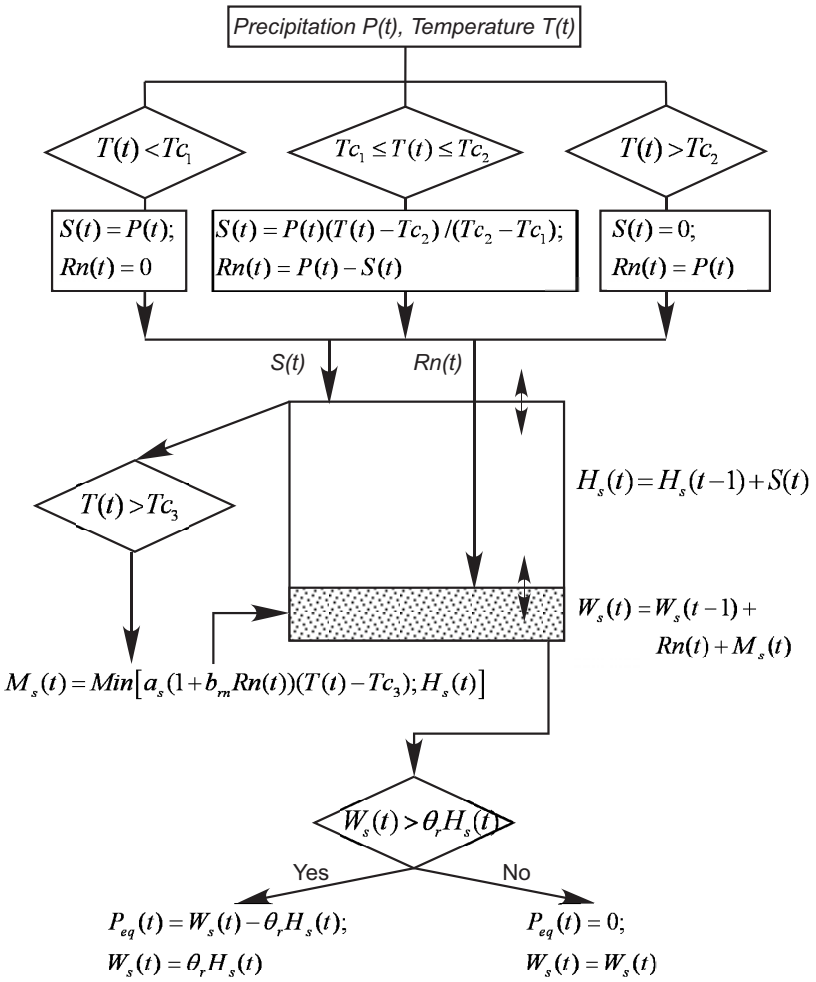

Figure 5.2. Snow storage unit used in the SOCONT-Alpine element in the HydroRoute model (adapted from Hamdi et al., 2005)

5.2.3 SOCONT-Alpine

The flowchart in figure 5.3 illustrates the SOCONT-Alpine element of the HydroRoute model. The element has two parts: glacier and non-glacier. Only the non-glacier part is described here since the Venoge catchment does not have any glaciers.The SOCONT-Alpine element uses snow storage units. The equivalent precipitation issued from them is divided into effective rainfall, P_{eff}, for runoff and infiltrated rainfall, P_{inf}. The quantity of rainfall that infiltrates depends on the degree of saturation (fullness), represented by the height, h_a (mm), compared to the capacity of the slow reservoir, represented by the total height, A (mm), of the reservoir and is governed by the equation shown in figure

5.3. The exponent y can be calibrated. The slow reservoir is drained by evapotranspiration, ET, and by baseflow, q_a. The ET depends on the input PET time series, which can be adjusted by a multiplication factor, F_{PET}, and also on the degree of saturation in the slow reservoir raised to the power x, another calibration coefficient. The baseflow is also a linear reservoir with a storage coefficient, k_a (1/h). The effective rainfall flows through a nonlinear runoff reservoir. The runoff specific discharge, q_r, depends on the calibration coefficient, β ($m^{4/3}/s$), the catchment mean slope, J (m/m), and the height in the runoff reservoir, h_r. The sum of the non-glacier specific discharges multiplied by the non-glacier area, A_{ngl} (ha), and the appropriate unit conversion factors will produce the non-glacier discharge, Q_{ngl} (m^3/s). The sum of the Q_g and the Q_{ngl} gives the total discharge, Q_{tot}, for the SOCONT-Alpine element.

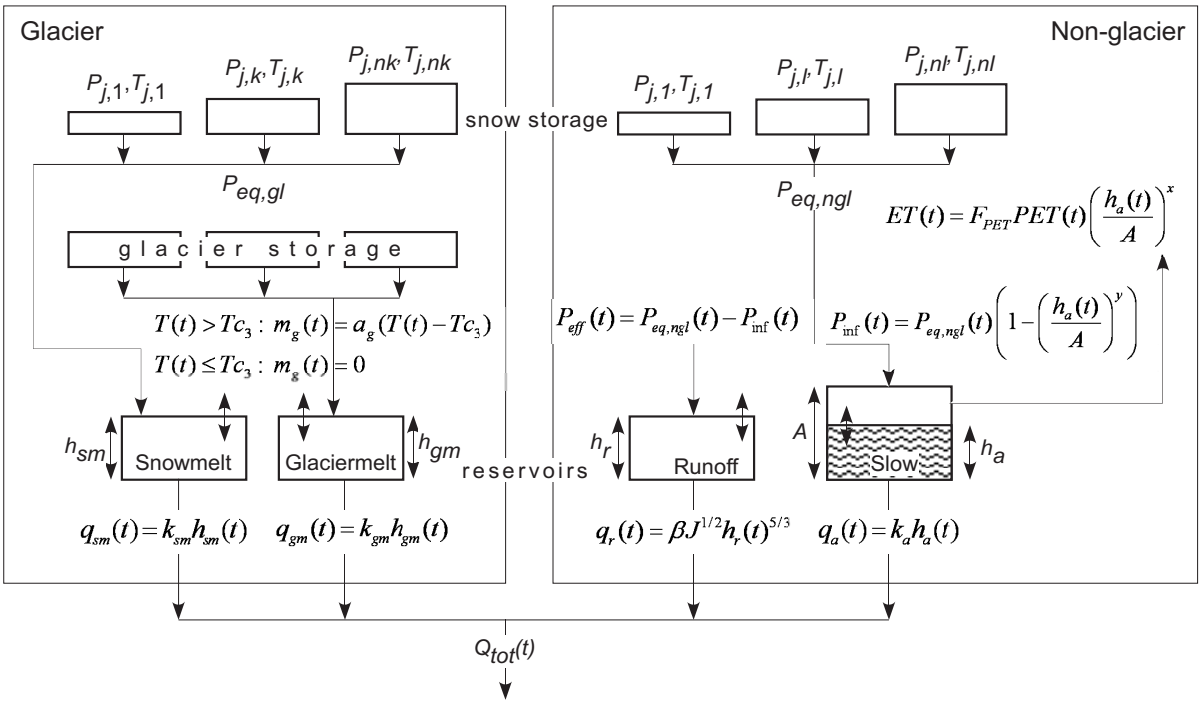

Figure 5.3. SOCONT-Alpine element of the HydroRoute model (adapted from Hamdi et al., 2005)

The snow storage and transfer reservoirs in the system need the continuity equation to calculate their respective heights. The generalized continuity equation applied is:

$$\frac{dh}{dt} = I(t) - O(t) \qquad \textit{Eq. 5.1}$$

where h (mm) is the height in the snow storage unit or reservoir and the I (mm/h) is the input to and O (mm/h) is the output from the reservoir. The continuity equations are solved implicitly by the Newton-Raphson method.

5.3 Subcatchment delineation

The delineation of the subcatchments (c.f. figure 3.5) follows that of the GESREAU database. This delimitation is based on the 1:25'000 maps in the database (Crausaz, 2000). This topographic delineation

possibly underestimates the real hydrographic basin (Prétorian, 1994), but the limited hydrogeologic information available is not sufficient to delineate a real basin. Subcatchments are regrouped to form the principal tributaries and contributing slopes (contributing areas around the river channel but with no tributary). These subcatchments are shown in figure 5.4. Notice the elevation bands, based on the 100 meter elevation contours, that are used in the large Upper Venoge subcatchment. Table 5.1 shows the mean elevation, area, and mean slope of each of the subcatchments, as well as the mean elevation and area of each band.

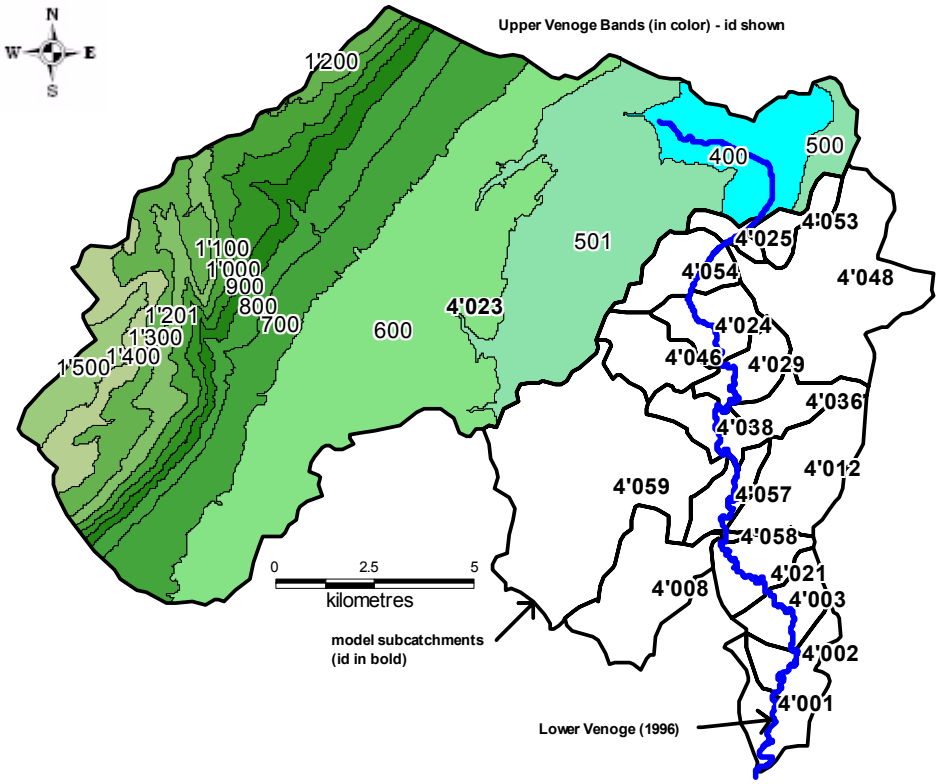

Figure 5.4. Delineation of the subcatchments for the hydrologic modeling. ID's of the subcatchments and Upper Venoge snow storage units are shown.

ID	Mean elevation (m.a.s.l.)	Area (ha)	Mean Slope (-)		Band	Mean elevation (m.a.s.l.)	Area (ha)
4001	401	297	0.051		400	472	912
4002	407	286	0.059		500	559	219
4003	423	309	0.075		501	568	2618
4008	478	733	0.065		600	655	4235
4012	505	668	0.077		700	741	1881
4021	431	329	0.084		800	847	892
4023	814	15046	0.135		900	947	615
4024	485	360	0.122		1000	1052	630
4025	482	110	0.086		1100	1152	687
4029	474	277	0.084		1200	1239	159
4036	510	269	0.076		1201	1256	511
4038	470	283	0.095		1300	1354	757
4046	554	382	0.069		1400	1444	567
4048	556	1350	0.061		1500	1559	365
4053	527	204	0.091				
4054	521	365	0.1				
4057	428	233	0.094				
4058	412	18	0.058				
4059	524	2254	0.059				

Table 5.1. Properties of the subcatchments and elevation bands as identified in figure 5.4

5.4 Data and modeling periods

5.4.1 Available data

Precipitation

The Venoge catchment is equipped with only one precipitation gage (nonrecording at Cossonay) (figure 5.5). Fortunately, the surrounding catchments are well equipped with the nonrecording gages of MeteoSwiss. Four automatic federal climate stations (ANETZ network of MeteoSwiss) surround the Venoge catchment, but are relatively far. Most ANETZ stations were implemented in 1978 providing a network of 10 minute and hourly stepped data. The Vaud canton has tried to overcome this lack of fine temporal resolution precipitation data by installing additional tipping bucket gages. Two of those gages (figure 5.5) are indirectly used in this study.

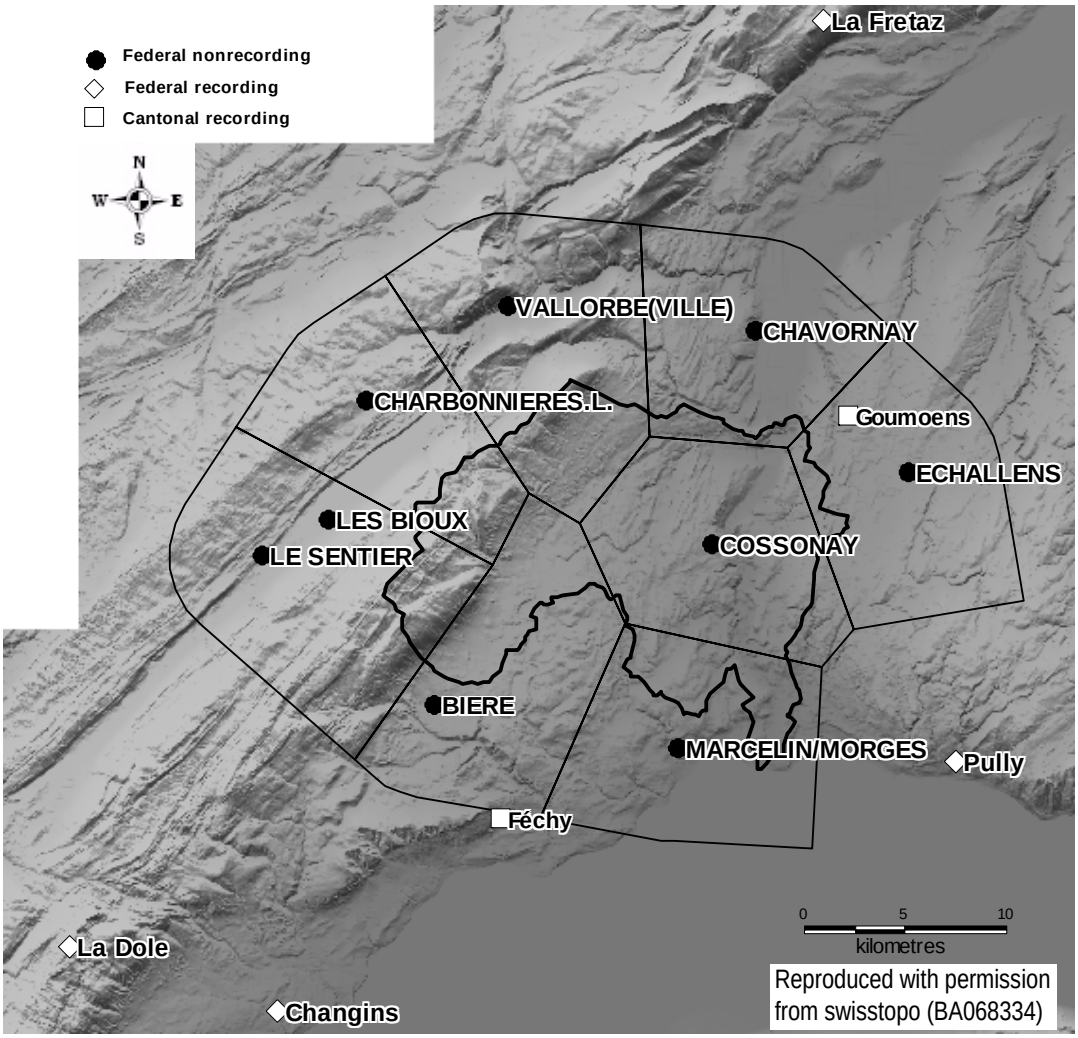

Figure 5.5. Precipitation gages used in the hydrologic modeling. Polygons show the zone of influence attributed to each nonrecording gage. Background image is the DTM25 © 1995, Swisstopo.

ISM ID	Station name	Elevation (m.a.s.l.)	Period	Gage type	start-2003	1934-2003	1961-2003	1975-2003	1983-2003
6038	CHARBONNIERES.L.	1135	7.1982 - present	nonrecording	1712				1712
6033	LES BIOUX	1025	7.1996 - present	nonrecording					
6030	LE SENTIER	1020	10.1900 - 6.1996	nonrecording	1551	1571	1639	1804	1739
6060	VALLORBE(VILLE)	762	1.1961 - present	nonrecording	1370		1370	1483	1427
8245	BIERE	695	5.1974 - present	nonrecording	1341			1389	1313
6100	ECHALLENS	618	1.1934 - present	nonrecording	1061	1061	1030	1087	1023
8180	COSSONAY	570	10.1919 - present	nonrecording	953	963	973	1034	965
6115	CHAVORNAY	439	1.1974 - present	nonrecording	889			925	897
8230	MARCELIN/MORGES	425	1.1961 - present	nonrecording	1051		1051	1149	1089
8290	Changins	430	1.1978 - present	tipping bucket					1023
8280	La Dole	1670	8.1978 - present	tipping bucket					1890
6185	La Fretaz	1202	1.1978 - present	tipping bucket					1333
8100	Pully	461	1.1978 - present	tipping bucket					1174
	Féchy	470	11.1992 - present	tipping bucket	1190				
	Goumoens	614	11.1992 - present	tipping bucket	937				

Table 5.2. Precipitation station data used in the hydrologic study. Mean annual precipitation is given for different periods. Les Bioux and Le Sentier stations are summed together.

Temperature

The temperature data for the Venoge catchment is also located outside of the catchment. The nearest stations are those of the ANETZ stations (figure 5.6). These stations are representative of the entire catchment considering the Dole station is located at 1670 meters, Fretaz at 1202 meters, and Pully at 461 meters.

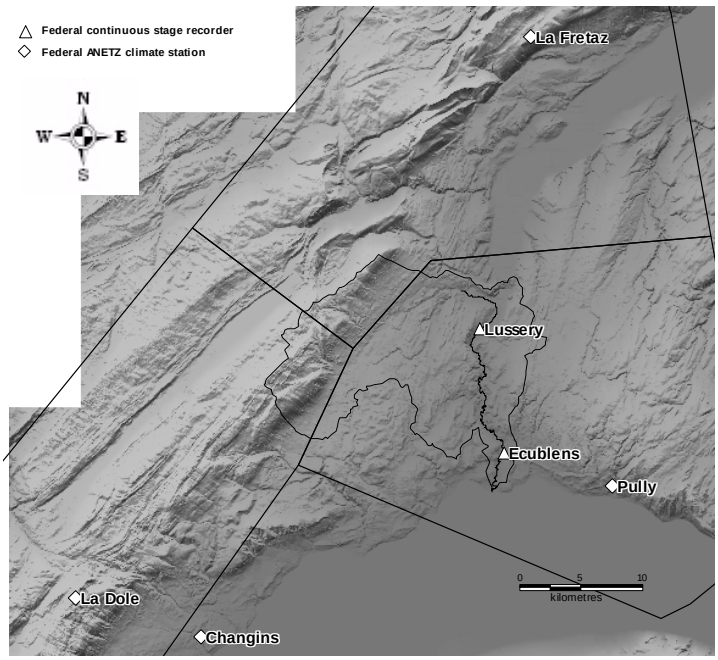

Figure 5.6. Climate and discharge stations used in the hydrologic model. The polygons show the zone of influence for each climate station. Background is the DTM25 © 1995, reproduced with permission from swisstopo (BA068334).

Discharge

Discharge measurements have been made by the Swiss National Hydrologic Service (SHN). Measurements exist for the station of Lussery and Ecublens. Daily measurements for Lussery exist from 1944-1974 and are continuous during the period 1974-1978. The measurements at Ecublens are continuous and started in 1979 and are still running. Without overlapping discharge series, the routing aspects of the Lower Venoge River cannot be calibrated.

Potential evapotranspiration

Potential evapotranspiration can be obtained from MeteoSwiss. This data was examined but found to seriously underestimate the PET (it is less than the average real evapotranspiration recorded in the Swiss hydrological atlas (Spreafico et al., 1992)). Other European sources of PET were available, but data for the streambank erosion modeling needed to be up-to-date. This requirement made it necessary to calculate the potential evapotranspiration. Calculation of the PET by the Penman-Monteith equations requires sunshine duration, relative humidity, wind, temperature, and global radiation data. This data, without interruptions, is available from MeteoSwiss, from 1981 to present.

The available data is summarized in table 5.3.

5.4.2 Modeling strategy

The ANETZ station data begins in 1978 and the Dole station data is only available from August 1978, which does not coincide well with the end of discharge measurements at Lussery in 1978. A 1978 simulation is possible for Lussery, but the use of calibrated model parameters based on only one year would be perilous. Maximum annual discharge values are available though for Lussery so they will be used to evaluate the simulated maximum annual discharges with the caution that is due.

A daily time step for the Venoge catchment is too long. Prétorian (1994) analyzed 19 runoff events from 1984-1991. The mean lag time of those events was 16 hours with values ranging from 6 to 27 hours. Mean rising limb time was 32 hours, mean hydrograph duration was 100 hours and the mean time of concentration was 66 hours. With a mean lag time of less than 24 hours, it is absolutely necessary to study the Lower Venoge River at a smaller time step. As mentioned in chapter 3.4, the impermeable urban area of the Venoge catchment is small, so that a small time step for simulating urban runoff is unnecessary. The temporal precipitation structure of the farther hourly rain gages will be used to disaggregrate the precipitation recorded at the daily nonrecording gages.

	1944-1974	1974-1977	1978	1979-1980	1981-1992	1993-2.2005	3.2005
Lussery Q	daily, max annual	instantaneous					
Ecublens Q				instantaneous			
Prec. - detailed							
Prec. - less detailed							
PET - Temp							
PET - PM							
Simulation Periods				validation		calibration	

Table 5.3. Summary of the available hydrological data and simulation periods

Discharge information is available at Ecublens from January 1979 - March 2005. This period is long enough for calibration and validation. From 1993 on, the cantonal hourly rain gages are also available so the calibration period is from August 1993 - August 2004. The August starting point is chosen to avoid water balance issues related to snow since all of the Jura snow typically melts by June. The validation period is chosen from August 1979 - August 1993. This permits the use of the Charbonnieres data, but it is assumed the associated error will be minimal due to the reasonable coverage of the surrounding Jura gages.

To completely exploit the Ecublens discharge series for the streambank erosion modeling, it is necessary to find a solution for the PET for 1979-1980. Recent advancements in this area (Oudin et al, 2005b) have shown that a simple temperature based PET model is sufficient for continuous rainfall-runoff modeling. Calibration will be done using Penman-Monteith calculated PET and simple temperature-based PET to evaluate the performance of the two PET calculations. Holes in the ANETZ temperature data for the 1978-1980 period will need to be corrected.

5.4.3 Corrected and derived data

Precipitation

The daily precipitation data of the nonrecording gages shown in figure 5.5, must be transformed to hourly data. This is done with the daily precipitation structures of the surrounding cantonal and federal recording gages. The method consists of applying the daily recorded precipitation volume proportionally onto the daily structure of a nearby recording gage. The optimal manner to do this procedure would be to apply the precipitation event volume onto the event volume of the recording gage, but its programming is much more complicated for a small gain. Occasionally, there are daily precipitation volumes without any precipitation measured at the recording gage. In this case, the precipitation will be uniform for that day. The other complication that occurs is that of the different processing of snow in the

precipitation gages by cantonal and federal measurement systems. Federal precipitation volumes take into account snow that falls during the recording period. Snow in the cantonal gages is measured at the time it melts. This proves to be a significant complication for using their data in combination with the data of the federal stations. For this reason, only the cantonal stations of Goumoens and Féchy are used. The modeling improvement that can be gained from the hourly recorded structures of these devices for 1993-2005 is greater than the few snow complications that occur at the elevations of these two stations. For the period 1993-2005, the precipitation structures-volumes combinations are the following: Féchy with Bière and Marcelin/Morges, Goumoens with Echallens, Cossonay, and Chavornay, La Dole with Sentier-Bioux and Charbonnieres, and La Fretaz with Vallorbe. For the period 1979-1992, the structure of the federal station of Pully was used in combination with the volumes of Echallens, Chavornay, Cossonay, and Marcelin/Morges, Changins was used with Bière, La Dole with the Sentier, and La Fretaz with Vallorbe. Prétorian (1994) analyzed the number of days a given precipitation intensity was exceeded for the majority of the nonrecording stations shown in figure 5.5 and it clearly shows that intense precipitation is more frequent at higher elevations. Ideally then, the rainfall structure should come from a station that is at the same altitude or higher then the daily volume station. This was for the most part respected, except for the Biere station. Further analysis would have been necessary to determine more precisely if the Dole station or the Changins and Féchy station would be more appropriate, but the Changins and Féchy stations were chosen because of the important elevation difference between Biere and Dole.

Temperature

Correction of ANETZ temperature during the period 1978-1980 was necessary. This was done in one of two ways. For holes that were greater than 6 hours, missing values were replaced from a nearby station. Replacement values were taken from the closest ANETZ station if possible, but otherwise from climate stations that measure temperature three times daily. The values were corrected for elevation differences with a standard lapse rate of -0.005 °C/m. For holes of 6 hours or less, a cubic spline interpolation was used to replace missing values.

Potential evapotranspiration

Potential evapotranspiration was calculated for the Venoge with two methods: Penman-Monteith (PM) and a temperature-based model. The PM method is documented in many sources (ASCE, 1996 or Allen, 1998 for example) and will not be described in detail here. PM PET hourly time series were calculated for the Pully, Dole, and Fretaz stations from January 1981 - August 2004.

Oudin et al. (2005a) demonstrated that lumped rainfall-runoff models only need long term mean PET values. In a second companion article (Oudin et al., 2005b), they proposed a simple temperature based model, which they called the "adjusted PE model with mean air temperature", and concluded that rainfall-runoff model efficiency can be improved by using simple temperature based PET models. This improvement is most likely due to adjustment factors in their PE formula that can compensate for model

structure deficiencies. Their model is issued from the Jensen-Haise and McGuinness models which take the following generalized form:

$$PET = \frac{R_e}{\lambda\rho}\frac{T_a + K_2}{K_1} \qquad for \qquad T_a + K_2 > 0$$
$$PET = 0 \qquad for \qquad T_a + K_2 \le 0 \qquad \text{Eq. 5.2}$$

where PET is the potential evapotranspiration (m/day), R_e is the extraterrestrial radiation (MJ/m^{2}day) which can be calculated with the latitude and Julian day, T_a is the mean daily air temperature (°C), λ is the latent heat flux (standard value is 2.45 MJ/kg), ρ is the density of water (kg/m^3) and K_1 and K_2 are coefficients to calibrate. Oudin et al. (2005b) indicate that the chosen values of K_1 and K_2 could depend on the model structure, but they assert that with values of 100 and 5 respectively, the model performance due to the PET should be optimized. Temperature based PET was calculated for the Pully, Fretaz, and Dole stations with the values of 100 and 0 for K_1 and K_2, respectively.

Muskingum parameters

No upstream and downstream hydrographs are available for the Lower Venoge River during the same period so it was decided to approach the hydrograph routing more as hydrograph translations (X=0.5) rather than attenuation to avoid a possible underestimation of the discharge peaks due to an exaggerated attenuation. Translation times are based on the K muskingum coefficient. This value can be estimated by dividing the length of the reach by the mean reach velocity (Musy and Higy, 1998). The estimated mean reach velocities are based on the HEC-RAS simulations used for the description of the Lower Venoge hydraulic geometry (c.f. chapter 3.7.4).

Muskingum id	K (s)
4025	209
4054	586
4024	907
4029	1144
4038	1290
4057	1403
4058	146
4021	1434
4003	1116
4002	865
4001	1284

Table 5.4. Muskingum K values for the Lower Venoge

5.5 Spatial interpolation of data

Estimates of hourly rainfall, temperature, and evapotranspiration must be provided to each HydroRoute subcatchment. These estimates can be based on the recorded or derived values of nearby stations or an areal estimate. The method used here follows the one presented by Hamdi et al. (2005). A brief description is given hereafter.

5.5.1 Precipitation

The first step in the precipitation interpolation is to correct for elevation. A precipitation correction factor is calculated according to:

$$r_{i,k} = \frac{\hat{P}_{an,i,k}}{P_{an,i}} = 1 + \frac{\phi_i(Z_k - Z_i)}{P_{an,i}} \qquad \text{Eq. 5.3}$$

where $r_{i,k}$ is the precipitation correction factor for the ith station and the kth band, $\hat{P}_{an,i,k}$ is the estimated mean annual precipitation based on station i for the kth band, $P_{an,i}$ is the mean annual precipitation for station i, ϕ is the lapse rate for station i as determined by a linear regression analysis, and Z_k and Z_i are the elevations of the kth band and ith station, respectively. The estimated precipitation for band k based on station i, $\hat{P}_{i,k}$, then is:

$$\hat{P}_{i,k} = r_{i,k} P_i \qquad \textit{Eq. 5.4}$$

where P_i is the precipitation of station i. The estimated precipitation of the kth band, $\hat{P}_k$, is calculated according to:

$$\hat{P}_k = \sum_{i=1}^{m} \alpha_{i,k} r_{i,k} P_i \qquad \textit{Eq. 5.5}$$

where $\alpha_{i,k}$ is a weight expressing the influence of the ith station on the kth band according to the overlap area of the Thiessen polygon of the ith station on the kth band.

The appropriate lapse rates are determined by a linear regression analysis of annual precipitation data (figure 5.7). A lapse rate of 1.21 was found with the linear regression using all of the 1983-2003 federal nonrecording stations. This lapse rate is too high for the Jura stations because for an elevation equivalent to La Dole, the estimated precipitation would be 2500 mm compared to the recorded 1900. A linear regression was performed with only the Jura stations providing a lapse rate of 0.84 that gives a better estimate for these high altitude stations.

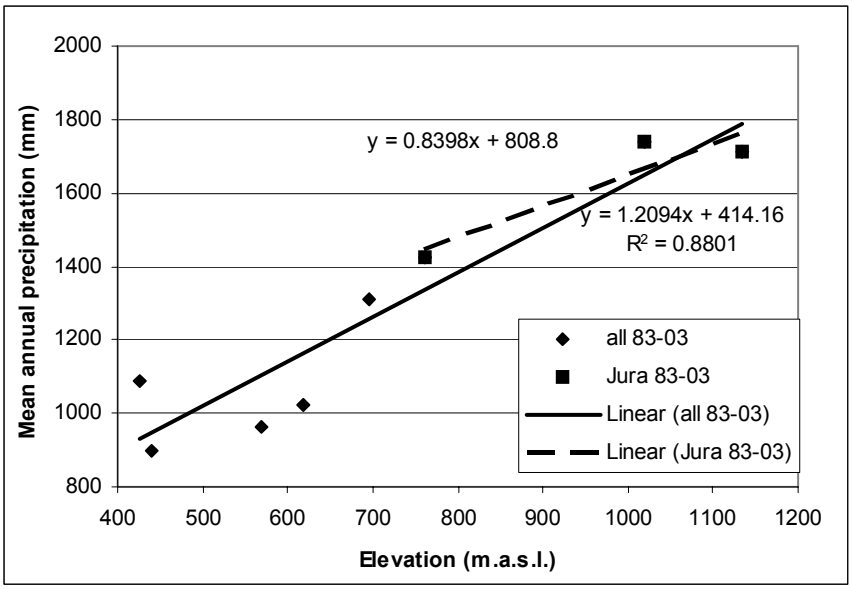

Figure 5.7. Analysis of the effect of elevation on mean annual precipitation to determine precipitation lapse rates

The Thiessen weights necessary for the precipitation spatial interpolation are based on the polygons shown in figure 5.5. The initial Thiessen polygons over the Jura mountains were adapted to prevent the Jura stations from having any influence on the rainfall interpolation on the plateau part of the catchment. Thiessen weights were generated based on their overlap with the snow storage units and subcatchments of figure 5.4. Each Lower Venoge subcatchment of figure 5.4 has one snow storage unit. With the band elevations, station elevations, station lapse rates, and thiessen weights matrix known, a spatial interpolation program was run and the precipitation series of the 18 subcatchments and 14 bands of the Jura subcatchment were produced for the period 1.1983-2.2005. The same procedure was run, but with

Thiessen weights adapted accordingly to replace the missing Charbonnieres station data, to produce the precipitation series for the period 1.1978-2.2005.

5.5.2 Temperature

The spatial interpolation of temperature follows a procedure that is similar to that of the precipitation. Rather than fixing the lapse rate for the entire interpolation period, it was decided to calculate a lapse rate for every time step. This will allow periods of temperature inversion (higher temperatures at higher elevations) to be taken into account. As for precipitation, the first step is to calculate an estimated temperature, $\hat{T}_{j,k}$, for the *k*th band with the *j*th temperature station according to:

$$\hat{T}_{j,k} = T_j + G_j(Z_k - Z_j) \qquad \textit{Eq. 5.6}$$

where T_j is the temperature of the *j*th station, G_j is the hourly lapse rate, and Z_k and Z_j are the elevations of the *k*th band and the *j*th station, respectively. The estimated temperature for each band then is determined as:

$$\hat{T}_k = \sum_{j=1}^{n} w_{j,k}\hat{T}_{j,k} \qquad \textit{Eq. 5.7}$$

where $w_{j,k}$ are the Thiessen determined weights. Here again, the initial Thiessen polygons were adapted so that the Dole and Fretaz Jura stations only influenced the Jura region. Since the Dole and Fretaz temperature series had been corrected to the beginning of 1978, only one temperature spatial interpolation had to be run. This run calculated the temperature series for the 14 Jura subcatchments bands. Due to the small elevation differences in the subcatchments of the Lower Venoge, the Pully temperature data was used directly with no correction. Figure 5.8 shows the hourly lapse rate calculated with the Dole, Fretaz, and Pully ANETZ stations for the year 2004. This example shows the inversion that can occur during the fall and winter months.

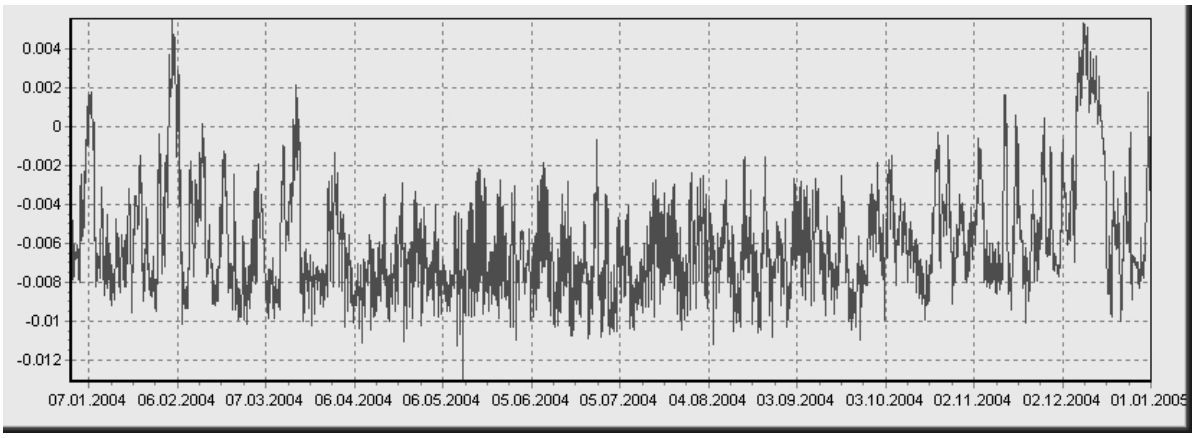

Figure 5.8. Hourly temperature lapse rate (°C/m) calculated with the Dole, Fretaz, and Pully ANETZ stations for the year 2004

5.5.3 Potential evapotranspiration

Potential evapotranspiration must be supplied to each subcatchment in the HydroRoute model. Since the Upper Venoge is encompassed in one subcatchment, it needs only one potential evapotranspiration series. The weights of 0.53, 0.21, and 0.26 for the three PET series: Pully, Fretaz, and Dole, respectively, are to be used for the calculation of the Upper Venoge PET according to Thiessen polygons (same as those used for temperature in figure 5.6). The Pully PET series is used for the Lower Venoge subcatchments.

5.5.4 Accuracy of data

The accuracy of the utilized data must be assessed. A qualitative assessment is possible based on the density of the gaging network and the spatial interpolation method.

The first question to ask is if the gaging network is sufficiently dense to accurately describe the spatial rainfall. The Cossonay daily rainfall gage covers nearly half of the Venoge catchment (figure 5.5). This indicates that the density is not sufficient. Huff (1970) measured areal precipitation in Illinois for areas of 50-550 mi² and suggested that gage spacing should be 65 km^2 per gage to ensure average sampling errors of less than 6% for hourly rainfall, but also that the storm type affects sampling errors. Duncan et al. (1993) also showed that the 5% accuracy gage spacing depends on the catchment and the storm types and pattern and calculated 5% accuracy values (standard deviation of the error equals 5%) for gage spacing in the range of 25-1000 km per gage. They also suggested though that for a 5% accuracy for peak flow estimates, a much higher gage density is needed in the range of 1-41 km^2 per gage. It can be deduced then from this recommendation and the Venoge catchment area that the minimum number of hourly recording gages necessary for the Venoge catchment is 6 and most likely more due to the orographic effects of the Jura slopes.

Andréassian et al. (2001) also looked at the gage density question in light of its effect on hydrologic modeling results. They showed that models have a capacity to adapt to poor rainfall input, but that the performance and the variability of model efficiency improved with increasing gage density.

Concerning spatial interpolation, Beven (2001) noted that a precipitation correction for elevation is justified in the case of orographic situations. Dirks et al. (1998) compared interpolation methods on a high density network and showed that areal-mean, thiessen, inverse-distance, and kriging methods performed similar. They concluded for high density networks that inverse-distance weighting should be used for a better interpolation of the precipitation field, but also for its simplicity. For low to medium density networks, Creutin and Obled (1982) showed that kriging outperformed Thiessen or areal-mean methods. Goovaerts (2000) suggested that multivariate geostatistical algorithms can be used to integrate DEM or radar information with ground gage information. These recommendations suggest that further work can be done to improve the spatial interpolation of precipitation for the Venoge catchment.

Hamdi et al. (2005) noted that the spatial interpolation of temperatures seems to be as delicate as precipitation interpolation. This remark is especially pertinent for the lack of temperature information available for the Jura slopes of the Venoge catchment. For the rest of the catchment, this lack of

temperature information should be less important because of the small snowfall recorded on the plateau part of the Venoge catchment.

5.6 Simulations and results

Two sets of calibration runs were done for the period August 1993 - August 2004, one with the PM PET and the other with the temperature-based PET. Validation runs were done for August 1979 - August 1993. The parameter setup of the model is explained first, and then the results of the simulations are presented.

5.6.1 Parameter estimation

It was necessary to estimate as many parameters as possible with standard values found in literature to avoid an excessive number of parameters to calibrate. Based on the work done by Hamdi et al. (2005), the critical temperature values for the snow/rainfall separation, Tc_1 and Tc_2, were taken to be 0°C and 2°C, respectively. They estimated the mean degree-day factor, a_s, to be 0.15 mm/h/°C for elevations in the range of 500-1000 meters, which corresponds to suggested literature values (ASCE, 1996). The value used for the Venoge was 0.16. The value of b_{rn} (h/mm) was estimated to be 0.3 h/mm. This value was calculated so that a strong rain pushes the combined degree-day factor, $a_s(1+b_{rn}*Rn)$, up to a value of around 0.3 which is the value found in literature for snowmelt during windy and heavy rain (ASCE, 1996). The snow water retention capacity, θ_r, was set to 0.1 (Hamdi et al., 2005). The critical temperature for snowmelt was determined from the Lussery discharge series, in which the Venoge spring snowmelt is clearly visible. The diurnal temperature effect and the snowmelt peaks are clearly visible in figure 5.9. The critical temperature was adjusted so that the snowmelt of the highest model snow storage unit finished according to the end of the snowmelt in the 1978 Lussery discharge series. The critical snowmelt temperature, Tc_3, was estimated to be 0.25°C. The remaining parameters are calibrated.

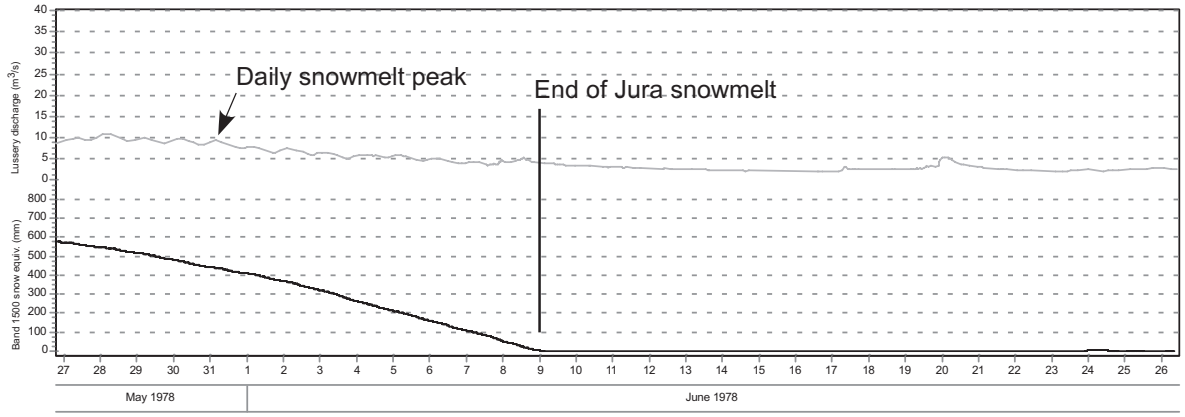

Figure 5.9. Estimation of the snowmelt temperature based on the end of the simulated Jura snowmelt and the snowmelt visible in the 1978 Lussery discharge series

5.6.2 Calibration

Adopted procedure

The HydroRoute model was adapted during this thesis to allow a global calibration. The parameters of each of the subcatchments as well as the global parameters are available for calibration. Beyond two subcatchments, the number of parameters to calibrate becomes unmanageable because no optimization routine is available in HydroRoute. It was necessary to add four coefficients to allow for a global calibration of the primary Venoge subcatchment parameters. These four coefficients are C_A, C_B, C_{ka}, C_{PET}. They are multiplied against each subcatchment A, β, k_a, and F_{PET}, respectively. No subcatchment differentiation of parameters was done except for the upstream β that was diminished because of the size of the subcatchment. The parameter A was set to 250 mm, β to 7500 $m^{4/3}/s$ (6500 for the Upper Venoge subcatchment), k_a to 0.00022 h^{-1}, and F_{PET} to 1. These parameters (except for the Upper Venoge β) correspond to those used in the Venoge study (Lance and Consuegra, 1997).

The adopted calibration procedure involved the simulation of 10'000 parameter sets generated via Monte-Carlo random sampling of uniform distributions of each of the coefficients. The uniform distributions for C_A, C_B, C_{ka} were from 0.5 to 1.5 and for C_{PET} the distribution was 1 to 1.75 for the PM PET series and 2 to 3.5 for the temperature-based PET. The Nash or Log-Nash objective function criteria is available for model performance evaluation. The Nash criterion was chosen to evaluate the model performance over the entire period, with all values below the threshold of 4 m^3/s (under-threshold), and with all values above 40 m^3/s (over-threshold). Using these three objective functions, should provide parameter sets that are optimal for the entire range of discharges.

Results

The objective function results for 25 of the 10'000 simulations are shown in tables 5.5 and 5.6. Columns 2-5 show the randomly generated coefficients used in the simulations. The three Nash criteria are given as well as their sum. The next three columns show the ranking of each of the Nash objective functions (1 to 10000). The next two columns present two ways to combine the information of the ranks, one by summing and one by choosing the maximum rank of the three. Combining the results of the three Nash criteria helped to find a parameter set that was better for high flows. The best Nash results (for the entire discharge series) for each of the two calibrations are 0.91 for the PM calibration and 0.89 for the temperature-based PET one. This confirms the hypothesis of Oudin et al. (2005) that a simple temperature-based PET is sufficient for hydrologic modeling. It should be noticed though, that the a posteriori "good" parameter distributions might be different depending on the parameters used in the temperature-based PET formula. As can be seen in the tables 5.5 and 5.6, the resulting "good" estimates of β are significantly different for the two calibrations. The reason for this can be seen in figure 5.10. The temperature-based PET (K_1=65, and K_2=0 of equation 5.2) produces lower winter and spring PET than that of PM. Since the majority of high flows for the Venoge are in the winter and spring, the β of the PM calibration must be higher due to the slow reservoir saturation that is lower. Figure 5.10 also shows that using the temperature-based PET with K_1=100 and K_2=7 is roughly equivalent to the PM equation for the Venoge catchment.

simulation number	C.ß	C.A	C.K	C.PET	Nash entire	Nash 40 m³/s	Nash 4 m³/s	sum Nash	rank Nash entire	rank Nash 40 m³/s	rank Nash 4 m³/s	sum ranks	maximum of ranks	comments
11	0.64	1.00	0.52	1.44	0.91	0.37	0.28	1.55	1	1564	737	2302	1564	best entire
286	1.00	1.26	0.51	1.08	0.86	0.59	-1.02	0.43	5280	1	7282	12563	7282	best high flow
8982	0.71	1.44	0.53	1.74	0.84	-1.45	0.61	-0.01	6786	8793	1	15580	8793	best low flow
5655	1.26	1.11	0.58	1.73	0.88	0.49	0.42	1.79	2595	499	222	3316	2595	best sum Nashs
9780	0.95	1.06	0.58	1.56	0.90	0.49	0.36	1.75	238	487	416	1141	487	best sum ranks
7331	1.01	1.06	0.59	1.60	0.89	0.50	0.38	1.77	463	438	343	1244	463	lowest maximum rank
3679	0.93	0.98	0.60	1.57	0.90	0.51	0.32	1.73	269	352	554	1175	554	
4953	0.84	0.94	0.57	1.55	0.90	0.50	0.30	1.70	181	409	641	1231	641	
7126	0.77	0.95	0.54	1.56	0.90	0.47	0.34	1.71	85	679	487	1251	679	
7720	0.91	1.08	0.57	1.51	0.90	0.48	0.32	1.70	108	604	556	1268	604	
2292	0.84	1.00	0.55	1.61	0.90	0.46	0.38	1.75	232	719	321	1272	719	
665	0.97	0.99	0.64	1.53	0.90	0.51	0.28	1.69	241	323	726	1290	726	
5706	0.94	1.00	0.51	1.63	0.89	0.52	0.37	1.78	610	297	389	1296	610	
1046	1.08	1.09	0.56	1.51	0.89	0.54	0.30	1.73	518	150	655	1323	655	
8937	0.78	0.95	0.50	1.63	0.90	0.47	0.37	1.74	285	686	368	1339	686	
9329	0.85	0.98	0.60	1.47	0.90	0.51	0.24	1.65	76	349	914	1339	914	
5087	1.01	1.01	0.64	1.51	0.90	0.52	0.26	1.68	288	264	819	1371	819	
9545	0.96	1.09	0.56	1.58	0.90	0.46	0.39	1.75	326	746	303	1375	746	
5322	0.97	0.96	0.62	1.56	0.90	0.51	0.30	1.70	376	347	664	1387	664	
5213	0.95	0.94	0.66	1.61	0.90	0.49	0.33	1.71	353	518	542	1413	542	
8301	0.83	1.02	0.59	1.48	0.90	0.47	0.28	1.65	35	645	736	1416	736	
2664	0.98	1.01	0.67	1.49	0.90	0.51	0.24	1.65	172	320	950	1442	950	
4309	0.93	0.96	0.53	1.54	0.89	0.52	0.28	1.70	466	286	714	1466	714	
612	0.84	0.93	0.56	1.50	0.90	0.51	0.24	1.65	219	366	900	1485	900	
834	1.09	1.05	0.65	1.63	0.89	0.49	0.38	1.76	653	483	351	1487	653	

Table 5.5. Calibration objective function results for 25 of the 10000 simulations using Penman-Monteith PET

simulation number	C.ß	C.A	C.K	C.PET	Nash entire	Nash 40 m³/s	Nash 4 m³/s	sum Nash	rank Nash entire	rank Nash 40 m³/s	rank Nash 4 m³/s	sum ranks	maximum of ranks	comments
1815	0.63	0.96	0.77	2.38	0.89	0.54	-0.10	1.33	1	101	3931	4033	3931	best entire
2197	0.85	0.84	1.09	2.55	0.89	0.61	-0.19	1.32	250	1	4886	5137	4886	best high flow
5090	0.55	1.47	0.52	3.23	0.80	-1.97	0.44	-0.73	8810	8810	1	17621	8810	best low flow
2178	0.81	0.94	0.68	3.04	0.88	0.58	0.19	1.65	1549	1558	909	4016	1558	best sum Nashs
5167	0.58	0.95	0.59	2.69	0.89	0.50	0.17	1.57	183	273	993	1449	993	best sum ranks
5924	0.62	1.02	0.70	2.84	0.88	0.29	0.21	1.39	754	785	753	2292	785	lowest maximum rank
8350	0.57	0.93	0.67	2.68	0.89	0.48	0.14	1.51	101	198	1266	1565	1266	
1230	0.56	0.99	0.58	2.55	0.89	0.46	0.14	1.49	96	193	1294	1583	1294	
6235	0.55	0.91	0.59	2.78	0.89	0.50	0.19	1.57	309	381	895	1585	895	
250	0.54	0.93	0.62	2.59	0.89	0.49	0.12	1.51	53	152	1404	1609	1404	
8442	0.54	0.95	0.62	2.76	0.89	0.39	0.20	1.48	352	421	845	1618	845	
8386	0.64	0.93	0.75	2.77	0.89	0.52	0.14	1.55	148	241	1255	1644	1255	
422	0.60	0.97	0.55	2.74	0.89	0.49	0.20	1.58	400	465	816	1681	816	
7516	0.53	0.92	0.54	2.77	0.89	0.49	0.20	1.58	394	459	830	1683	830	
7114	0.63	1.05	0.59	2.66	0.89	0.40	0.19	1.48	378	443	865	1686	865	
8276	0.60	0.92	0.67	2.86	0.89	0.50	0.19	1.58	382	447	889	1718	889	
5066	0.68	0.97	0.63	2.71	0.89	0.55	0.16	1.60	275	350	1100	1725	1100	
368	0.58	0.90	0.57	2.77	0.89	0.55	0.18	1.62	359	427	970	1756	970	
2480	0.60	0.92	0.63	2.60	0.89	0.56	0.11	1.56	71	168	1547	1786	1547	
7027	0.59	1.00	0.70	2.61	0.89	0.39	0.11	1.40	111	207	1482	1800	1482	
876	0.61	0.91	0.74	2.68	0.89	0.54	0.10	1.53	41	140	1623	1804	1623	
6534	0.72	1.00	0.74	2.68	0.89	0.52	0.12	1.53	147	240	1423	1810	1423	
1063	0.67	0.94	0.80	2.72	0.89	0.52	0.10	1.52	77	174	1618	1869	1618	
8282	0.62	1.06	0.65	2.71	0.89	0.30	0.20	1.38	552	601	847	2000	847	
2460	0.74	0.90	0.87	2.89	0.89	0.58	0.11	1.58	228	312	1499	2039	1499	

Table 5.6. Calibration objective function results for 25 of the 10000 simulations using temperature-based PET

All of the parameter sets of tables 5.5 and 5.6 had problems reproducing the extreme discharge events (figure 5.12). The HydroRoute model doesn't save output variables for multiple runs so it was unfeasible to test a lot of simulations for their extreme value distributions. Parameters were changed from the initial parameter set until an acceptable result in terms of the entire Nash, high flow Nash, and the extreme value distribution was found. The parameter set found was: $\beta = 7500$ (except for the Upper Venoge $\beta = 6500$), A=250, k_a=.00018, and F_{PET}=2.5 for the temperature-based PET calibration. The entire Nash was

0.88, the high flow Nash 0.47, and the low flow Nash -0.08. The low flow Nash is not good, but in the case of streambank erosion, it does not need to be better. It should be remembered that the high and low flow Nash criteria are very strict so the reader should not be shocked by these values. Figure 5.13 shows the results of the Gumbel frequency analysis. The fitted, simulated maximum annual discharges at the Ecublens station correspond very well to the observed 1993-2004 trend, which is different from the 1979-2004 trend (figure 5.13). The Lussery 1993-2004 fitted maximum annual discharges doesn't correspond well though to the Lussery 1948-1978 gumbel fit (figure 5.14). This can be explained by the two very important high flows that occurred during the 1993-2004 period. The 2004 high flow was one that was particularly generated from the Upper Venoge catchment precipitation. Replacing those two high flows by lower flows typical of the 1948-1978 period produced the fictive Lussery fitted line that is shown in figure 5.14.

The high flows as well as the low flows are relatively well reproduced as illustrated in figure 5.11. The variability around the regression line shows the error due to the model structure and especially the error due to the inaccuracies of the input data. The regression line's slope is 1.00 showing that there is no bias in the calibrated result.

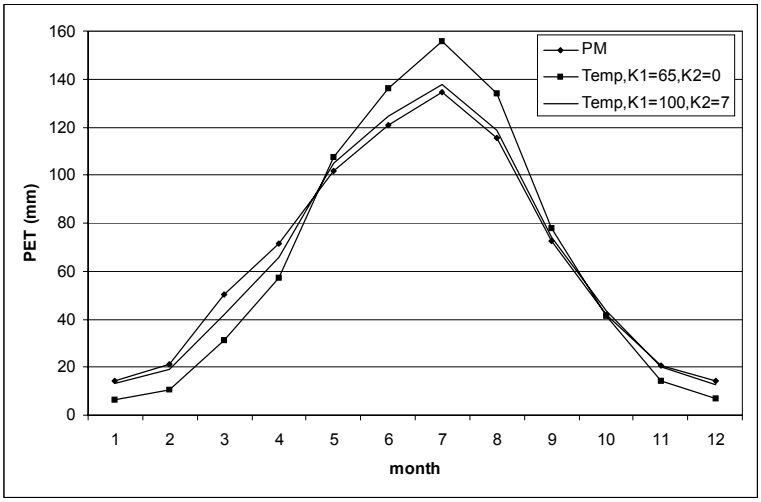

Figure 5.10. Comparison of mean monthly PET calculated with PM and the temperature-based method

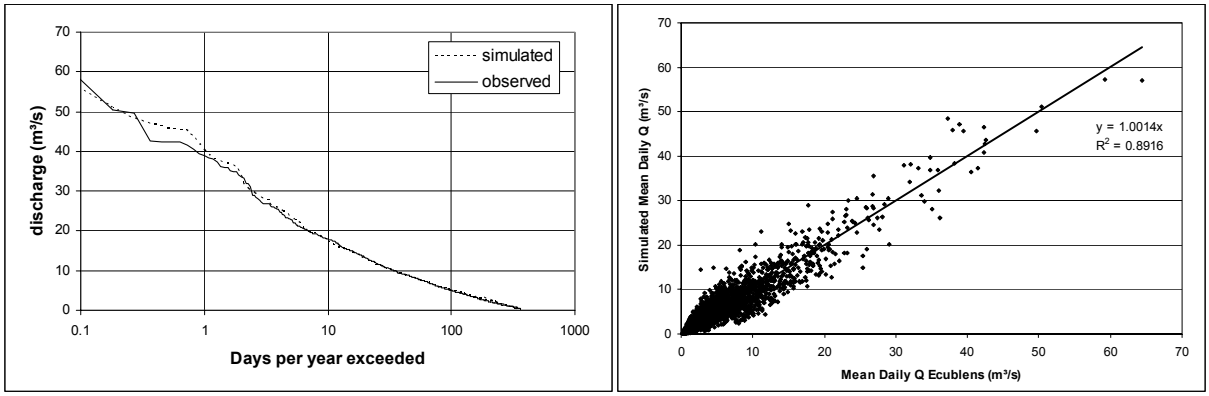

Figure 5.11. Flow duration curve (left) and the observed vs. simulated mean daily flows (right) for the period 1994-2004.

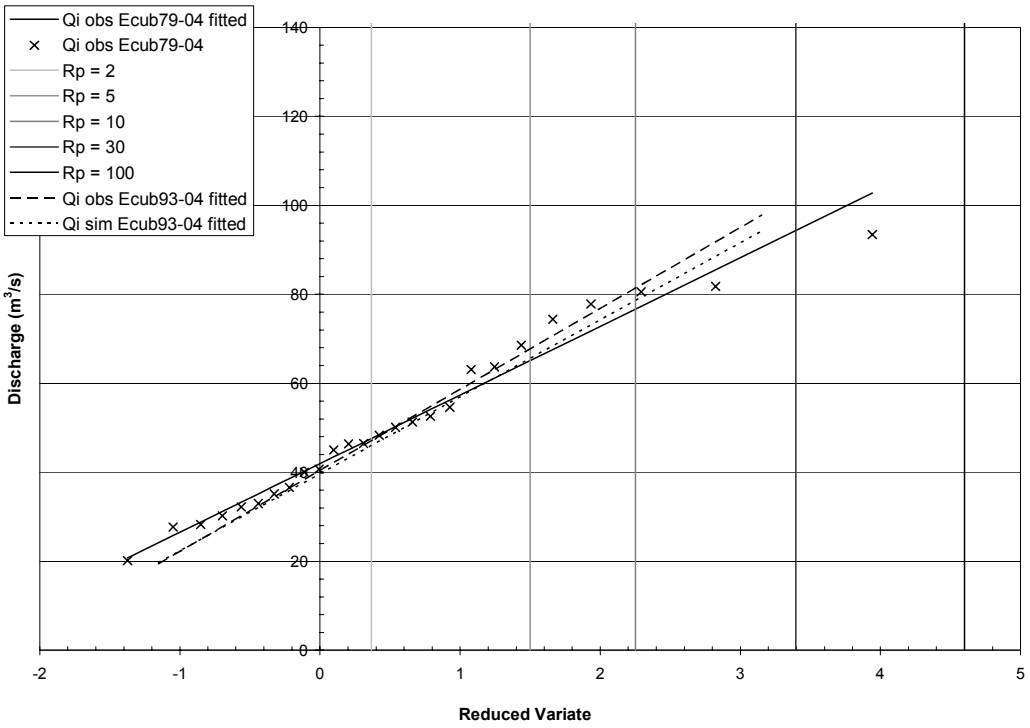

Figure 5.12. Comparison of maximum annual discharge behavior of the best "sum of Nash" of the temperature-based PET calibration versus observed discharges using a Gumbel (EVI) frequency analysis

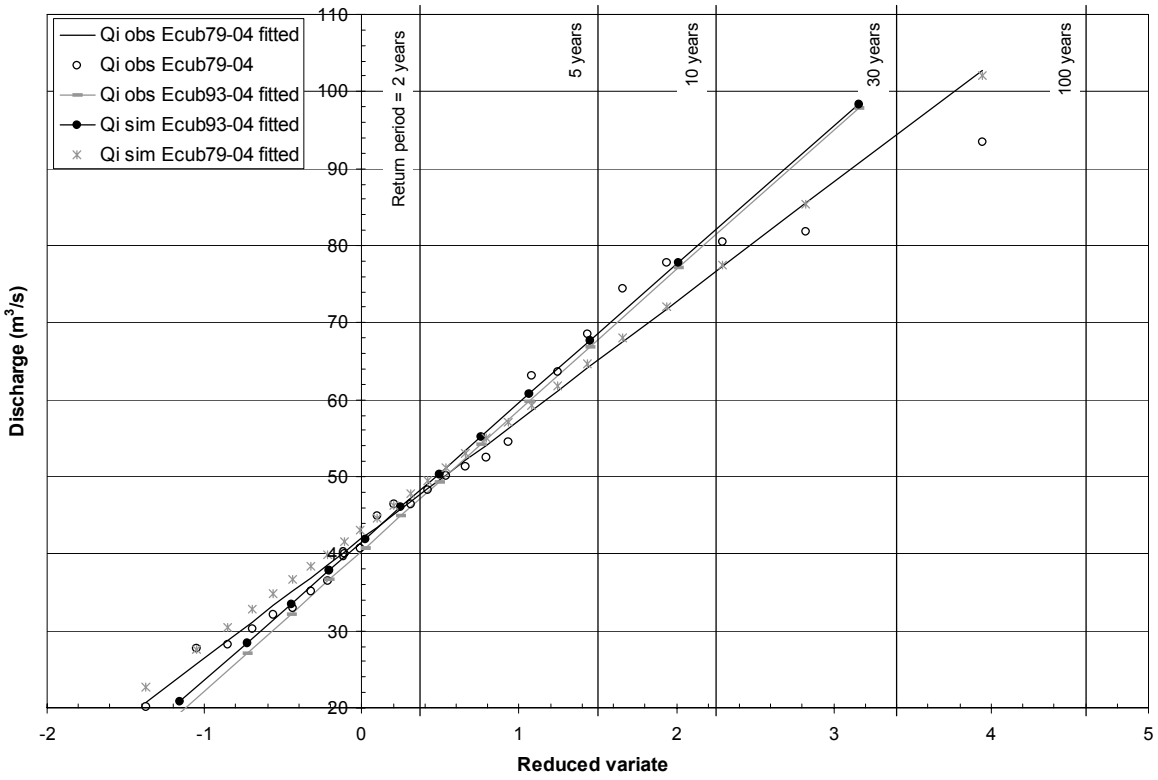

Figure 5.13. Gumbel frequency analysis of maximum annual discharges for the station of Ecublens, observed and simulated

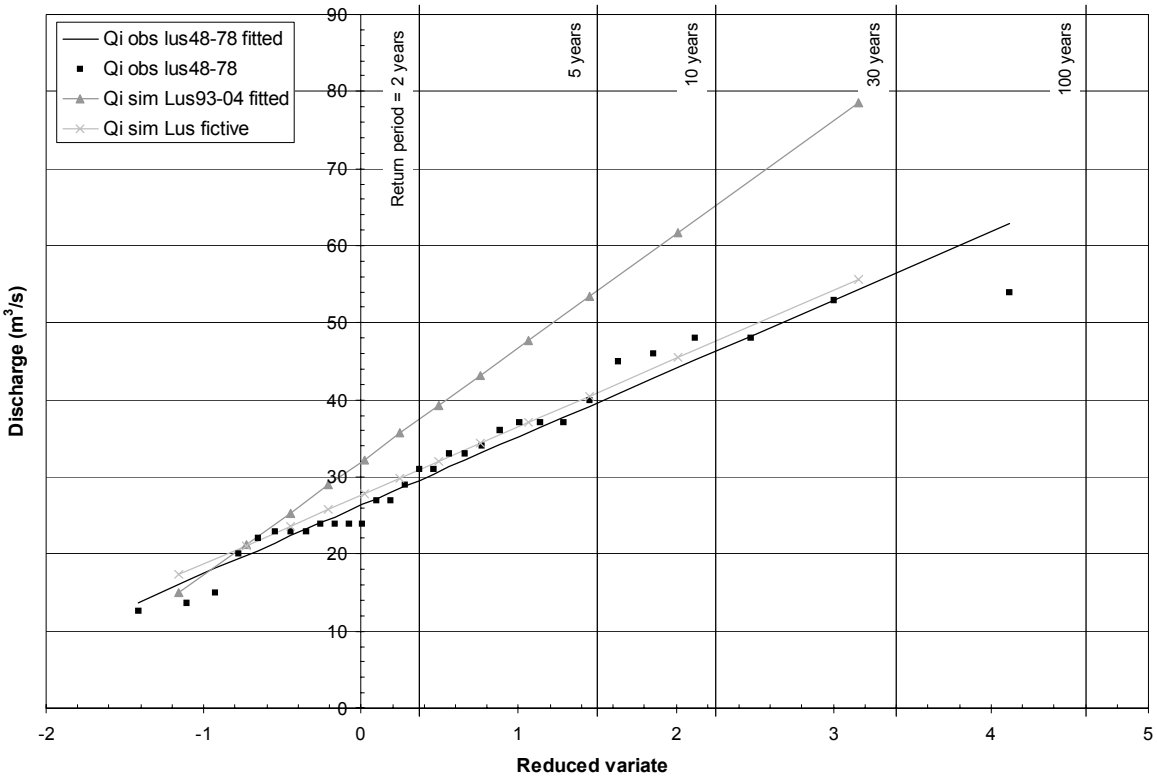

Figure 5.14. Gumbel frequency analysis of maximum annual discharges for the station of Lussery, observed and simulated

5.6.3 Validation

A simulation for the period August 1978 - August 1993 was run to validate the calibration. It was run only with the temperature-based PET. The resulting entire Nash is 0.83, the high flow Nash is 0.13, and the low flow Nash is -0.47. These results are lower than the calibration, even considerably for the high and low flow Nashs, but this is to be expected because the station Charbonnieres was not available, and especially because of the lack of the two cantonal recording precipitation gages that provide a better temporal structure for the majority of the catchment.

Although, the hourly discharge estimates of the simulation were degraded, the gumbel frequency analysis of the 1979-2004 shows a very good fit with the observed series (figure 5.13).

5.7 Distributed hydrographs for streambank erosion modeling

The goal of the work presented in this chapter is to produce hydrographs for the upstream and tributary inputs to the streambank erosion study reach. The calibration of the hydrologic model provided good results and the validation is within the values expected. The simulated values for Jan. 1, 1979 - Aug. 22, 1993 and the calibration simulated values for Aug. 23,1993 - February 28, 2005 were used for generating the hydrograph inputs for the streambank erosion study reach. With a historical discharge series

available though, its information should be capitalized on for the simulation of the historical period. It is proposed then to correct the simulated discharges according to the observed discharge with the following formula:

$$Q_{est,j} = \frac{Q_{obs,i}}{Q_{sim,i}} Q_{sim,j} \qquad \textit{Eq. 5.8}$$

where $Q_{est,j}$ is the estimated discharge for catchment j, the $Q_{obs,i}$ is the observed discharge at station i, $Q_{sim,i}$ is the simulated discharge at station i, and the $Q_{sim,j}$ is the simulated discharge for subcatchment j. This correction of simulated discharges was done to produce the estimated discharges of the combined subcatchments upstream and including subcatchment 4057, and the subcatchments 4012, 4058, 4008, 4021, 4003, and 4002 (see figure 5.4 for the subcatchment locations). Figure 5.15 illustrates the correction of simulated discharges for the January 14, 2004 flood.

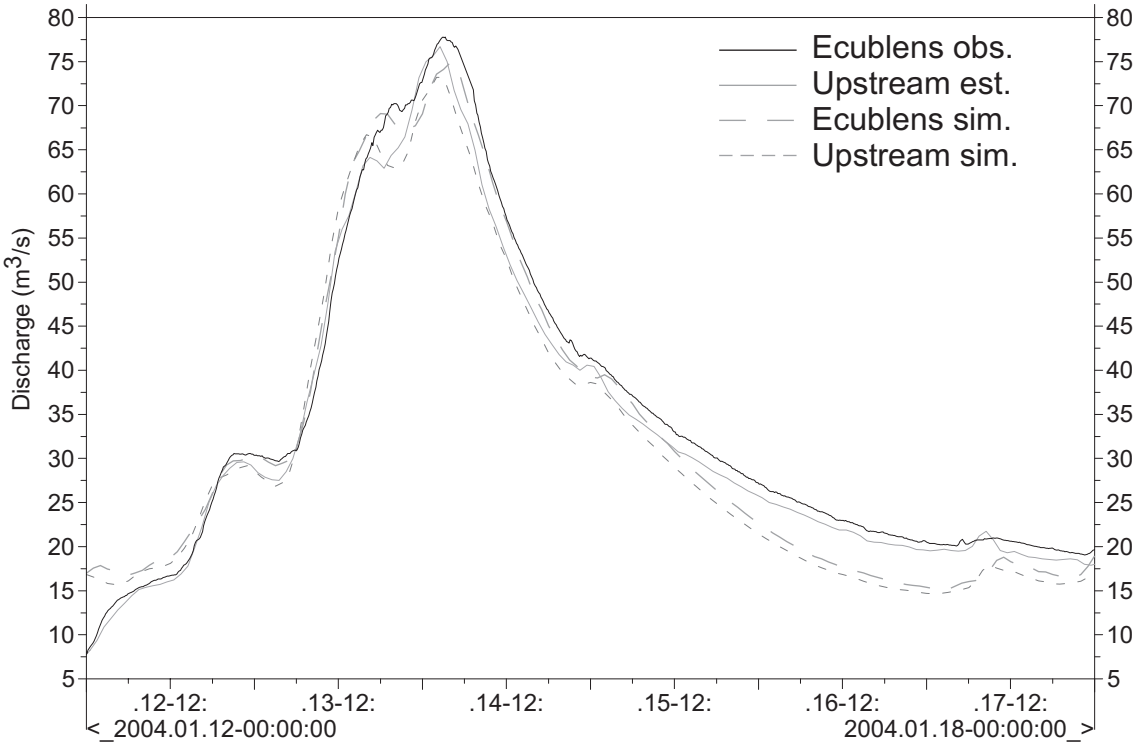

Figure 5.15. Simulated and historically corrected discharges

5.8 Extreme hydrographs and scenarios

The historical period for the Lower Venoge River is long enough to provide an adequate picture of the effect of high, low and typical precipitation years on the river flows. As a simpler alternative to the generation of discharge with stochastically generated meteorological data, it is proposed here to generate 300 years of Lower Venoge River discharge based on the discharge series created in section 5.7. Twenty-five years of discharge for the Lower Venoge River is available from 1980-2004. It is proposed to use the high flows during these years to generate extreme hydrographs and to replace the historical floods with the generated ones.

5.8.1 Flood volume and duration frequency analysis

Streambank erosion depends not only on the event peak discharge, but also on the event mean discharge. Thus, when generating flood hydrographs it is necessary to take into consideration frequency analysis of not only the peak discharges, but also of the flood volumes and durations. One possible approach is the QDF (discharge-duration-frequency) approach (Musy and Higy, 1998). Frequency analysis is performed on the mean discharge for various time steps and then can be graphed together (figure 5.16). A hydrograph of a given frequency can then be constructed based on the QDF curve of that frequency and typical rising limb times. This approach can lead to unrealistic hydrographs (single peak instead of multi-peaks), though, so it is preferred to generate hydrographs based on historical ones. As all floods above 9 m³/s will be simulated for streambank erosion, volume and duration frequency is analyzed specifically at that threshold and the results are given in table 5.7.

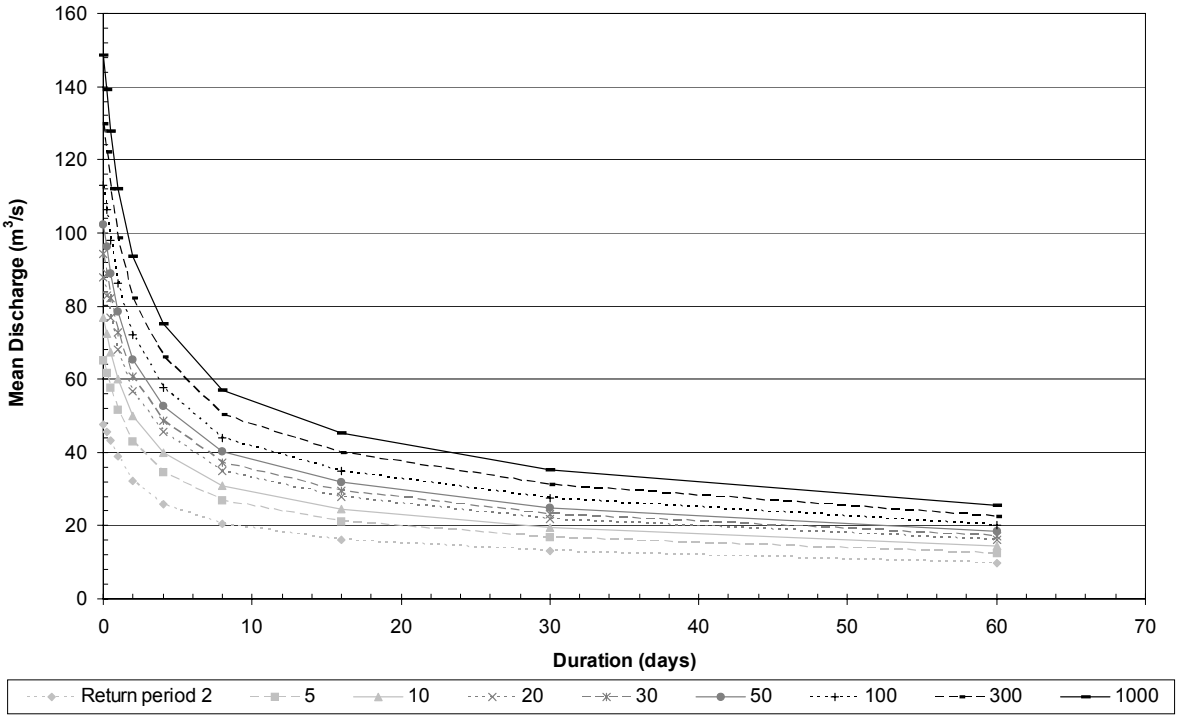

Figure 5.16. Mean discharge-duration-frequency curves for the Ecublens Venoge River recording station

Frequency analysis of instantaneous peak discharge, volume and duration were performed with the HYFRAN© (HYdrological FRequency ANalysis) software. The Gamma distribution is recommended by the software for fitting the annual series of the Venoge River Ecublens data, although the Gumbel distribution gives a good fit to the data also. It is preferred to work with the Gumbel distribution as there is not enough years of data to confirm either the Gamma or Gumbel distribution and the Gumbel distribution predicts higher rare flood peaks, volumes, and durations.

Return period (years)	Q (m³/s)	Vol. (m³)	Dur. (days)
25	92.7	5.41E+07	32.95
27	94.1	5.51E+07	33.56
30	95.6	5.63E+07	34.22
33	97.3	5.75E+07	34.96
38	99.2	5.89E+07	35.78
43	101.4	6.05E+07	36.71
50	103.8	6.24E+07	37.77
60	106.8	6.46E+07	39.04
75	110.3	6.72E+07	40.58
100	114.9	7.07E+07	42.57
150	121.3	7.55E+07	45.36
300	132.3	8.38E+07	50.13
1000	151.4	9.81E+07	58.39

Table 5.7. Gumbel frequency analysis results for instantaneous peak discharges, and flood volumes and durations of the Venoge River for the Ecublens recording station

5.8.2 Venoge River historically based flood hydrographs

To estimate a 300 year discharge series, the 25 year historical record will be repeated twelve times. Of course this historical record needs to be correctly completed with higher return period floods. Twelve floods respecting the characteristics of table 5.7 must be generated and inserted properly into the 300 year series. Six historical hydrographs were selected for the generation of these twelve hydrographs. The characteristics of those 6 historical hydrographs are placed in the context of the annual floods in table 5.8.

The low probability floods are generated by associating one of the low probability floods of table 5.7 with a historical flood and then are generated in three steps: firstly, all discharges are increased to raise the desired length of the hydrograph above the limit of 9 m³/s, secondly, discharges of one or multiple peaks of the historical flood are increased so that the peak discharge is respected, and finally, all other non-peak discharges are increased or decreased to produce the required flood volume. This procedure assumes that the return period of the instantaneous peak discharge, volume, and duration of low probability floods is equal. This assumption is not valid on an event basis as evident in table 5.8, but on average the volume and duration of the flood does increase with increasing flood peak discharge. Putting the low probability volumes and durations together with the same probability peak discharge will be a conservative estimation of low probability hydrographs for streambank erosion modeling. The twelve low probability floods as well as the 1000 year flood, which will be used as the extreme flood, are shown in figure 5.17. These low probability floods are proportioned into the upstream input and tributary hydrographs based on the subcatchment areas compared to the Ecublens measuring station catchment area.

Event start date	Q peak (m^3/s)	Volume (m^3)	Duration (days)	Return period Q (years)	Return period volume (years)	Return period duration (years)
01.01.1987 22:06	20.1	3.12E+06	2.30	1.0	1.1	1.0
09.12.1994 18:58	24.4	3.99E+06	2.82	1.1	1.1	1.0
30.11.1996 00:27	27.7	5.84E+06	4.39	1.1	1.1	1.1
03.02.2003 16:00	28.3	2.78E+06	2.09	1.2	1.0	1.0
29.06.1997 18:58	30.2	1.02E+07	8.22	1.2	1.2	1.3
02.03.1989 23:58	32.2	4.90E+06	3.31	1.3	1.1	1.0
18.01.1998 20:26	35.1	5.59E+06	4.48	1.3	1.1	1.1
22.12.1991 01:33	36.6	7.15E+06	4.08	1.4	1.1	1.1
23.01.1986 15:45	40.0	5.56E+06	3.10	1.5	1.1	1.0
10.10.1988 02:05	40.7	1.02E+07	5.12	1.6	1.2	1.1
01.05.1983 12:06	46.4	4.33E+07	31.88	1.7	10.4	21.5
25.12.1999 22:10	46.5	1.23E+07	6.83	1.8	1.3	1.2
22.01.1985 17:49	48.3	1.01E+07	5.59	1.9	1.2	1.1
31.01.1984 17:07	50.1	1.72E+07	11.51	2.1	1.7	1.7
29.02.2000 16:36	51.3	9.83E+06	5.75	2.3	1.2	1.1
20.01.1995 21:52	52.6	2.94E+07	15.16	2.5	3.6	2.4
28.09.1993 13:09	54.6	3.56E+07	22.81	2.7	5.7	6.1
15.11.1992 11:26	63.1	2.53E+07	14.89	3.1	2.7	2.3
31.12.1981 01:32	63.4	2.61E+07	15.28	3.5	2.8	2.4
31.01.1980 18:46	63.7	2.06E+07	11.32	4.0	2.0	1.6
26.01.1979 21:29	68.5	9.74E+06	5.11	4.7	1.2	1.1
14.02.1990 02:31	74.4	2.34E+07	9.83	5.8	2.4	1.4
12.01.2004 00:54	77.8	2.36E+07	10.69	7.4	2.4	1.5
03.03.2001 12:08	80.5	6.78E+07	33.02	10.4	78.8	25.3
07.12.1982 23:05	81.8	3.68E+07	18.58	17.3	6.2	3.5
09.11.2002 20:45	93.4	3.97E+07	23.23	52.0	7.8	6.5

Table 5.8. Annual peak floods recorded at the Ecublens Venoge River recording station. Events shaded in grey are those selected for the generation of low probability floods.

5.8.3 Discharge scenarios

Three 300 year discharge time series (scenarios) are constructed based on the simulated historical discharges from 1980-2004 and the low probability floods of figure 5.17. The base 300 years are constructed by repeating the period 1980-2004 twelve times to form a period from 1980-2179. The twelve events to be inserted into the 300 year period are chosen in a random order. This is done for each of the three scenarios (table 5.9 and figure 5.18) and for each tributary and the upstream input within each scenario.

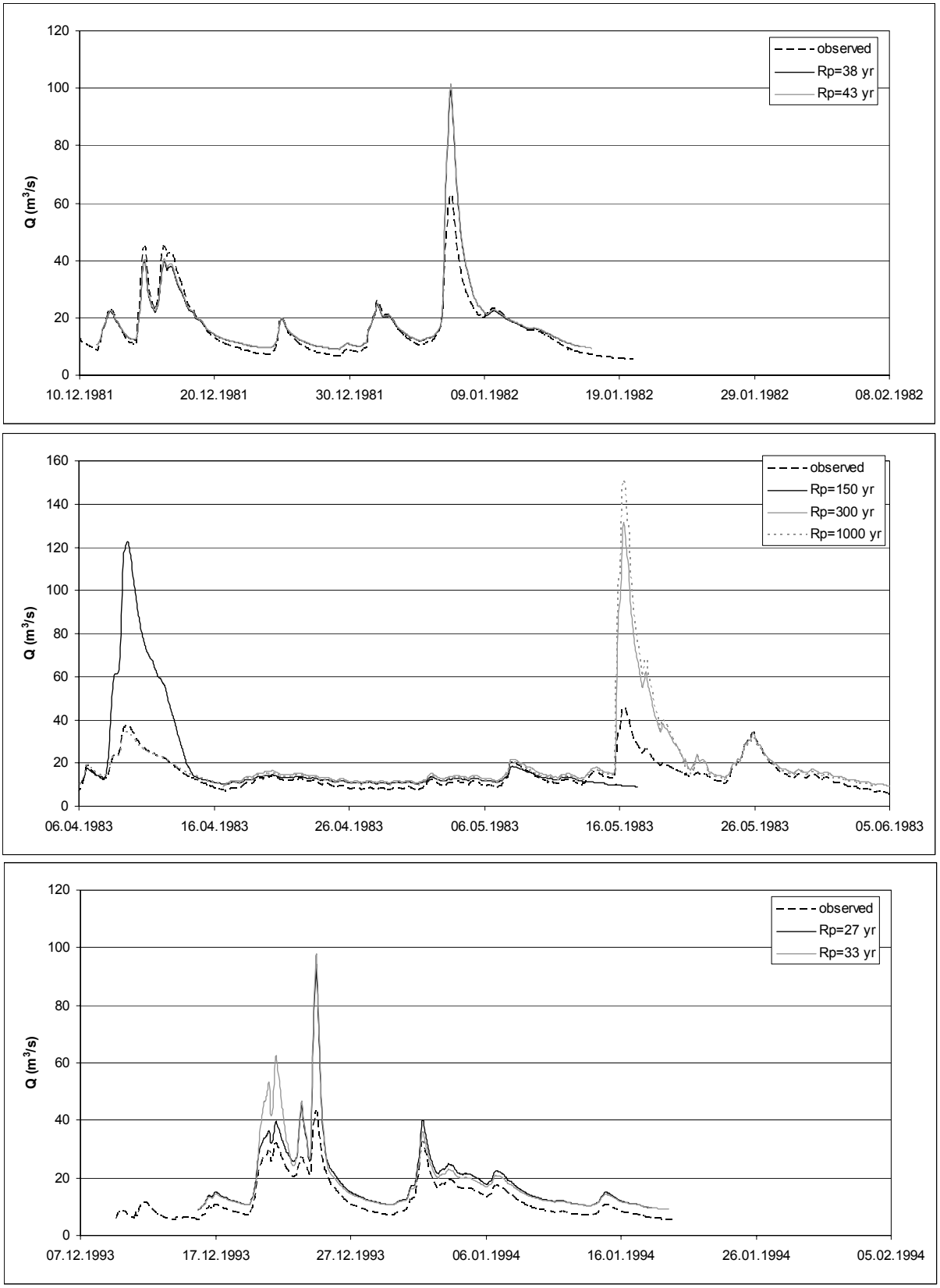

Figure 5.17. Low probability floods generated from historical floods

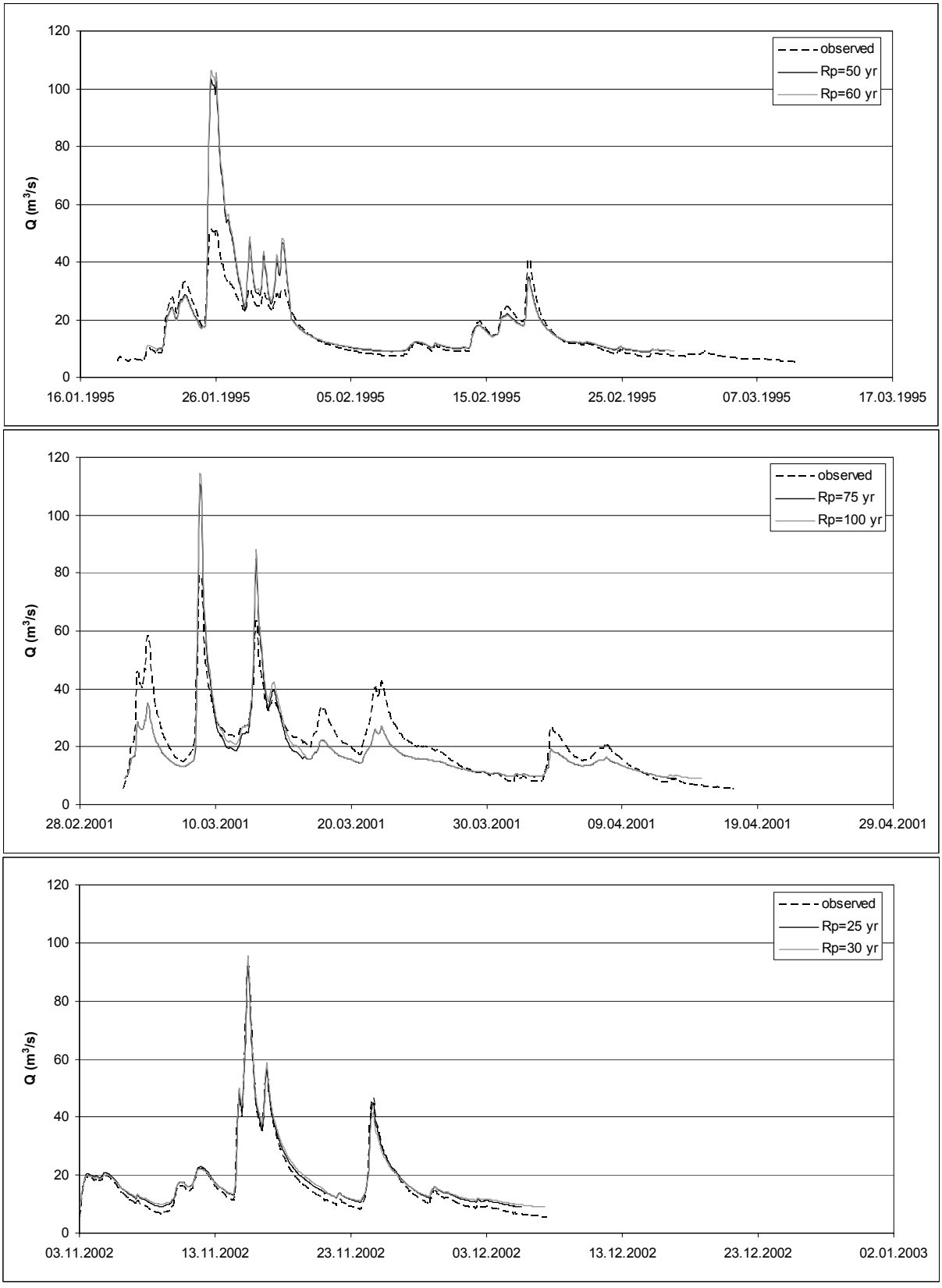

Figure 5.17 (cont.). Low probability floods generated from historical floods

Scenario 1		Scenario 2		Scenario 3	
Return Period	Year	Return Period	Year	Return Period	Year
150	1983	30	2002	27	1993
300	2008	150	2008	60	2020
50	2045	100	2051	50	2045
100	2076	38	2056	33	2068
25	2102	43	2081	43	2081
33	2118	300	2108	100	2126
30	2152	60	2145	150	2133
27	2168	75	2176	30	2177
75	2201	25	2202	38	2181
43	2206	27	2218	75	2226
60	2245	50	2245	25	2252
38	2256	33	2268	300	2258
1000	2283	1000	2283	1000	2283

Table 5.9. Insertion of low probability floods into the 300 year record to form three 300 year scenarios. The 1000 year flood is added to the end of each scenario.

To respect the historical frequency analyses, it is necessary to take out the historical flood that corresponds to the date of the low probability flood and to take out the floods that had return periods higher than 25 years. This is the case for the 2001 (high volume and duration) and 2002 (high peak discharge) floods. These floods are eliminated from each of the scenarios.

The resulting 300 year scenarios each contain 2826 streamflow events with flow greater than 9 m³/s.

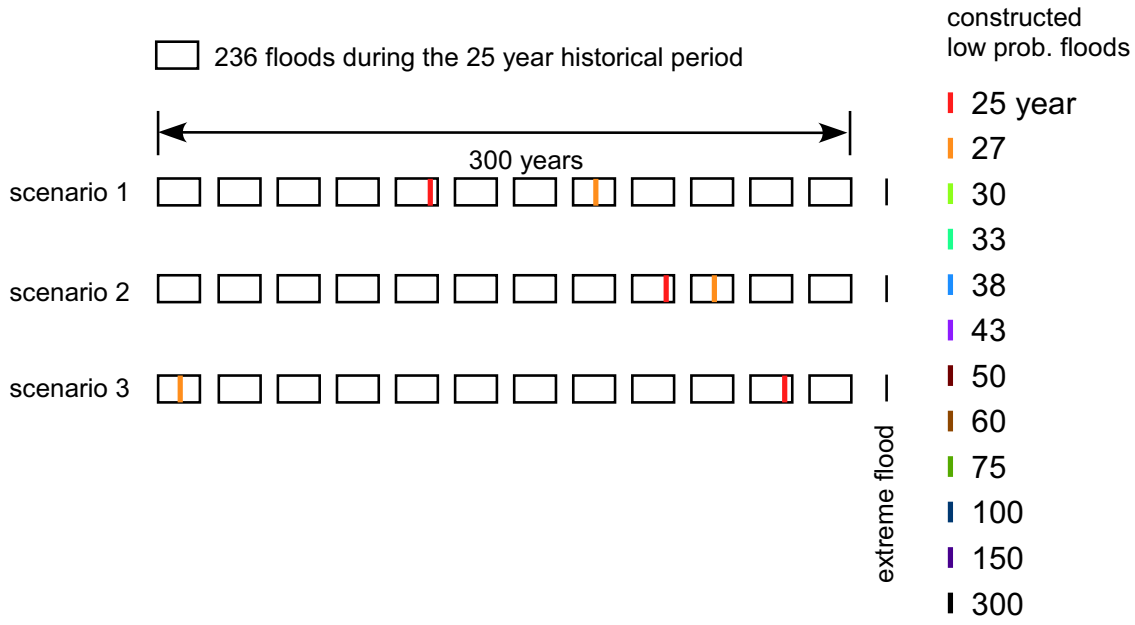

Figure 5.18. Example illustrating the insertion of the 25 and 27 year return period floods into the three 300 year series. One rectangle represents the 236 floods of the 25 year historical period.

Only three 300 year scenarios are constructed here to serve as an example. More should be constructed, but to do so an automated method would be necessary. Rather than automating such a method, it would be preferable to generate meteorological scenarios (Wojcik and Buishand, 2003) for input into the hydrologic model to generate many discharge series.

5.9 Summary and conclusions

Hydrologic data for the Venoge catchment was collected. Although, the data measured within the basin is largely insufficient, using the surrounding data allows for reasonable estimates of hydrologic input

data. Daily precipitation is disaggregated to hourly precipitation via the 10 minute recording gages. Precipitation, temperature, and PET are spatially interpolated for each Venoge subcatchment. PET is calculated by both the Penman-Monteith method as well as a temperature based method.

The model HydroRoute was used to do continuous hydrologic modeling. This model is able to take into account snowfall and snowmelt, which is important for the Jura mountains of the Venoge catchment. The Upper Venoge is modeled as one big subcatchment with many snow storage units, while the Lower Venoge is divided into many subcatchments to provide a detailed evolution of the Lower Venoge River flows.

Calibration coefficients were added to HydroRoute. These calibration coefficients allow a regional calibration of subcatchment parameters. One of the calibration coefficients is multiplied against the subcatchment PET. This calibration coefficient can be important to overcome evapotranspiration deficiencies in the model structure.

Calibration of the four calibration coefficients was done for the Venoge catchment using Monte-Carlo simulations. The best calibration yielding a Nash value of 0.91 is an excellent result for continuous hydrologic modeling although the stricter criteria of using the Nash criteria on the high flows or the low flows shows the difficulty of reproducing hydrograph peaks and low flows precisely. Validation gave poorer results as expected due to the diminished quantity of input data for this period. The Nash criteria was insufficient for finding parameter estimations to reproduce high flows adequately. Output of high flow statistics by the HydroRoute model would permit an improved model calibration of high flows.

Temperature based PET produced an equally good calibration as that done with the Penman-Monteith PET. This verified the hypothesis of Oudin et al. (2005a) that temperature based PET is sufficient for continuous hydrologic modeling. Other model parameters can be affected though if the temperature based PET gives an annual PET series that is significantly different than more sophisticated PET calculations such as Penman-Monteith.

The simulated January 1979 - March 2005 discharges were proportioned according to the discharge observed at the Ecublens recording station to improve the historical estimations for the Lower Venoge tributary inputs.

Frequency analysis of the instantaneous peak flow, flow duration, and flow volume was done for the Ecublens observed discharge series. This provides the criteria to respect in adapting historical high flow events to generate low probability flood events. Twelve low probability flow events are generated and combined in a 300 year flow series based on the 25 year historical period. This procedure was repeated three times to produce three series of 300 years. An extreme flood is added onto each of the 300 year discharge scenarios.

More than three discharge scenarios should be produced, although three discharge scenarios for the Venoge case will be sufficient to serve as an example in the streambank erosion hazard mapping methodology. To produce more scenarios, the scenario generation would need to be automated, or better yet, discharge scenarios should be generated based on stochastically generated meteorological data.

Chapter 6

Geofluvial Streambank Erosion Hazard Modeling and Danger Mapping

6.1 Introduction

As described in chapter 2.3.2, geofluvial modeling combines mechanistic fluvial and bank failure models to be able to perform streambank erosion hazard modeling. To calculate bank failures and their probabilities it is necessary to use this type of model. The methodology for calculating and mapping a streambank erosion hazard was outlined in chapter 2.4. The topographic, hydraulic, geotechnical, and hydrologic data that is used in connection with the geofluvial model, CCHE1D in this case, was presented in chapters 4 and 5.

This chapter will firstly show how the model is setup and then calibrated. Bank parameters will be spatialized to permit the simulation of streambank erosion throughout the reach. Finally, the streambank erosion hazard simulations will permit their mapping.

6.2 Model setup

The modeling reach is from station kilometer 10.516 to station kilometer 2.538 (map shown in figure A.3 of the appendix). Although, the data has been presented in the previous chapters, the procedure to bring that data into the required CCHE1D format is summarized here:

1. CCHE1D calculation nodes. After the channel centerline has been digitized and smoothed, nodes from that polyline are extracted according to cross section and hydraulic structure placement and

according to the spatial resolution needed. The procedure is fully described in chapter 2.4.2.

2. Hydraulic structures. If structures are to be modeled, the appropriate CCHE1D dbf files must be prepared. For the Venoge, only one inline weir is modeled as a drop structure, that of the recording station at kilometer 4.908. Bridges are modeled as regular cross sections with ineffective flow areas where flow obstruction occurs.
3. Channel and link CCHE1D files. These files are prepared based on the node and hydraulic structures. Scripts for the GIS, Mapinfo Professional® in this study, were developed to prepare these files.
4. Grain size classes. Bed and bank data require grain size distributions of the bed and bank material. The size classes must be specified for the model. This is done in the CCHE1D *_sedclas.dbf file.
5. Grain size fractions. Each Grain Size Distribution (GSD) for the bed and bank material must be divided into the grain size classes by indicating the fraction of material in each class. This grain size fraction information is put into the *_grfrac.dbf file.
6. Bed data. According to the sampling locations, polygons in the GIS are made to show the area of influence of each sample. These polygons become the basis for the CCHE1D *_sedbed.dbf file. Each *_sedbed.dbf entry contains attributes defining if the bed is erodible or not, and if so to what depth, and also the bed porosity, and identifier of the grain size fraction histogram. Nodes must be updated with the identifier of the bed data that applies to that node.
7. Bank data. Polygons are drawn in the GIS to represent homogeneous bank areas. These polygons are the graphical representations of each entry in the *_sedbank.dbf file. Each entry must define each of the required bank soil properties as described in detail in chapter 4.6. Each entry must also contain the identifier that links it to its grain size fractions. Nodes must be updated with the identifier of the bank data that applies to that node.
8. Cross sections. This step requires several sub-steps using the cross section tool developed during this thesis. They are described in detail in chapter 4.4 and are summarized here:
   - Cross sections points are identified by their station number which is the downstream distance to the outlet in meters for this study.
   - Cross section positions and transverse distances are calculated using the cross section tool.
   - Bank definition points are chosen.
   - Cross sections are interpolated linearly onto each node.
   - Manning values are based on the homogeneous roughness zones as shown in chapter 4.4.1 and ineffective flow areas are attributed to the appropriate cross sections points.
   - Cross section lines for the CCHE1D program are generated by a script in the GIS based on the cross section points CCHE1D file.
9. Baseflow. A text file is prepared according to the CCHE1D user's manual specification (Vieira and Wu, 2002). The baseflow for the Venoge is set at 9 m^3/s since the hydrographs to be simulated begin at roughly this value.
10. Upstream boundary condition. The upstream boundary condition is prepared with a program that takes a discharge time series and multiplies it against a sediment load curve to prepare the CCHE1D *.bc file. This is fully described in chapter 4.7.
11. Downstream boundary condition. A text file is prepared for CCHE1D specifying the rating curve at the downstream outlet. This is also described in chapter 4.7.
12. CCHE1D input file. This file is generated automatically if using the ArcView® interface of the CCHE1D program. Otherwise, it must be prepared manually. This was done by running the

ArcView interface for an example and reusing it for the Venoge case. Many important parameters are specified in this file. The various parameters used for the Venoge are:

- Sediment transport equation: code 2, Wu-Wang formula
- Bed material porosity: code 2, default method
- Roughness method: code 1, user specified
- Washload method: code 2, default method
- Suspended load adaptation length method: code 1, user specification, $\alpha = 0.5$ for the Venoge
- Bed adaptation length: code 3, method based on alternate bar spacing
- Mixing layer method: code 2, related to the bed material diameter
- Timestep: 1 hour, no significant difference was found between 1 hour and 1 minute timesteps
- Dynamic or Diffusive Wave: Diffusive; significant differences occur only in the vicinity of the weirs

13. CCHE1D output definition file, *_mp_df.txt. This file indicates to the CCHE1D program the variables that need to be output and at what locations and what times. The variables that can be output and the output formats are described in the user's manual (Vieira and Wu, 2002).

The following files are used specifically for this thesis and are not required by the standard CCHE1D program:

14. Second output definition file, "jb_output_def.txt." This is a second file used for output of other CCHE1D variables that can not be exported via the standard CCHE1D file.
15. Simulation type file, "inicon.txt". The CCHE1D program can be run with or without the initial conditions run. This can be helpful for repetitive simulations.
16. Centerline and erosion parameters file. This file contains the x and y coordinates of each node as well as the variables k_1, k_2, b, and k_5 of equation 2.22, and α of equation 2.16.

It is reminded here that the above steps are necessary when running CCHE1D without the ArcView® interface. The manner of preparing data for CCHE1D using the ArcView® interface is fully described in the user's manual (Vieira and Wu, 2002).

Once the above steps have been completed, it is possible to run the CCHE1D program from a command line. To facilitate the program execution, a program was written to allow CCHE1D to be run in batch mode. This program asks for the location of the CCHE1D executable and the location of the input files and will run CCHE1D repeatedly until all input files have been run.

In step 8 above, cross sections were linearly interpolated. To replace the cross sections with cross sections that respect radius of curvature (see chapter 4.4 for details), the Manning roughness values of the linearly interpolated cross sections are calibrated with historical water surface elevations. Water depth values exported from CCHE1D then permit the cross section tool to calibrate bed topography parameters and to interpolate cross sections respecting the centerline radius of curvature. These new cross sections are once again prepared as in step 8.

6.3 Calibration

6.3.1 Water surface elevation

The first step in the calibration procedure is to calibrate the Water Surface Elevations (WSE's). This is possible if historical WSE's are available. They were available or measured during this thesis and were reported in chapter 4.2. The majority of WSE's were measured during the October 26, 2004 event so it is used as the basis for simulating WSE's. For higher discharge values reported in table 4.2, those observed WSE's were used qualitatively only. For WSE's from 1996, the observed WSE was adjusted if a significant difference in the bottom thalweg exists between 1996 and 2004. The Manning values were changed and updated in the cross section points file according to the homogenous roughness zones as shown in chapter 4.4.1 until the differences in simulated and observed WSE's were acceptable. Typical Manning values for the are 0.04 for the bed, 0.07 for the banks, and 0.11 for the overbanks. The results are shown in figure 6.1 and table 6.1.

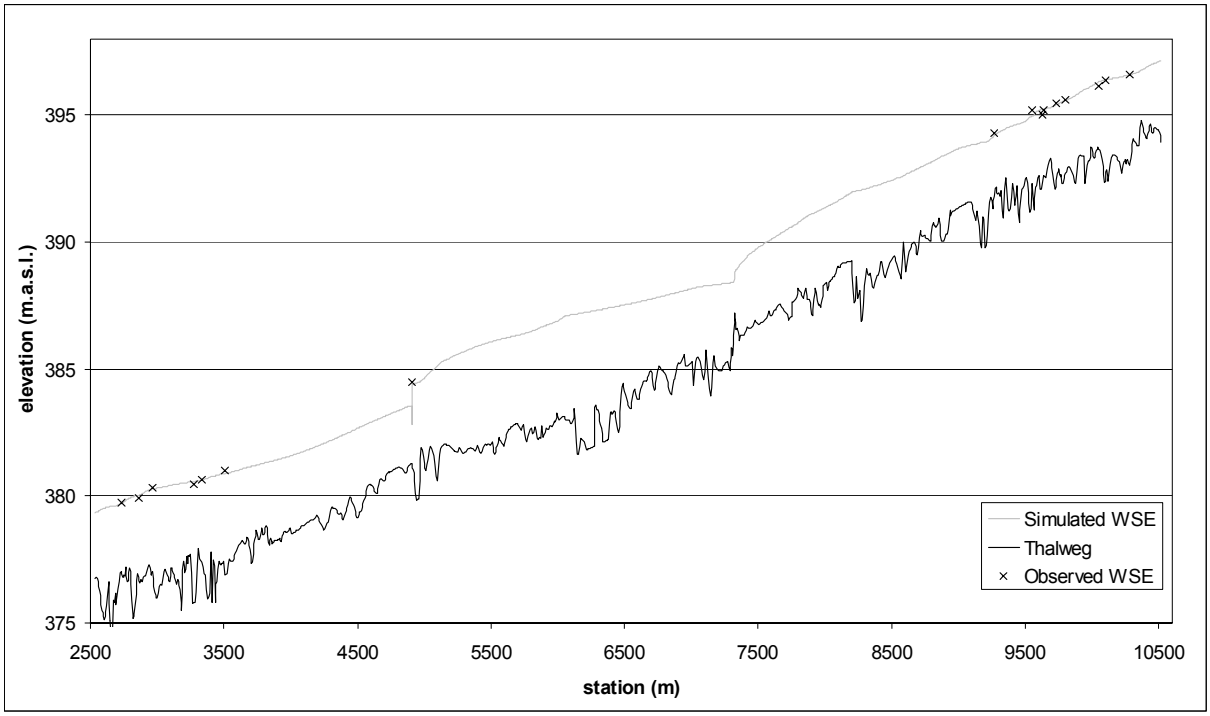

Figure 6.1. Comparison of observed and simulated water surface elevations for the October 26, 2004 high flow event

6.3.2 Bank erosion

The next step in the calibration procedure is to calibrate the bank erosion and according to calibrated values estimate bank property values for other banks where erosion was not monitored. Initial simulations to calibrate bank erosion showed the gamma toe shear stress correction function (figure 6.2) to produce erosion in a less localized manner than that observed in the field. To try to localize erosion to the very small areas as observed, the gamma function was changed as shown in figure 6.2.

The calibration period for bank erosion is from January 12, 2004 through March 29, 2005. Historically corrected simulated data are available through February 28, 2005. For the month of March 2005, input hydrographs are determined according to the subcatchment area in relation to the area of the Ecublens stage recorder catchment and the measured discharge. When running the simulations with sediment transport a few cross sections significantly changed their bottom elevation. To avoid problems with changing bed elevations, the bed elevations were fixed for the bank erosion calibration.

distance to outlet (m)	point id	discharge (m^3/s)	observed maximum WSE	simulated WSE	difference (m)
10323	360	50	396.42	396.50	0.08
10282	361	55	396.61	396.59	-0.02
10104	limni1	57	396.37	396.41	0.04
10053	2.1	57	396.14	396.31	0.17
9804	4.1	60	395.61	395.59	-0.02
9728	limni6	60	395.49	395.41	-0.09
9635	7.1	60	395.18	395.24	0.06
9625	7.4	60	395.03	395.23	0.20
9549	8.3	60	395.21	394.96	-0.25
9269	limni-eros11	60	394.31	394.20	-0.11
8213	371	55	392.24	391.90	-0.34
7771	390	50	390.49	390.44	-0.05
5241	461	50	385.22	385.26	0.04
4910	limni Ecublens	60	384.47	384.41	-0.06
3510	15.2	60	381.00	380.89	-0.11
3330	limni14	60	380.65	380.63	-0.02
3275	20.2	60	380.45	380.57	0.12
3005	470	55	379.89	380.20	0.30
2963	471	60	380.35	380.27	-0.08
2859	16.4	60	379.93	380.02	0.09
2734	limni-eros17	60	379.74	379.72	-0.02

Table 6.1. Comparison of historical and simulated WSE's

With incorporation of tension cracking in the CCHE1D bank failure algorithm, failure widths were typically in the 40-80 cm range, which was observed in the field, so that specific calibration of failure width was not sought. Also, without cross sections measured immediately before and after the erosion monitoring period at each erosion monitoring point, it is impossible to try to simulate the bank failures at a precise time. Thus, it was decided to compare erosion measurements with simulated bank erosion. An average erosion width for each measuring vertical during the calibration period was calculated based on the measured values given in table A.1 of the appendix. This eroded width is then compared with the simulated eroded width. The simulated eroded width, in terms of bank properties, is dependant on the critical shear stress and porosity. Assuming the measured bank porosity to be correct, bank erosion calibration was performed by changing the critical shear stress until simulated erosion was equivalent to the observed erosion.

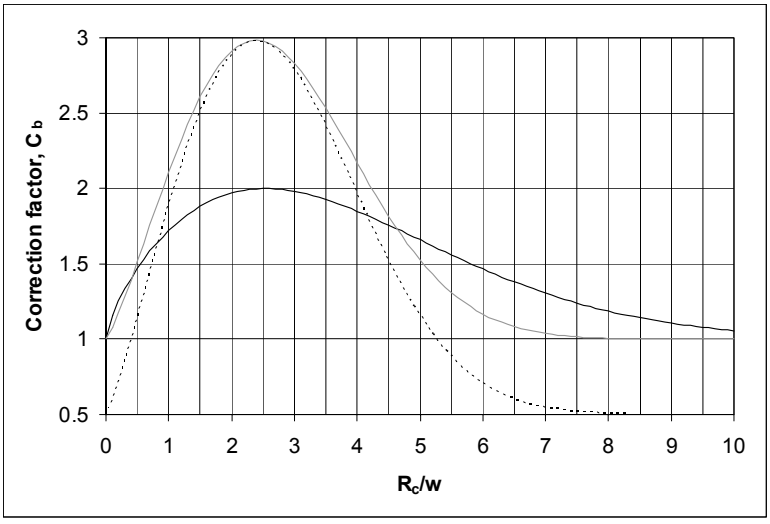

Figure 6.2. Final toe shear stress correction factor (in grey) as a function of the ratio of radius of curvature to width used in the streambank erosion modeling. Test case curve is the dashed line.

bend	estimated eroded bank width (m)	cross section id	simulated erosion width (m)	difference (cm)	critical shear stress (N/m²)	sum of differences (cm)	% difference
1.1	-0.01	10080	0.293	-30	5.3	10.2	0.01
1.2	0.06	10080	0.293	-23			
1.3	0.01	10074	0.363	-35			
2.1	0.12	10053	0.637	-52			
2.2	0.37	10045	0.723	-35			
2.3	0.40	10045	0.723	-32			
2.4	0.46	10045	0.723	-26			
2.5	0.74	10039	0.759	-2			
2.6	0.94	10033	0.759	18			
3.1	1.26	10022	0.921	34			
3.2	1.11	10022	0.921	19			
3.3	2.63	10016	0.877	175			
4.1	0.54	9804	0.651	-12	5.2	9.4	0.02
4.2	0.49	9804	0.651	-16			
4.3	0.55	9796	0.734	-18			
5.1	1.64	9788	0.864	78			
5.2	0.95	9782	0.803	14			
5.3	0.28	9776	0.657	-37			
6.1	0.30	9728	1.474	-118	4.45	-5.7	0.00
6.2	0.21	9728	1.474	-126			
6.3	1.73	9722	1.624	11			
6.4	1.76	9716	1.853	-9			
6.5	1.47	9716	1.853	-38			
6.6	2.39	9709	1.8	59			
6.7	1.63	9709	1.8	-17			
6.8	2.30	9701	1.44	86			
6.9	2.22	9701	1.44	78			
6.91	1.40	9694	1.113	29			
6.92	1.20	9686	0.799	40			
7.1	2.93	9635	1.902	102	3	-34.6	-0.02
7.2	4.71	9635	1.902	281			
7.3	2.19	9625	2.843	-66			
7.4	1.54	9625	2.843	-131			
7.5	2.39	9625	2.843	-45			
7.6	2.55	9620	4.31	-176			
8.1	0.48	9557	1.036	-56	5.2	0.9	0.00
8.2	0.56	9557	1.036	-48			
8.3	1.79	9549	0.745	105			
9.1	1.81	9460	1.491	32	4.2	4.8	0.01
9.2	1.49	9455	1.204	28			
9.3	0.48	9449	1.035	-55			
10.1	0.17	9348	0.346	-18	4.95	-2.2	-0.01
10.2	0.09	9339	0.716	-63			
10.3	0.09	9339	0.716	-63			
10.4	2.06	9330	0.658	141			

Table 6.2. Results of the bank erosion calibration. Calibration of the bank critical shear stress is based upon groups of measured verticals as shown by areas outlined in solid black.

The results of the bank erosion calibration are shown in table 6.2. The results vertical by vertical (line by line in table 6.2) are poor as shown by the difference in the eroded width and the simulated eroded width, although the average eroded width throughout a bend was reproduced as shown by the percentage difference (table 6.2). The important differences vertical by vertical are assumed to come from the varying flow conditions from one vertical to another during one event to another. A bank failure a few meters upstream will influence the flow conditions for the next vertical downstream. It can also be assumed that the bends will not continue to progress in the same proportions as observed during the calibration period as this would eventually produce an extremely jagged bank line.

bend	estimated eroded bank width (m)	cross section id	simulated erosion width (m)	difference (cm)	critical shear stress (N/m²)	sum of differences (cm)	% difference
11.1	0.68	9262	0.92	-24	5.25	18.0	0.02
11.2	0.22	9255	1.172	-95			
11.3	0.54	9248	1.053	-51			
11.4	1.28	9241	1.054	22			
11.5	2.02	9234	1.269	75			
11.6	2.54	9224	1.389	115			
11.7	1.09	9224	1.389	-30			
11.8	1.27	9214	1.209	6			
12.1	0.18	9176	0.94	-76	3.25	-16.2	-0.01
12.2	1.69	9167	1.418	27			
12.3	3.35	9167	1.418	194			
12.4	2.32	9158	3.206	-88			
12.5	3.35	9158	3.206	15			
12.6	3.37	9150	4.239	-87			
13.1	0.17	9080	0.218	-5	3.75	-8.9	-0.03
13.2	0.69	9073	0.573	12			
13.3	0.95	9073	0.573	38			
13.4	0.74	9073	0.573	17			
13.5	0.19	9067	0.89	-71			
14.1	0.04	3357	0.113	-7	6.4	-6.2	-0.12
14.2	0.04	3348	0.153	-11			
14.3	0.20	3339	0.152	4			
14.4	0.23	3339	0.152	8			
15.1	1.12	3519	1.095	3	4.35	17.6	0.03
15.2	0.75	3510	1.066	-32			
15.3	1.85	3500	0.892	96			
15.4	0.76	3492	0.883	-13			
15.5	1.12	3476	0.856	27			
15.6	0.32	3468	0.944	-63			
16.1	0.04	2882	0.887	-85	4.8	-8.0	-0.02
16.2	0.93	2870	0.86	7			
16.3	0.85	2864	0.747	11			
16.4	1.14	2859	0.602	54			
16.5	0.55	2853	0.499	5			
17.1	0.11	2728	2.362	-225	3.75	9.8	0.01
17.2	0.46	2716	2.1	-164			
17.3	1.15	2710	2.198	-105			
17.4	2.71	2703	2.541	17			
17.5	4.85	2693	2.852	199			
17.6	4.79	2688	1.914	288			
18.1	0.31	2670	0.149	16	4.3	-3.2	-0.02
18.2	0.03	2670	0.149	-12			
18.3	0.40	2664	0.171	23			
18.4	0.27	2664	0.171	10			
18.5	0.12	2658	0.197	-8			
18.6	0.18	2646	0.311	-13			
18.7	0.10	2640	0.282	-18			
19.1	0.02	3447	0.16	-14	5.7	0.0	0.00
19.2	0.15	3440	0.162	-1			
19.3	0.39	3433	0.166	22			
19.4	0.06	3420	0.131	-7			
20.1	0.36	3284	0.206	15	6.05	0.3	0.01
20.2	-0.04	3275	0.178	-22			
20.3	0.21	3266	0.141	7			

Table 6.2 (cont.). Results of the bank erosion calibration. Calibration of the bank critical shear stress is based upon groups of measured verticals as shown by areas outlined in solid black.

The calibration of critical shear stress is based on the cumulative bend erosion. It is worthwhile though to consider the behavior of the model event by event. As explained above, the cumulative erosion results for each bank profile are often poor so that event by event the results will be expected to be even poorer. For each bank profile and for each event, the three or four measurements (top, mid top, mid bottom, and bottom) were averaged to estimate a mean bank profile erosion. These mean values are only estimates of the event bank profile erosion. This is not only due to the fact that the point measurements are limited, but it is also largely due to the fact that the bank toe is not fully represented in the point measurements. These mean values were compared to the simulated mean bank profile erosion event by event. The absolute value of the difference of simulated and measured average profile erosion were summed over the 100 profiles. This sum of the differences is compared to the total measured average profile erosion to calculate a percentage difference. The results are shown graphically in figure 6.3. Firstly, the sums of all of the measured and simulated erosion at the measured profile locations are given, and secondly the percentage difference is shown with the right vertical axis. In terms of the global erosion, the model respects relatively well the measured quantity although the graph suggests slightly too much erosion for small discharge events and not enough for higher events. The percentage difference results are very poor. This is especially true for the lower discharge/volume events. Without putting the exact starting bank configuration into the model (the cross sections are from summer 2004 while the simulations start in January 2004) and without taking into account the effect of bank soil and tree falls on the 3-D flow field, it is inevitable to have poor results profile by profile. This should not be considered though to invalidate the model, but rather qualify the results of the model as indicative of global bend and reach erosion rather than specific location erosion.

As seen in figure 6.3, the lower discharge/volume event erosion appears to be overestimated and the higher discharge/volume events underestimated. This behavior is most likely a result of the erodibility coefficient equation used in the model. The CCHE1D model equation (c.f. equation 2.7), based on the work of Arulanandan et al. (1980), is compared to the erodibility coefficient equation in the work of Simon and Thomas (2002) (figure 6.4) in which the erodibility coefficient, $k = 0.1\tau_c^{-0.5}$. It can be seen that the low calibrated shear stress values result from the Arulanandan et al. (1980) formula. Using the Simon and Thomas (2002) formula would produce a higher calibrated critical shear stress that would permit proportionally more erosion to occur in the higher discharge/volume events. This result confirms that the equation of Simon and Thomas (2002) is an improvement over the Arulanandan et al. (1980) formula, although in the article by Hanson and Simon (2001), the equation is different by a factor of 2. Such a difference shows the need to further research the erodibility coefficient equation.

Measuring date	28.01.04	18.03.04	24.05.04	26.07.04	30.08.04	09.11.04	17.01.05	28.02.05	11.04.05
Erosion sim. (cm)	5227	147	359	380	360	2270	373	765	860
Erosion meas. (cm)	6082	478	342	73	431	2539	119	445	244
% difference by profile	74	548	188	129	240	114	180	122	101

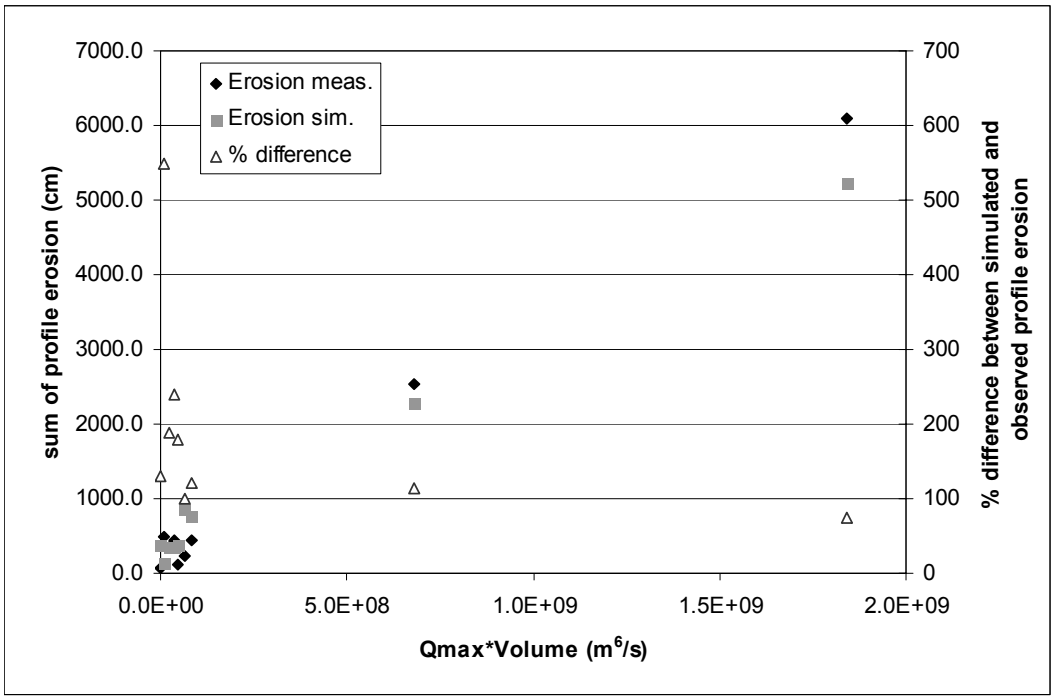

Figure 6.3. Comparison of total measured and simulated erosion as well as the average absolute percentage difference for measured and simulated profile erosion

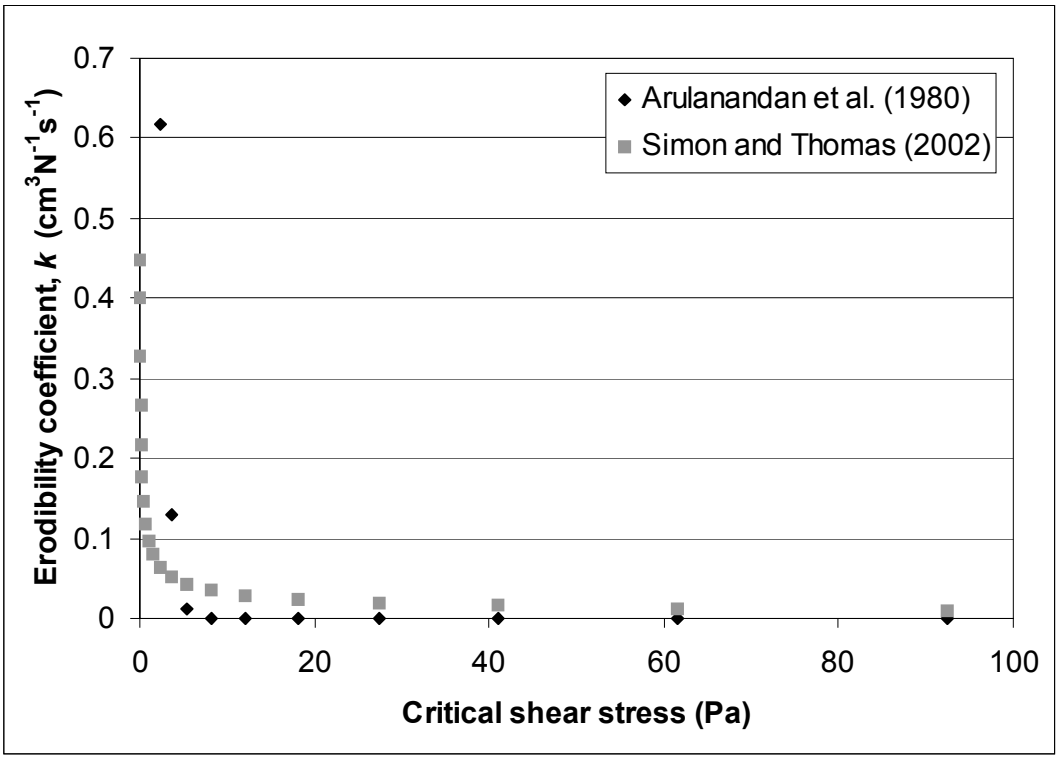

Figure 6.4. Comparison of two equations for erodibility as a function of critical shear stress.

6.3.3 Critical shear stress estimation

With the calibrated bank critical shear stresses, it is now possible to investigate if there are relationships between them and the various soil properties described in chapter 4.6 in view of developing an equation to estimate critical shear stress for non-calibrated banks. Firstly, correlation coefficients are explored to gain an appreciation of the correlations between the variables. Besides the variables given in table 4.9, characteristic grain sizes (D10, D30, D50, D60, D90, Dm), derived values of %silt/%clay, % cohesive, % large silt-fine sand (0.02-0.316 mm), % fine sand (0.05-0.316 mm), fraction bare observed, fraction bare laser, and vegetation height laser values were also explored for correlation. The variable, fraction bare observed, is a subjective judgement of the fraction of the bank observed to have no vegetation or root coverage, while fraction bare laser is derived from the LIDAR topographic data. It is assumed that the ratio of terrain LIDAR points to surface LIDAR points should be indicative of the vegetatative cover. This ratio is expressed in the variable fraction bare laser. The difference between surface point elevations and terrain point elevations can be considered to be representative of the vegetation height and is given by the variable vegetation height laser. Little correlation exists between these variables and the calibrated critical shear stress values. Only variables that have a correlation coefficient greater than the absolute value of 0.4 with critical shear stress are shown in the correlation matrix in table 6.3.

	τc	*n*	γ	Cu	Ip	Cud	Ccd	fract. bare obs
Critical shear stress, τc	1.00							
Porosity, *n*	0.50	1.00						
Natural unit weight, γ	-0.43	-0.84	1.00					
Shear vane, Cu	-0.43	-0.32	0.41	1.00				
Plasticity Index, Ip	-0.44	-0.16	0.24	0.61	1.00			
Uniformity Coef, Cud	-0.47	-0.24	0.03	0.32	0.72	1.00		
Curvature Coef., Ccd	-0.45	-0.01	-0.06	0.40	0.86	0.86	1.00	
fract. bare observed	-0.74	-0.49	0.50	0.71	0.61	0.40	0.44	1.00

Table 6.3. Correlation matrix of critical shear stress and soil properties

The poor correlation coefficients confirm the suggestion of other authors (Briaud et al., 2001, and Hanson and Simon, 2002 for example) that critical shear stress is poorly correlated with other soil variables and must be measured. This does not preclude an attempt at a multiple linear regression, though, to see if a combination of variables can explain the calibrated shear stresses for a given study reach. Stepwise regression was performed in Matlab® based on the same variables explored above in the correlation analysis. A multiple regression using just two variables, % fine sand - large silt, and fraction bare observed explained 75% of the variation (table 6.4). Although, this regression can not be used outside of the reach from which it was obtained, it does indicate the importance of these two variables.

bend	critical shear stress	% fine sand and large silt	fract. bare observed
1-3	5.3	63.09	0.25
4-5	5.2	48.32	0.25
6	4.45	64.22	0.40
7	3	75.27	0.50
8	5.2	54.84	0.50
10	4.95	65.71	0.25
11	5.25	59.84	0.30
12	3.25	47.38	0.80
13	3.75	56.65	0.40
15	4.35	63.05	0.50
16	4.8	63.50	0.30
17	3.75	62.80	0.50
18	4.3	1.79	0.75
19	5.7	14.37	0.30
20	6.05	66.59	0.05

SUMMARY OUTPUT

Regression Statistics	
Multiple R	0.87
R Square	0.75
Adjusted R Square	0.71
Standard Error	0.48
Observations	15

ANOVA

	df	*SS*	*MS*	*F*	*p value*
Regression	2	8.34	4.17	18.14	0.0002356
Residual	12	2.76	0.23		
Total	14	11.10			

	Coeff.	*Stand. Error*	*t Stat*	*P-value*	*Lower 95%*	*Upper 95%*
Intercept	7.500	0.563	13.312	0.0000	6.273	8.728
% fine sand - large silt	-0.022	0.007	-3.183	0.0079	-0.037	-0.007
fract. bare obs	-4.192	0.705	-5.944	0.0001	-5.729	-2.656

RESIDUAL OUTPUT

Bend	*Predicted*	*Residuals*	*Stand. Residuals*
1-3	5.06	0.24	0.54
4-5	5.38	-0.18	-0.42
6	4.40	0.05	0.10
7	3.74	-0.74	-1.67
8	4.19	1.01	2.27
10	5.00	-0.05	-0.11
11	4.92	0.33	0.74
12	3.10	0.15	0.34
13	4.57	-0.82	-1.85
15	4.01	0.34	0.76
16	4.84	-0.04	-0.09
17	4.02	-0.27	-0.60
18	4.32	-0.02	-0.04
19	5.93	-0.23	-0.51
20	5.82	0.23	0.52

Table 6.4. Results of a multiple linear regression to explain calibrated critical shear stress

Without numerous particle size distributions and observations of vegetation density on bank faces in areas of the study reach not monitored for erosion, it was decided to attribute a mean calibrated critical shear stress value of 4.6 Pa to all other banks in the study reach. This value was then increased or decreased based upon the location of erosion scars (see figure 4.1) and upon the approximate river centerline movement from 1964 (from the 1996 Venoge study, Lance and Consuegra, 1998).

6.3.4 Sediment transport

Sediment transport can only be considered qualitatively because there are not enough cross sections spanning a long enough period to quantify significant bed elevation changes in the Venoge River and no bedload or suspended sediment measurements were taken.

Sediment transport including bank erosion was simulated for the historical period from January 1979 through March 2005. The areas from km 4.950 to km 5.527 and km 5.819 to km 6.102 seemed to have excessive bed erosion. It seems to be excessive compared to a lack of bed lowering indicators based on

field observations. Bed lowering occurred upstream from the damaged "Abbaye" weir in the zone km 7.335-7.884 during 2001 and 2002, but this zone was supposedly stabilized by a temporary reparation to the weir in 2002.

Bed sediment size was increased in the excessive bed lowering areas until a relative stability was ensured for the 1979-2005 simulation. The change in the D_{50} seems excessive though, as the values from km 4.950 to km 5.527 were changed from approximately 1 cm to 4.5 cm, and from 1.1 to 4 cm for km 5.819 to km 6.102, and from 1.3 to 7 cm for km 7.335 to km 7.884. As the maximum sampled D_{50} for the last 20 kilometers of the Venoge River is 4 cm (see figure 4.33), there seems to be data problems in these areas.

Besides the adjustments to bed sediment sizes, it was also noticed that significant deposition was occurring near the upstream boundary condition. This was corrected by multiplying the sediment transport curves of figure 4.38 by 0.75 such that a reasonable balance between deposition near the inlet and erosion following the depositions was obtained (figure 6.5).

6.4 Streambank erosion hazard simulations and danger mapping

6.4.1 Streambank erosion danger map

With the calibration of the Venoge River study reach completed, it is now possible to simulate bank erosion and failures with the 300 year scenarios shown in chapter 5.8. The objective of this simulation is to be able to analyze the empirical frequency of the bank failures to calculate the probability of a given failure width. As explained in chapter 2.4.2 concerning the changes made to the CCHE1D model for this thesis, to calculate the probability of failure for a current bank, flow conditions and bank geometry should not change during the simulations. To do this, bank geometry is not changed after a bank failure, but new bank failures are not allowed to occur until nearly all basal sediments in the virtual reservoir have been emptied.

Besides the adjustments made to the sediment transport as shown in the previous section, 6.3.4, there are still important bed fluctuations that are occurring during the 25 year period. These fluctuations will change the flow conditions and bank geometry situations. Thus, it is decided for the 300 year simulations to fix the river bed. This option is available in the CCHE1D sediment transport calculations.

To practically handle the 300 year simulations with the computer resources at hand, the 300 years are divided into 100 year simulations. This means that the initial bank conditions are repeated 3 times rather than once. This is deemed a reasonable compromise for banks that are initially stable, but become unstable during the course of the simulations due to toe erosion. If the simulation period is too long, the probability of failure of such banks will be overestimated. If the simulation period is too short, though, the bank will never fail. Thus, the length of the simulations should be at least as long as the period of validity designated for the maps, in other words, the length of time before the maps will be renewed. In the case of the Venoge River, it would be suggested to renew the maps every 10 years or so. Of course,

erosion in active meanders will most likely change during the 10 years as the erosion attack will migrate downstream, but the bank failure probabilities can be roughly assumed to follow the bend migration path during this period. Due to some poor cross section interpolations, it is preferred to go beyond this 10 year simulation length. How much beyond this 10 year simulation length is reasonable is unknown. For convenience, a 100 year simulation length was chosen. This simulation time takes roughly 13 hours on a 2.8 Ghz desktop personal computer. This is convenient for running simulations during the evening on several workstations and recovering the results the next work day. Thus, the three 300 year simulations were divided among 9 workstations.

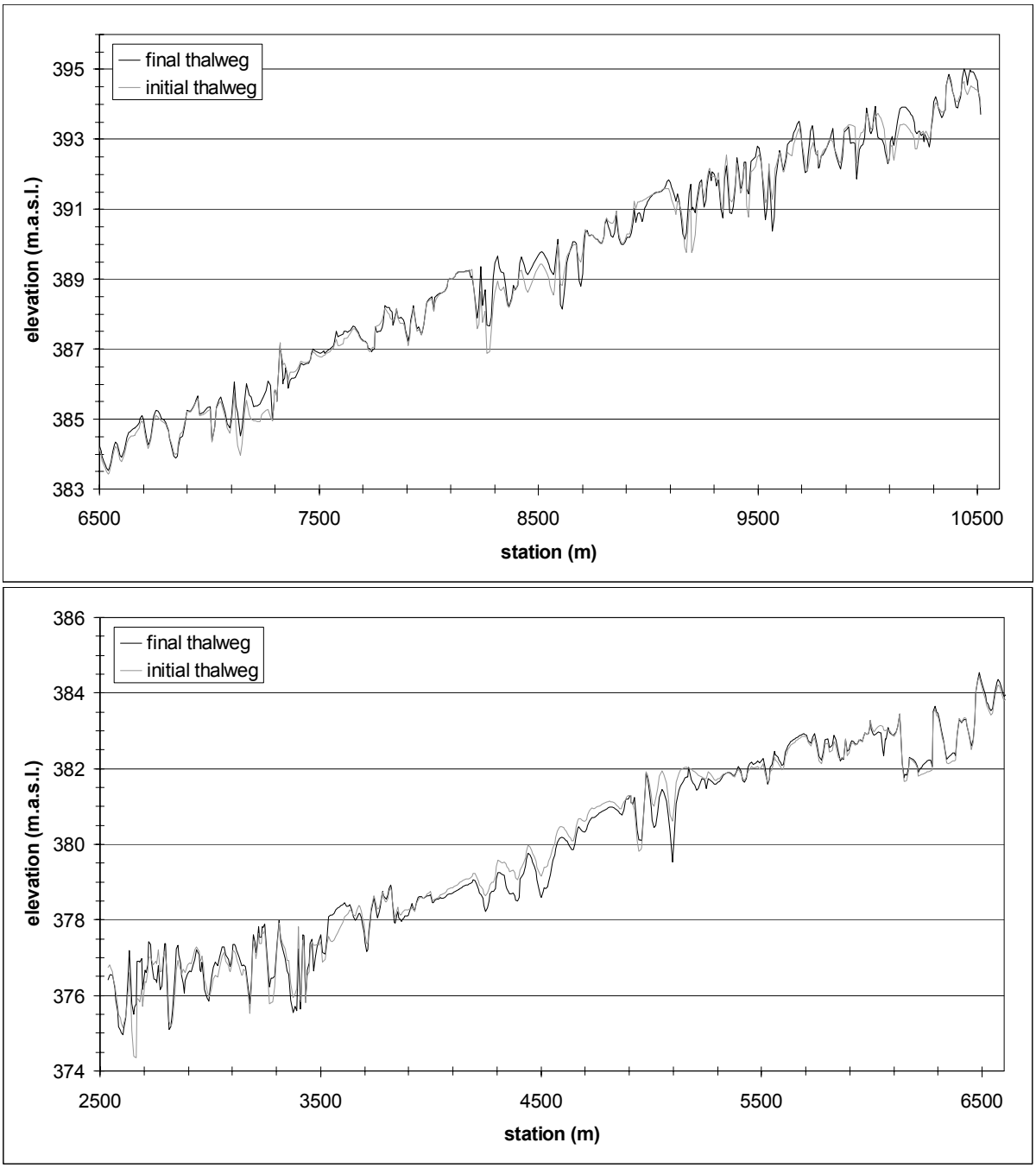

Figure 6.5. Bed elevation changes simulated with the 26 year discharge record

The bank failure results for the simulations are output in a text file. The three 100 year bank failure text files are combined to form the 300 year bank failures. These bank failures are read by a program which ranks the failures and calculates a frequency according to the number of events. This event frequency is transformed into an annual frequency according to the Langbein-Takeuchi relation (Meylan and Musy, 1999):

$$F_A(x) = \exp\{-\lambda[1 - F_E(x)]\} \qquad \textit{Eq. 6.1}$$

where $F_A(x)$ is the annual cumulative probability, λ is the number of events divided by the number of years, and $F_E(x)$ is the event cumulative probability. Examples of bank failures and their probabilities are given in figure 6.6. The top left graph shows a bank that fails infrequently while the bottom right graph shows very frequent failures. The multiple steps in the bottom right graph are due to multiple bank failures in a single event. For banks to have a more varied bank failure width response, the CCHE1D program would need to include pore-water pressure modeling. This would force the bank geometry to steepen when the bank has enough matric suction to resist bank failure causing a different failure geometry the next time the bank is saturated enough to fail. Varied bank failure response is also most likely due to heterogeneities in the bank which could be incorporated in the model if those heterogeneities are quantified (with probability distributions of cohesion and friction angle in the bank for example).

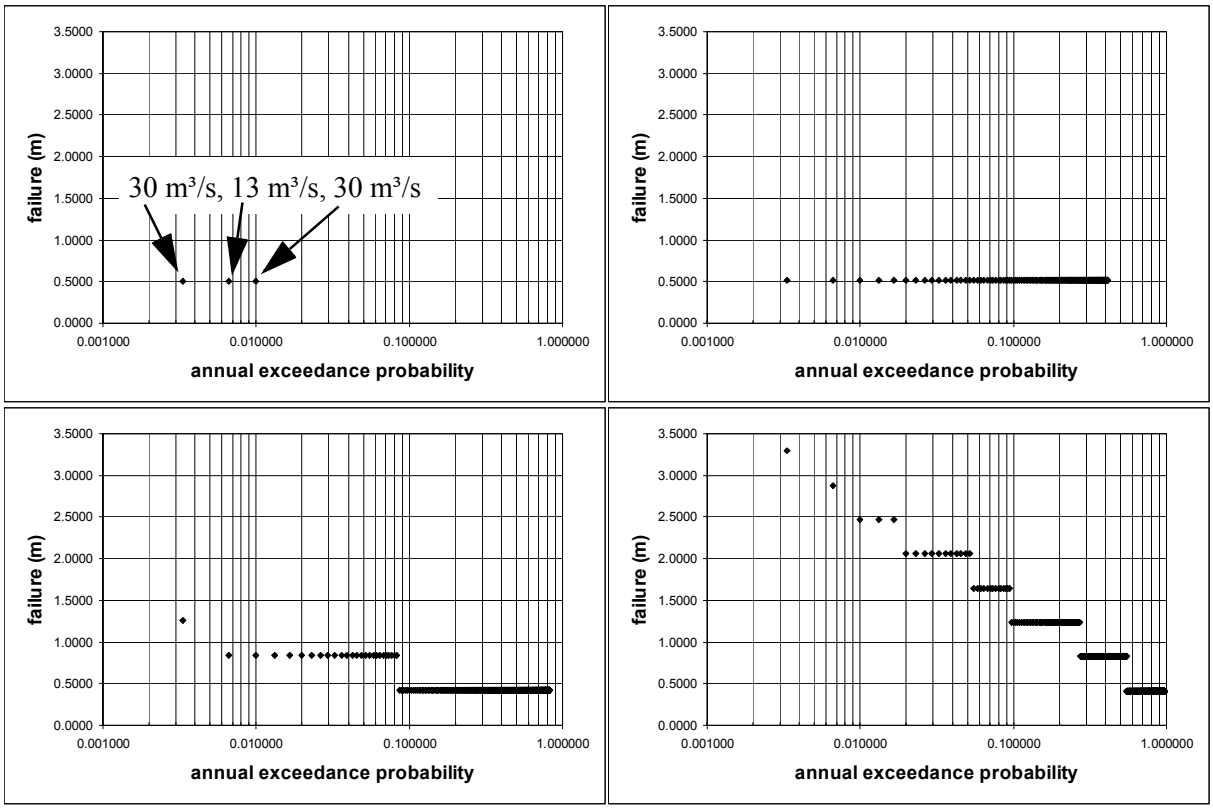

Figure 6.6. Examples of bank failure widths and probabilities for the following cross sections: km 2.693 right (top left), km 10.080 left (top right), km 10.016 (bot. left), and km 2.949 (bot. right)

With the bank failure widths and their probabilities quantified, it is possible to quantify the danger level of the streambank erosion hazard according to the recommendations of the Federal Office for Water and Geology (figure 1.3). For example, the bank represented in the top left graph of figure 6.6 would have a

weak danger level because its value is just less than 0.5 meters and a failure can be expected only every one hundred years on average. It can also be noticed in this graph that the events causing the failures are all below the one year return period maximum annual discharge showing that bank failures often are not correlated with the maximum event discharge. The top right and bottom left graphs of figure 6.6 show medium streambank erosion dangers, while the bottom right graph shows a high streambank erosion danger. The danger levels are calculated for each bank and are mapped (figure 6.7 and appendix 7). There are very few weak dangers on the map and they are hardly visible because of their size. This is due to the stringent criteria of all 30 year return period failures being classified as a medium or high danger. It seems reasonable though that nearly all of the bank failures should be classified as medium or high dangers because of the dangerousness of a failure.

It should be noticed that danger levels have been calculated where bank protection exists. This was possible in the simulation with a fixed bed calculation. With a non-fixed bed simulation, taking out all of the bank protection would have caused too much sediment supply causing significant bed changes. Danger levels at the bank protection in this map are not the final danger levels. These danger levels would have to be combined with the probability of failure of the bank protection works to determine a final danger level.

Besides the erosion danger level, the mean annual erosion is also represented in the map according to the length of the bar. This information is provided to qualify the danger level. It is meant to show where the erosion is active. It is not meant to show where the river will progress in the future. For actively eroding banks, the cross section and planform geometry will progressively change, changing in turn the mean annual erosion widths. Besides, the bars showing the danger level, a buffer is placed around the river channel outline showing the possible river extension during an extreme flood. This value is set here as 1.5 times the maximum simulated bank failure of the river. The maximum extreme failure of 10.53 meters for a cross section is at km 9.614 so that the extreme danger buffer is set to 16 meters around the existing bank tops. It seems reasonable to imagine, that obstructions in the river could deflect the river flow to cause excessive shearing velocities beyond that which was simulated, thus permitting the use of a multiplication factor. The average width of the Venoge River in the study reach is approximately 24 meters. It would be prudent to use this value as the security distance for a management strategy such as the one shown in figure 1.4.

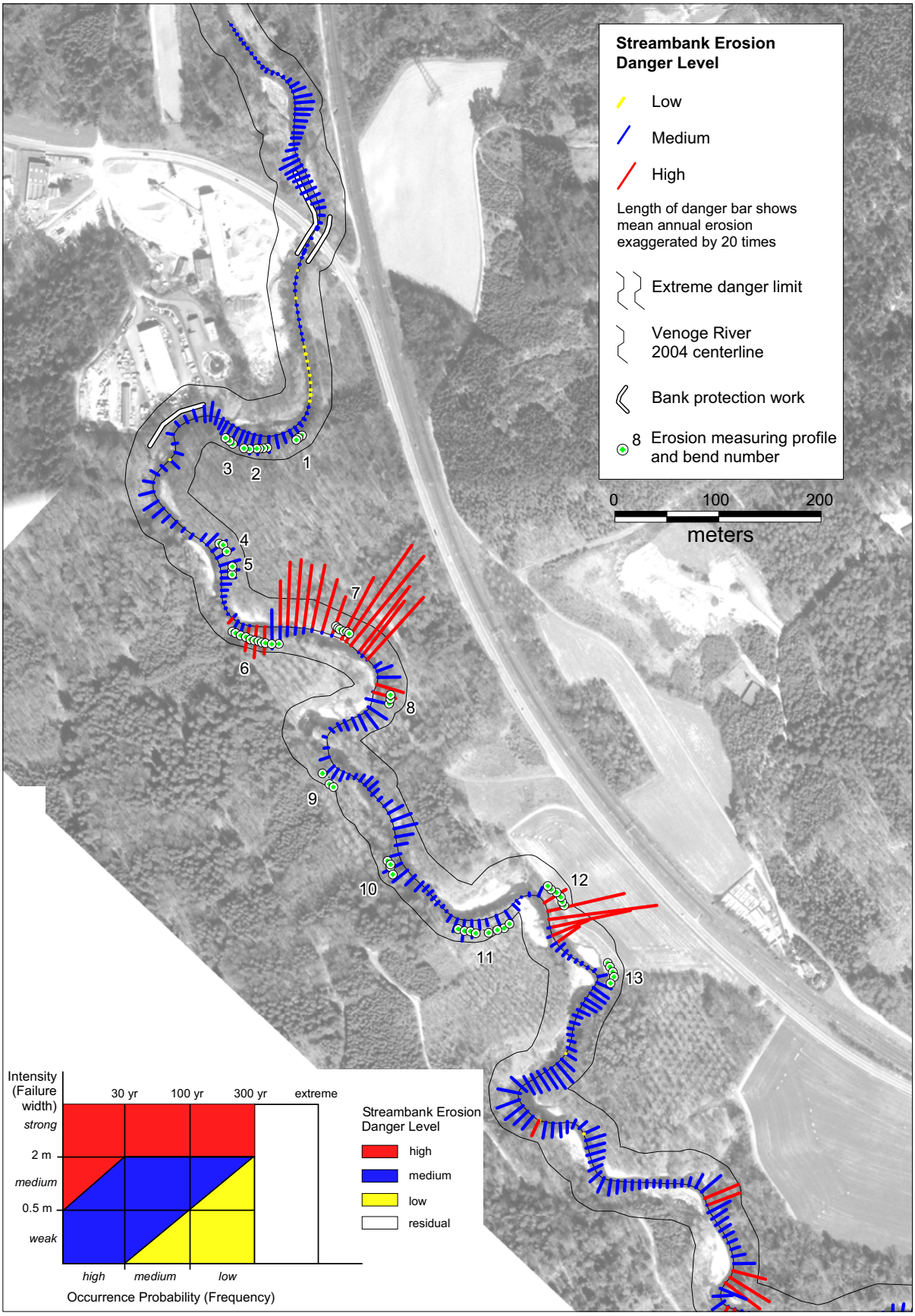

Figure 6.7. Streambank erosion danger map based on CCHE1D simulations and the FOWG danger matrix (bottom left inset). Bank protection failure probability is not taken into account.

6.4.2 Streambank erosion hazard results

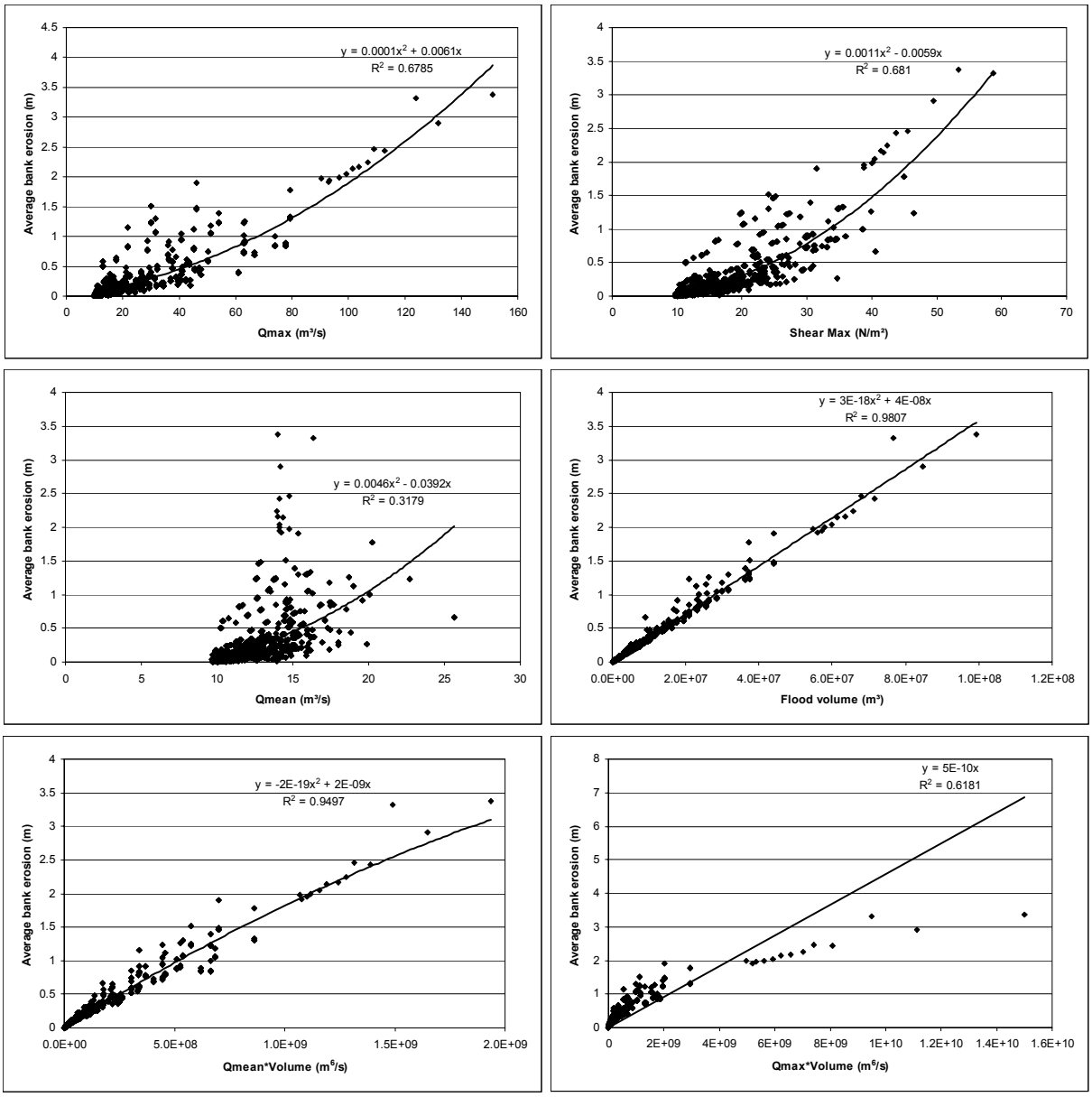

Figure 6.8. Results of the streambank erosion simulations for the right bank at kilometer 2.693

The correlation between measured streambank erosion and flood variables was shown in figure 4.12. With the streambank erosion simulated for a period of 300 years, it is possible to examine the model behavior to determine if it mimics the behavior shown in the graphs of figure 4.12. Maximum event discharge (Qmax), event flood volume (event start and end at 9 m³/s), mean event discharge (Qmean), maximum shear stress, Qmean*volume, and Qmax*volume are compared against the average bank erosion. Graphs for the right bank of node 1123 (km 2.693) serve as an example in figure 6.8. It can be seen in these graphs that the flood volume is the best indicator of the bank erosion that will occur while the indicator Qmax*volume is not linear as seen in figure 4.12. The rare flood values of Qmax*volume are much greater though in figure 6.8 so it is difficult to conclude if the difference in behavior is due to the very few observations in figure 4.12 or due to the model behavior. Figure 6.3 would seem to indicate

though that the model does not erode enough at high shear stresses so that the erosion shown in figure 6.8 might be underestimated for the high discharge/volume events. The CCHE1D model should be tested with the Simon and Thomas (2002) erodibility coefficient and erosion rate formulas to see what difference it would make on the erosion values for high discharge/volume events.

6.5 Streambank erosion simulation tests

It can be noticed in the danger map (figure 6.7) that there are a lot of straight reaches with medium danger levels. This result is most likely due to shear stresses that have not been diminished (or critical shear stresses that are not high enough) due to the significant vegetation that lines these straight sections. Thompson et al. (2004) have used shear stress partitioning theory to estimate the shear stress exerted on the vegetation and non-vegetation surfaces. They have shown that with significant vegetation, the particle shear stress is significantly reduced (down to 13% in their experiments). With this reasoning in mind, it would seem appropriate to reduce the bottom end of the shear stress correction function (figure 6.2) to 0.5 rather than 1.0. This should significantly reduce the simulated erosion in straight river reaches.

To test this hypothesis, a test case is run. The test case consists of using a trapezoidal channel with the average dimensions and roughness for the study reach. This same cross section is used for every node. The average slope of the study reach is used and does not vary throughout the reach. The bank and bed properties are also homogeneous throughout the test case study reach. With this test, variability in erosion due to hydraulic, soil, and vegetation conditions is removed. The test case is run for the calibration period of January 2004 through March 2005.

The result of the test case is shown visually for the upstream detailed study reach (figure 6.9). It can be seen that with the shear stress correction of 1 in straight sections that erosion often occurs on both sides of the stream compared to none or one-sided erosion when the correction is 0.5. The Venoge channel width is stable which would suggest the use of the correction factor for straight sections of 0.5 compared to 1 for vegetated banks.

A second test is performed to verify the necessity of smoothing the channel centerline (c.f. chapter 2.4.2). This test case uses the same hypothetical test reach as in the first case. Four cases are tested: a smoothed channel with no upstream weighting ($\alpha = 0.99$), a smoothed channel with upstream weighting as for the Venoge ($\alpha = 0.05$), an unsmoothed channel with no upstream weighting ($\alpha = 0.99$), and an unsmoothed channel with typical Venoge upstream weighting ($\alpha = 0.05$). It can be seen in figure 6.10 that for an accurately digitized centerline, smoothing is unnecessary when the upstream weighting is significant, but when no upstream weighting is used, the smoothing procedure is necessary.

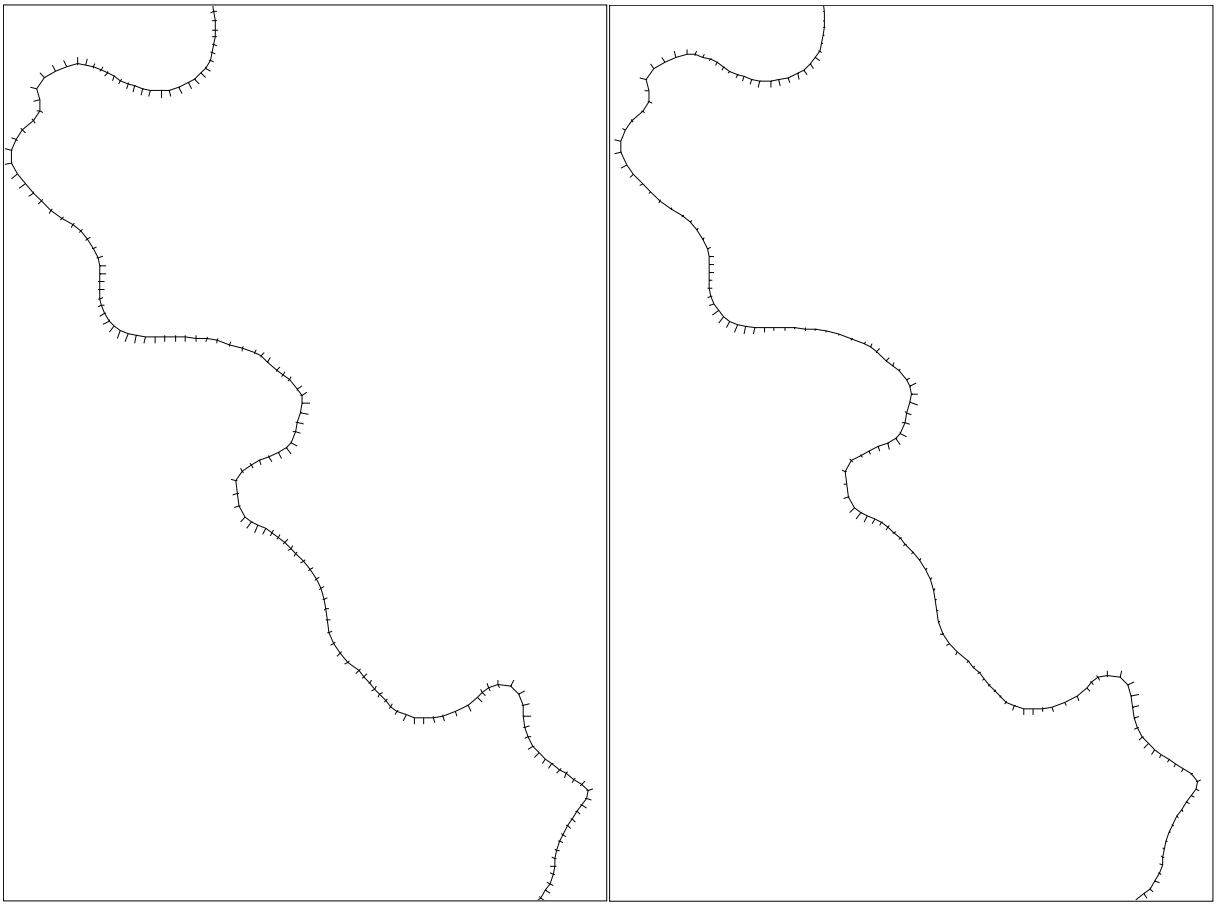

Figure 6.9. Comparison of erosion results when the shear stress correction function does not reduce the average shear stress in straight sections (left) or reduces it to half (right). The simulated eroded distances are shown by the lines perpendicular to the channel centerline.

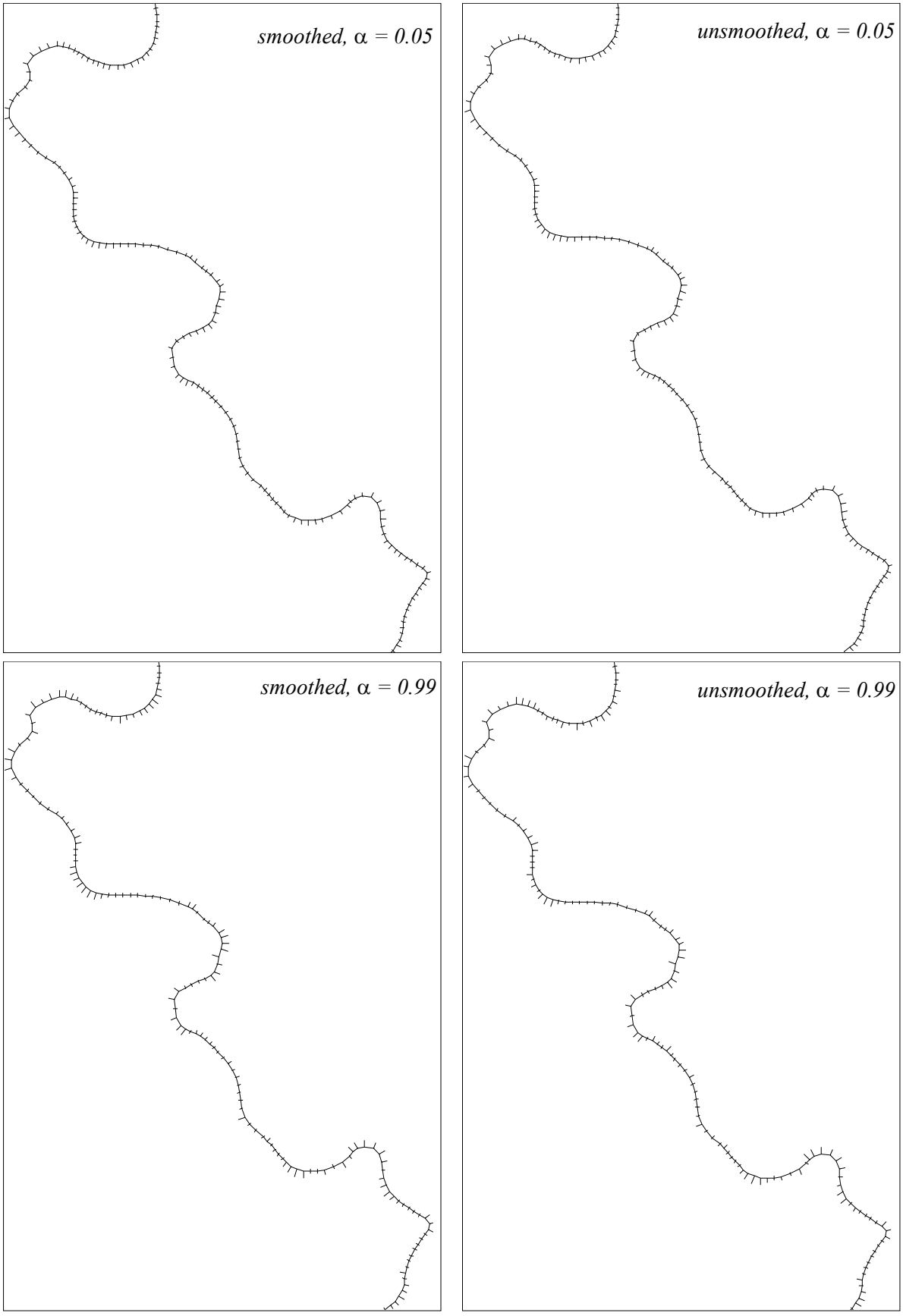

Figure 6.10. Test case erosion to determine the importance of centerline smoothing. The simulated eroded distances are shown by the lines perpendicular to the channel centerline.

Chapter 7

Conclusions and Future Research Recommendations

7.1 Conclusions

The streambank erosion hazard can be viewed from two aspects: land-use management and flood event management, which can be restated in the questions: "Where will the river be in 30 or 60 years?" and "How much will the stream erode its bank during a 100 year flood?" This research investigated the second question. Knowing the event streambank erosion behavior can also be helpful for land-use management by providing a streambank intervention distance that dictates when streambanks must be protected to avoid damage to vulnerable objects.

This research proposes a methodology for streambank erosion hazard mapping. It must begin with geomorphological mapping. This step is paramount for understanding the sediment sources of the river reach in question. In this step, the fluvial geomorphologist reads the field signs that indicate the current erosional and depositional behavior of the river.

Geomorphological mapping can be followed by streambank erosion hazard modeling and mapping. The model CCHE1D was adapted in this research to be able to calculate the width of a streambank failure and its probability, as needed for the calculation of the streambank erosion danger according to the directives of the Swiss Federal Office for Water and Geology. A bank toe shear stress correction function was added to the CCHE1D model to correct the 1-D toe shear stresses based on channel planform curvature, as well as an upstream weighting function to permit the phase lag of maximum bend erosion compared to maximum bend curvature. These shear stress correction functions properly placed the maximum erosion at the outside of meander bends, but permitted too much erosion in straight river reaches.

Tension cracking was added to the bank failure algorithm of the CCHE1D model. Tension cracking significantly affects the failure width of slab failures so it must be taken into account for this type of failure mode. It needs to be further researched so that algorithms can be improved to better predict tension crack depth and placement.

For the special case of determining bank failure probability, the CCHE1D model was modified so that bank geometry does not change after a bank failure. Bank failure sediments are placed in the virtual basal sediment reservoir of CCHE1D and a new bank failure can not occur until the basal sediments have been eroded away. This strategy allows bank geometry and flow conditions to stay the same throughout simulations so that a probability of a given bank failure width can be calculated.

The Lower Venoge River fieldwork showed the difficulties associated with the input data necessary for streambank erosion hazard modeling. Monitoring erosion allows for an understanding of the erosion and failure processes to be gained. This step is absolutely necessary so that the modeler can select a streambank erosion hazard model that includes the observed processes. For the monitoring to be more practical, it can be restricted to a few banks that are representative of the different bank types found on the river.

Estimation of the mean bank critical shear stress is extremely important in the CCHE1D modeling. Attempts have been made in this research and by other researchers to correlate critical shear stress with other measured soil properties, but no equations have proven to be globally satisfactory. Critical shear stress must be measured by an apparatus such as the submerged jet device (Hanson and Cook, 2004) or calibrated as done in this research. A multiple linear regression equation involving the percentage of fine sand - large silt and the fraction of the non-vegetated bank surface explained 75% of the variation for the monitored bends. Such a regression equation can be used for the reach for which it was developed.

Calibration of critical shear stress was done by comparing simulated cumulative bend erosion (9 events) to that which was measured. If the channel topography is known precisely at two different times, with two or more sets of orthophotos or high resolution (1-2 m) DTM, then these remote sensing data can replace erosion measurements.

The topographic needs for streambank erosion are enormous. Streambank erosion is usually very localized so that the computational network must be refined. This requires an enormous amount of cross sections which are impractical to survey. Thus, remotely sensed topographic data must be used or cross sections must be interpolated respecting channel curvature. Standard LIDAR data, such as the national Swisstopo data used in this research, is insufficient for describing the topography of vegetated channels and is not water penetrating. Thus, a cross section interpolation tool was developed to interpolate cross sections with respect to curvature. This tool was used to interpolate 78 measured cross sections to provide cross sections for the 1149 computational nodes. Although this tool needs to be used in various channel contexts before giving firm suggestions on its use, it would appear in a homogeneous zone (similar bank and bed conditions, and river slope) that one cross section for every fourth bend pool would be approximately sufficient. The bank toe definition point is very important in the interpolation program and its influence on the interpolation and on the subsequent calculations should be further investigated.

A qualification is warranted, though, concerning the topographic needs. For slowly migrating channels, the initial topographic description will be important. Without a correct topographic description, the bank might fail too soon or remain stable too long during the simulation. For fast migrating channels, a precise description is unnecessary if the simulation time is long enough. Such banks will have the opportunity to fail many times throughout the simulation.

Depending on the type of geotechnical failures observed, more or less attention should be given to collecting data on the cohesion and friction angle of the banks. For the Venoge River, soil fall and cantilever failures are the dominant process so that specific calibration of the cohesion and friction angle parameters was not undertaken. In a case where planar and curved failures are wider, cohesion and friction angle should be measured by laboratory analysis or by an in situ device such as the Iowa Borehole Shear Tester.

Bed and bank particle size data are required by the CCHE1D model. These data can be rough if the streambank erosion simulations are conducted with a fixed bed.

Flood volume was shown to be a very important indicator of reach erosion. This shows the necessity of streambank erosion modeling to be unsteady. High flow hydrographs are necessary and usually need to be produced by continuous hydrologic modeling. The spatial interpolation of data and the semi-distributed approach used in the hydrologic modeling in this thesis serve as an example how to generate spatially coherent input data for the streambank erosion modeling. Temperature based potential evapotranspiration was shown to be sufficient for the hydrological modeling compared to more data intensive formulas.

Three 300 year simulations were conducted with the CCHE1D model. Bank failures were output from the model for the 1149 cross sections covering the 8 kilometers of study reach. The probability of a given bank failure width was calculated based on its empirical frequency. For a given bank and for a given probability, the median bank failure width of the three 300 year scenarios was used as the final bank failure width. Danger levels were calculated and mapped for each bank based on the directives of the Swiss Federal Office for Water and Geology.

Bank failure width for an extreme event was also calculated. The maximum simulated for the study reach was 10.5 meters. This failure width was multiplied by a safety factor for the extreme failure width of 16 meters to be mapped on the danger map. It is assumed that such a multiplication should be made due to extreme shear stress conditions that might occur during an extreme flood. Research should be done to better determine this multiplication factor or the method by which a simulation should be conducted to best reproduce extreme shear stress conditions.

Erosion hazards in straight reaches of the study reach are too high. This would suggest that the toe shear stress correction should be less than one. This is a reasonable assumption because of vegetation which most likely reduces particle shear stress in these zones.

The streambank erosion hazard mapping methodology succeeded in producing the streambank erosion danger map. The methodology can be used for other alluvial, single threaded, subcritical flow rivers. Curved failure surfaces are not implemented in CCHE1D, so reaches with such geotechnical problems should not be modeled with it. The planar failure algorithm with tension cracking might not work

appropriately for steep, high (> 8 m) banks. Also in such a case, unsaturated conditions might begin to have important stability effects. Unsaturated conditions are not taken into account by the CCHE1D bank failure algorithm.

When large failure width (>10 m) geotechnical problems are present, the model could be used in combination with a geotechnical model. CCHE1D can be used to estimate the toe erosion, while the geotechnical failure should be explored by an appropriate geotechnical model.

It must be remembered that CCHE1D is a 1D model. Vegetation can only be taken into account by adapting the critical shear stress and bank failure parameters. The effect of bank soil and vegetation falls into the river, which in turn affect the bank shear stresses, can not be taken into account. This was quite evident in the very poor correlation between measured and observed event bank profile erosion. Average bend erosion was calibrated so that the average bend migration is expected to be realistic. Observed and measured reach erosion were relatively well correlated. The tendency to overestimate lower discharge/ volume events and underestimate higher discharge/volume events should be further investigated. Changing the erodibility coefficient equation might correct this problem.

It can be concluded from this research that streambank erosion hazard mapping is possible with the results of geofluvial 1-D models. The amount of input data for this type of modeling is prohibitive though and will restrict its use to cases in which the streambank erosion problem has significant impacts. Research must be conducted to reduce data acquisition costs for this type of modeling to be used more regularly.

7.2 Future research recommendations

The following recommendations can be given for improving streambank erosion modeling in the CCHE1D model:

- Confining and pore pressure effects should be included in the bank failure algorithm to better reproduce natural variability in bank failure width. Bank failures should not be restricted to failing through the bank toe.
- Rather than using a virtual basal sediment tank for failed material, it would be better to slough the material onto the toe area of the bank. This would entail improving cross section deposition.
- Channel migration modeling could be explored with CCHE1D, but the cross section deposition would have to be improved. It is debatable whether a geofluvial 1-D model should be used for channel migration modeling. It is most likely preferable to concentrate on including bank erosion and bank failure algorithms in a 2-D sediment transport model.

The following recommendations can be given for completing the streambank erosion hazard modeling research on the Lower Venoge River:

- Critical shear stress must be measured for the bends monitored for erosion. The in situ jet apparatus described by Hanson and Cook (2004) could be used for this. Knowing these values will allow the improvement and validation of the shear stress correction function used in this thesis. In this respect, 3-D hydraulic modeling could also be conducted to better understand the shear stress being applied to the toe and its phase lag with maximum bend curvature, but it would be difficult to correctly

quantify the actual particle shear stress due to vegetation effects.

- Stochastically generated meteorological scenarios should be generated for the Venoge catchment to produce more discharge scenarios. The use of many discharge scenarios will give a higher confidence in the calculated failure width probabilities.
- For more precision in failure width, more needs to be known about the soil fall and slab failures of the Venoge River. This entails better knowledge of the bank topography just before and after the failure. New monitoring tools must be researched and developed to do this.
- Event based modeling should be compared against continuous modeling once enough discharge scenarios have been modeled. In the fluvial erosion dominated case of the Lower Venoge River, event modeling will probably be sufficient. As in any event modeling, the proper initial conditions must be chosen though, and this is especially true for the bank topography of slowly eroding banks. Thus, research would need to be done to determine how to properly choose the initial conditions of the banks.

Other diverse recommendations are:

- A sensitivity analysis should be done to quantify the influence of the CCHE1D shear stress correction and bank parameters.
- Data acquisition methods must continually be pushed to be less costly and time consuming. Important advances have been made with LIDAR topographic data, although this data is usually insufficient for accurately describing the channel topography unless special measures are taken (water penetrating LIDAR and sufficient resolution for vegetated banks). Water penetrating LIDAR should be used in a stream such as the Venoge River to quantify its potential in that setting. Otherwise, other rapid land-based laser techniques should be tested in combination with standard LIDAR data (such as that used in this thesis) for accurately describing the channel topography. Research also must be continued on maximizing the potential of the data on hand. One aspect of this was started in this research by improving the channel description by proper interpolation methods. The streamwise interpolation of channel points presented in this research should be improved with more sophisticated interpolation algorithms. More rapid critical shear stress, cohesion, and friction angle testing also need to be developed.
- The channel migration modeling of the 1996 HYDRAM Venoge study should be further researched. This model is practical because it does not require hydraulic modeling. A relation of event erosion compared to channel migration should be possible to find by taking into account bank erosion theory and the hydrologic events that produced the channel migration.

References

Abernethy, B. and I. D. Rutherfurd (1998). "Where along a river's length will vegetation most effectively stabilise stream banks?" Geomorphology **23**(1): 55-75.

Abramson, L. W., T. S. Lee, et al. (2002). Slope stability and stabilization methods. New York, Wiley.

Allen, R. G. (1998). Crop evapotranspiration guidelines for computing crop water requirements. Rome, Fao.

Andreassian, V., C. Perrin, et al. (2001). "Impact of imperfect rainfall knowledge on the efficiency and the parameters of watershed models." Journal of Hydrology **250**(1-4): 206-223.

Arulanandan, K., E. Gillogley, et al. (1980). Development of a quantitative method to predict critical shear stress and rate of erosion of natural undisturbed cohesive soils. Vicksburg, Mississippi, U.S. Army Engineers Waterways Experiment Station.

ASCE (1996). Hydrology handbook. New York, NY, American Society of Civil Engineers.

ASCE Task Committee (1998a). "River width adjustment. I: Processes and mechanisms." Journal of Hydraulic Engineering-Asce **124**(9): 881-902.

ASCE Task Committee (1998b). "River width adjustment. II: modeling." Journal of Hydraulic Engineering-Asce **124**(9): 903-917.

Beven, K. J. (2001). Rainfall-runoff modelling the primer. New York, John Wiley.

Blackmar, W. (1995). Documentation of hydrologic, geomorphic, and sediment transport movements on the Goodwin Creek Experimental Watershed, Northern Mississippi, for the period 1982-1993. Research Report #3. Oxford, MS, USDA-ARS, National Sedimentation Laboratory.

Blaisdell, F. W., L. A. Clayton, et al. (1981). "Ultimate dimension of local scour." Journal of the Hydraulics Division, ASCE **107**(HY3): 327-337.

Blanckaert, K. and W. H. Graf (2001). "Mean Flow and Turbulence in Open-Channel Bend." Journal of Hydraulic Engineering **127**(10).

Blick (2005). Engelberg ist keine Insel mehr. Zurich, retrieved from http://www.blick.ch/news/schweiz/hochwasser/artikel25138, October 22, 2005.

Borah, D. K. and P. K. Bordolai (1989). Stream bank erosion and bed evolution model. Sediment Transport Modeling. Proceedings of the international symposium. S. Wang. New York, ASCE.

Bravard, J.-P. and F. Petit (1997). Les cours d'eau. Dynamique du système fluvial. Paris, Colin.

Briaud, J. L., F. C. K. Ting, et al. (2001). "Erosion function apparatus for scour rate predictions." Journal of Geotechnical and Geoenvironmental Engineering **127**(2): 105-113.

Bridge, J. S. (1976). "Bed topography and grain size in open channel bends." Sedimentology, Int. Associatin of Sedimentologists **23**: 407-414.

Bridge, J. S. (2003). Rivers and floodplains forms, processes, and sedimentary record. Oxford, Blackwell.

Bujard, P. (2005). Failure of the Abbaye weir. Morges, personal communication.

Burrough, P. and R. McDonnell (1998). Principles of geographical information systems. Oxford [etc.], Oxford University Press.

Charlton, M. E., A. R. G. Large, et al. (2003). "Application of airborne LiDAR in river environments: The River Coquet, Northumberland, UK." Earth Surface Processes and Landforms **28**(3): 299-306.

Chorley, R. J., S. A. Schumm, et al. (1984). Geomorphology. London New York, Methuen.

Chow, V. T., D. R. Maidment, et al. (1988). Applied hydrology. New York [etc.], McGraw-Hill.

Church, M. A., D. G. McLean, et al. (1987). River Bed Gravels: Sampling and Analysis. Sediment Transport in Gravel-bed Rivers. C. R. Thorne, J. C. Bathurst and R. D. Hey. Chichester etc., John Wiley and Sons.

Collet, L. W. (1955). Notice Explicative. Feuille 5. Carte géologique générale de la Suisse. 1:200'000. Berne.

Consuegra, D., Beck, J., and Musy, A. (2000). Gestion quantitative des eaux de la Seymaz et de ses affluents. Etude Hydrologique et Hydraulique. Diagnostic de l'état actuel des dangers liés aux inondations et à l'érosion, EPFL, HYDRAM.

Consuegra, D., J.-M. Lance, et al. (1999). "Modélisation conceptuelle de la dynamique érosive d'un cours d'eau." Ingénieurs et Architectes Suisses(9).

Consuegra, D. and E. Vez (1996). AMIE - Analysis et Modélisation Intégrées du cheminement des Eaux en zones habitées, modélisation hydrologique, Application au bassin versant de la Haute Broye. Lausanne, EPFL-HYDRAM.

Couper, P. (2003). "Effects of silt-clay content on the susceptibility of river banks to suaerial erosion." Geomorphology **1338**: 1-14.

Crausaz, P.-A. (2000). Du rôle intégrateur des systèmes d'information à référence spatiale dans la gestion institutionnelle des eaux: analyse, méthodes, limites et perspectives. HYDRAM. Lausanne, EPFL.

Creutin, J. D. and C. Obled (1982). "Objective Analyses and Mapping Techniques for Rainfall Fields - an Objective Comparison." Water Resources Research **18**(2): 413-431.

Cunge, J. A., F. M. Holly, et al. (1980). Practical aspects of computational river hydraulics. Boston - Mass. a.o., Pitman.

Custer, W. (1935). Notice Explicative. Feuille 1222. Cossonay. Atlas géologique de la Suisse. 1:25'000. Berne.

Daniels, M. D. and B. L. Rhoads (2004). Riparian Vegetation and Fluvial Geomorphology. Riparian vegetation and fluvial geomorphology. S. J. Bennett and A. Simon. Washington, DC, American Geophysical Union**:** 282 S.

Darby, S. E. (2005). "Refined hydraulic geometry data for British gravel-bed rivers." Journal of Hydraulic Engineering-Asce **131**(1): 60-64.

Darby, S. E., A. M. Alabyan, et al. (2002). "Numerical simulation of bank erosion and channel migration in meandering rivers." Water Resources Research **38**(9).

Darby, S. E. and I. Delbono (2002). "A model of equilibrium bed topography for meander bends with erodible banks." Earth Surface Processes and Landforms **27**(10): 1057-1085.

Darby, S. E. and C. R. Thorne (1994). "Prediction of Tension Crack Location and Riverbank Erosion Hazards Along Destabilized Channels." Earth Surface Processes and Landforms **19**(3): 233-245.

Darby, S. E. and C. R. Thorne (1996). "Numerical simulation of widening and bed deformation of straight sand-bed rivers .1. Model development." Journal of Hydraulic Engineering-Asce **122**(4): 184-193.

Darby, S. E., C. R. Thorne, et al. (1996). "Numerical simulation of widening and bed deformation of straight sand-bed rivers .2. Model evaluation." Journal of Hydraulic Engineering-Asce **122**(4): 194-202.

De Souza, P. B., D. Consuegra, et al. (1994). CODEAU: A database package for the assessment and analysis of hydrometeorological data. Hydroinformatics '94 proceedings of the First International Conference on Hydroinformatics, Delft, Netherlands, 19-23 September 1994, Rotterdam [etc.], Balkema.

Diplas, P. and A. J. Sutherland (1988). "Sampling Techniques for Gravel Sized Sediments." Journal of Hydraulic Engineering **114**(5): 484-501.

Dirks, K. N., J. E. Hay, et al. (1998). "High-resolution studies of rainfall on Norfolk Island Part II: Interpolation of rainfall data." Journal of Hydrology **208**(3-4): 187-193.

Duncan, M. R., B. Austin, et al. (1993). "The Effect of Gauge Sampling Density on the Accuracy of Streamflow Prediction for Rural Catchments." Journal of Hydrology **142**(1-4): 445-476.

Edijatno and C. Michel (1989). "Un modèle pluie-débit journalier à trois paramètres." La Houille Blanche **2**: 113-121.

Engelund, F. (1974). "Flow and bed topography in channel bends." Journal of Hydraulics Division-Asce **100**(11): 1631-1648.

Fehr, R. (1987). "Einfache Bestimmung der Korngrössen-verteilung von Geschiebematerial mit Hilfe der Linienzahlanalyse." Schweizer Ingenieur und Architekt **38**.

FEMA (1999). Riverine Erosion Hazard Areas. Mapping Feasibility Study, Federal Emergency Management Agency**:** 154.

Franca, M. (2005). A field study of turbulent flows in shallow gravel-bed rivers. Civil Engineering PhD dissertation. Lausanne, EPFL.

Fripp, J. B. and P. Diplas (1993). "Surface Sampling in Gravel Streams." Journal of Hydraulic Engineering-Asce **119**(4): 473-490.

Furbish, D. J. (1991). "Spatial autoregressive structure in meander evolution." Geological Society of America Bulletin **103**: 1576-1589.

Goovaerts, P. (2000). "Geostatistical approaches for incorporating elevation into the spatial interpolation of rainfall." Journal of Hydrology **228**(1-2): 113-129.

Graf, W. H. and M. S. Altinakar (2002). Fluvial hydraulics flow and transport processes in channels of simple geometry. Chichester, Wiley.

Graf, W. L. (1984). "A Probabilistic Approach to the Spatial Assessment of river Channel Instability." Water Resources Research **20**(7): 953-962.

Graf, W. L. (2001). "Damage control: Restoring the physical integrity of America's rivers." Ann. Assoc. Am. Geog. **91**: 1-27.

Grattier, M. (1980). "Les Sols du Plateau Vaudois." Mémoires de la Société vaudoise des Sciences Naturelles **16**(3): 188.

Grissinger, E. H. (1982). Bank erosion of cohesive materials. Gravel-bed rivers. Fluvial processes, engineering and management (First International workshop on gravel-bed rivers; Gregynog, 23-27 June 1980). R. D. Hey, J. C. Bathurst and C. R. Thorne. Chichester a.o., Wiley**:** XV, 875.

Hamblin, W. K. and E. H. Christiansen (1998). Earth's dynamic systems. Upper Saddle River, N.J., Prentice Hall.

Hamdi, Y., B. Hingray, et al. (2005). "Un modèle de prévision hydro-météorologique pour les crue du Rhône supérieur en Suisse." Wasser Energie Luft(11/12 2005).

Hanson, G. J. (1990). "Surface Erodibility of Earthen Channels at High Stresses .1. Open Channel Testing." Transactions of the Asae **33**(1): 127-131.

Hanson, G. J. and K. R. Cook (2004). "Apparatus, test procedures, and analytical methods to measure soil erodibility in situ." Applied Engineering in Agriculture **20**(4): 455-462.

Hanson, G. J. and A. Simon (2001). "Erodibility of cohesive streambeds in the loess area of the midwestern USA." Hydrological Processes **15**(1): 23-38.

Hanson, G. J. and A. Simon (2002). "Discussion of "Erosion function apparatus for scour rate predictions" by J. L. Briaud, F. C. K. Ting, H. C. Chen, Y. Cao, S. W. Han, and K. W. Kwak." Journal of Geotechnical and Geoenvironmental Engineering **128**(7): 627-628.

Hersberger, D. S. (2003). Wall roughness effects on flow and scouring in curved channels with gravel bed. Lausanne, Laboratoire de Constructions Hydrauliques Ecole Polytechnique Fédérale de Lausanne.

Hession, W. C., J. E. Pizzuto, et al. (2003). "Influence of bank vegetation on channel morphology in rural and urban watersheds." Geology **31**(2): 147-150.

Hey, R. D. (1997). Stable River Morphology. Applied fluvial geomorphology for river engineering and management. C. R. Thorne, R. D. Hey and M. D. Newson. Chichester [etc.], Wiley**:** VI, 376 S.

Hey, R. D., G. L. Heritage, et al. (1991). Streambank Protection in England and Wales. R&D Note 22. London, National Rivers Authority**:** 75.

Hey, R. D. and C. R. Thorne (1983). "Accuracy of Surface Samples from Gravel Bed Materials." Journal of Hydraulic Engineering-Asce **109**(6): 842-851.

Hey, R. D. and C. R. Thorne (1986). "Stable Channels with Mobile Gravel Beds." Journal of Hydraulic Engineering-Asce **112**(8): 671-689.

Hickin, E. J. and G. C. Nanson (1975). "The Character of Channel Migration on the Beatton River, Northeast British Columbia, Canada." Geological Society of America Bulletin **86**: 487-494.

Howard, A. D., and Knutson, T.R. (1984). "Sufficient Conditions for River Meandering: A Simulation Approach." Water Resources Research **20**(11): 1659-1667.

Huff, F. A. (1970). "Sampling Errors in Measurement of Mean Precipitation." Journal of Applied Meteorology **9**: 35-44.

Hutchinson, J. N. (1995). Landslide hazard assessment. Landslides proceedings of the sixth international symposium 10-14 February 1992, Christchurch. D. H. Bell. Rotterdam [etc.], Balkema**:** 3 vol.

HydroScientific (1999). The Photo-Electronic Erosion Pin (PEEP) System: User guide for models PEEP 110 and PEEP 200. Stratford-upon-Avon.

Irish, J. L. and W. J. Lillycrop (1999). "Scanning laser mapping of the coastal zone: the SHOALS system." Isprs Journal of Photogrammetry and Remote Sensing **54**(2-3): 123-129.

Jacobs Babtie (2005). SAFER - Flood risk assessment and survey on the River Enrick, Geomorphological appraisal. Glasgow, Jacobs Babtie.

Johannesson, H., and Parker, G. (1989). Linear theory of river meanders. River meandering. S. Ikeda, and Parker, G. Washington D.C., American Geophysical Union. **Water Resources Monograph 12:** 103-126.

Jowett, I. G. (1998). "Hydraulic geometry of New Zealand rivers and its use as a preliminary method of habitat assessment." Regulated Rivers-Research & Management **14**(5): 451-466.

Kellerhals, R. and D. I. Bray (1971). "Sampling procedures for coarse fluvial sediments." Journal of the Hydraulics Division **97**(HY8): 1165-1180.

Kienholz, H. and B. Krummenacher (1995). Légénde modulable pour la cartographie des phénomènes. Bern, Office Fédéral de l'environnement, des forêts, et du paysage (OFEFP) and Office Fédérale des eaux et de la géologie (OFEG) Suisse.

Knighton, D. (1998). Fluvial forms and processes a new perspective. London [etc.], Arnold [etc.].

Kondolf, G. M. (1997). "Application of the pebble count: Notes on purpose, method, and variants." Journal of the American Water Resources Association **33**(1): 79-87.

Lamouroux, N. and H. Capra (2002). "Simple predictions of instream habitat model outputs for target fish populations." Freshwater Biology **47**(8): 1543-1556.

Lancaster, S. T., and Bras, Rafael L. (2002). "A simple model of river meandering and its comparison to natural channels." Hydrological Processes **16**: 1-26.

Lance, J.-M. and D. Consuegra (1997). Bassin Versant de la Venoge. Etude des risques liés aux inondations. Etude hydrologique, IATE/HYDRAM, EPF Lausanne.

Lance, J.-M. and D. Consuegra (1998). Bassin versant de la Venoge. Etude des dangers liés à l'érosion, IATE/HYDRAM, EPF Lausanne.

Lance, J.-M., R. Thielen, et al. (1997). Bassin Versant de la Venoge. Etude des risques liés aux inondations. Diagnostic de l'état actuel, IATE/HYDRAM, EPF Lausanne.

Lane, E. W. (1953). "Design of stable channels." Transactions, ASCE **120**: 1234-1260.

Lane, S. N., J. H. Chandler, et al. (1994). "Developments in Monitoring and Modeling Small-Scale River Bed Topography." Earth Surface Processes and Landforms **19**(4): 349-368.

Langendoen, E. J. (2000). CONCEPTS-Conservational Channel Evolution and Pollutant Transport System. Research Report No. 16. Oxford, USDA-ARS National Sedimentation Laboratory.

Lawler, D. M. (1993). "The Measurement of River Bank Erosion and Lateral Channel Change - a Review." Earth Surface Processes and Landforms **18**(9): 777-821.

Lawler, D. M., C. R. Thorne, et al. (1997). Bank Erosion and Instability. Applied fluvial geomorphology for river engineering and management. C. R. Thorne, R. D. Hey and M. D. Newson. Chichester [etc.], Wiley**:** VI, 376 S.

Leopold, L. B. and T. Maddock (1953). The hydraulic geometry of stream channels and some physiographic implications. Washington, United States Government Printing Office.

Leopold, L. B. and M. G. Wolman (1957). River channel patterns. Washington, United States Government Printing Office.

Loat, R. and A. Petrascheck (1997). Danger naturels : recommandation : Prise en compte des dangers dus aux crues dans le cadre des activités de l'aménagement du territoire. Bienne, OFEG, OFAT, OFEFP.

Mandal, J. N. and D. G. Divshikar (1995). Soil testing in civil engineering. Rotterdam [etc.], Balkema.

Maxey, G. B. (1964). Geology. Handbook of Applied Hydrology. V. T. Chow. New York, McGraw-Hill.

Metzger, R. (2003). Modélisation des inondations par approches déterministe et stochastique avec prise en compte des incertitudes topographiques pour la gestion des risques liés aux crues. HYDRAM. Lausanne, EPFL.

Meylan, P. and A. Musy (1999). Hydrologie Fréquentielle. Bucarest, Editions *H*G*A.

Mosselman, E. (1992). Mathematical Modeling of Morphological Processes in Rivers with Erodible Cohesive Banks. PhD thesis. Delft, The Netherlands, Delft University of Technology.

Mosselman, E. (1998). "Morphological modelling of rivers with erodible banks." Hydrological Processes **12**(8): 1357-1370.

Musy, A. and C. Higy (1998). Hydrologie Appliqué. Lausanne, Course book.

Musy, A. and C. Higy (2004). Hydrologie. Lausanne, Presses Polytechniques et Universitaires Romandes.

Nanson, G. C. and J. C. Croke (1992). "A Genetic Classification of Floodplains." Geomorphology **4**(6): 459-486.

Northwood Technologies (2001). Vertical Mapper 3.0 User guide. Ontario.

Osman, A. M. (1985). Channel width response to changes in flow hydraulics and sediment load. PhD thesis. Fort Collins, Colorada State University.

Osman, A. M. and C. R. Thorne (1988). "Riverbank Stability Analysis .1. Theory." Journal of Hydraulic Engineering-Asce **114**(2): 134-150.

Oudin, L., F. Hervieu, et al. (2005b). "Which potential evapotranspiration input for a lumped rainfall-runoff model? Part 2 - Towards a simple and efficient potential evapotranspiration model for rainfall-runoff modelling." Journal of Hydrology **303**: 290-306.

Oudin, L., C. Michel, et al. (2005a). "Which potential evapotranspiration input for a lumped rainfall-runoff model? Part 1 - Can rainfall-runoff models effectively handle detailed potential evapotranspiration inputs?" Journal of Hydrology **303**: 275-289.

Parker, G. and E. D. Andrews (1986). "On the time development of meander bends." Journal of Fluid Mechanics **162**: 139-156.

Petrie, J. (1998). The Accuracy of River Bed Sediment Samples. University of Virginia - Civil Engineering. Blacksburg, Virginia.

Petrie, J. and P. Diplas (2000). "Statistical approach to sediment sampling accuracy." Water Resources Research **36**(2): 597-605.

Piégay, H. and S. A. Schumm (2003). System Approaches in Fluvial Geomorphology. Tools in fluvial geomorphology. G. M. Kondolf and H. Piégay. Chichester, Wiley**:** 688 S.

Prétorian, R. (1994). Analyse hydro-météorologique et modélisation hydrologique synthétique du transfert de de l'acheminement entre sous-bassins versant de la Venoge". Lausanne, HYDRAM.

Primault, B. (1972). Etude mésoclimatique du Canton de Vaud. Lausanne, Office Cantonal Vaudois de l'Urbanisme.

Rakotondranaly, N. (2001). Développement et Validation d'une Méthodologie pour l'Identification et l'Evaluatiion des Dangers liés à l'Erosion des Berges des cours d'eau. Lausanne, EPFL/HYDRAM.

Rice, S. and M. A. Church (1996). "Sampling surficial fluvial gravels: the precision of size distribution percentile estimates." Journal of Sedimentary Research **66**(3): 654-665.

Rice, S. P. and J. K. Haschenburger (2004). "A hybrid method for size characterization of coarse subsurface fluvial sediments." Earth Surface Processes and Landforms **29**(3): 373-389.

Richards, K. (1982). Rivers form and process in alluvial channels. London New York, Methuen.

Richardson, W. R. (2002). "Simplified Model for Assessing Meander Bend Migration Rates." Journal of Hydraulic Engineering **128**(12): 1094-1097.

Rodi, W. (1993). Engineering turbulence modelling and experiments 2 proceedings of the Second International Symposium on Engineering Turbulence Modelling and Measurements, Florence, Italy, 31 May - 2 June, 1993. Amsterdam [etc.], Elsevier.

Rosgen, D. and H. L. Silvey (1996). Applied river morphology. Pagosa Springs, CO, Wildland Hydrology.

Schaefli, B., B. Hingray, et al. (2005). "A conceptual glacio-hydrological model for high mountainous catchments." Hydrology and Earth System Sciences **9**.

Schneider, T. (2001). Caractérisation multicritère des formations géologiques du canton de Vaud et de leur prédispositions face aux Dangers Naturels. "Géologie de Ingénieur et de l'Environnement" Postgraduate Diploma Presentation. Lausanne.

Schumm, S. A. (1981). "Evolution and response of the fluvial system, sedimentologic implications." Society of Economic Paleontologists and Mineralogists Special Publication **31**: 19-29.

Schumm, S. A. (2005). River variability and complexity. New York, Cambridge Univeristy Press.

Selby, M. J. (1993). Hillslope materials and processes. Oxford, Oxford University Press.

Shields, A. (1936). Anwendung der Aehnlichkeitsmechanik und der Turbulenzforschung auf die Geschiebebewegung. Berlin, Eigenverlag der Preussischen Versuchsanstalt für Wasserbau und Schiffbau.

Simon, A., A. Curini, et al. (2000). "Bank and near-bank processes in an incised channel." Geomorphology **35**(3-4): 193-217.

Simon, A. and P. W. Downs (1995). "An Interdisciplinary Approach to Evaluation of Potential Instability in Alluvial Channels." Geomorphology **12**(3): 215-232.

Simon, A. and C. R. Hupp (1986). Channel evolution in modified Tennessee channels. Proceedings of the 4th Federal Interagency Sedimentation Conference, Las Vegas, Nevada, US Government Printing Office, Washington D.C.

Simon, A. and R. E. Thomas (2002). "Processes and forms of an unstable alluvial system with resistant, cohesive streambeds." Earth Surface Processes and Landforms **27**(7): 699-718.

Simon, A., R. E. Thomas, et al. (2002). "Case study: Channel stability of the Missouri River, eastern Montana." Journal of Hydraulic Engineering-Asce **128**(10): 880-890.

Smart, G. M. (1984). "Sediment Transport Formula for Steep Channels." Journal of Hydraulic Engineering **110**(3).

Spreafico, M., Schweiz Landeshydrologie und -Geologie, et al. (1992). Hydrologischer Atlas der Schweiz. Bern, Edmz.

Stewardson, M. (2005). "Hydraulic geometry of stream reaches." Journal of Hydrology **306**(1-4): 97-111.

Swisstopo MNS/MNT-MO., retrieved from http://www.swisstopo.ch/fr/products/digital/height/dom_dtmAV, October 21, 2005.

Swisstopo MNT25, retrieved from http://www.swisstopo.ch/fr/products/digital/height/dhm25, October 21, 2005.

Swisstopo Status of Updates, retrieved from http://www.swisstopo.ch/pub/down/products/analog/maps/status_de-fr-en-it.pdf, October 22, 2005.

Taylor, D. W. (1948). Fundamentals of soil mechanics. New York, Wiley.

Terzaghi, K., R. B. Peck, et al. (1996). Soil mechanics in engineering practice. New York [etc.], Wiley.

Thoma, D. P., S. C. Gupta, et al. (2005). "Airborne laser scanning for riverbank erosion assessment." Remote Sensing of Environment **95**(4): 493-501.

Thompson, A. M., B. N. Wilson, et al. (2004). "Shear stress partitioning for idealized vegetated surfaces." Transactions of the Asae **47**(3): 701-709.

Thorne, C. R. (1981). Field measurements of rates of bank erosion and bank material strength. Erosion and Sediment Transport Measurement, Forence Symposium, International Association of Hydrological Sciences Publication.

Thorne, C. R. (1982). Processes and Mechanisms of River Bank Erosion. Gravel-bed rivers fluvial processes, engineering and management (record of the proceedings of the International workshop on engineering problems in the management of gravel-bed rivers = First International workshop on gravel-bed rivers; Gregynog, 23-27 June 1980). R. D. Hey. Chichester a.o., Wiley**:** XV, 875.

Thorne, C. R. (1997). Channel Types and Morphological Classification. Applied fluvial geomorphology for river engineering and management. C. R. Thorne, R. D. Hey and M. D. Newson. Chichester [etc.], Wiley**:** VI, 376 S.

Thorne, C. R. and N. K. Tovey (1981). "Stability of Composite River Banks." Earth Surface Processes and Landforms **6**(5): 469-484.

Tolhurst, T. J., K. S. Black, et al. (1999). "Measuring the in situ erosion shear stress of intertidal sediments with the Cohesive Strength Meter (CSM)." Estuarine, Coastal, and Shelf Science **49**: 281-294.

USACE (2002). HEC-RAS River Analysis System. User's Manual. Version 3.1. Davis, CA, USA, US Army Corp of Engineers.

Vereinigung Schweizerischer Strassenfachleute (1997a). Identifikation der Lockergesteine Labormethode mit Klassifikation nach USCS méthode de laboratoire avec classification selon l'USCS. Zürich, Vss.

Vereinigung Schweizerischer Strassenfachleute (1999b). Bodenkennziffern. Zürich, Vss.

Vieira, D. and W. Wu (2002). One-Dimensional Channel Network Model CCHE1D 3.0 - User's Manual. Oxford, National Center for Computational Hydroscience and Engineering.

Winterbottom, S. J. and D. J. Gilvear (2000). "A GIS-based approach to mapping probabilities of river bank erosion: Regulated River Tummel, Scotland." Regulated Rivers-Research & Management **16**(2): 127-140.

Wojcik, R. and T. A. Buishand (2003). "Simulation of 6-hourly rainfall and temperature by two resampling schemes." Journal of Hydrology **273**(1-4): 69-80.

Wolman, M. G. (1954). "A Method of Sampling Coarse River-Bed Material." Transactions, American Geophysical Union **35**(6): 951-956.

Wood, A. L., A. Simon, et al. (2001). "Bank-toe processes in incised channels: the role of apparent cohesion in the entrainment of failed bank materials." Hydrological Processes **15**(1): 39-61.

Wu, T. H., P. E. Beal, et al. (1988). "In-situ shear test of soil-root systems." Journal of Geotechnical Engineering **114**(12): 1376-1394.

Wu, W. and D. Vieira (2002). One-Dimensional Channel Network Model CCHE1D 3.0 - Technical Manual. Oxford, National Center for Computational Hydroscience and Engineering.

Wu, W. and S. Y. Wang (2004). "Depth-averaged 2-D calculation of flow and sediment transport in curved channels." International Journal of Sediment Research **19**(4): 241-257.

Appendix

Appendix 1 Textural triangles of the Vaud plateau

Appendix 1.1 Molassic and Morainic particle distributions

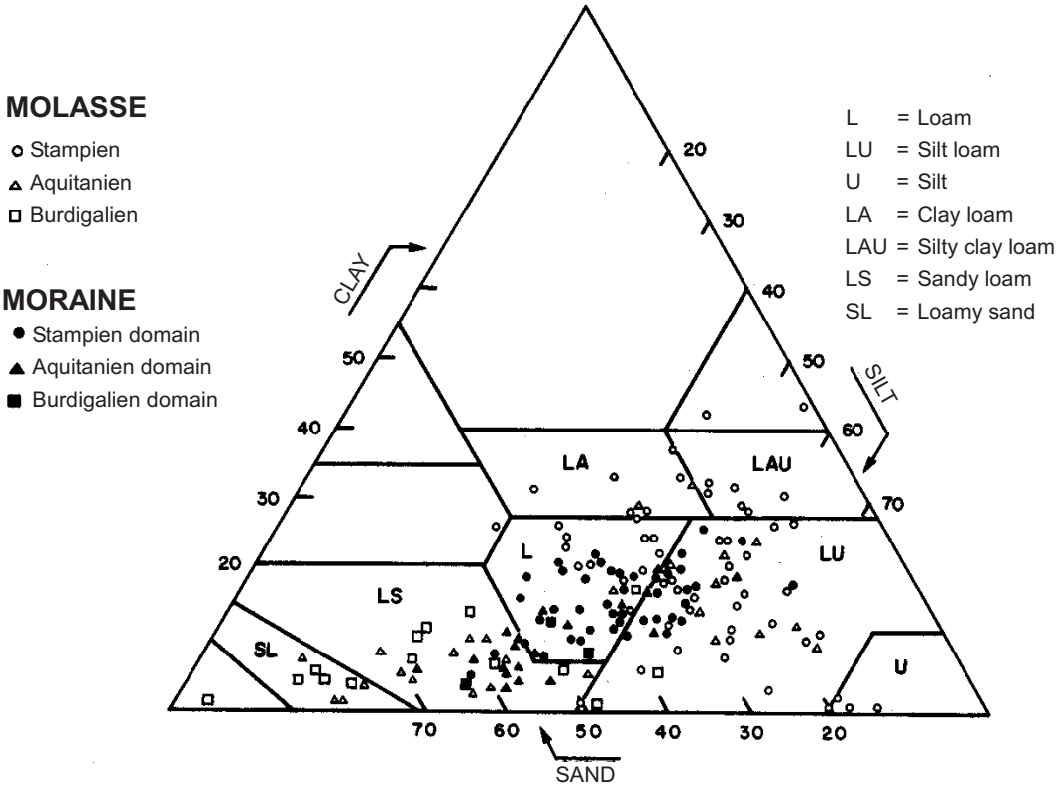

Figure A.1. Textural triangles (FAO) of the Vaud plateau morainic and molassic particle distributions (adapted from Grattier, 1980)

Appendix 1.2 Alluvial soil particle distributions

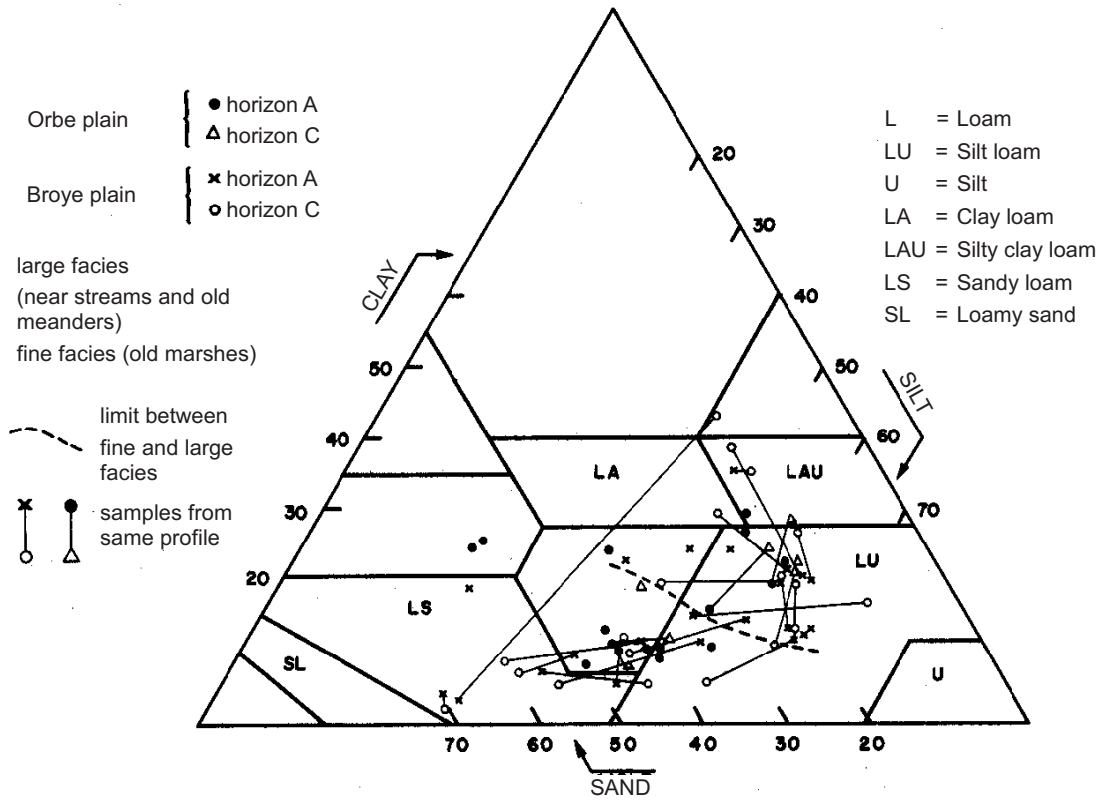

Figure A.2. Textural triangles (FAO) of the Vaud plateau alluvial soil particle distributions (adapted from Grattier, 1980)

Appendix 2 Map of the Lower Venoge Study Reach

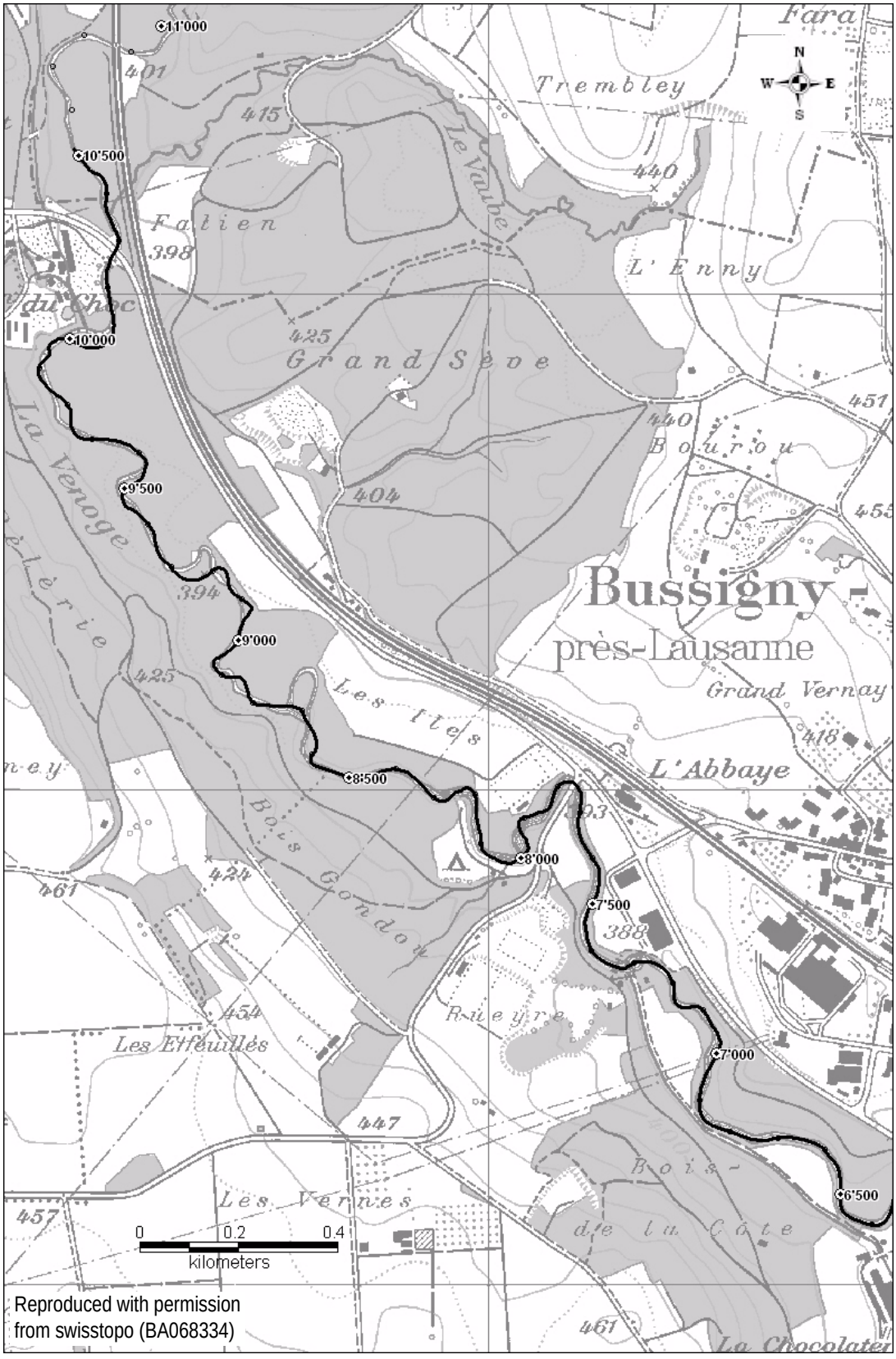

Figure A.3. Upstream section of the study reach of the Lower Venoge River (background: CP25 ©1997, Swisstopo). Distance in meters from outlet is shown by points. 2004 centerline in black.

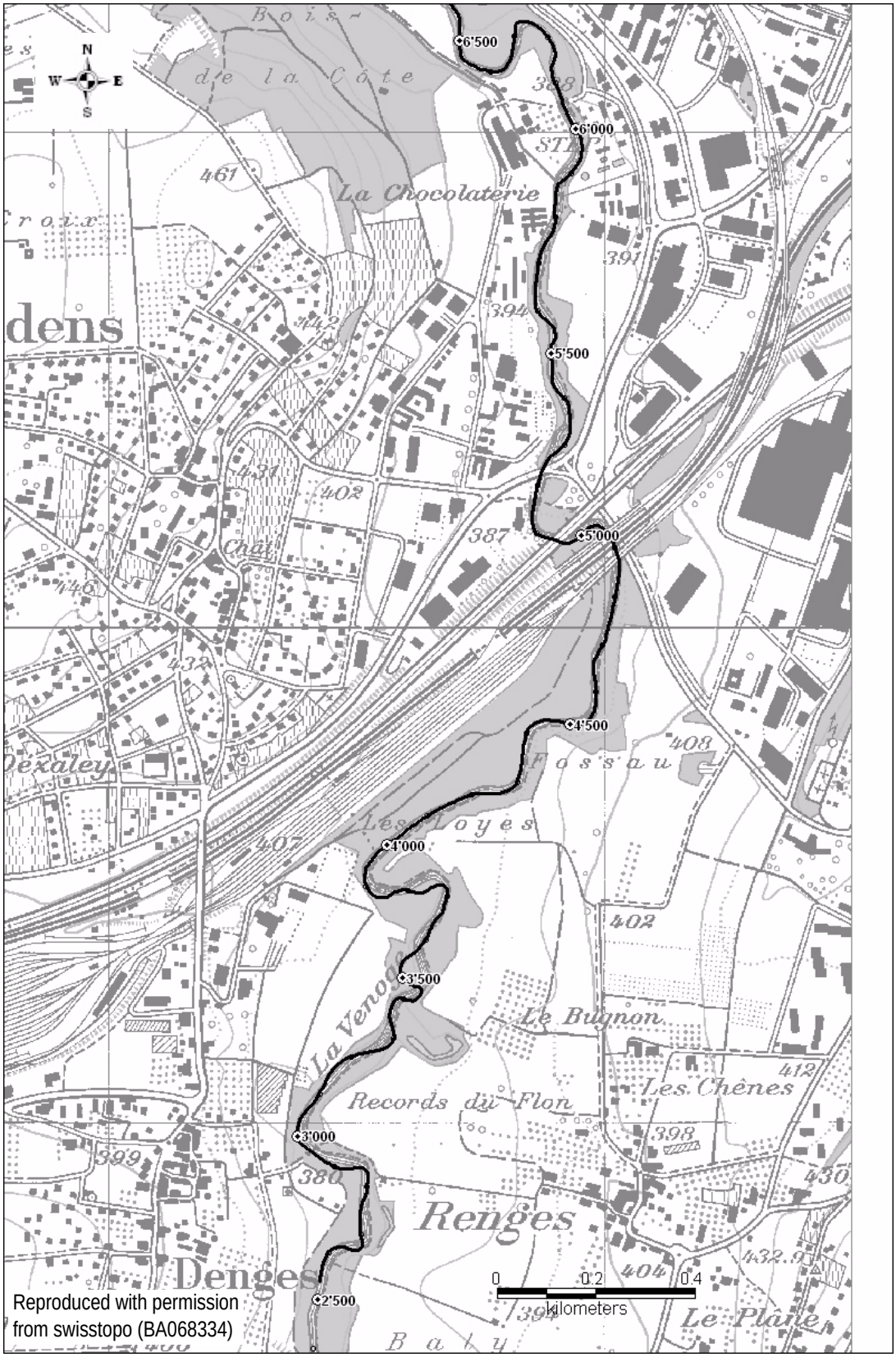

Figure A.3 (cont.). Downstream section of the study reach of the Lower Venoge River (background: CP25 ©1997, Swisstopo). Distance in meters from outlet is shown by points. 2004 centerline in black.

Appendix 3 Lower Venoge River and tributary GSD's

		class number	1	2	3	4	5	6	7	8	9	10	11	12	13	14	15	16	17	18	19	20
		representative diameter (cm)	0.0001	0.0011	0.004	0.008	0.021	0.066	0.18	0.35	0.58	0.85	1.20	1.69	2.39	3.38	4.78	6.76	9.56	13.52	19.12	27.04
		lower (cm)	0	0.0002	0.002	0.005	0.010	0.032	0.10	0.25	0.45	0.70	0.99	1.40	1.98	2.80	3.96	5.60	7.92	11.20	15.84	22.40
		upper (cm)	0.0002	0.0020	0.005	0.010	0.032	0.100	0.25	0.45	0.70	0.99	1.40	1.98	2.80	3.96	5.60	7.92	11.20	15.84	22.40	31.68
river	distance to outlet (m)	field id																				
Venoge	22654	1	0.004	0.009	0.008	0.009	0.023	0.040	0.05	0.05	0.05	0.05	0.05	0.07	0.08	0.09	0.11	0.13	0.16	0.02	0.00	0.00
	22091	2	0.004	0.008	0.007	0.008	0.020	0.036	0.05	0.04	0.04	0.04	0.05	0.06	0.07	0.08	0.10	0.12	0.14	0.10	0.03	0.02
	20513	5	0.005	0.012	0.010	0.011	0.029	0.052	0.07	0.06	0.06	0.06	0.07	0.08	0.10	0.12	0.07	0.05	0.05	0.05	0.00	0.03
	19687	6	0.004	0.009	0.007	0.008	0.022	0.039	0.05	0.05	0.05	0.04	0.05	0.06	0.07	0.09	0.11	0.13	0.11	0.02	0.06	0.02
	18848	8	0.004	0.008	0.007	0.007	0.020	0.035	0.05	0.04	0.04	0.04	0.05	0.06	0.07	0.08	0.10	0.11	0.14	0.12	0.02	0.00
	18602	9	0.004	0.009	0.008	0.009	0.024	0.043	0.06	0.05	0.05	0.05	0.06	0.07	0.08	0.10	0.12	0.14	0.12	0.01	0.00	0.00
	18323	10	0.004	0.008	0.007	0.008	0.021	0.037	0.05	0.05	0.04	0.04	0.05	0.06	0.07	0.08	0.10	0.12	0.13	0.04	0.03	0.03
	17706	11	0.004	0.010	0.008	0.009	0.025	0.044	0.06	0.05	0.05	0.05	0.06	0.07	0.08	0.10	0.12	0.14	0.11	0.00	0.00	0.00
	17276	a1	0.006	0.012	0.011	0.012	0.032	0.056	0.07	0.07	0.07	0.06	0.08	0.09	0.11	0.13	0.15	0.04	0.00	0.00	0.00	0.00
	17157	12	0.004	0.009	0.008	0.009	0.023	0.041	0.05	0.05	0.05	0.05	0.06	0.07	0.08	0.09	0.11	0.13	0.10	0.07	0.00	0.00
	16733	13	0.005	0.011	0.010	0.011	0.029	0.052	0.07	0.06	0.06	0.06	0.07	0.08	0.10	0.12	0.14	0.08	0.04	0.00	0.00	0.00
	16195	14	0.006	0.013	0.011	0.012	0.033	0.059	0.08	0.07	0.07	0.07	0.08	0.09	0.11	0.13	0.13	0.01	0.02	0.00	0.00	0.00
	16041	b3	0.006	0.014	0.012	0.013	0.035	0.062	0.08	0.08	0.07	0.07	0.08	0.10	0.13	0.12	0.06	0.06	0.00	0.00	0.00	0.00
	15468	15	0.005	0.011	0.010	0.011	0.029	0.052	0.07	0.06	0.06	0.06	0.07	0.08	0.10	0.12	0.14	0.10	0.01	0.00	0.00	0.00
	15085	16	0.003	0.007	0.006	0.007	0.019	0.034	0.04	0.04	0.04	0.04	0.05	0.05	0.07	0.08	0.09	0.11	0.13	0.13	0.05	0.00
	14569	17	0.004	0.008	0.007	0.008	0.021	0.037	0.05	0.05	0.04	0.04	0.05	0.06	0.07	0.09	0.10	0.12	0.14	0.04	0.03	0.02
	13578	19	0.005	0.011	0.009	0.010	0.027	0.048	0.06	0.06	0.06	0.06	0.07	0.08	0.09	0.11	0.11	0.12	0.04	0.03	0.00	0.00
	13499	20	0.004	0.009	0.008	0.009	0.024	0.043	0.06	0.05	0.05	0.05	0.06	0.07	0.08	0.10	0.12	0.14	0.12	0.01	0.00	0.00
	12021	22	0.005	0.011	0.010	0.011	0.029	0.051	0.07	0.06	0.06	0.06	0.07	0.08	0.10	0.12	0.14	0.12	0.01	0.00	0.00	0.00
	11728	d1	0.005	0.011	0.010	0.011	0.029	0.052	0.07	0.06	0.06	0.06	0.07	0.08	0.10	0.12	0.14	0.08	0.03	0.00	0.00	0.00
	11200	d2	0.005	0.012	0.010	0.011	0.030	0.053	0.07	0.06	0.06	0.06	0.07	0.09	0.10	0.12	0.14	0.09	0.01	0.00	0.00	0.00
	10624	23	0.005	0.010	0.009	0.010	0.026	0.047	0.06	0.06	0.06	0.05	0.06	0.08	0.09	0.11	0.13	0.11	0.07	0.02	0.00	0.00
	10329	d3	0.005	0.012	0.010	0.011	0.030	0.054	0.07	0.07	0.06	0.06	0.07	0.09	0.10	0.12	0.15	0.07	0.01	0.00	0.00	0.00
	10058	28	0.006	0.012	0.010	0.012	0.031	0.055	0.07	0.07	0.07	0.06	0.07	0.09	0.11	0.13	0.15	0.06	0.00	0.00	0.00	0.00
	9867	e2	0.005	0.011	0.009	0.010	0.027	0.048	0.06	0.06	0.06	0.05	0.07	0.08	0.09	0.11	0.13	0.15	0.03	0.00	0.00	0.00
	9726	e3	0.005	0.011	0.009	0.010	0.027	0.049	0.06	0.06	0.06	0.06	0.07	0.08	0.09	0.11	0.13	0.13	0.05	0.00	0.00	0.00
	9600	29	0.006	0.012	0.010	0.012	0.031	0.055	0.07	0.07	0.07	0.06	0.07	0.09	0.11	0.13	0.08	0.10	0.04	0.00	0.00	0.00
	9399	e4	0.005	0.010	0.008	0.009	0.025	0.045	0.06	0.06	0.05	0.05	0.06	0.07	0.09	0.10	0.12	0.14	0.09	0.00	0.00	0.00
	9247	30	0.005	0.010	0.009	0.010	0.026	0.047	0.06	0.06	0.06	0.05	0.06	0.08	0.09	0.11	0.13	0.15	0.04	0.01	0.00	0.00
	9100	31	0.005	0.011	0.010	0.011	0.029	0.051	0.07	0.06	0.06	0.06	0.07	0.08	0.10	0.12	0.14	0.09	0.04	0.00	0.00	0.00
	8875	e5	0.005	0.011	0.009	0.011	0.028	0.050	0.07	0.06	0.06	0.06	0.07	0.08	0.10	0.11	0.14	0.10	0.04	0.00	0.00	0.00
	8625	e6	0.005	0.011	0.009	0.010	0.027	0.048	0.06	0.06	0.06	0.05	0.06	0.08	0.09	0.11	0.13	0.12	0.06	0.00	0.00	0.00
	8562	e7	0.006	0.013	0.011	0.012	0.032	0.058	0.08	0.07	0.07	0.07	0.08	0.09	0.11	0.13	0.16	0.01	0.00	0.00	0.00	0.00
	8169	32	0.006	0.012	0.010	0.011	0.030	0.054	0.07	0.07	0.06	0.06	0.07	0.09	0.10	0.12	0.15	0.05	0.03	0.00	0.00	0.00
	7127	33	0.006	0.012	0.010	0.012	0.031	0.056	0.07	0.07	0.07	0.06	0.08	0.09	0.11	0.13	0.15	0.03	0.02	0.00	0.00	0.00
	6496	34	0.007	0.014	0.012	0.014	0.037	0.065	0.09	0.08	0.08	0.07	0.09	0.11	0.13	0.15	0.05	0.01	0.00	0.00	0.00	0.00
	5714	35	0.007	0.015	0.013	0.014	0.038	0.068	0.09	0.08	0.08	0.08	0.09	0.11	0.13	0.15	0.03	0.00	0.00	0.00	0.00	0.00
	5226	36	0.007	0.014	0.012	0.013	0.036	0.064	0.08	0.08	0.08	0.07	0.09	0.10	0.12	0.11	0.09	0.02	0.00	0.00	0.00	0.00
	4729	g1	0.006	0.014	0.012	0.013	0.035	0.062	0.08	0.08	0.07	0.07	0.08	0.10	0.12	0.13	0.12	0.01	0.00	0.00	0.00	0.00
	4528	g2	0.006	0.013	0.011	0.012	0.032	0.057	0.08	0.07	0.07	0.06	0.08	0.09	0.11	0.13	0.15	0.02	0.00	0.01	0.00	0.00
	3451	g3	0.007	0.015	0.013	0.014	0.038	0.068	0.09	0.08	0.08	0.08	0.09	0.11	0.13	0.16	0.02	0.00	0.00	0.00	0.00	0.00
	3283	g4	0.007	0.016	0.013	0.015	0.040	0.070	0.09	0.09	0.08	0.08	0.10	0.11	0.14	0.13	0.01	0.01	0.00	0.00	0.00	0.00
	2889	37	0.007	0.015	0.013	0.014	0.038	0.068	0.09	0.08	0.08	0.08	0.09	0.11	0.13	0.13	0.05	0.00	0.00	0.00	0.00	0.00
	2702	h1	0.007	0.014	0.012	0.014	0.036	0.065	0.09	0.08	0.08	0.07	0.09	0.10	0.12	0.15	0.05	0.02	0.00	0.00	0.00	0.00
	2538	38	0.006	0.013	0.011	0.013	0.033	0.059	0.08	0.07	0.07	0.07	0.08	0.10	0.11	0.14	0.09	0.06	0.00	0.00	0.00	0.00
	2083	41	0.008	0.016	0.014	0.016	0.042	0.074	0.10	0.09	0.09	0.09	0.10	0.12	0.14	0.09	0.02	0.00	0.00	0.00	0.00	0.00
	1522	39	0.006	0.012	0.010	0.011	0.030	0.054	0.07	0.07	0.06	0.06	0.07	0.09	0.10	0.12	0.09	0.08	0.05	0.00	0.00	0.00
	1101	40	0.006	0.013	0.011	0.012	0.033	0.059	0.08	0.07	0.07	0.07	0.08	0.10	0.11	0.13	0.11	0.04	0.00	0.00	0.00	0.00
Molomba	125	3	0.004	0.008	0.006	0.007	0.019	0.034	0.05	0.04	0.04	0.04	0.05	0.06	0.07	0.08	0.09	0.11	0.13	0.15	0.01	0.00
	25	4	0.004	0.008	0.007	0.008	0.021	0.037	0.05	0.05	0.04	0.04	0.05	0.06	0.07	0.08	0.10	0.12	0.14	0.09	0.01	0.00
Sorge	340	21	0.004	0.009	0.007	0.008	0.022	0.039	0.05	0.05	0.05	0.04	0.05	0.06	0.07	0.09	0.11	0.13	0.15	0.07	0.00	0.00
	85	18	0.005	0.011	0.009	0.010	0.028	0.049	0.07	0.06	0.06	0.06	0.07	0.08	0.09	0.11	0.13	0.13	0.03	0.00	0.00	0.00
Vaube	165	24	0.005	0.010	0.009	0.010	0.026	0.046	0.06	0.06	0.06	0.05	0.06	0.07	0.09	0.11	0.13	0.15	0.06	0.00	0.00	0.00
	45	25	0.005	0.010	0.008	0.009	0.025	0.045	0.06	0.06	0.05	0.05	0.06	0.07	0.09	0.10	0.12	0.13	0.05	0.02	0.04	0.00
Arena	100	27	0.006	0.012	0.010	0.012	0.031	0.055	0.07	0.07	0.07	0.06	0.07	0.09	0.10	0.12	0.15	0.03	0.01	0.02	0.00	0.00
	70	26	0.007	0.015	0.013	0.014	0.038	0.068	0.09	0.08	0.08	0.08	0.09	0.11	0.13	0.08	0.09	0.02	0.00	0.00	0.00	0.00

Figure A.4. Grain size fractions as determined by the Fehr method for the Lower Venoge, the Ruisseau de Molomba, the Vaube, and the Arena

Appendix 4 River Enrick streambank classification

Type	Photograph	Description	Stability
Tree lined bank		Cobble or coarse gravel bank, lined with trees. Cobbles often covered by moss indicating high stability. The stability is encouraged by tree roots. Banks often low.	High
Cobble bank		Cobble or coarse gravel banks, often with a fine gravel and sand matrix. Generally free from vegetation. Banks usually around 1 m high sloping at 45°.	Low
Vegetated valley-side slope		Valley side bluff consisting of reworked Quaternary deposits. Covered by vegetation including trees and mixed scrub.	Moderate but vulnerable to large floods.
Eroding valley-side slope		Valley side bluff consisting of reworked Quaternary deposits. Free from vegetation often with accumulation of material at toe. Mass failures common.	Low – Frequent failures during high flows.
Fine grained bank		River bank composed entirely of fine sand, silts and clay. These banks are highly cohesive. Presence of moss on bank face indicative of stability.	High

Figure A.5. Classification of streambanks used in the project SAFER on the River Enrick (Jacobs Babtie, 2005)

Composite bank		Bank consists of two layers. A coarse cobble-gravel horizon at base over laid by fine sandy sediments. Thickness of horizons varies. Fluvially derived – alluvium.	Low-moderate
Point bar	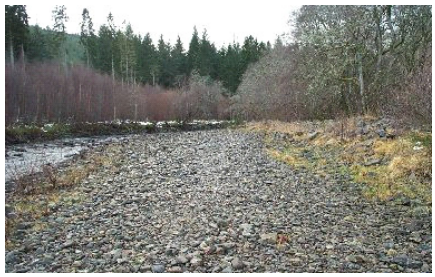	River bank very low or absent due to the presence of a gravel bar. In most cases the bar surface is at the same elevation as the surrounding low floodplain.	Moderate - High
Rip-rapped bank		Bank composed of large boulders placed to protect the bank from fluvial entrainment. The size of boulders vary, the larger the boulder the greater the stability.	High
Walled		Bank protected by a wall of interlocking river cobbles. These are not cemented.	High
Bedrock		River bank formed entirely of bedrock. With the exception of the gorge upstream of Corrimony, these tend to occur along only one bank.	Very High

Figure A.5 (cont.). Classification of streambanks used in the project SAFER on the River Enrick (Jacobs Babtie, 2005)

Appendix 5 Textural triangles of the Lower Venoge River

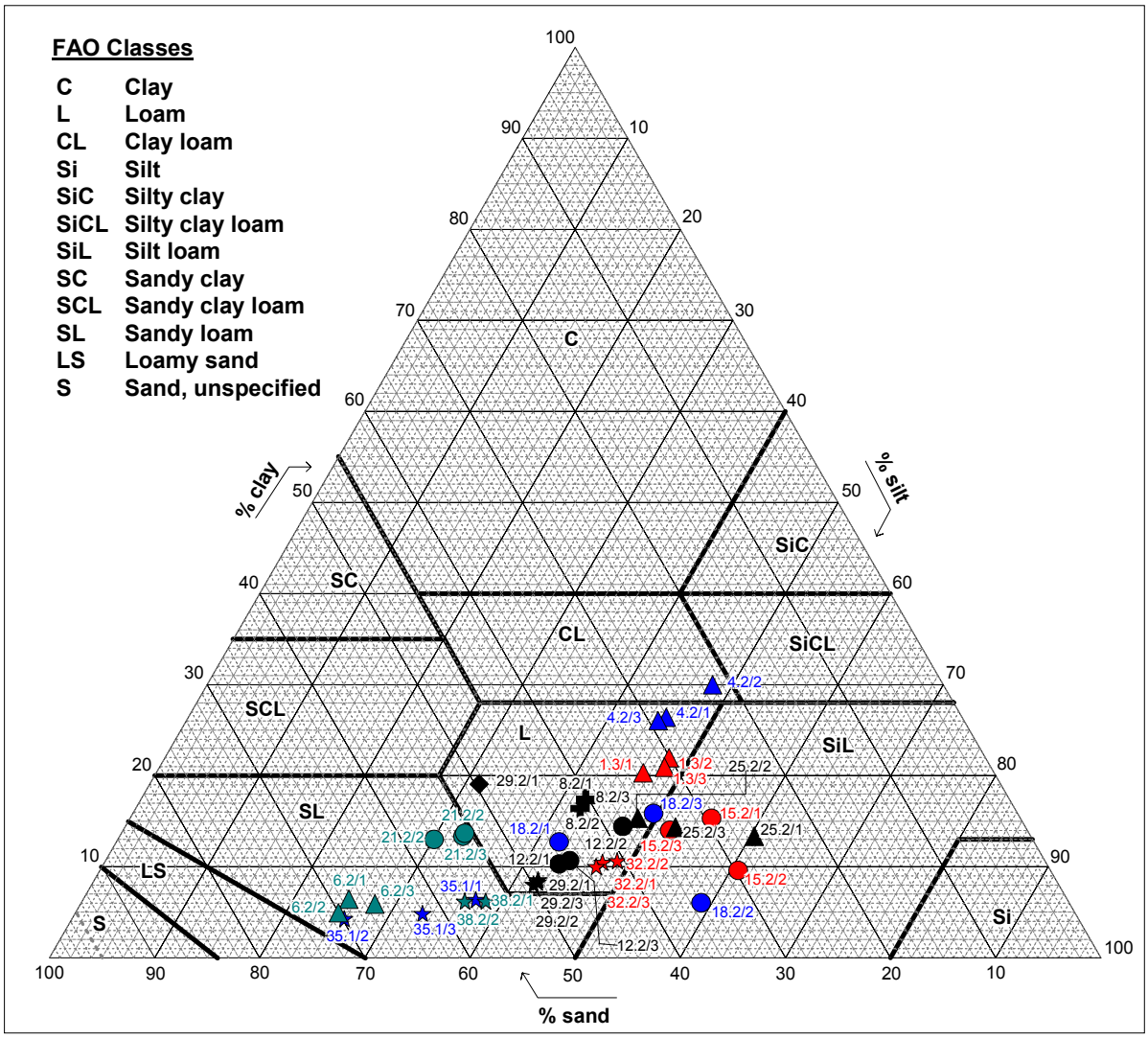

Figure A.6. FAO textural triangle representation of Lower Venoge 2004 level 2 investigation PSD's

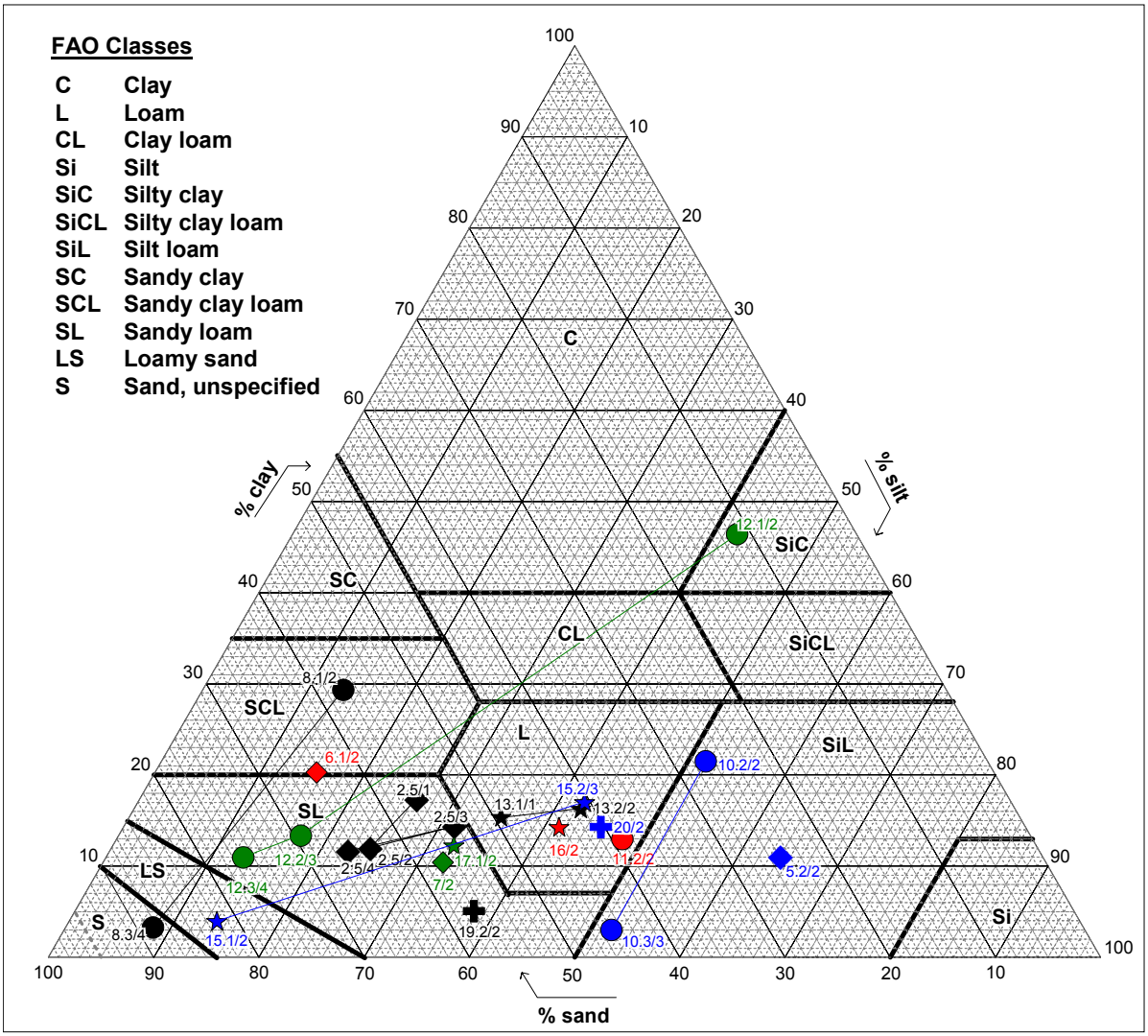

Figure A.7. FAO textural triangle representation of Lower Venoge 2004 level 1 investigation PSD's. Lines join PSD's sampled from different depths of a same bank.

Appendix 6 Cumulative measured bank positions changes

date / bend	depth	04.12.03	28.01.04	18.03.04	24.05.04	26.07.04	30.08.04	09.11.04	17.01.05	28.02.05	11.04.05	26.09.05
1.1	note:											
bank top	-20	0	0	0	0	0	0	0	0	0	0	0
top	-30	0	1	1.5	1.5	1.5	2	2	3	3	4	4
mid top	-108	0	2	2.5	1.8	0	0	1	1	1	1	1
bottom	-147	0	-3	-2.8	-2.8	-2.8	-7.5	-6	-7	-9	-8	-9
1.2	note:											
bank top	-35	0	0	0	0	0	0	0	0	0	0	0
top	-45	0	6	6	6	6	6	6	6	7	9	10.5
mid top	-90	0	2.5	3	3.5	3.5	3.5	5	6	6	10	12
bottom	-125	0	2	1	0	-1	-2	-2	-2	-4	-1.5	-1.5
1.3	note:											
bank top	-21	0	0	0	0	0	0	0	0	-6	-6	-6
top	-30	0	1.5	1.5	1.5	1.5	1.5	1	1	1	1	1
mid top	-96	1	1.5	1.5	2	1.5	1	1	1.5	1.5	2.5	1.5
bottom	-151	0	2.5	3	1.4	0	-0.5	-3	-4	-3.5	0.5	3.5
2.1	note:											
bank top	-20	0	0	0	0	0	0	3	3	3	3	3
top	-52	0	5.5	6	5.5	5.5	5.5	7	8.5	8.5	10.5	12.5
mid top	-70	0.5	5.5	5.5	5.2	5.5	5.5	7	7	7	17	18.5
bottom	-100	0	1	3	1.5	1.5	1.5	1.5	1.5	2.5	8	9
2.2	note:											
bank top	-23	0	0	0	0	-2	-20	-7	46	46	46	46
top	-50	0	4	3.5	3.5	3.5	3.5	10	10	2.7	5.5	7
mid top												
bottom	-100	0	2.3	2.8	2.8	2.8	60.3	61.3	61.3	65	69	72
2.3	note:											
bank top	-61	0	0	0	0	-10	-10	-10	-10	-10	-10	-10
top	-90	0	10	1	5	12	12	10	9	9	12	16
mid top	-130	0	22	25	25	35	21	81	80	98	98	101
bottom	-160	0.6			7.6	-0.4	-0.4	1.6	1.6	16.6	9.6	9.6
2.4	note:											
bank top	-34	0	31	31	36	36	36	36	38	41	46	46
top	-40	0	38	39	39	39	47	50	48	37	37	22
mid top	-80	0	7	7	7	7	7	7	7	16	22	22
bottom	-120	1			1	4	13	60	69	73	79	85
2.5	note:											
bank top	-21	0	83	83	83	83	83	83	83	83	83	83
top	-50	0		86	86	86	86	86	86	86	95	95
mid top	-90	0		78	78	78	65	74	74	56	69	76
bottom	-120	0			58.5	50	46	61	45.5	55	59	67
2.6	note:											
bank top	-28	0	83	83	83	83	83	88	88	88	93	103
top	-40	0		92	92	92	92	89	94	94	117	122
mid top	-80	0		83	83	83	66	82	92	92	92	78
bottom	-110	0		72	74	58	54	81	73	73	73	80
3.1	note:											
bank top	-15	0	124	124	127	127	128	143	147	147	147	147
top	-30	0		119.5	120.5	121.5	119.5	122.5	121.5	124.5	124.5	124.5
mid top	-80	0.2		117.7	117.7	117.7	117.7	126.7	124.7	124.7	126.7	130.7
bottom	-120	0		117	120	120	118	124	123	124	127	132
3.2	note:											
bank top	-11	0	132	137	142	142	142	142	142	137	137	137
top	-30	0		109.5	106.5	106.5	106.5	110.5	110.5	110.5	110.5	60.5
mid top	-70	0		104	104	104	112	110	110	110	115	115
bottom	-120	0		104	102	102	102	102	104	108	108	108

Table A.1. Cumulative bank position change. Medium gray shaded cells indicate bank failures (>20 cm).

date / bend	depth	04.12.03	28.01.04	18.03.04	24.05.04	26.07.04	30.08.04	09.11.04	17.01.05	28.02.05	11.04.05	26.09.05
3.3	note:											
bank top	-10	0	175	175	175	175	175	278	313	313	313	313
top	-40	0		173	173	173	173	253	265	259	259	259
mid top	-80	0		170	170	170	170	255	260	270	270	280
bottom	-110	0		173	173	173	173	272	259	259	259	259
4.1	note:											
bank top	-41	0	0	0	5	5	5	88	88	88	88	88
top	-85	0	0	0	0	0	0	68	58	58	58	58
mid top	-125	0	1.5	1.5	34	29.5	78.5	48.5	55.5	55.5	55.5	65.5
bottom	-180	0	1	43	43	43	62	35	26	43	47	62
4.2	note:											
bank top	-6	0	0	65	65	65	65	110	110	110	110	110
top	-48	0.8	8.5	66	63	63	63	68	89	89	89	89
mid top	-93	0	9	44	30	51	37	36	36	36	36	36
bottom	-138	-1.5	-14		17	22	12	30	11	15	23	23
4.3	note:											
bank top	-19	0	0	0	-10	-10	0	35	35	35	50	50
top	-35	-2	14.5	17.5	20.5	11.5	16.5	91.5	83.5	85.5	87.5	95.5
mid top	-60	0		3	95	82	86	162	163	173	165	155
mid bot	-100			3	29	17	17	48	48	33	42	44
bottom	-140				-76	-76	-76	-79	-73	-73	-73	-69
5.1	note:											
bank top	-4	0	96	111	106	106	106	134	136	131	173	177
top	-15	0		111	122	113	113	158	160	160	160	160
mid top	-75	0		114	114	117.5	117.5	162	163	176.7	179.7	183.7
bottom	-135	-0.5		109.5	105.5	114.5	114.5	140.5	138.5	127.5	153.5	154
5.2	note:											
bank top	-22	0	9	9	9	9	9	9	9	9	9	9
top	-75	-0.4	1	2	2	2	2	2	94	94	96	96
mid top	-130	0	2	2	2	2	2	10	99	94	96	97
bottom	-160	0	2.5	2.5	2.5	-0.5	-0.5	-0.5	89.5	89.5	91.5	91.5
5.3	note:											
bank top	-17	0	4	4	4	4	4	4	-1	-4	-4	-4
top	-75	0	9	6	6	6	6	15	15	19	19	1.5
mid top	-95	0	11	13	13	20	21	30	30	40.5	45.5	-3.5
bottom	-150	0	2	2	2	0.5	-3	1.5	3	3	20.5	-25.5
6.1	note:											
bank top	-19	0	0	8	18	18	18	18	18	18	18	43
top	-80	0	1	2	2	2	2	2	8	32	36	41
mid top	-130	0	3.5	19.5	-4.5	24.5	-12.5	-2.5	-7.5	-7.5	23.5	30.5
bottom	-160	0	2.5		1.5	5.5	5.5	11.5	-0.5	9.5	29.5	35.5
6.2	note:											
bank top	-39	0	0	0	15	15	15	15	0	35	35	70
top	-60	0	2.5	2.5	2.5	1.5	-3.5	16.5	2.5	48.5	48.5	48.5
mid top	-100	0	38	41	41	41	34	49	37	-20	-15	-3
bottom	-150	0	8	51	10	10	10	17	4	35	30	30
6.3	note:											
bank top	-5	0	90	95	90	95	95	125	165	165	175	175
top	-30	0	90	101	101	101	101	118	170.5	127.5	180	180
mid top	-80	0	90	101.5	90.5	101.5	101.5	119.5	179.5	179.5	179.5	191.5
bottom	-130	0	90	93	93	99	95	126	129	153	160	178
6.4	note:											
bank top	-23	0	127	135	130	130	130	130	133	135	140	200
top	-50	0	127	136	136	136	136	140	140	140	140	194
mid top	-110	0	127	132	132	132	132	132	149	175	176	198
bottom	-150	0	127	139	149	149	149	163	172	200	212	221
6.5	note:											
bank top	-39	0	81	81	96	96	96	96	96	96	96	116
top	-40	0	81	107	107	107	107	111	103	103	103	126
mid top	-100		81	84	92	92	92	168	188	206	206	229
bottom	-150	0	81	57	75	80	80	106	113	132	132	140

Table A.1. Cumulative bank position change. Medium gray shaded cells indicate bank failures (>20 cm).

date / bend	depth	04.12.03	28.01.04	18.03.04	24.05.04	26.07.04	30.08.04	09.11.04	17.01.05	28.02.05	11.04.05	26.09.05
6.6	**note:**											
bank top	**-7**	0	157	162	162	162	162	232	277	277	282	282
top	**-30**	0	157	163	163	163	163	308	239	239	239	256
mid top	**-80**		157	161	161	161	161	340	290	254	254	254
bottom	**-130**	0	157	159	159	159	153	325	209	209	224	224
6.7	**note:**											
bank top	**-5**	0	160	160	160	160	160	380	380	380	380	380
top	**-40**	0	160	163	163	163	167	338	338	328	336	336
mid top	**-110**		160	156	156	156	156	165	159	179	154	154
bottom	**-150**	0	160	189	189	176	163	116	116	covered	covered	covered
6.8	**note:**											
bank top	**-11**	0	160	165	175	175	175	247	247	252	270	270
top	**-30**	0	160	177	165	165	180	248	248	248	259	266
mid top	**-80**		160	158	168	168	176	219	219	242	214	214
bottom	**-120**	0	160	156	188	170	170	245	240	232	216	216
6.9	**note:**											
bank top	**-7**	0	144	144	144	144	144	159	159	259	259	259
top	**-40**	0	144	141	129	140	151	196	196	243	243	243
mid top	**-100**		144	144	144	144	149	178	178	208	208	208
bottom	**-140**	0	144	132	163	138	132	208	208	204	214	covered
6.91	**note:**											
bank top	**-6**	0	91	91	96	96	96	121	121	121	121	121
top	**-40**	0	91	86	90	90	90	116	123	116	125	124
mid top	**-90**		91	92	92	92	92	176	176	191	175	191
bottom	**-120**	0	91	80	80	80	80	184	184	153	121	158
6.92	**note:**											
bank top	**-5**	0	67	72	82	82	82	92	127	132	132	132
top	**-20**	0	67	67	72	72	72	138	122	114.5	126	123
mid top	**-80**		68	71	71	71	71	142	122	113	123	127
bottom	**-120**	0	68	65	65	65	59	146	117	107	112	150
7.1	**note:**											
bank top	**-58**	0	104	169	204	204	314	319	314	324	329	329
top	**-74**	0	104	158	200	200	320	320	320	320	320	320
mid top	**-114**	0	104	151	165	170	268	270	270	276	276	276
bottom	**-144**	0	104		217	217	269	269	269	282	282	269
7.2	**note:**									measurement error		
bank top	**-26**	0	190	231	281	281	501	506	516			521
top	**-69**	26	216	256.5	322.5	322.5	532.5	540.5	535.5			533.5
mid top	**-109**	40	230	299	334	378	464	478	457			464
bottom	**-129**	40	230		312	356	418	427	420			428
7.3	**note:**											
bank top	**-5**	0	129	154	249	249	254	254	254	256	254	264
top	**-30**	0	129	140	238	238	238	238	238	238	238	238
mid top	**-60**	0	129	129	214	208	204	204	204	204	208	208
bottom	**-90**	0	129	130.5	202.5	207.5	205.5	206.5	206.5	206.5	209.5	209.5
7.4	**note:**											
bank top	**-4**	0	79	99	141	141	134	134	144	154	154	154
top	**-30**	0	79	109	132	137	150	142	142	151	151	151
mid top	**-70**	0	79	120	142	146	146	142	142	142	153	161
bottom	**-100**	0	79		130.5	137	137	130	130	140	157	163
7.5	**note:**											
bank top	**-32**	0	204	243	253	253	253	248	253	253	258	258
top	**-50**	0		235	235	235	235	230	230	234	243	248
mid top	**-80**	0		236.5	236.5	236.5	231.5	232.5	232.5	232.5	239.5	256.5
bottom	**-110**	0		232	232	232	232	229	224	224	235.5	244
7.6	**note:**											
bank top	**-40**		200	275	281	281	281	281	290	290	290	290
top	**-60**		200	270	270	270	260	266	266	266	266	266
mid top	**-90**		200	257	251	251	258	252	261	261	261	261
bottom	**-110**		200	230	230	230	230	231	231	231	237	237

Table A.1. Cumulative bank position change. Medium gray shaded cells indicate bank failures (>20 cm).

date / bend	depth	04.12.03	28.01.04	18.03.04	24.05.04	26.07.04	30.08.04	09.11.04	17.01.05	28.02.05	11.04.05	26.09.05
8.1	**note:**											
bank top	**-32**	0	10	10	15	15	15	70	70	70	85	85
top	**-80**	0	8	8	11	11	11	5	12	12	12	18
mid top	**-125**	0	32	32	28.5	32	32	79	79	79	85	85
bottom	**-160**	0		0		0	0	41	41	46	46	46
8.2	**note:**											
bank top	**-18**	0	0	10	10	10	10	10	5	5	60	75
top	**-45**	0	7	7	7	7	7	43	44	44	40	55
mid top	**-100**	0	0	2	2	2	2	37	40	50	53	53
bottom	**-160**	0	8	8	13	10	10	69	77	77	74	74
8.3	**note:**											
bank top	**-14**	0	183	183	183	183	183	183	183	183	183	209
top	**-70**	0		183	183	183	183	183	183	183	183	190
mid top	**-105**	0		185	185	185	185	185	185	191		
bottom	**-220**	0		181	176	172.5	171.5	171	170	167.5	175.5	
9.1	**note:**											
bank top	**-24**	0		150	150	150	150	380	380	380	380	380
top	**-90**	0		161	161	161	161	300	300	300	300	300
mid top	**-125**	0		149	149	149	136	269	249	239	243	251
bottom	**-185**	0		142	135	140	140	140				
9.2	**note:**											
bank top	**-7**	0		150	148	148	148	148	150	150	145	145
top	**-50**	0		151	151	151	151	153	153	153	153	153
mid top	**-100**	0		153	141	134	126	157	157	152	129	163
bottom	**-120**	-3.5		155.5	152.5	145.5	150.5	169.5	231.5	167.5	163.5	227.5
9.3	**note:**											
bank top	**-16**	0		150	152	152	152	152	152	152	152	152
top	**-40**	0		53	53	53	62	61	61	57	57	57
mid top	**-100**	0		56	56	56	56	52	97	49	31	31
bottom	**-140**	-1		65	65	70	61	68	68	68	57	73
10.1	**note:**											
bank top	**0**	0	0	0	0	0	0	3	3	3	3	3
top	**-60**	0	1	2	2	2	2	2	2	3	4	4
mid top	**-110**	0	4	4	4	4	4	4	4	8	8	12.5
bottom	**-160**	0	4	6	7.5	13.5	31.5	34.5	35.5	35.5	39	42
10.2	**note:**											
bank top	**0**	0	4	4	4	4	4	4	4	4		-11
top	**-65**	0.4	1	2.5	2.5	2.5	2.5	2.5	2.5	1.5	6	8.5
mid top	**-110**	0	2.8	0.8		-0.2	0.8	4.3	5.8	9.8	13.8	13.8
bottom	**-160**	0	0.6	0.6			1.6	2.1	3.1	3.6	7.1	7.1
10.3	**note:**											
bank top	**0**	0	13	13	13	17	17	1	1	1		1
top	**-70**	0	0	0	0	0	0	0	0	6	6	6
mid top	**-110**	0	0	0	0	0.5	12	12	12	12	14	14
bottom	**-150**	-0.9	1	1	0	0	0	0	2	3	7	17
10.4	**note:**											
bank top	**-19**	0	23	123	123	138	163	262	263	263	263	263
top	**-50**	0	0.3	100.3	125.3	126.8	173.3	207.3	207.3	205.3	218.3	218.3
mid top	**-90**	0	0.5	100.5	146.5	144.5	175.5	201.5	203.5	205.5	207.5	210.5
bottom	**-120**	0	3.5	103.5	158.5	158.5	158.5	168.5	185.5	200.5	193.5	191.5
11.1	**note:**											
bank top	**-18**	0	0	0	0	0	0	15	15	15	15	15
top	**-70**	0	3	5	5	5	5	59	5	57	61	46
mid top	**-140**	0	-2	-1	-1	-1	-1	64	64	60	57	57
bottom	**-180**	0	4	4	2	2	0.5	84	64	67	85	54
11.2	**note:**											
bank top	**-18**	0	85	85	93	93	93	93	90	90	90	90
top	**-60**	0	80	76	76	76	76	76	76	76	76	76
mid top	**-100**	-1	39	33	33	33	33	33	33	33	33	33
bottom	**-150**	-0.5	28	-47	-47	-47	-47	-49	-49	-49	-42	-45

Table A.1. Cumulative bank position change. Medium gray shaded cells indicate bank failures (>20 cm).

date bend	depth	04.12.03	28.01.04	18.03.04	24.05.04	26.07.04	30.08.04	09.11.04	17.01.05	28.02.05	11.04.05	26.09.05
11.3	note:											
bank top	-22	0	1	1	3	3	3	3	58	58	58	58
top	-60	0	4	5	5	5	5	23	34	34	34	50
mid top	-130	0	40	53	49	49	49	74	37	77	70	70
bottom	-180	0	40	40	30	34	34	39	54	37	58	46
11.4	note:											
bank top	-7	0	0	0	0	0	0	0	0	0	0	0
top	-80	0	7	9	9	9	9	9	13	138	154	154
mid top	-120	0	3.5	0.5	0.5	-1.5	-1.5	-1.5	1	121.5	140.5	140.5
bottom	-175	0	3.5	5	5	6.5	6	8	5	74	89	53
11.5	note:											
bank top	-11	0	100	100	105	105	105	105	108	248	248	258
top	-60	0	100	100	99	98	99	99	105	194	193	218
mid top	-120	0	100	104	103	103	105	105	109	165	194	206
bottom	-170	0	100		98	102	102	97	107	175	219	224
11.6	note:											
bank top	-14	0	125	131	133	133	133	290	290	290	290	290
top	-56	0	125	139	139	139	139	230	236	236	259	259
mid top	-116	0	125	124	137	137	137	232	232	227	246	250
bottom	-156	0	125	129	129	126	133	218	255	262	256	262
11.7	note:											
bank top	-20	0	132	132	135	180	132	132	140	132	135	135
top	-70	0	132	132	132	179	131	133	133	128	145	149
mid top	-130	-1.5	130.5	106.5	106.5	154.5	105.5	106.5	112.5	129.5	84.5	107.5
bottom	-150	0	132	132	126	174	128	126	133	111	98	133
11.8	note:											
bank top	0	0	132	132	127	134	134	134	134	136	132	132
top	-40	0		131	131	131	131	131	135	135	135	135
mid top	-90	0		132	132	132	132	137	137	132	132	143
bottom	-130	-1.5		121.5	121.5	118.5	122.5	116.5	115.5	110.5	113.5	113.5
12.1	note:											
bank top	0	0	0	0	-1	-1	-1	-5	-11	-5	4	4
top	-70	0	1	2	2	2	2	3	3	5	5	6
mid top	-120	0	1	2	2	2	2	4	4	8.5	12	12
bottom	-175	0	0	1.5	2.7	10	14	17	30	35	36.5	41.5
12.2	note:											
bank top	-7	0	0	0	0	0	0	92	90	90	113	113
top	-55	0	33.5	33.5	33.5	33.5	33.5	163.5	163.5	169.5	170.5	171.5
mid top	-95	0	35	35	36	36	36	160	160.5	167.5	167.5	169.5
bottom	-190	0	35	38	38	36	38	161	164	170.5	168	173.5
12.3	note:											
bank top	-14	0	160	160	165	165	165	285	295	300	307	307
top	-70	0	180	178	178	178	280	404	404	407	411	411
mid top	-120	0	180	181	179	181	180	290	289	293	294	295
bottom	-170	0	180	183	166	176	137	291	304	296	301	318
12.4	note:											
bank top	0	0	150	155	160	160	160	215	220	225	225	250
top	-55	0		151	151	151	151	216	219	232	238	240
mid top	-115	-1		149	149	149	149	215	215	224	224	224
bottom	-175	0		138	125	130	130	235	235	235	235	246
12.5	note:											
bank top	0	0	212	209	235	235	235	302	300	355	365	364
top	-60	0		216	216	226	218	319	319	345	345	345
mid top	-140	0		213	213	213	213	306	306	321	321	321
bottom	-190	0		205	205	187	202	323	303	331	340	340
12.6	note:											
bank top	-9	0	245	245	235	235	235	313	313	370	370	380
top	-68	0	245	245	245	245	245	327	332	353	353	353
mid top	-138	0	245	252	245	250	250	336	336	342	342	342
bottom	-188	0	245	224	224	218	224	307	307	325	316	349.5

Table A.1. Cumulative bank position change. Medium gray shaded cells indicate bank failures (>20 cm).

date / bend	depth	04.12.03	28.01.04	18.03.04	24.05.04	26.07.04	30.08.04	09.11.04	17.01.05	28.02.05	11.04.05	26.09.05
13.1	note:											
bank top	-12	0	0	0	0	0	0	0	-8	-8	-8	-8
top	-90	0	1.5	2	3	3	2	8	8	8	7	10
bottom	-125	0	0	1	1	1	7	23	27	27	27.5	27.5
13.2	note:											
bank top	-8	0	0	0	0	0	0	35	40	50	63	63
top	-30	0	3	4	4	4	4	55	55	68	68	68
mid top	-80	0	1.5	4	4	4	4	30.5	54	64.5	64.5	64.5
bottom	-135	0	1	1	2	2	3	68	62	74	75	78
13.3	note:											
bank top	-9	0	0	0	0	0	10	120	118	117	125	125
top	-56	0	0	0	0	1	21	74	68	81	91	94
mid top	-100	0	0	1.5	1.5	1.5	37.5	66	63	86	94	97
bottom	-180	0	3	29.5	44.5	50	52.5	11				103
13.4	note:											
bank top	-4	0	0	0	0	0	0	40	38	75	80	85
top	-40	0	4	7	7	7	7	62	56	71	74	76
mid top	-95	0	2	4	4	4	4	43	43	61	64	64
bottom	-160	-1	11.5	24.5	25.5	25.5	57	30.5	54.5	77.5	83.5	88.5
13.5	note:											
bank top	-23	0	0	0	1	1	1	1	1	11	11	11
top	-65	0	5.5	4	4	4	4	3.5	3.5	3.5	3.5	3.5
mid top	-95	0	6	7	7	8	8	10.5	11.5	14	16	16
bottom	-150	0	3	5.5	13	12	12	12	14	28.5	36	36.5
14.1	note:											
bank top	-35	0	0	0	0	0	0	0	0	0	0	0
top	-120	0	0	-4	-0.5	-0.5	-0.5	-0.5	-0.5	-1.5	1	0
mid top	-210	0	2	2	2	3	3	3	2	2	3	3
bottom	-260	0	2	4	4	4	4	4	4	8	8	16
14.2	note:											
bank top	-36	0	0	0	0	0	0	0	0	0	0	0
top	-160	0	5	5	5	5	5	5	7	7	9	8
mid top	-230	0	6.5	2.5	2.5	2.5	0.9	-7.5	2	0.5	2	2
bottom	-255	0	1.5	1.5	-0.5	1	1	1.5	1.5	1.5	1.5	6
14.3	note:											
bank top	-50	0	0	0	0	0	0	0	0	0	0	0
top	-175	0	5	4	8.2	6.5	3.5	18	18	16.5	18	18
mid top												
bottom	-220	0	-1	6	4	4	9	20	20	21	21	21
14.4	note:											
bank top	-63	0	0	0	0	0	0	0		0		
top	-100	0	7	6	8	10.5	10.5	21	21.5	20	21	21.5
mid top	-130	0	19	18	18	18	19.5	21	24.5	26.5	30	39
bottom	-175	0	3	4.5	6.5	6	6	10.5	8.5	15	18.5	20
15.1	note:											
bank top	-20	0	115	115	125	125	125	125	125	125	135	140
top	-50	0	115	110	116	111	118	113	113	113	121	156
mid top	-100	-1	114	92	89	93	94	96	91	97	110	149
bottom	-160	0	115	113	108	108	101	107	113	113	105	153
15.2	note:											
bank top	-12	0	80	90	90	90	90	105	110	110	110	115
top	-50	0	80	81	81	81	76	76	69	69	84	90
mid top	-110	-0.8	79.2	87.7	65.2	87.2	87.2	84.2	72.2	89.2	83.2	105.2
bottom	-160	0	80	97	81	71	71	58	58	45	57	83
15.3	note:											
bank top	-10	0	70	90	95	95	95	390	390	385	385	395
top	-74	0	70	68	74	70	70	353	362	354	354	346
mid top	-144	0	70	18	36	26	30	153				
bottom	-184	0	70		80	80	80	48				

Table A.1. Cumulative bank position change. Medium gray shaded cells indicate bank failures (>20 cm).

date / bend	depth	04.12.03	28.01.04	18.03.04	24.05.04	26.07.04	30.08.04	09.11.04	17.01.05	28.02.05	11.04.05	26.09.05
15.4	note:											
bank top	-5	0	55	55	45	45	45	131	130	130	130	130
top	-60	0	55	55	55	61	56	72	79	79	79	79
mid top	-120	0	55	60	60	60	60	63	78	87	87	70
bottom	-170	0	55		57	53	37	55	55	55	61	35
15.5	note:											
bank top	-24	0	78	78	78	78	78	88	88	93	93	93
top	-50	1	79	89	89	89	89	90	90	90	97	100
mid top	-100	0	78	87	81	78	78	87	77	100	108	108
bottom	-160	-1	77		61	67	61	68	98	112	132	135
15.6	note:											
bank top	-28	0	40	40	42	42	42	42	52	37	37	37
top	-70	0	20	22	22	22	22	25	25	29	29	29
mid top	-120	0	11.5	4.5	5.5	4.5	0	9.5	9.5	19.5	19.5	24.5
bottom	-170	0	11		1	-6	-7	34	34	36	46	46
16.1	note:											
bank top	-5	0	0	0	0	0	0	0	0	0	0	0
top	-65	0	6	6	6	6	6	7	7	5	9.5	10.5
mid top	-110	-8	-4	-4	-4	-4	-2.5	-2.5	-2.5	-4.5	-4.5	-2
bottom	-155	-2	9	5	5	4	3	3.5	3.5	3.5	7.5	7.5
16.2	note:											
bank top	-7	0	87	87	92	92	92	122	122	127	127	127
top	-40	0	87	85	85	85	94	111	111	111	111	111
mid top	-100	0	87	90	90	90	90	92	92	82	82	82
bottom	-140	0	87	91	91	97	84	89	89	94	86	92
16.3	note:											
bank top	-12	0	80	80	80	80	80	80	85	80	80	80
top	-40	0	80	80	80	80	80	87	87	87	87	87
mid top	-130	0	80	80	80	80	89	90	90	90	94	102
bottom	-170	0	80		76	76	56	75	75	75	75	95
16.4	note:											no stakes
bank top	-17	0	92	92	97	97	97	137	137	137	137	
top	-40	0	90	90	90	96	92	106	106	106	106	
mid top	-110	0	92	92	92	92	92	97	97	110	113	
bottom	-150	8	99		100	100	100	106	103	118	124	
16.5	note:											
bank top	-10	0	0	0	3	3	3	3	13	8	28	28
top	-55	0	6	8.5	8.5	8.5	8.5	8.5	8.5	17.5	25.5	25.5
mid top	-120	7.5	20	29.5	29.5	29.5	29.5	27.5	27.5	53.5	64.5	69.5
bottom	-150	8	38		51	41	41	40	40	74	74	60
17.1	note:											
bank top	-52	0	0	0	1	1	1	1	1	1	1	1
top	-105	0	18	17	17	17	17	15.5	17	15	15	15
mid top	-150	0	1	2.5	2.5	2.5	2.5	3	3	9.5	12.5	12.5
bottom	-180	0		2	2	0	0	2	2	6.5	6.5	5.5
17.2	note:											
bank top	-16	0	0	0	0	0	0	0	5	5	5	5
top	-60	0	2	2.5	2.5	2.5	2.5	34.5	34	34	35	35
mid top	-100	0	8	2	1	3	16	16.5	16.5	28	28	31
bottom	-150	0	15	34.5	34	34	59	61	57	75.5	75.5	77
17.3	note:											
bank top	-7	0	46	46	56	56	211	211	211	211	211	211
top	-70	0	48	106	106	106	167	204	206	206	206	206
mid top	-130	0	25	52	52	52	116	80	83	83	88	88
bottom	-180	0	38		48	62	87	87				
17.4	note:											
bank top	-14	0	92	127	157	157	287	287	287	287	312	312
top	-50	0	92	162	178	178	315.5	318	322	327	327	327
mid top	-110	0	92	149	236	236	283	271	271	271	271	283
bottom	-150	-3	89		238	245	206	208	213	226	214	235

Table A.1. Cumulative bank position change. Medium gray shaded cells indicate bank failures (>20 cm).

date bend	depth	04.12.03	28.01.04	18.03.04	24.05.04	26.07.04	30.08.04	09.11.04	17.01.05	28.02.05	11.04.05	26.09.05
17.5	note:											
bank top	0	0	200	200	200	200	200	557	560	560	560	560
top	-60	0		203	203	203	203	526	549	549	549	556
mid top	-110	0		202	202	202	207	485	492	492	505	505
bottom	-160	0			200	200	212	210				444
17.6	note:											
bank top	-18	0	215	240	230	235	435	555	555	560	575	580
top	-60	0		242	250	250	267	566	579	595	595	604
mid top	-110	0		247	270	270	271.5	504	555	563	592	575
bottom	-160	0			248	249	250	459		489		
18.1	note:											
bank top		0	50	50	50	50	50	50	50	50	50	50
top		-5	45		44.5	44.5	44.5	46	44.5	41.8	44	43
mid top		-2	48		47.5	47.5	47.5	51.5	51.5	50	51	50
mid bot		-1	49									
bottom		0	5		4	5	-0.2	0.5	0.5	-2.5	-2.5	-2.5
18.2	note:											
bank top		0	0	0	2	15	15	15	15	5	5	5
top		-0.2	3	4	2.5	4	5	5	5	7	6	6
mid top		-1	1	-1	0.5	-0.5	2	0.5	-3.5	-3	-3	-3
mid bot		-0.5	6	6	7	7	5.3	5	-2.5	1	2	3
bottom		0	12	11.5	9	9	9	7.5	7.5	5	5	5
18.3	note:											
bank top		0	50	50								
top		-1.5	48.5									
mid top		30	80									
mid bot		30	80									
bottom		-3	47									
18.4	note:											
bank top		0	0	0	0	0	0	0				
top		0	1.5	1.5	1.5	1.5	1.5	41.5				
mid top		-1	-1	-0.5		-4.5	2	19.5				
mid bot		0	6	6								
bottom		-1	-10			-9.5	12.3	19.8				
18.5	note:											
bank top		0	0	0	0	0	0	0	0	0	0	0
top		-1	2	-5	-10	-12	-10.5	-5	-3.5	-5	-5	-12
mid top		-0.5	10	5	0	-7.5	0.3	12.3	12.8	12.8	12.8	10.8
mid bot		-0.5	15	14.5	9	5	6.2	24	23	24	26.5	25
bottom		0.5	9		9.2	-1	-4.2	7.5	9	11.5	12	14
18.6	note:											
bank top		0	0	0	0	0	0	0	0	0	0	0
top		-1	5	7	5.5	7	7	7	7	4.5	6	6
mid top		0	8.5	9	9	9	9	10	10	6.5	13	13.5
mid bot		0	20	18.5	20.5	21	20	22	22	25.5	28	29.5
bottom		0	9	12.5	12	11.5	11	12.5	12.5	19	26	28
18.7	note:											
bank top		0	0	0	20	20	20	20	20	20	20	20
top		-0.5	11	0	0	0	0	4	4	2.5	3	5
mid top		-1	8	-3	0.5	-2	-2	3	4.5	4.5	5.5	27.5
mid bot		0	13	-2	-2	-2	-2	4.5	3	11	13.5	20
bottom		0	18		-1	0	0	4	3	13	17	19.5
19.1	note:											
bank top	0	0	0	5	9	9	9	9	9	9	9	9
top	-40	0	3	1.5	1.5	1	1.4	1.5	1.5	0.5	1.5	1.5
mid top	-85	0	0.5	0.5	0.5	0.5	0.5	0.5	-1	-2	-1	-0.5
bottom	-150	0	0.5	2	2	2	2	2.5	2.5	1.5	4.5	4.5
19.2	note:											
bank top	0	0	0	0	35	35	35	35	35	35	35	35
top	-60	-4	7	6.5	6.5	6.5	16.5	24.5	23.5	19	21	23.5
mid top	-110	-1	4	4	3	0.3	0.3	4.5	3	3	3	4

Table A.1. Cumulative bank position change. Medium gray shaded cells indicate bank failures (>20 cm).

date / bend	depth	04.12.03	28.01.04	18.03.04	24.05.04	26.07.04	30.08.04	09.11.04	17.01.05	28.02.05	11.04.05	26.09.05
bottom	-140	0	14.2	14.2	13.7	12.2	11.6	18.2	16.2	16.7	21.2	21.7
19.3	note:											
bank top	-5			0	0	0	0	5	5	20	40	40
top	-50			-12	-2	-1	0	19	41	38	35	57
mid top	-85			-14	22	-12	-7	40	25	59	38	42
bottom	-125			-1	20	-3	1.5	29	4	66	44	53
19.4	note:											
bank top		0	0	0	0	0	0	3	3	2	2	2
top		0	9.5	11.5	11.5	11.5	11	11	11.5	9.5	16.5	20.5
mid top		0	1	2.5	2.5	2.5	3	3	3.5	8.5	7.5	13
bottom		-1	-0.5	-4.5	-3	-3.5	-5.9	-5.9	-5.4	-6.4	-5.4	-6.4
20.1	note:											
bank top	-19	0	0	0	0	0	0	0	0	0	0	0
top	-95	0	-4	-4	0	0	48	43.5	46	41.5	42	42
mid top	-120	0	3	4	4	18	46	41.5	44	41	42	42
bottom	-180	0	-7.5	-7.5	-7.5	15.5	27	20.5	24.5	22.2	24	28
20.2	note:											
bank top	-21	0	62	62	62	62	62	72	72	72	72	72
top	-80	-8		-9	-8	-7	-8.8	-9	-10	-13	-13	-18
mid top	-150	-5.5		-5.5	-5.5	-9.5	-5.5	-9.5	-11	-14.5	-13.5	-13.5
bottom	-205	-3.5	12	13.5	16	14	12.5	12	11	11.5	13.5	14.5
20.3	note:											
bank top	-50	0	0	0	10	10	10	3	3	3	3	3
top	-90	0	7	8	7	8	9.5	10	11.5	16	16	19
mid top	-120	0	4	5	4	4	4	6	8.5	15	21.5	24.5
bottom	-150	0	2.5		3	8	19.5	25.5	27	27.5	26	23.5

Table A.1. Cumulative bank position change. Medium gray shaded cells indicate bank failures (>20 cm).

Appendix 7 Streambank erosion danger maps of the Venoge River

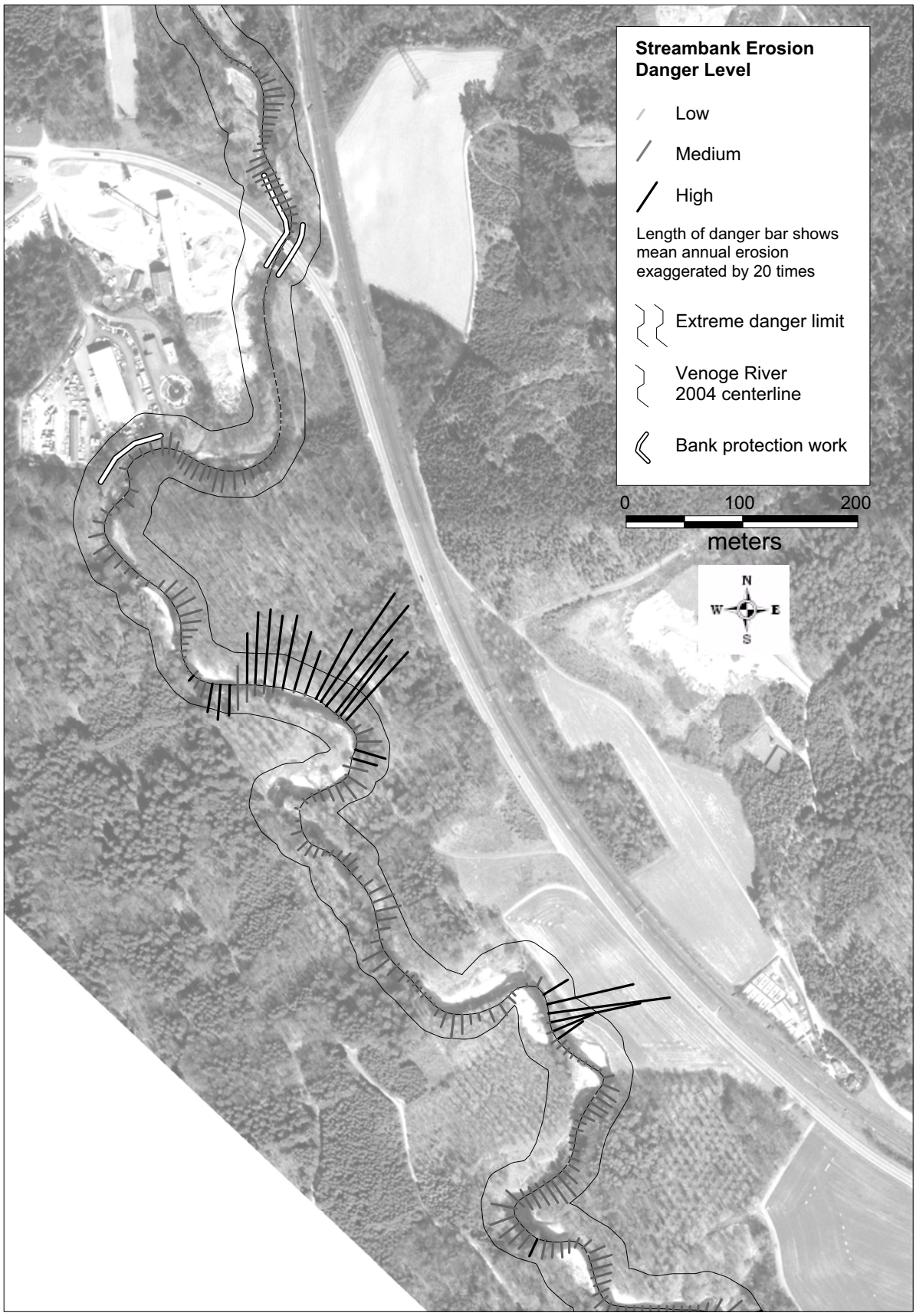

Figure A.8. Streambank erosion danger map of the Venoge River (bank protection failure probability not taken into account)

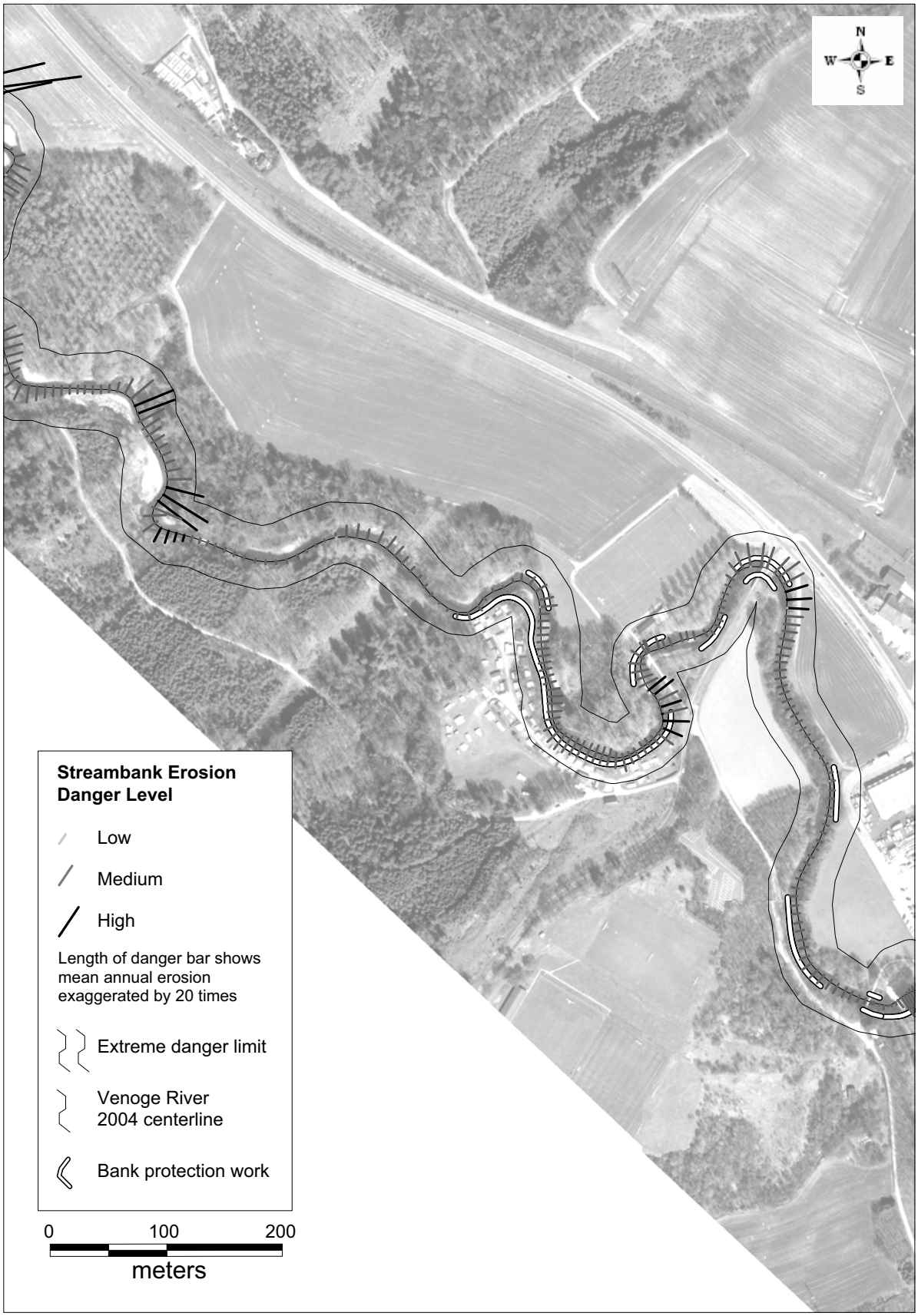

Figure A.8 (cont.). Streambank erosion danger map of the Venoge River (bank protection failure probability not taken into account)

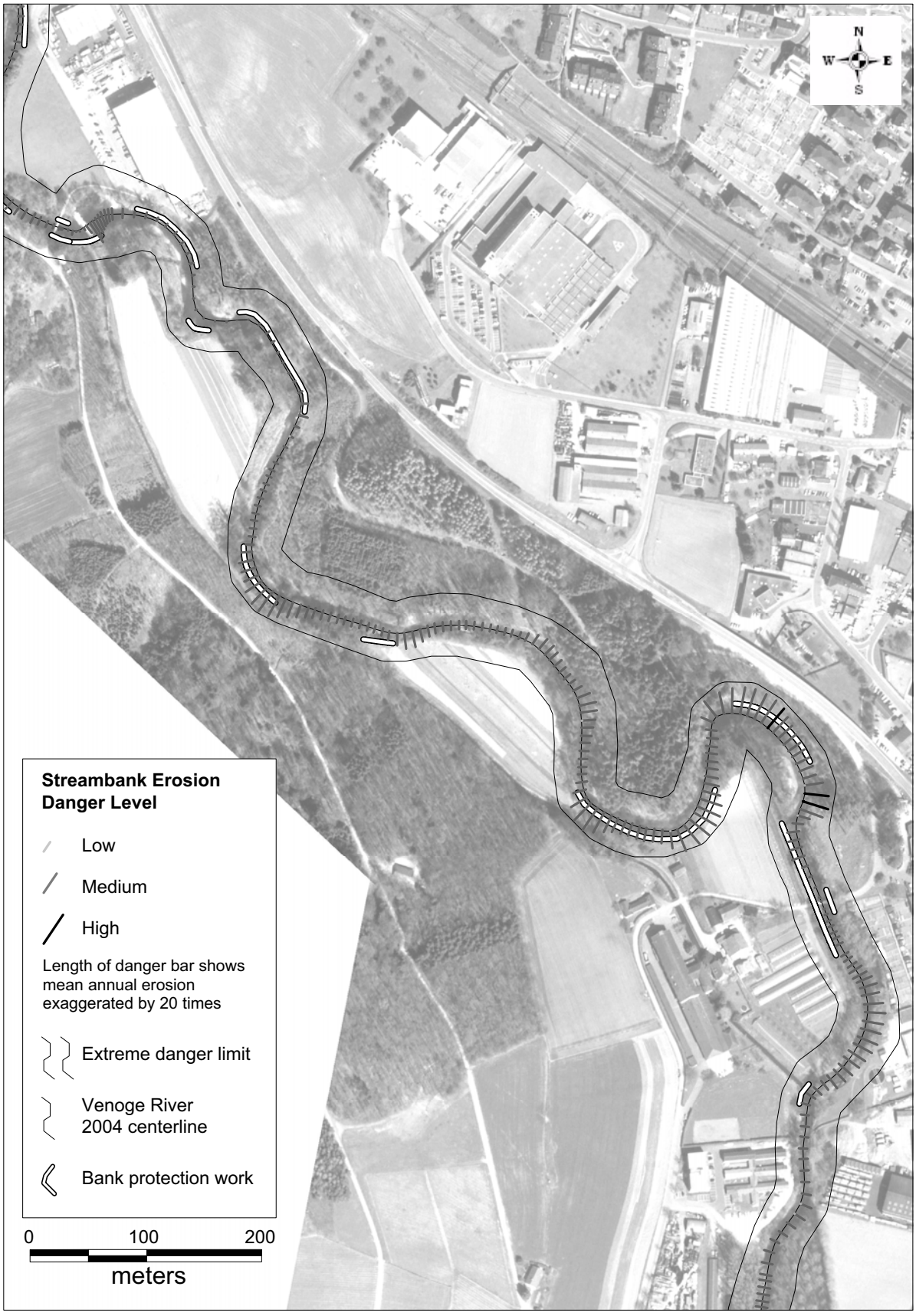

Figure A.8 (cont.). Streambank erosion danger map of the Venoge River (bank protection failure probability not taken into account)

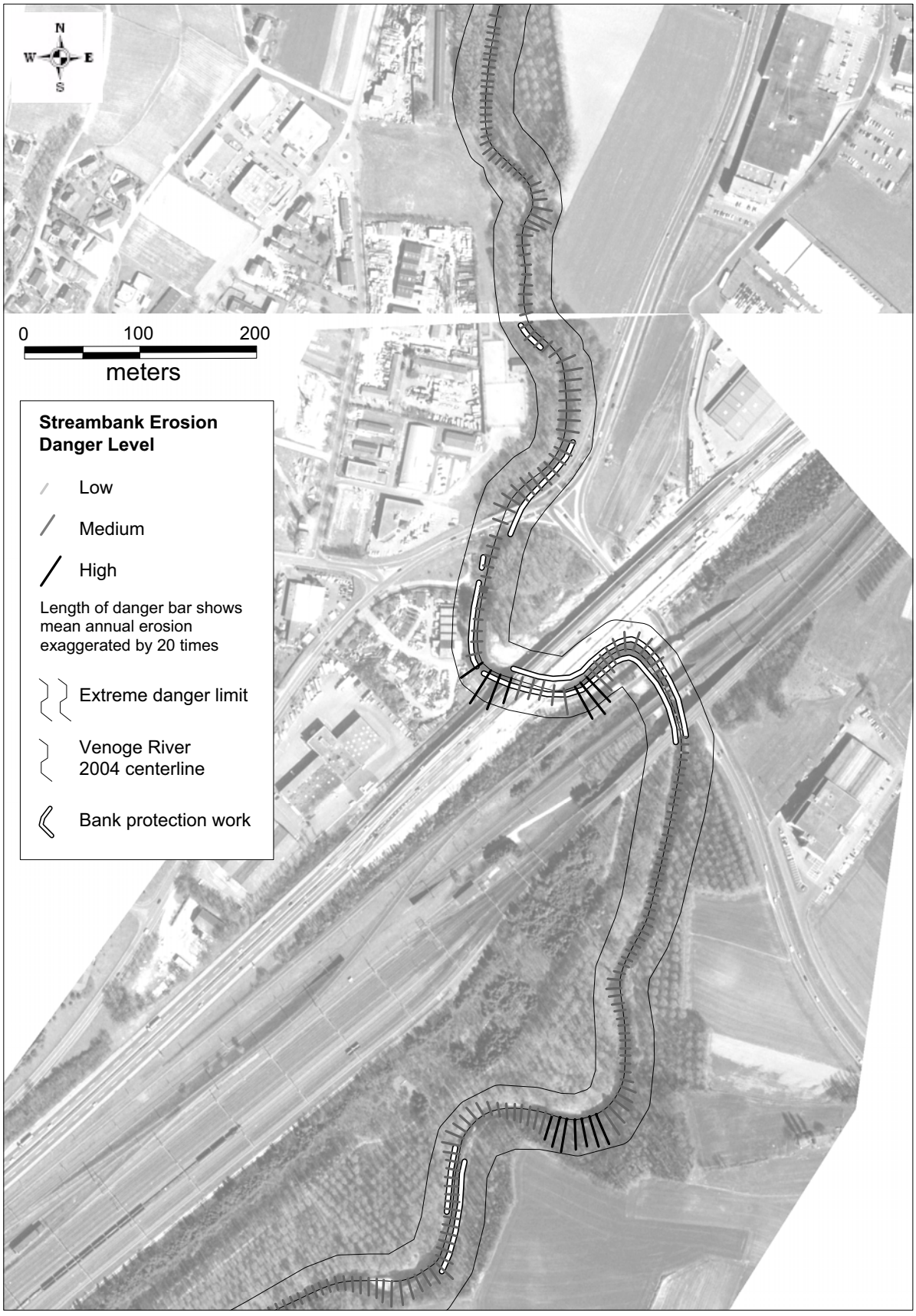

Figure A.8 (cont.). Streambank erosion danger map of the Venoge River (bank protection failure probability not taken into account)

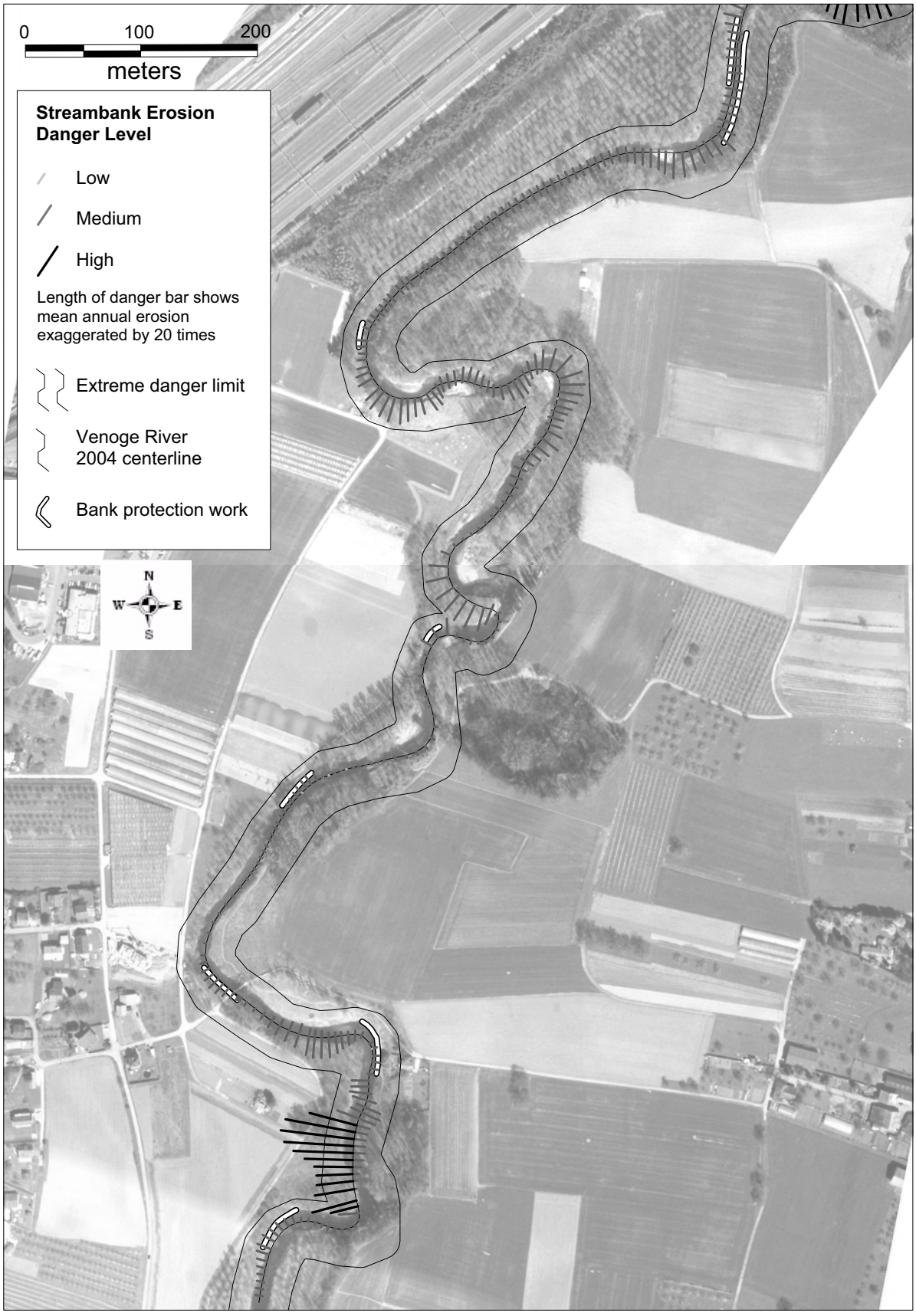

Figure A.8 (cont.). Streambank erosion danger map of the Venoge River (bank protection failure probability not taken into account)

JOHN RAYMOND BECK

PERSONAL INFORMATION

Marital status: Married, three children
Nationality: American
Date of birth: February 15, 1971 at Cedar Rapids, Iowa, USA

EDUCATION

DOCTORAL THESIS **2002-2006**
SWISS FEDERAL INSTITUTE OF TECHNOLOGY, EPFL, LAUSANNE, SWITZERLAND
Dissertation: "Streambank Erosion Hazard Mapping: Concepts, Methodology and Application on the Venoge River (Switzerland)"

POST-GRADUATE SPECIALIZATION IN HYDROLOGY **1998-1999**
SWISS FEDERAL INSTITUTE OF TECHNOLOGY, EPFL, LAUSANNE, SWITZERLAND
Master's thesis: "Methodology for the Evaluation of Flood Hazards: Application on the Seymaz Watershed."

BS CIVIL ENGINEERING WITH HONORS AND HIGHEST DISTINCTION **1989-1993**
UNIVERSITY OF IOWA, IOWA CITY, IOWA
GPA 4.00/4.00
Honors Paper: "The Effects of Long Combination Vehicles on Rigid Pavement Damage"

HIGH SCHOOL DIPLOMA **1985-1989**
IOWA MENNONITE SCHOOL, KALONA, IOWA
Valedictorian

COMPUTER EXPERIENCE:
Microsoft Office, Adobe Framemaker, Canvas, MapInfo, HEC-RAS, HEC-HMS, Visual OTTHYMO
Programming experience in Pascal, Fortran, and Delphi.

LANGUAGES:
English (mother tongue)
French (fluent)
Chadian Arabic (medium speaking abilities)
Spanish (medium written skills)

PROFESSIONAL EXPERIENCE

HYDROLOGY AND LAND IMPROVEMENT LABORATORY **1/2000-6/2006**
SWISS FEDERAL INSTITUTE OF TECHNOLOGY, EPFL, LAUSANNE, SWITZERLAND
Assistant researcher on the following projects:
- Quantitative water management of the Seymaz and its tributaries
- Flood Risk Scenarios and Hydrological Mapping (FRHYMAP), IRMA-SPONGE
- Flood Analysis and Management of the Orlice River (FLAMOR), Czech Republic
- Strategies and Actions/Implementations for Flood Emergency Risk Management (SAFER)

MENNONITE CENTRAL COMMITTEE **6/1994-6/1998**
WINNIPEG, MANITOBA, CANADA
Volunteer worker in Chad, Africa
Managed a team of 11 people doing community development work: building wells and micro-dams and pumps, promoting proper water hygiene, managing cereal banks, and creating a public library.

CONNIE BELIN CENTER,
SUMMER INSTITUTE FOR CREATIVE ENGINEERING AND INVENTIVENESS 5/93-9/93
UNIVERSITY OF IOWA, IOWA CITY, IOWA, USA
Coordinated summer 3 week camp on hydropower for 30 gifted high school students

BARR ENGINEERING COMPANY 5/1992-8/1992
MINNEAPOLIS, MINNESOTA, USA
Assisted surveyors during summer internship

ACTIVITIES/HONORS

American Society of Civil Engineers University of Iowa chapter vice president (spring '93) and executive committee (Fall '93)
Chi Epsilon University of Iowa chapter president ('93) and vice president (Fall '92)
Inducted as a member of Tau Beta Pi (Fall '92)
Student Body President of Iowa Mennonite School ('88-89)

PUBLICATIONS

Beck, J. (2005). Streambank erosion hazard mapping on the Venoge River, Switzerland. Increasing the Awareness of Flooding to Improve the Risk Management of Flood Events, Heidelberg, Germany.

Beck, J., R. Metzger, et al. (2001). FRHYMAP - WP3: Security Deficit Risk Analysis on the Upper Alzette River - Luxembourg. Lausanne, EPFL**:** 17 pp. + appendices.

Beck, J., R. Metzger, et al. (2002). Flood risk analysis based on security deficits. Experimental Hydro-climatological Atlas of the Alzette River Basin - Grand-duchy of Luxembourg. L. Pfister and L. Hoffman. Luxembourg**:** pp. 43-55.

Beck, J., R. Metzger, et al. (2002). Flood risk assessment based on security deficit analysis. Geophysical Research Abstracts. 27th General Assembly of the European Geophysical Society, Nice, France.

Beck, J., R. Metzger, et al. (2002). Two Dimensional Modeling of Floods in an Urban Environment. The International Conference Preventing and Fighting Hydrological Disasters, Timisoara, Romania.

Beck, J., P. Valenta, et al. (2003). Flood Analysis and Mitigation on the Orlice River. Final Report. Lausanne, EPFL, CTU, VUMOP, IH**:** 145.

Beck, J., P. Valenta, et al. (2003). "Flood Analysis and Mitigation on the Orlice River (FLAMOR)." ERWG Letter **14**: 8-11.

Consuegra, D., J. Beck, et al. (2000). Gestion quantitative des eaux de la Seymaz et de ses affluents: Etablissement de scénarios de gestion. Lausanne, IATE/HYDRAM.

Consuegra, D., J. Beck, et al. (2000). Gestion quantitative des eaux de la Seymaz et de ses affluents. Etude Hydrologique et Hydraulique. Diagnostic de l'état actuel des dangers liés aux inondations et à l'érosion. Lausanne, IATE/HYDRAM.

Metzger, R., A. Musy, and J. Beck (2001). Flood Risk Procedures and Management: A comprehensive approach based on the Swiss experience. 19th European Regional Conference of ICID on Sustainable Use of Land and Water, Brno and Prague.